

# **An Investigation into an All Polymer Knee Joint Replacement**

**Temitope Simon Adesina**

A dissertation submitted in partial fulfilment of the requirements  
for the degree of Doctor of Philosophy  
of the  
University College London

Centre for Material Research  
Institute of Orthopaedics and Musculoskeletal Science  
University College London  
Royal National Orthopaedic Hospital  
Stanmore HA7 4LP  
United Kingdom

I, Temitope Simon Adesina, confirm that the work presented in this thesis is my own. Where information has been derived from other sources, I have confirmed that this has been indicated in the thesis.

-----*Name*

-----*Date*

## **DEDICATION**

This work is dedicated to the memory of my late wife, Monisola, my jewel of inestimable value and a diligent mother to our sons.

## **ABSTRACT**

My thesis describes a series of tests aimed at investigating the suitability of polyetheretherketone (PEEK), carbon fibre reinforced polyetheretherketone (CFR-PEEK), polyethylene and acetal in an all polymer, metal free total knee replacement. Central to this study was the investigation of the wear performance of these polymers as bearing materials under two different loading conditions and in comparison, to contemporary metal on polyethylene (MoP) bearings. The concept of an all polymer total knee replacement (TKR) is intended to realise physiological stress distribution within periprosthetic bone, reduce stress shielding and bone loss and eliminate biological activity to particulate metal alloy. The hypothesis was that an all polymer bearing will generate reduced or similar amounts of wear when compared with the traditional metal-on-plastic bearing and may provide an alternate metal-free method of replacement. Following unidirectional pin on plate testing, wear of the different bearing combinations was assessed using gravimetric analysis, digital photography, surface profilometry and scanning electron microscopy (SEM). Characterization of wear particles generated from these bearing combinations was conducted following digestion of the particle containing lubricant fluid using an acid digestion method with isolated particles subjected to SEM analysis and an automated image analysis sequence. Subsequently, the inflammatory response of depyrogenated, endotoxin free wear particles retrieved from the pin-on-plate test was cultured with monocytes and cytokine production (TNF- $\alpha$ , IL-1 $\beta$  and IL-6) quantified as measured using ELISA.

The key findings from my thesis were that using a pin on plate test setup designed to simulate a simplified knee couple, PEEK pins articulated against

moderately cross-linked polyethylene plate exhibited comparable wear loss, a similar wear quantity, morphology and inflammatory potential to the contemporary metal on polyethylene articulations. CFR-PEEK was found unsuitable as a bearing surface in an all polymer TKR.

Based on this, my hypothesis can be accepted as it may be possible to replace CoCr in TKR. However, before translation to clinical use, exhaustive appraisal of new bearing components is necessary to confer confidence in their appropriateness and safety. An all polymeric PEEK-on-a highly crosslinked polyethylene (XLPE) bearing may be a promising alternative to MoP in total knee arthroplasty.

## IMPACT STATEMENT

Total knee arthroplasty (TKA) is established as the mainstay of treatment in advanced osteoarthritis of the knee with approximately 100,000 knee replacement procedures carried out in England, Wales and Northern Ireland in 2020. It is widely accepted that wear induced aseptic loosening and stress shielding are causes of failure with contemporary knee designs.

My study investigated polyetheretherketone, a lightweight polymer, which has a low Young's modulus as an alternative to cobalt chromium femoral components in TKA. The main finding and contribution to knowledge was that using a pin on plate device designed to simulate a simplified knee couple, PEEK pins representing femoral components articulated against highly cross-linked polyethylene (XLPE) tibial inserts in metal free knees exhibited comparable wear loss and inflammatory potential to the contemporary metal on polyethylene articulations. Based on these results, it may be possible to replace cobalt chromium in total knee replacement with PEEK which may be beneficial because of the low elastic modulus and elimination of the potential biological activity to metal alloy. Advantages of an all polymer TKA include a more physiological stress distribution in the distal femur, better visualisation of the bone implant interface using plain radiographs, artefact free CT or MRI imaging and cheaper manufacture of prostheses.

Though largely preliminary, the results also afford interesting opportunities and ideas for further scholarship and research before clinical translation, such as the need for more rigorous tribological testing of candidate biomaterials and

investigation of the biological response to particulate wear debris from the all polymer articulation. Furthermore, if successful, the novel implant may reduce failure and improve longevity of TKA designs, permitting extension of this treatment option to younger and more active patients in whom concern of early failure and need for revision surgery is of important clinical consideration. It is also postulated that the PEEK-on-XLPE knee design may reduce the financial burden on Health Services such as the NHS; specifically the costs related to implant procurement and revision arthroplasty.

## **ACKNOWLEDGEMENTS**

I would like to thank everyone who helped me throughout the course of this project. Most importantly, my supervisors – Professor Melanie Coathup for her critical, painstaking and constant input to my research, without her help and support, it would have been impossible to complete this work. I could not have asked for a better supervisor. Also, to Professor Gordon Blunn for getting me started on this interesting project and his help during my study.

Many thanks to the staff and students at the IOMS including Keith Rayner, Mark Harrison, Bob Skinner and Dr Jay Meswania for their technical advice and help with the design work. Rebecca Porter, Idonnya Aghoghogbe, Rawiya Al Hosni and Anita Sanghani-Kerai for their help with my cell work. Sara Ajami, Anna Panagiotidou and Maryam Tammadon for their “little help” in making this thesis happen.

I would also like to thank ORUK for funding part of this work. I am also grateful to Invibio, Orthoplastics, Evonik and Clariant for supplying some of the materials used in this study free of charge.

Last but not the least – to Temitayo, Temidayo and Temilolu for all the encouragement, love and support. And to God, for everything.



## **PRESENTATIONS**

Work presented in this thesis has been presented as follows:

### **World Biomaterial Congress, Montreal, Canada, May 2016.**

Polyetheretherketone as an Alternative Bearing Surface in Total Knee Arthroplasty.

Podium presentation: Temitope S Adesina

### **ORS Meeting, Orlando, Florida 2016.**

Polyetheretherketone as a bearing surface in a metal free knee.

Poster presentation: Gordon W Blunn

### **International Society for Technology in Arthroplasty, Vienna, October 2015**

Wear performance of polyetheretherketone in an all polymer total knee arthroplasty.

Podium presentation: Temitope S Adesina

### **British Orthopaedics Research Meeting, Liverpool Sept 2015.**

Wear performance of polyetheretherketone in an all polymer total knee replacement.

Podium presentation: Temitope S Adesina

**European Orthopaedic Research Meeting, Bristol, Sept 2015.**

Polyetheretherketone in an all polymer total knee arthroplasty.

Podium presentation: Temitope S Adesina

**2<sup>nd</sup> International PEEK Meeting, Washington DC 2015.**

The use of PEEK-on-UHMWPE and CFR-PEEK-on-UHMWPE as a bearing combination in Total Knee Arthroplasty.

Poster presentation: Temitope S Adesina

<b>Contents</b>	<b>Page No</b>
<b>Chapter 1: Thesis Introduction</b>	
1. Introduction.....	33
1.1. Overview.....	33
1.2. The Knee Joint.....	34
1.2.1. Functional Anatomy.....	34
1.2.2. Knee Joint Kinematics.....	38
1.2.3. Loads and Forces.....	42
1.3. Knee Arthritis.....	44
1.3.1. Epidemiology.....	44
1.3.2. Pathology.....	45
1.3.3. Treatment Overview.....	46
1.4. Total Knee Replacement.....	47
1.4.1. Developmental History.....	47
1.4.2. Biomaterials Used in Knee Replacement.....	51
1.4.3. Ultra-High Molecular Weight Polyethylene.....	52
1.4.4. Implications of Wear.....	56
1.5. Alternative Materials in Joint Replacement.....	59
1.5.1. Polyacetal.....	59
1.5.2. Polyacryletherketone (PAEK).....	61
1.5.2.1. Clinical Use of PAEK.....	63
1.5.3. Polyetheretherketone.....	64
1.5.3.1. Pre-Clinical Assessment of PEEK.....	65
1.5.3.1.1. Wear Assessment.....	65

1.5.3.1.2. Biological Assessment.....	67
1.5.3.2. Uses of PEEK and PEEK Composites.....	69
1.6. Wear Testing of Biomaterials.....	72
1.7. Aims and Hypotheses.....	75
1.8. Thesis Structure.....	77
<b>2. Chapter 2: Wear Analysis</b>	<b>78</b>
2.1. Introduction.....	78
2.2. Materials and Method.....	81
2.2.1. Test Specimens and Articulations.....	81
2.2.2. Test Set-Up.....	83
2.2.3. Contact Stresses.....	84
2.2.4. Volumetric Wear Loss.....	87
2.2.5. Surface Characterisation.....	88
2.2.6. Statistical Analysis.....	89
2.3. Results (High Load) .....	90
2.3.1. CFR-PEEK Pin Articulations.....	90
2.3.1.1. Volumetric Wear Loss.....	90
2.3.1.2. Surface Characterisation.....	91
2.3.1.2.1. Qualitative Analysis.....	91
2.3.1.2.2. Scanning Electron Microscopy.....	93
2.3.2. PEEK and Acetal Pin Articulations.....	94
2.3.2.1. Volumetric Wear Loss.....	95
2.3.2.2. Surface Characterisation.....	98
2.3.2.2.1. Qualitative Analysis.....	98

2.3.2.2.2.Surface Profilometry.....	101
2.3.2.2.3.Scanning Electron Microscopy.....	102
2.3.3. CoCr Pin Articulations.....	104
2.3.3.1.Volumetric Loss.....	104
2.3.3.2.Surface Characterisation.....	105
2.3.3.2.1.Qualitative Analysis.....	105
2.3.3.2.2.Surface Profilometry.....	106
2.3.3.2.3.Scanning Electron Microscopy.....	107
2.4. Results (Low Load) .....	111
2.4.1. CFR-PEEK Pin Articulation.....	112
2.4.2. PEEK Pin Articulations.....	113
2.4.3. CoCr Pin Articulation.....	114
2.5. Discussion.....	117
<b>3. Chapter 3: Wear Particle Analysis</b>	<b>126</b>
3.1. Introduction.....	126
3.2. Materials and Methods.....	127
3.2.1. Specimen parameters.....	127
3.2.2. Purification of reagents.....	128
3.2.3. Articulations tested.....	128
3.2.4. Sample digestion/ Isolation of particles.....	128
3.2.5. Scanning electron microscopy (SEM).....	129
3.2.6. Characterisation of wear particles.....	130
3.2.7. Quantification of wear particles.....	131
3.2.8. Protocol for separating PEEK from XLPE particles.....	132

3.2.9. Statistical analysis.....	133
3.3. Results.....	133
3.3.1. Qualitative analysis.....	133
3.3.2. Particle size analysis.....	138
3.3.3. Particle morphology.....	141
3.3.4. Particle quantification.....	145
3.3.5. PEEK-XLPE Particle separation protocol.....	146
3.4. Discussion.....	151
<b>4. Chapter 4: Inflammatory Response to PEEK, XLPE and UHMWPE Particles</b>	<b>157</b>
4.1. Introduction.....	157
4.2. Materials and Methods.....	160
4.2.1. Particle Preparation and Characterisation.....	160
4.2.2. Depyrogeneration of Particles.....	161
4.2.3. Endotoxin Testing Using Gel Clot LAL.....	162
4.2.4. Cells.....	164
4.2.4.1. Flow Cytometry – CD14+ expression.....	165
4.2.5. Particle Preparation for Monocyte-Particle Challenge.....	166
4.2.6. Monocyte-Particle Challenge.....	167
4.2.7. Assessment of Cell Activity.....	169
4.2.7.1. Monocyte Metabolism.....	169
4.2.7.2. Monocyte Viability.....	169
4.2.7.3. Cytokine Analysis.....	169
4.2.7.4. Phagocytosis and Particle Uptake.....	170

4.2.8. Statistical Analysis.....	170
4.3. Results.....	170
4.3.1. Particle Isolation and Characterisation.....	170
4.3.2. Particle Size Distribution.....	172
4.3.3. Endotoxin Testing.....	175
4.3.4. Flow Cytometry.....	178
4.3.5. Biological Activity of Cells.....	179
4.3.5.1. Cell Metabolism.....	179
4.3.5.2. Cell Viability.....	181
4.3.5.3. Particle Uptake.....	182
4.3.5.4. Enzyme Linked Immunosorbent Assay (ELISA).....	183
4.3.5.4.1. Standard Curves.....	183
4.3.5.4.2. IL-6 Assay.....	184
4.3.5.4.3. IL-1 $\beta$ and TNF- $\alpha$ .....	186
4.4. Discussion.....	187
<b>5. General Discussions and Conclusions</b>	<b>194</b>
5.1. General Discussions.....	195
5.2. Future Directions.....	197
5.2.1. Future Tribological Testing.....	197
5.2.2. Further Investigation of Inflammatory Potential.....	200
5.2.3. Limitations of the Study.....	202
<b>Appendices</b>	
1. Laboratory Protocols.....	204

2. Chapter 2 Statistics.....	220
3. Chapter 3 Statistics.....	223
4. Chapter 4 Statistics.....	228
<b>Bibliography.....</b>	<b>230</b>



## LIST OF FIGURES

<b>Figure</b>	<b>Caption</b>	<b>Page No.</b>
1.1	A diagram showing the anterior knee in the flexed position.	35
1.2	Superior view through the knee joint.	37
1.3	The six degrees of freedom of the knee (Shenoy et al, 2013)	39
1.4	Four-bar linkage formed by fixed femur and tibia with intervening anterior and posterior cruciate ligaments guiding femoral roll back	42
1.5a	X-ray image of the knee showing advanced osteoarthritis of the medial compartment and femora-tibial bone contact.	47
1.5b	Total knee replacement in the left knee.	47
1.6	Rolling and sliding in knee joint.	75
2.1	Schematic representation of pin on plate set up.	83
2.2	Six station pin-on-plate testing device. Insert shows single station.	84
2.3	Black discoloration of lubricant fluid (white arrow).	91
2.4a	Average volume loss from CFR-PEEK pins showing transition to steady wear at 500,000 cycles.	91
2.4b	Average steady volume loss from UHMWPE plates articulated against CFR-PEEK pins.	91

2.5a	CFR-PEEK pin pictured after 3656 cycles coupled with CFR PEEK plate.	92
2.5b	CFR PEEK plate coupled with CFR-PEEK pin pictured after 3656 cycles. Arrow depicts direction of travel.	92
2.5c	CFR PEEK pin coupled with PEEK plate pictured after 83117 cycles, transfer films noted on the test specimen.	92
2.5d	PEEK plate against CFR-PEEK plate shows corresponding area of transfer. Arrow depicts direction of travel.	92
2.5e	PEEK pin articulated against UHMWPE plate at the end of wear test 1.65 million cycles.	93
2.5f	UHMWPE plate coupled with PEEK pin pictured after 1.65 million cycles. Arrow depicts direction of travel.	93
2.6a	Typical CFR-PEEK finishing.	94
2.6b	CFR-PEEK pin articulated against UHMWPE plate showing, protruding and broken carbon fibers.	94
2.7a	Typical machining cut as seen with SEM examination of UHMWPE plate.	94
2.7b	Flake-like cut out from the worn surface of UHMWPE articulated against CFR-PEEK.	94
2.8a	Volume loss from PEEK pins articulated against UHMWPE plates.	96
2.8b	Volume loss from UHMWPE plates articulated against PEEK pins.	96

2.9a	Volume loss from PEEK pins (articulated against XLPE plates).	97
2.9b	Volume loss from XLPE plate articulated against PEEK pins.	97
2.10a	Volume loss from Acetal pins coupled with XLPE plates.	97
2.10b	Variations in volume loss from XLPE plates articulated against Acetal pins.	97
2.11a	Volume loss from PEEK pins (articulated against Acetal plates).	97
2.11b	Volume loss from Acetal plates (articulated against PEEK pins).	97
2.12a	Volume loss from PEEK pins (articulated against PEEK plates).	98
2.12b	Volume loss from PEEK plates (articulated against PEEK pins).	98
2.13a	Light burnishing on PEEK pin articulated against XLPE plate at the end of wear test.	99
2.13b	XLPE plate coupled with PEEK pin pictured after 2 million cycles.	99
2.13c	PEEK pin articulated against acetal plate pictured after 2 million cycles.	99
2.13d	Acetal plate coupled with PEEK pin pictured after 2 million cycles.	99
2.13e	Light scratches observed on PEEK pins at the end of test with UHMWPE.	99

2.13f	UHMWPE plate articulated with PEEK at the end of 2 million cycles.	99
2.13g	Surface of acetal pin after a 2 million wear cycle coupled with XLPE.	100
2.13h	XLPE plate coupled with acetal pin.	100
2.13i	Large wear scar on PEEK pin coupled with PEEK plate, pictured after wear testing (2 million cycles).	100
2.13j	Corresponding wear scar on PEEK plate at the end of test.	100
2.13k	Flattening of PEEK pin coupled with PEEK plate (left). Comparison made with unused PEEK pins of similar dimensions.	100
2.14	R <sub>a</sub> values of all polymeric articulations (Mean ± SE) pre-test and post-test.	101
2.15	Typical machine finish of pre-test PEEK pin surfaces.	103
2.16	PEEK pin coupled with UHMWPE post testing.	103
2.17	Typical machine surface finish of PEEK plate as seen before wear testing.	103
2.18	PEEK plate after wear test coupled with PEEK pin. Similar features observed on PEEK pin.	103
2.19	XLPE surface (coupled with PEEK) at low magnification.	103
2.20	XLPE surface (coupled with PEEK) at high magnification with areas of delamination and surface cracks.	103

2.21	Volumetric wear loss generated from UHMWPE plates against CoCr Pins over the 2 million cycle period.	105
2.22	Volumetric wear from XLPE plates (against CoCr Pins).	105
2.23	Volumetric wear from PEEK plates (against CoCr Pins).	105
2.24a	XLPE plate after 2 million cycles.	106
2.24b	PEEK plate after 2 million cycles.	106
2.24c	UHMWPE plate after 2 million cycles.	106
2.25	R <sub>a</sub> values of CoCr pins (Mean ± SE) articulated against various polymeric counterfaces pre-test and post-test.	107
2.26a	Deep grooves (R <sub>a</sub> -635.59±9.87nm) seen on CoCr pins coupled with CFR-PEEK.	108
2.26b	Scratches seen on CoCr Pins coupled with PEEK.	108
2.26c	Scratches on CoCr pins coupled with polyethylene.	108
2.27a	CFR-PEEK plate surface showing areas of carbon fibre detachment.	108
2.27b	PEEK surface showed a “polished” appearance post wear test.	108
2.27c	XLPE surface (against CoCr) at low magnification.	109
2.27d	XLPE surface (against CoCr) at high magnification with evidence of micro-delamination and surface cracks shown by block arrows.	109
2.28	Average wear (± SD) of materials tested to 2MC.  Asterisk depicts significance p<0.05 (Mann Whitney U test) when compared to volumetric wear loss of CoCr vs. XLPE combination.	110

2.29	Wear rate of CoCr-on-UHMWPE, CoCr-on-XLPE, PEEK-on-XLPE and PEEK-on-UHMWPE.	111
2.30a	Negligible wear observed from the CFR-PEEK pin when coupled with XLPE at contact stresses of 50N	112
2.30b	Variations in SE noted in wear from XLPE plates coupled with CFR-PEEK	112
2.31a	No appreciable wear observed from PEEK pin coupled with UHMWPE.	113
2.31b	Variations in SE observed in UHMWPE plates coupled with PEEK pins	113
2.32a	No appreciable wear observed from PEEK pin coupled with XLPE.	114
2.32b	No significant wear noted after 750,000 cycles from XLPE plates coupled with PEEK	114
2.33	Wear profile of XLPE plates coupled with CoCr pins	114
2.34	Average wear ( $\pm$ SD) of materials tested to 2MC at low stresses. Asterisk depicts significance when compared to volumetric wear loss of CoCr vs. XLPE articulation.	116
2.35	Graphical Representation comparing wear in CoCr vs. XLPE, PEEK vs. XLPE, PEEK vs. UHMWPE.	116
3.1	Particle laden filter membrane showing particles from the CoCr vs PEEK articulation	134
3.2	Few particles were obtained from CoCr vs XLPE articulations	134

3.3a	CoCr-on-XLPE displayed on polycarbonate filter membrane	135
3.3b	Typical outline of particles (CoCr-on-XLPE) for automated sequence analysis.	135
3.4a	Displayed particles from CoCr-on-UHMWPE articulation.	135
3.4b	Representative particle outline from CoCr-on-UHMWPE articulation.	135
3.5a	SEM image of PEEK particles from CoCr-on-PEEK articulation.	136
3.5b	ImageJ rendered outline of PEEK particles from CoCr-on-PEEK articulations.	136
3.6a	Particles from CFR-PEEK-on-UHMWPE articulation as viewed by SEM	136
3.6b	ImageJ rendered outline of particles from CFR-PEEK-on-UHMWPE articulations.	136
3.7a	SEM image of particles from PEEK-on-XLPE couples	137
3.7b	Outline of particles from PEEK-on-XLPE articulation.	137
3.8a	Displayed particles from PEEK-on-UHMWPE articulation.	137
3.8b	Representative particle outline from PEEK-on-UHMWPE articulation	137
3.9a	Displayed particles from PEEK vs PEEK articulation.	138
3.9b	Representative particle outline from PEEK-on-PEEK articulation	138

3.10	Particle sizes (ECD) of analysed wear particles from seven articulations.	140
3.11	Summary of the morphological characteristics of the different articulations.	144
3.12	SEM image of proprietary supplied polyethylene particles (Ceridust 3715)	146
3.13	SEM image of proprietary supplied PEEK (VESTAPEEK)	146
3.14	Digested lubricant containing Ceridust and PEEK powder.	147
3.15	Digested lubricant layered over chloroform: methanol mixture (2:1).	147
3.16	Separation into layers after centrifugation	148
3.17	Particles collected on to 0.05micron pore filter membrane.	148
3.18	Retrieved ceridust with described separation protocol. The double peak at approximately $2900\text{cm}^{-1}$ is characteristic of the hydrocarbon bond of polyethylene (C-H).	149
3.19	FT-IR spectrum of plain ceridust showing similarities to the tracing of retrieved ceridust after separation.	149
3.20	FT-IR spectrum of retrieved VESTAPEEK particles after separation. Distinctive features of PEEK spectra exhibited mainly in the fingerprint region showing carbonyl bond (C=O), ether bond (C-O-C) and aromatic benzene ring (-C <sub>6</sub> H <sub>4</sub> -) (Nguyen and Ishida, 1986)	150



3.21	FT-IR spectrum of proprietary received VESTAPEEK showing carbonyl bond (C=O), ether bond (C-O-C) and aromatic benzene ring.	150
4.1a	XLPE particles of different sizes laden on the membrane filter	171
4.1b	XLPE particles viewed from another region on the same membrane as Fig 4.1a	171
4.2	a, b and c show the SEM images of PEEK, XLPE and UHMWPE particles respectively while d, e and f show the outline of PEEK, XLPE and UHMWPE as analysed with ImageJ.	172
4.3	Histograms showing the particle size range for XLPE, UHMWPE and PEEK.	173
4.4	Histogram showing the morphological variations observed in particle types.	175
4.5	a). Gate applied to identify monocyte population b). Histogram showing overlay of negative population (red) onto stained cells (green) permits identification of positive cells expressing CD14. c) and d) Gated cells split at intersection to identify isotype population and cell elaborating CD14, over 70% of cells expressed CD14.	179
4.6	Box and Whisker plot showing Alamar blue absorbance results in each of the test groups investigated.	181

4.7	(a, b & c) Live/Dead staining of cells after test as observed with a widefield fluorescence microscope (Apotome, Zeiss, Germany)	182
4.8	Showing birefringent particles within cells.	182
4.9a	Seven-Point XY scatter plot showing standard curve for lyophilised TNF- $\alpha$ protein	183
4.9b	Seven-Point XY scatter plot showing standard curve for lyophilised IL-1 $\beta$ protein	183
4.9c	Seven-Point XY scatter plot showing standard curve for lyophilised IL-6 protein	183
4.10a	IL-6 levels by CD14+ monocytes 12 hours after particle challenge.	184
4.10b	IL-6 levels as observed in positive controls after 12 hours	184
4.11a	IL-6 release by CD14+ monocytes 24 hours after particle challenge.	185
4.11b	Showing IL-6 levels in positive controls after 24 hours.	185

## LIST OF TABLES

<b>Table</b>	<b>Caption</b>	<b>Page No.</b>
1.1	Examples of UHMWPE in clinical use.	55
1.2	Typical average mechanical and thermal properties of some clinically relevant materials	62
1.3	Showing femoral profile measurements of some prosthetic designs.	73
2.1	Articulations tested (Pin vs. Plate).	82
2.2	Typical average elastic modulus and Poisson's ratio of material tested	85
2.3	Articulations and calculated contact stresses under a 1KN load.	86
2.4	Articulations and calculated contact stresses using 50N load.	86
2.5	Density of materials used.	88
2.6	Volume loss for PEEK and acetal pin articulations ranked from lowest to highest wearing couples.	96
2.7	Volume loss for CoCr pin articulations ranked from lowest to highest wearing couples.	104
2.8	Articulations tested at low stresses (Pin versus Plate).	112
2.9	Volume loss for articulations tested at with 50N load	115
3.1	List of articulations used in wear debris analysis	128

3.2	Particle sizes (ECD) of various articulations in descending order.	139
3.3	Aspect ratio of wear debris, showing mean $\pm$ SD, median and range.	142
3.4	Analysis of particle roundness from different bearing couples.	143
3.5	Form factor description from each articulation	143
3.6	CoCr-on-UHMWPE, PEEK-on-XLPE and CoCr-on-XLPE generated a statistically similar number of wear particles. Asterisks highlight combinations that are statistically different to CoCr-on-XLPE articulations.	145
4.1	Showing set-up for assessment of test sensitivity and validity	163
4.2	Setup for evaluating test interference.	164
4.3	Test setup in sterile 48 well plate, colour coding represents each participant.	168
4.4	Endotoxin standard incubated with lysate.	176
4.5	Positive product control (PPC) incubated with lysate	176
4.6	Results of LAL testing using gel clot method.	177
4.7	Alamar blue test results – Kruskal Wallis (Absorbance) p= 0.182.	180
4.8	Kruskal Wallis IL-6 concentration compared with negative control at 12 and 24 hours; p= 0.585 and 0.310 respectively	186

## ABBREVIATIONS

A	Area
ACL	Anterior Cruciate Ligament
A <sub>Filter</sub>	Area of filter membrane
AM	Acetoxymethyl
APC	Allophycocyanin
AR	Aspect Ratio
ASTM	American Society for Testing and Materials
BSA	Bovine Serum Albumin
CD	Cluster of Differentiation
CFR-PBT	Carbon Fibre Reinforced Polybutyleneterephthalate
CFR-PEEK	Carbon Fibre Reinforced Polyetheretherketone
CNC	Computerised Numerical Controlled
CO <sub>2</sub>	Carbon Dioxide
CoCr	Cobalt Chromium
CoCrMo	Cobalt Chromium Molybdenum
CT	Computerised Tomography
DEXA	Dual Energy X-ray Absorptiometry
ECD	Equivalent Circle Diameter
EDTA	Ethylenediaminetetraacetic Acid
ELISA	Enzyme Linked Immunosorbent Assay
EU	Endotoxin Unit
FDA	Food and Drug Administration
FF	Form Factor

FTIR	Fourier Transform Infrared Spectroscopy
Gy	Gray
Hc	High Carbon
HCl	Hydrochloric Acid
HNO <sub>3</sub>	Nitric Acid
HSS	Hospital for Special Surgery
ICIC	Inflammatory Cell Induced Corrosion
ICLH	Imperial College London Hospital
IDE	Investigational Device Exemption
IL-6	Interleukin 6
IL-8	Interleukin 8
IL-1 $\beta$	Interleukin 1 beta
LAL	Limulus Amoebocyte Lysate
Lc	Low Carbon
LPS	Lipopolysaccharide
m	Metre
M	Molar
Mc	Million Cycle
MoM	Metal on Metal
MoP	Metal on Polyethylene
MRI	Magnetic Resonance Imaging
N	Newton
NaOH	Sodium Hydroxide
N <sub>(T)</sub>	Total number of particles
OA	Osteoarthritis

OD	Optical Density
P	Perimeter
PAEK	Poly Aryl Ether Ketone
PAN	PolyacrlNitrile
Pa	Pascal
PBMC	Peripheral Blood Mononuclear Cells
PBS	Phosphate Buffered Saline
PEK	Polyetherketone
PEEK	Polyetheretherketone
PEEKK	Polyetheretherketoneketone
PEKEKK	Polyetherketoneeetherketoneketone
PEKK	Polyetherketoneketone
PCL	Posterior Cruciate Ligament
PMMA	Polymethylmethacrylate
PPC	Positive Product Control
R	Roundness
Ra	Surface Roughness
Rpm	Revolutions per minute
SEM	Scanning Electron Microscope
TCP	Tissue Culture Plate
THR	Total Hip Replacement
Ti6Al4v	Titanium Alloy
TKA	Total Knee Arthroplasty
TKR	Total Knee Replacement
TNF- $\alpha$	Tumour Necrosis Factor - alpha

UHMWPE

Ultra-High Molecular Weight Polyethylene

v/v

Concentration of substance in solution (volume per volume)



## CHAPTER ONE: INTRODUCTION

### 1.1 OVERVIEW

Contemporary designs in total knee replacement (TKR) utilise metal on polyethylene (MoP) bearing couples. The commonly used orthopaedic metal alloys have a modulus that is 10 – 20 times greater than that of bone with cobalt chrome being the stiffest of all orthopaedic alloys (Chen and Thouas, 2015). This mismatch in elastic modulus between bone and implanted alloy results in the stiffer metallic component bearing more load than bone to which it is fixed, subsequently shielding the bone from stress. Stress shielding deprives bone of the mechanical stresses required to maintain its structure thereby becoming porotic and more likely to fracture under stress (Williams et al., 1987, Andersen et al., 2018). Also, wear particles generated within the bearing surfaces and at the bone-implant (or bone-cement) interface induce a cellular response with activated macrophages and giant cells producing pro-inflammatory cytokines (Matthews et al., 2000a). This biological event called aseptic loosening, has been reported to lead to periprosthetic bone resorption and osteolysis, leading to loosening and implant failure (Maguire et al., 1987, Sharkey et al., 2014). Based on these highlighted issues, the use of a low wearing, low modulus material is attractive in implant design and may be a suitable alternative to conventional hard bearing prostheses. Such a novel implant may also extend consideration for joint replacement to include more active and younger patients.

My thesis investigated the use of polyetheretherketone (PEEK) composites, polyethylene and polyacetal as bearing surfaces in an all polymer TKR. My

research covered the measurement of material wear of these polymers using a pin on plate test, characterisation of the wear particles generated followed by assessment of the inflammatory response of these wear particles.

The ensuing literature review describes relevant published information as it relates to the anatomy of the knee, loads and motion across the knee joint, it also provides a brief description of knee arthritis, the evolution of contemporary TKR designs and biomaterials used in TKR. The review forms the basis and my rationale for investigating PEEK, PEEK composites and polyacetal as alternatives to metal alloys in TKR.

## 1.2 KNEE JOINT

### 1.2.1 Functional Anatomy of the Knee Joint

The anatomy of the knee joint has been well characterised and this section provides an overview that is relevant in understanding the requirements in knee joint replacement. The knee joint is the largest joint in the body and is comprised of a complex synovial hinge consisting of two articulations (Chummy and Sinnatamby, 1999). Firstly, the patellofemoral joint located between the patella and trochlea groove of the distal femur and secondly, the articulation between the distal femur and proximal tibia, also known as the tibiofemoral joint (Figure 1.1).

The patellofemoral joint is a sellar joint and its main role in terms of knee stability, is through its effect on the extensor mechanism. The patella increases

the moment arm of the extensor force from its centre of rotation, thereby reducing the force required to extend the knee (Goldblatt and Richmond, 2003). It may or may not be resurfaced during TKR procedures.

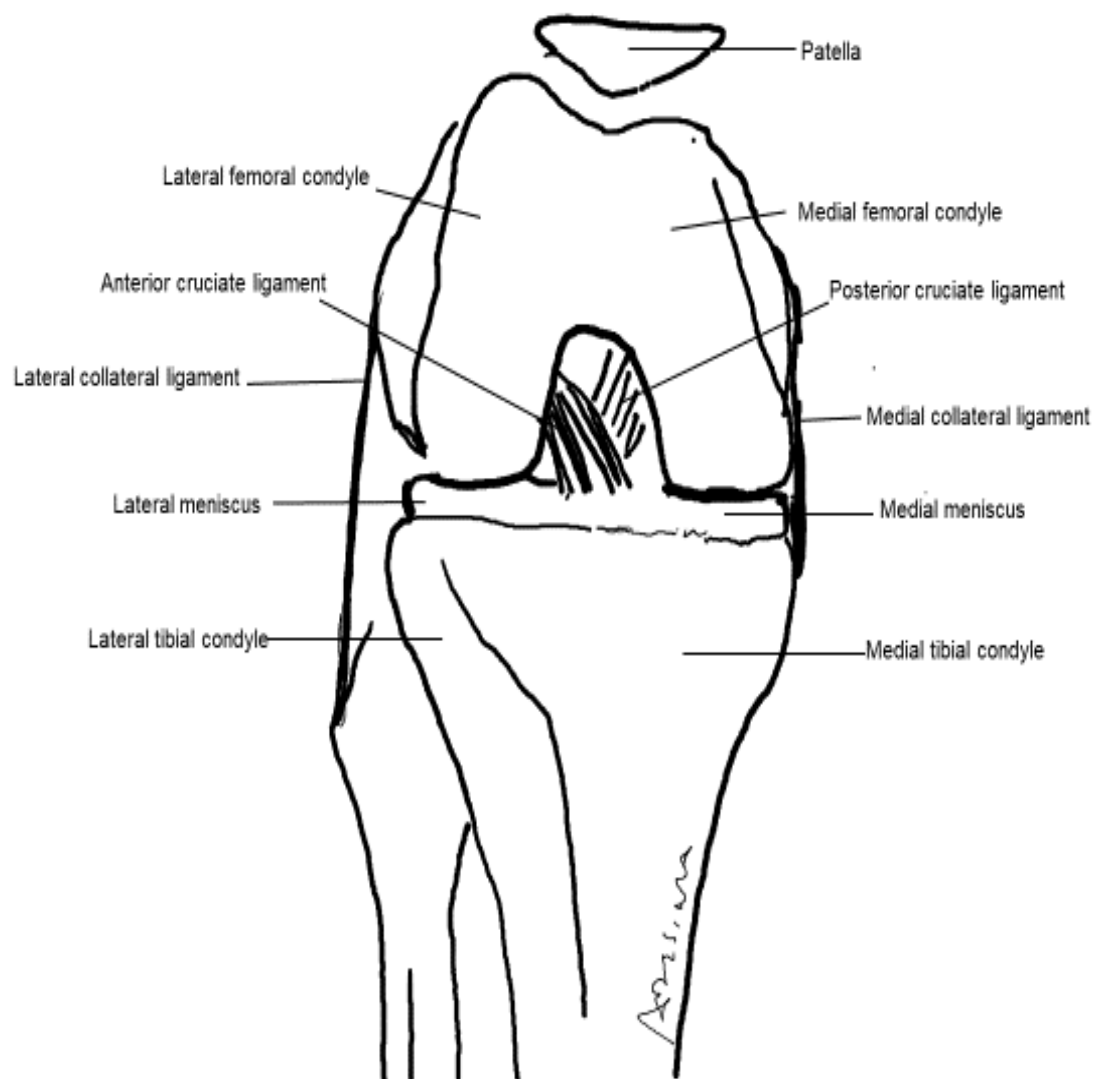


Fig 1.1: A diagram showing the anterior knee in the flexed position

The tibiofemoral articulation is a condyloid joint, where the articular surface of the distal femur consists of two condyles, the convex medial and lateral condyles separated by the shallow intercondylar groove anteriorly and deep intercondylar notch posteriorly. In the sagittal plane, the femoral condyles can be viewed as cam-shaped with the medial condyle subtending a longer radius of curvature, it also extends more distally in the coronal plane. The articular surfaces of the femoral condyles articulate with the corresponding medial and the lateral plateaus of the proximal tibia. The medial tibial plateau is oval with a shallow concavity while the lateral tibial plateau is circular and slightly convex. The asymmetrical compartments of the tibial plateau are separated by the intercondylar eminence (Hamilton, 1982).

The articular surface of the proximal tibia is partially covered by two c-shaped fibrocartilage structures referred to as the medial and lateral meniscus (Figure 1.2). The menisci provide some depth for the shallow and incongruent bony architecture of the tibiofemoral articulation. The menisci are thick in their outer margin and taper to a thin inner edge. The outer margin of the medial meniscus is firmly adherent to the knee capsule in its entire length while the lateral meniscus has a loose fixation to the joint capsule allowing for greater translation of the lateral meniscus compared to the medial meniscus (Miller and Thompson, 2016).

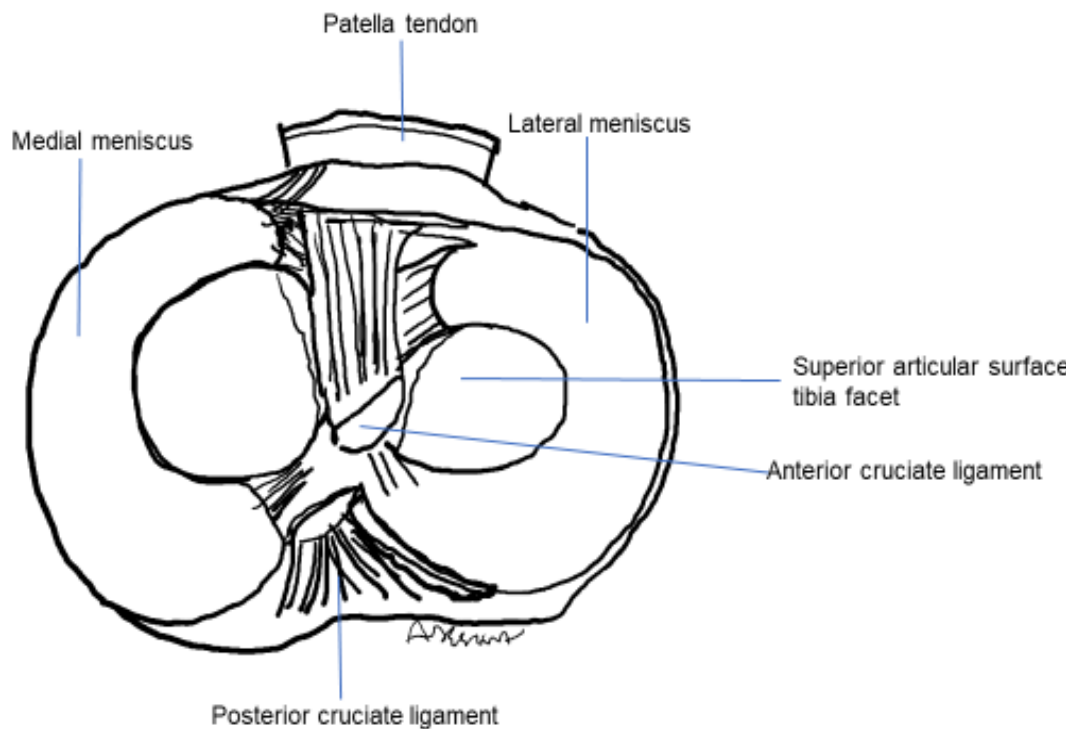


Figure 1.2: Superior view through the knee joint.

The bony architecture of the knee offers limited stability to the joint with most restraint provided by ligaments located across the joint (Garino and Beredjiklian, 2007). The femur and tibia are held together by the joint capsule and strong ligaments attached to the bones significantly increase the stability of the joint. The major ligamentous restraints are the collateral ligaments (lateral and medial) and the cruciate ligaments (anterior and posterior). The anterior cruciate ligament (ACL) is attached to the medial surface of the lateral femoral condyle close to its posterior aspect and extends with insertion on the tibia in front and lateral to the medial tibial spine on the intercondylar eminence. The posterior cruciate ligament (PCL) is attached to the lateral aspect of the medial condyle and extends with attachment within a depression between the

two tibial plateaus approximately a centimetre from the tibial articular surface. The ACL prevents anterior translation of the tibia while the PCL prevents posterior translation of the tibia on the femur. Both cruciate ligaments also provide rotational stability to the knee joint.

The lateral and medial collateral ligaments provide varus and valgus restraint to the knee respectively. The medial collateral ligament is a flat band like structure with a superficial and deep layer. The superficial layer extends from the medial epicondyle and fans out as a broad triangular ligament to its insertion on the tibia. The deep layer, which is a condensation of the joint capsule, is attached to the medial meniscus around the mid portion of its length. The lateral collateral ligament is a cord like structure, separate from the knee joint capsule and extends from the lateral epicondyle of the femur to the head of the fibula. The joint is lubricated by synovial fluid produced by the synovial membrane. The synovial fluid combined with the special attributes of the articular surface produce a very low co-efficient of friction.

### **1.2.2 Knee Joint Kinematics**

The knee joint is by far the most complex joint in the body. Knee joint kinematics entails movement of the joint without consideration for the forces causing motion. All joints are defined by six degrees of freedom with 3 rotations and 3 translations (Ramsey and Wretenberg, 1999, Lafortune et al., 1992). The rotations are internal-external, flexion-extension and abduction and adduction movements, while the translations are medial-lateral shift, anterior-posterior shift and compression-distraction motion (Figure 1.3). Some degrees

of freedom are larger and therefore more important, with flexion and extension movements being the primary motion of the knee joint (Buckwalter et al., 2000).

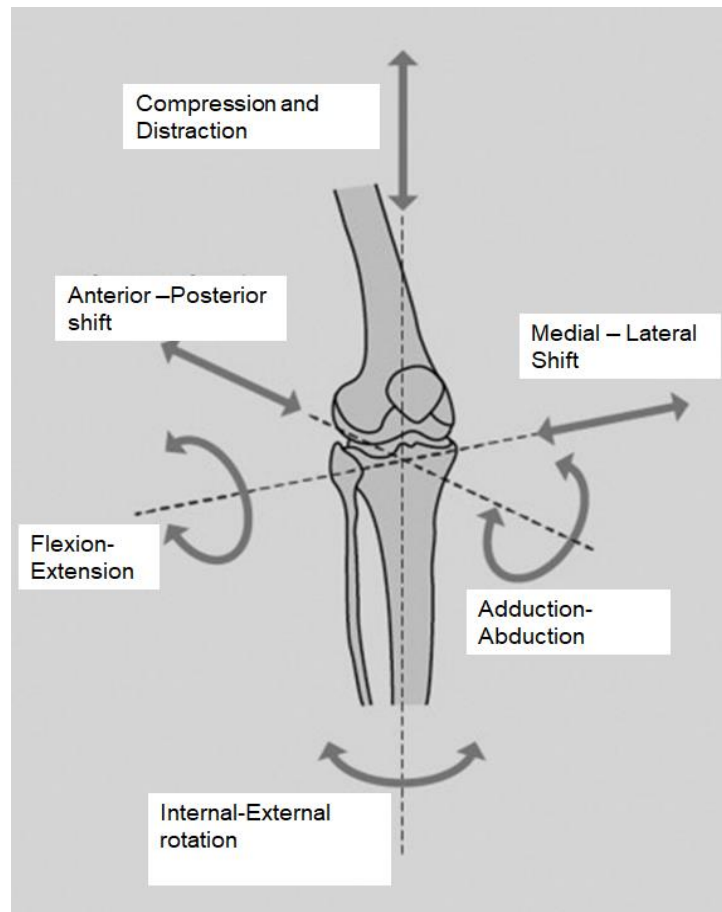


Figure 1.3: The six degrees of freedom of the knee (Shenoy et al., 2013)

Knee motion has been reported by many investigators using various descriptive parameters such as angular motion between the femur and tibia (Lafortune et al., 1992, Ramsey and Wretenberg, 1999), relative motion of the femur and tibial articular surfaces (Kanisawa et al., 2003, Komistek et al., 2003), relative movement of the condyles (Kurosawa et al., 1985) or movement of contact points during the gait cycle (Iwaki et al., 2000). These coupled with the challenges in measurement, the different methods of

investigation and systems used in reporting results provide a vast array of information simply too extensive to concisely review. In addition, widely used measurement methods such as exoskeletal linkages with instrumented goniometers and reflective markers, are subject to error due to their non-rigid fixation to the skin and are themselves subject to movement artefact following muscle contraction. This movement can result in uncertainties regarding their position in relation to bony landmarks (Reinschmidt et al., 1997). Furthermore, other methods of analysis such as fluoroscopy and X-ray imaging are carried out in 2-D and improved understanding may therefore require that these techniques are combined with other modalities in order to evaluate the 3-D kinematics of the knee (Freeman and Pinskerova, 2005).

Lafortune et al. 1992, used markers attached to pins, which were securely fixed within the bone in a bid to provide an accurate description of angular motion during gait. While this provided more valid experimental results when compared to markers attached to the skin, the invasiveness of the test method was an ethical drawback of the study. They reported the mean kinematic model in each of the five volunteers recruited in the study (Lafortune et al., 1992). This study showed that flexion-extension motion occurred in 2 phases with an initial 20° of flexion during heel strike, followed by a period of knee extension and a second phase of flexion peaking at 60° early in the swing phase. The observed sequence of abduction was limited with values ranging from 1.2° abduction to a maximum mean value of 6.4°. Tibiofemoral rotation during stance was reported to be less than 5°. This study related angular motion in the knee with phases of the gait cycle and showed that flexion-extension is the largest rotation in the knee joint during the gait cycle.



Anatomical demonstration of the relative motion of the articular contact points was examined by Iwaki et al 2000 using MRI studies in six male cadavers. Observation of the medial and lateral femoral condyles in the sagittal plane showed the medial femoral condyle to be composed of arcs produced by two circles, with the first (more anteriorly placed) reported as the extension facet while the second, the flexion facet. It was also demonstrated that the medial compartment appeared similar to a constrained ball-in-socket joint in which the medial femoral condyle did not exhibit anterior-posterior motion up to 110° of knee flexion. The lateral condyle was observed to rollback with flexion. In tibiofemoral flexion, different events occur in the medial and lateral compartment with a predominantly sliding motion seen in the medial compartment and rolling coupled with sliding motion observed in the lateral compartment. These movements result in an external rotation of the tibia along a medial pivot – the so-called ‘screw home mechanism’ especially seen in full knee extension.

Due to its articular geometry and ligament restraints, flexion in the knee takes place around a changing transverse axis and has been described as incorporating rotation (rolling) and translation (sliding) movements. These movements produce a mean posterior translation of the femur on the tibia averaging 21mm around a medially based pivot. O'Connor and his associates (O'Connor et al., 1989) proposed that knee motion was dependent on its geometry in the sagittal planes and that movement was guided by a four-bar linkage consisting of the femur, tibia and cruciate ligaments. This theory was based on a geometric simulation of knee movement. It was suggested that for

the knee to flex fully, the femur must rollback on the tibia to prevent impingement and that the changing or so called instantaneous centre of rotation of the knee joint, coincides with the cross over point of the cruciate ligaments. This observation coupled with the decreasing radius of curvature of the femoral condyles as the knee flexes, are important components of the femoral rollback mechanism (Figure 1.4).

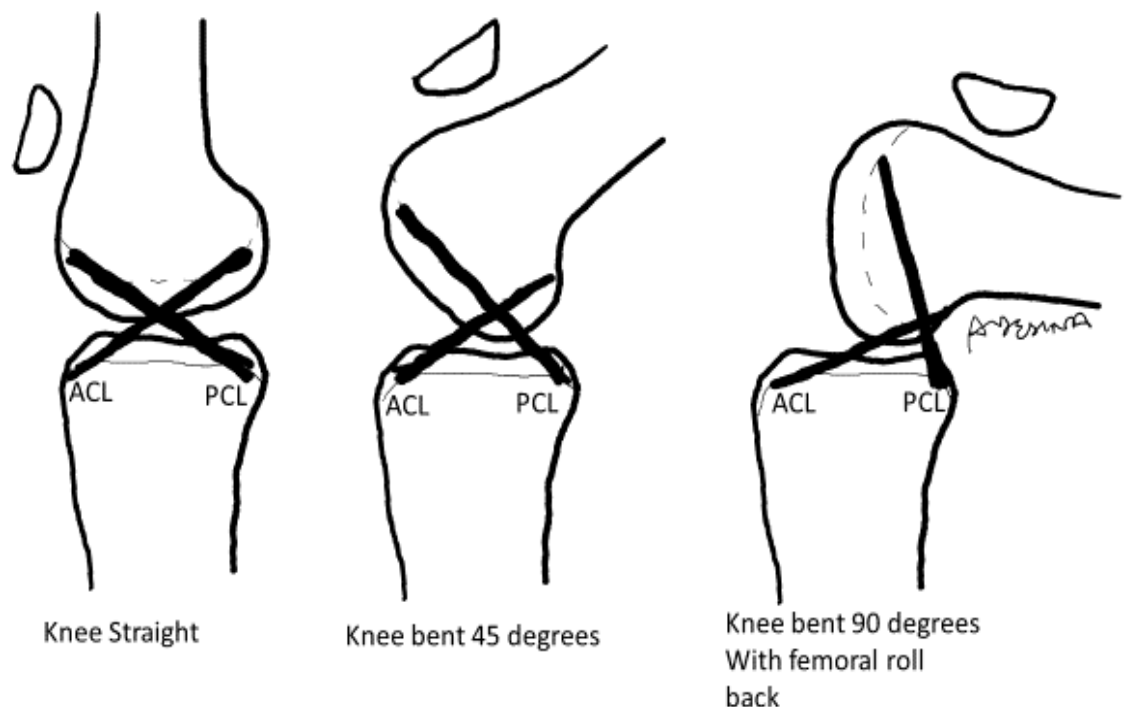


Figure 1.4: Four-bar linkage formed by fixed femur and tibia with intervening anterior and posterior cruciate ligaments guiding femoral roll back.

### 1.2.3 Loads and Forces

Estimation of the forces within the knee has received much attention partly due to the impact that they have on the initiation and progression of knee arthritis and also partly because of the effect on the durability of knee implants (D'Lima

et al., 2012). Forces and moments around the knee differ considerably with varying activities and are difficult to assess requiring a combination of techniques for estimation. Historically and in a series of experiments, Morrison (Morrison, 1970) developed a model using data obtained from gait analysis and ground reaction force in combination with geometrical measurements of the limb. Estimated forces were lowest during level walking and highest when descending stairs or walking down a slope. This study showed that external forces generated due to muscular activities, accounted for most of the forces acting on the joint, however impact loading on heel strike for example during descent down a slope also contribute significantly. A similar result was noted by another researcher who showed that the tibiofemoral compressive force averaged 3.9 times and 8 times body weight for level walking and downhill walking respectively (Kuster et al., 1997). Additionally, more strenuous activities were reported to generate higher forces.

Many methods have been used to demonstrate the connection between knee kinematics and forces causing motion. The multiplicity of methods and assumptions in problem solving have led to wide projections even for a common activity such as walking, where predictions have ranged from 1.7 times body weight (Komistek et al., 2005), 7 times body weight (Seireg and Arvikar, 1975) and 8 times body weight (Kuster et al., 1997) using different methods of evaluation. Difficulty in accurately modelling the forces within the knee is multifactorial and has been related to the complex articular geometry, complex muscular activity and importance of soft tissue involvement in maintaining knee stability (D'Lima et al., 2012).

In the native knee, tibiofemoral compressive forces are transmitted to the joint surfaces and a significant proportion of these are dispersed through the menisci. The meniscus is a composite material consisting of a strong collagen fibre scaffold encasing and supporting a weak glycosaminoglycan gel, forming a “shock absorber” within the knee. Following meniscectomy and after applying loads of 2.2KN, identical to peak loads while walking, a reduction in the articulating area is seen (Maquet et al., 1975) thereby increasing contact stresses. The tibiofemoral contact area changed from 20cm<sup>2</sup> to 12cm<sup>2</sup> in full extension and from 11cm<sup>2</sup> to 6cm<sup>2</sup> at 90° of flexion in the normal and in the menisectomised knee respectively. This suggests a significant proportion of load is dissipated through the menisci. In experimental studies using cadavers, contact areas have been reported to decrease by 10% in partial meniscectomy and 75% in total meniscectomy whereas peak load contact stresses surge by 65% in partial meniscectomy and up to 235% in total meniscectomy (Baratz et al., 1986). In the replaced knee joint, stresses are borne by the intervening polymer and in most cases exceed its yield strength of approximately 23MPa (Sobieraj and Rimnac, 2009) .

## 1.3 KNEE ARTHRITIS

### 1.3.1 Epidemiology

The most common form of arthritis is osteoarthritis followed by the inflammatory arthritides such as rheumatoid arthritis (Kean et al., 2004). The National Joint Registry for England and Wales 2017 shows that 96% of knee replacement procedures were carried out secondary to the debilitating effect

of osteoarthritis. The Framingham Osteoarthritis Study, a population based study with over 35 years observational period, showed that in individuals over 45 years, radiographic osteoarthritis occurred in 19% while the prevalence in individuals over 80 years of age was 43% (Felson et al., 1987). Knee osteoarthritis occurs more commonly in females with a female to male ratio ranging from 1:5 to 4:1. Other important risk factors identified in the study include obesity, trauma and occupation; especially jobs that are physically demanding and where repeated knee bending is required (Felson, 1988, Calce et al., 2018).

### **1.3.2 Pathology**

Osteoarthritis is characterised by joint swelling, pain and stiffness (Hwang and Kim, 2015). The aetiology is poorly understood and considered multifactorial. Though commonly referred to as being secondary to “wear and tear”, there appears to be a genetic predisposition (van Meurs, 2017). It is considered idiopathic if no underlying cause is found and secondary if arthritis developed subsequent to an identifiable cause such as cruciate ligament injury or meniscal tear. Factors that could predispose to osteoarthritis include excess joint load resulting in tissue failure or alteration in cartilage and bone biochemistry or physiology (Mobasheri, 2012).

In the early stage of the disease, there is thickening of the cartilage layer, increased water content and associated increased synthesis of proteoglycans. Following disease progression, the cartilage layer wears unevenly with areas bearing maximum loads wearing and thinning out the most (Xia et al., 2014).

Collagenase and lysosomal protease production is increased causing cartilage loss. The enzymes also decrease hyaluron content despite increased hyaluron production. Later in the disease, chondrocyte metabolism increases as the cells try to replicate, causing increased cellularity, but this is short-lived with subsequent tissue hypocellularity (Goldring and Goldring, 2007). Reduction in proteoglycan content ensues and integrity of the cartilage layer is lost as clefts appear within the cartilage. Bone beneath the cartilage is exposed and the subchondral bone response to destruction of overlying cartilage includes appositional growth with sclerosis, bone cysts secondary to microfracture and formation of osteophytes. Synovial thickening and inflammation follows (Fitzgerald et al., 2002). Since cartilage is to a large extent avascular, the repair and regenerative potential is limited. With disease progression, erosion of cartilage results in bone on bone contact in its most advanced stage (Figure 1.5a) and this leads to pain and disability.

### **1.3.3 Treatment Overview**

Different modalities of treatment have been described in the treatment of knee OA and depend on the level of deterioration. Physical therapy, lifestyle modification including weight loss, analgesia, intra-articular injections and surgical management are all described treatment options in common use (Dieppe and Lohmander, 2005). Total knee replacement, shown in figure 1.5b, is the only successful treatment for advanced degenerative disease of the knee joint (Nelson et al., 2014).



Figure 1.5a: X-ray image of the knee showing advanced osteoarthritis of the medial compartment and femora-tibial bone contact.

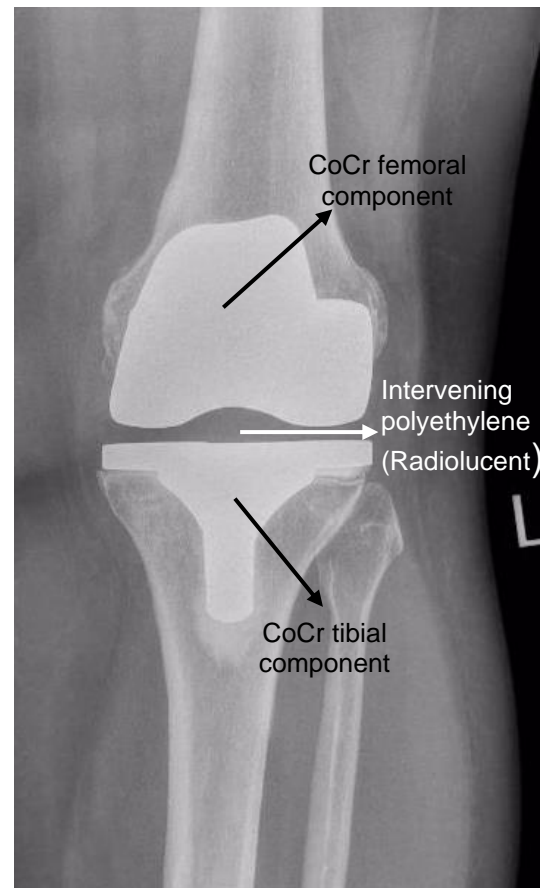


Figure 1.5b: Total knee replacement in the left knee.

## 1.4 TOTAL KNEE REPLACEMENT

### 1.4.1 Developmental History

Joint resurfacing procedures are generally needed to treat advanced, symptomatic articular surface degeneration. Surface degeneration may follow osteoarthritis, inflammatory arthropathy, trauma and infection. It was not until the late 1960s that innovative approaches to condylar replacement of the knee experienced rapid expansion. No other joint replacement enjoyed a better collaboration between engineers and clinicians, with both groups of experts

making a constructive contribution to the development of the knee replacement as known today.

Prior to this era, various pain-relieving procedures were carried out to treat knee deformity and symptomatic articular degeneration with limited success. Examples of these procedures include soft tissue interposition between resected femoral and tibia surfaces, metallic interposition, tibial hemiarthroplasty, resection arthroplasty and even knee fusion (Song et al., 2013). The hinged knee prosthesis by Walldius (Walldius, 1957), provided fair results compared with other methods in use at the time. However, the simple hinge could not substitute the complex kinematics of the knee, furthermore, loosening in the medium term and infection accounted for relatively high failure rates (Walldius, 1960). Certainly, the hinged knee design continued to experience design advancements and presently has a role in the management of severe deformities, severe ligament instability and revision procedures (Utting and Newman, 2004, Cottino et al., 2017).

Gunston's polycentric knee arthroplasty heralded the development of condylar resurfacing arthroplasty and evolution of contemporary knee arthroplasty designs. Gunston adopted the philosophy of low friction arthroplasty in his bicompartamental knee design as championed by Charnley (Gunston, 1971). Introduction of high density polyethylene as a bearing surface in joint replacement and use of polymethylmethacrylate (PMMA) as a grout or fixation material for orthopaedic prosthetic implantation are two important factors that enabled the realisation of technologies necessary for the development of the non-hinged condylar replacement (Robinson, 2005).



The non-hinged prosthetic knee joint was developed to produce a knee with a satisfactory range of motion, stability, excellent survivorship and a design that focussed on two main philosophies. The first was an anatomical approach, which endeavoured to preserve all soft tissue constraints around the knee joint, especially both cruciate ligaments. The other approach pursued an engineering solution to the complex knee kinematics by advocating resection of both cruciate ligaments to simplify the knee mechanics and applying moveable surfaces with inherent stability and maximum contact areas, reducing contact stresses at the bearing surface (Robinson, 2005).

One of the early designs based on this functional approach was that by Freeman and Swanson (Freeman et al., 1973). It utilised a metallic femoral component, which articulated against a tibial polyethylene groove in a “roller-in-trough” design. Both the femoral and tibial components were manufactured with the same radius of curvature. One observation following clinical use of this design was the inherent side to side instability. Newer designs subsequently evolved through three further advancements based on continued clinical evaluation (Freeman et al., 1985). The three advancements were (i) the Freeman-Swanson knee with a femoral component that had a central cut-out to accommodate a middle tibial polyethylene eminence, (ii) the Imperial College London Hospital (ICLH) knee which had a longer anterior flange to accommodate the patella and (iii) the subsequent Freeman-Samuelson design which had a central groove on its femoral component to enhance patella-femoral articulation.

A major advance in the total knee story was development of the Duocondylar anatomical knee replacement with symmetrical femoral condyles, which

preserved both cruciate ligaments (Ranawat and Shine, 1973). This implant was designed at the Hospital for Special Surgery (HSS), New York, USA. Clinical experience from the Duocondylar knee led to the evolution of a second generation of HSS knees. First was the Duopatella, a minimally constrained knee replacement, which selectively preserved the posterior cruciate ligament (PCL). The second was the total condylar knee, which has been described as the first truly successful functional design that typically sacrificed both cruciate ligaments. With the excision of both cruciate ligaments as exemplified in the total condylar knee, posterior subluxation of the artificial joint was reported in about a quarter of patients and knee flexion was noted to average only 90°, thought to be due to PCL deficiency (Insall et al., 1979). A further modification of the total condylar knee design was by way of a central polyethylene spine and a horizontal femoral cam that was introduced to impart PCL-like function on the construct. During knee flexion, the horizontal femoral cam engages the posterior aspect of the polyethylene spine effecting a femoral rollback, preventing posterior impingement and permitting more flexion while also improving stability (Insall et al., 1982). Thus, it appears that both designs from the 2<sup>nd</sup> generation of HSS knees evolved into two main design philosophies, the cruciate sacrificing (posterior stabilised) and the cruciate retaining TKRs. Both designs had a middle tibial eminence to prevent instability in the medial-lateral axis. It was suggested that this additional constraint may lead to increased loosening at the polyethylene bone interface. To mitigate the effect of asymmetrical loading, a tibial peg was designed to provide an additional site of fixation to the tibial plate (Robinson, 2005).

Most of the design concepts and innovation in contemporary knee arthroplasty had occurred by the early 80s, however the success of knee replacement surgery was interspersed with failure. While it may be impossible to provide a detailed account of innovations, it is considered important to highlight some landmark events as the knee designs evolved. Eftekhari is credited with implanting the earliest metal backed tibial insert with the goal of preventing polyethylene creep (Eftekhari, 1983). Subsequent advancement in his design included use of three polyethylene insert sizes to facilitate appropriate ligament tension and knee balancing. The polyethylene inserts were press-fit into the metallic tray (Eftekhari, 1983). Murray developed the Variable Axis Knee and introduced modularity into his metal-backed tibial tray design (Robinson, 2005). The idea was not only to permit a less difficult method of tibial component adjustment but also to allow for polyethylene exchange in case of wear. The concept continues to be an important consideration in present day TKR. In a bid to reduce contact stresses in the polyethylene insert, Buechel and Pappas developed a mobile bearing knee design and the first rotating platform total knee replacement (Buechel and Pappas, 1986).

#### **1.4.2 Biomaterials Used in Knee Replacement**

Historical and contemporary TKR designs have largely used metallic femoral components. Cobalt chrome is the dominant metal used, however stainless steel has also been used in the past. Following favourable laboratory testing and in a bid to reduce wear and extend implant longevity, ceramic alternatives have been introduced. Oxidized zirconium-niobium (Oxinium) is an enduring

alternative to cobalt chrome in contemporary practice, however cost limits its use (Walker et al., 2010). Furthermore, clinical and registry data do not demonstrate a clear reduction in the revision rate or show advantage when compared to CoCr (Vertullo et al., 2017). Oxinium does not contain chromium or nickel, which have been linked to metal sensitivity following the use of CoCr. The concept of metal sensitivity in TKR is debated (Granchi et al., 2008, Middleton and Toms, 2016). Also, the main biomaterials used to resurface the femoral condyles are stiff and may induce stress shielding.

#### **1.4.3 Ultra-High Molecular Weight Polyethylene**

Following its introduction as a bearing surface by Sir John Charnley, polyethylene is the material of choice for tibial inserts in contemporary TKR and the most commonly used bearing surface in arthroplasty procedures (Ingham and Fisher, 2005, Ilalov et al., 2013). Ultra-high molecular weight polyethylene (UHMWPE) belongs to a group of polyethylene polymers with  $(C_2H_4)_n$  repeating units where  $n$  represents the degree of polymerisation (Sobieraj and Rimnac, 2009). It is a semi-crystalline thermoplastic with both crystalline and amorphous regions. The crystalline region is characterised by chains folded into well aligned lamellae while the lamellae orientation in the amorphous region is random. GUR1020 and GUR1050 are the two UHMWPE resins currently in use in the field of orthopaedics (Kurtz, 2004).

In the 1990s, it was observed that terminal sterilisation of UHMWPE using gamma irradiation led to oxidation of the plastic especially after long term storage and a characteristic zone of oxidation was noted within the subsurface

layer (Blunn, 2013). At the time, gamma sterilisation in air was commonly used and the preferred method over ethyl oxide sterilisation because of cost and relative ease of use (Kurtz et al., 1999). Subsequently, it was observed that irradiation led to chain scission initiating free radical generation. This had an impact on the mechanical properties of the polyethylene including embrittlement, decreased wear resistance and increased polymer generated debris (Bracco and Oral, 2011). Once formed, free radical production is an autocatalytic process in the presence of oxygen. To mitigate against this autocatalytic process, modification of the sterilisation technique, such as vacuum-packaging or sterilisation in inert gas was adopted. These modifications did not prevent free radical production, but this approach eliminated an oxidative source (Sobieraj and Rimnac, 2009). Around this period, it was noted that sterilisation in the absence of an oxidative source was beneficial resulting in improved mechanical properties of UHMWPE (Blunn, 2013). This observation and the requirement to develop an improved biomaterial, triggered interest and subsequent production of highly cross-linked UHMWPE. In general, highly cross-linked polyethylene is manufactured by either electron beam or gamma irradiation at high doses relative to the sterilisation dose. This is followed by free radical elimination before machining and lastly, terminal sterilisation (Sobieraj and Rimnac, 2009).

To reduce oxidative degradation, the first generation crosslinking protocols employed two main thermal treatments to eliminate unreacted free radicals. The first approach was to heat the irradiated plastic below its melt transition temperature in order to prevent dissolution of the crystalline phase. It follows that any free radicals trapped within the crystalline phase will not be

extinguished. The second approach engaged an above melt transition temperature to the irradiated polymer (Oral and Muratoglu, 2011). Melting leads to dissolution and reconstitution of the crystalline phase significantly reduces the prospect of having residual free radicals. One major downside of melting is that it decreases overall crystallinity, leading to a trade-off with regards to the mechanical properties of the polymer with a reduction in fatigue strength reported (Collier et al., 2003, Oral et al., 2006).

Efforts to decrease wear through crosslinking but with the additional aim of maintaining the mechanical properties especially fatigue strength and fracture resistance, led to the development of contemporary methods of eliminating free radicals. These new second generation approaches led to the development of highly cross-linked polyethylenes. Methods developed include sequential irradiation and annealing of polyethylene, vitamin E incorporation and use of solid state deformation (Table 1.1). With sequential irradiation and annealing, the process of low dose irradiation followed by a period of annealing is repeated several times. This process is reported to extinguish most free radicals. X3™ (Stryker) is an example of sequentially irradiated UHMWPE with irradiation using 30 KGy in 3 cycles to make a total radiation dose of 90KGy (Dumbleton et al., 2006). Vitamin E incorporation is carried out largely by two methods. The first method is to mix the liquid Vitamin E antioxidant with UHMWPE resin powder, the mixture is consolidated by compression molding before irradiating the blend. The second approach allows diffusion of the Vitamin E into the radiation cross-linked bulk UHMWPE (Bracco and Oral, 2011). Vitamin E is an antioxidant that acts as a scavenger, mopping up excess free radicals that do not cross-link. Solid state deformation as a

technique for modification of radiation cross-linked polyethylene entails annealing of the polymer before ram extrusion through a die. It has been shown that the mechanical deformation step helps to align the crystalline plane along the principal axis of deformation and orientate molecular chains within the amorphous zone (Kurtz et al., 2006).

**Table 1.1:** Examples of UHMWPE in clinical use

	Cross-linking	Free Radical Elimination	Terminal Sterilisation	Examples
Conventional UHMWPE	Not Applicable	Not Applicable	Gamma Irradiation ~ 25KGy	
First Generation	50-100 KGy	Melting	EtO or Gas Plasma	Marathon (Depuy) Longevity, Durasul (Zimmer) XLPE (Smith and Nephew)
	~100 KGy	Annealing	Radiation sterilisation	Crossfire (Stryker)
Second Generation	Multiple Crosslinking ~ 30KGy (3 times)	Sequential annealing (3 times)		X3™
	50KGy	Barstock preheated to below T <sub>m</sub> ; solid state deformation; stress relief processing; machined to acetabular liners	Glass plasma sterilisation	ArComXL Biomet
	~100KGy	Vitamin E doping Homogenisation	Gamma irradiation ~25 kGy	E1 Biomet

#### **1.4.4 Implications of wear**

All joints wear. To attain the level of efficiency of the natural synovial joint, the artificial joint replacement must maintain the elements of lubrication, friction and wear. Wear is the loss of material from the articulating surfaces. The consequence of wear is one of the most important factors affecting longevity of contemporary joint replacement implants. Surfaces, irrespective of how smooth they may appear have a degree of roughness due to surface projections called asperities. Asperities come into contact when surfaces are in loaded contact and it is the interaction between these asperities that dictates the wear mechanism. Mechanical wear may be adhesive, abrasive or may follow surface fatigue (Fisher, 1994). With adhesive wear, asperities are welded together and break off with relative motion. Abrasive wear occurs when a harder material with relatively high surface roughness is in relative motion against a softer material. The abrasive phenomenon may follow two patterns. First, 2-body wear occurs when two surfaces are in contact or 3-body wear occurs when debris trapped between the articulating surfaces initiate the wear process. Surface fatigue occurs with cyclical loading especially when the loads are higher than the fatigue strength of the counterface, leading to subsurface crack propagation and delamination.

Accumulation of particulate debris especially submicron sized particles (Green et al., 1998), within the periprosthetic tissue elicits a cascade of biological events, which leads to periprosthetic tissue inflammation, release of pro-inflammatory cytokines, initiation of bone lysis, followed by implant loosening and failure (Ingham and Fisher, 2005). Tissues adjacent to resorbed bone have been shown to contain many macrophages and giant cells (Schmalzried



et al., 1992). Phagocytosed debris has also been demonstrated within these inflammatory cells (Mirra et al., 1982). In the past, the source of debris led to divergent views in the literature. One school of thought suggested that polyethylene particles generated within the articulating surfaces, were engulfed by macrophages that ultimately initiated the biological response. Howie and co-workers reported a significant connection between periprosthetic bone lysis and the number of wear plastic particles (Howie et al., 1988). Mechanical fatigue failure of the PMMA cement mantle has also been postulated as an alternative source of particulate debris. Micromotion between the bone-cement interface or cement-implant interface due to differential elastic moduli may generate cement particles or even abrade metal surfaces. Loss of “holding” cement may lead to implant loosening. This process may be contributory in generating wear debris especially in the medium term but may not be central to loosening as wear induced aseptic loosening has been extensively reported in non-cemented arthroplasties.

Initiation of endosteal lysis is complex and multifactorial. It is particle related, with monocyte-macrophage cell lines playing a central role in the pathogenesis of osteolysis. Pathogenesis is driven by pro-inflammatory enzymes released by phagocytic cells that increase osteoclastogenesis thereby shifting normal bone metabolism towards catabolism and decreased osteoblastic activity (Kandahari et al., 2016b). Revell and his associates were among the first investigators to show an association between large volumes of peri-implant polyethylene wear debris and periprosthetic bone loss secondary to osteolysis (Revell et al., 1978). Using a semi quantitative assessment technique, histological examination of periprosthetic tissue was carried out and inference

drawn based on the degree of polyethylene debris noted in samples. A significant difference was found with regards to the presence of large numbers of macrophages containing infiltrates, giant cells, tissue necrosis and bone resorption in samples with large quantities of polyethylene debris when compared to samples with minimal or no detectable polyethylene particles. The overall conclusion was that periprosthetic tissue necrosis was related to polyethylene particulate debris. Schmalzreid also showed an association between the presence of polyethylene laden macrophages and resultant bone loss in localised sites distant from the bearing surface. It is thought that joint pressure during the gait cycle may push joint fluid within the effective joint space resulting in debris being transported to sites distant to the articulation. Also, the localised regions of bone loss are thought to be due to cells moving through clefts present within the cement mantle (Schmalzried et al., 1992). Following a review of available literature at the time, Dumbleton noted that osteolysis was rarely observed when the wear rate was below 0.1mm/year. Subsequent to this observation, it was proposed that a “practical wear threshold of 0.05mm/year would eliminate osteolysis” (Dumbleton et al., 2002). Above this critical wear threshold, it was expected that the risk of osteolysis would increase. Wilkinson and colleagues suggested a continuous dose-response relationship rather than a critical threshold based on their observation that osteolysis did occur in 9% of patients recruited into their study who had wear rates less than 0.05mm/year (Wilkinson et al., 2005). One of the downsides to the critical threshold concept is that it suggests wear volume is the dominant entity predisposing to osteolysis. Work by various investigators have shown that while wear is central to initiation of endosteal lysis, particle

size, composition and possible host-response variability are important factors that determine the course of particulate disease (Matthews et al., 2000a). Particle size appears to be a major determinant of the observed cellular response *in vitro* (Kandahari et al., 2016a). Particles below 150nm are internalised by pinocytosis and may not initiate pro-inflammatory activities while particles in the phagocytosable range i.e. 150nm-10µm stimulate cellular elaboration of cytokines which induce osteoclastic and periprosthetic bone resorbing activities. Particles over 20µm appear to initiate multinucleated giant cell formation and usually do not elicit immediate osteolytic activity (Jiang et al., 2013, Cobelli et al., 2011).

## 1.5 ALTERNATIVE MATERIALS IN JOINT REPLACEMENT

### 1.5.1 Polyacetal

Polyacetal (polyoxymethylene, acetal homopolymer or polyformaldehyde) is an engineered thermoplastic manufactured based on formaldehyde polymerisation (Penick et al., 2005). Clinical use of polyacetal, especially in orthopaedics is based on its beneficial properties with regards to lubrication, hardness and resistance to creep (Shen and Dumbleton, 1976). Polyacetal has previously been used to fabricate hip replacement prostheses, for example the Christiansen hip (Christiansen, 1969, Christiansen, 1974), although studies showed limited success. A study by Edidin and Kurtz investigated wear of polyacetal in a multidirectional hip joint simulator and results suggested that failure of the implant may have been due to implant design rather than material composition (Edidin and Kurtz, 2000). Polyacetal has previously been

investigated for use in an all polymer TKR following favourable laboratory testing (McKellop et al., 1993). Using a ten-station hip joint simulator with UHMWPE cups undergoing a 46-degree biaxial excursion against either a polyacetal 'femoral' head or CoCr head, the wear test was run for 1,000,000 cycles at 45 cycles/min. Specimens were cleaned, inspected and weighed at 200,000 cycles interval. A comparison of frictional torque at the start of the investigation and end of test showed a greater frictional torque at the end of the experiment in the CoCr-UHMWPE bearing group when compared to the polyacetal-UHMWPE combination. The mean wear rate of UHMWPE was reported to be 61% greater against CoCr heads when compared to the polyacetal bearing material. In addition, the total volumetric wear (cup and head) was on average 23% lower in the all polymer station. Following this encouraging *in vitro* model, it was suggested that polyacetal in combination with UHMWPE afforded a potentially good combination for use in TJA.

Subsequently, a follow-up clinical evaluation of an all polymer TKR was performed with the aim of investigating answers to two specific questions (Bradley et al., 1993). Firstly, was the wear generated at the bearing surface acceptable? Secondly, would the polyacetal femoral component fail either mechanically or biologically? However, the clinical trial failed for two other reasons. Firstly, implantation in the majority of cases, relied on cementless fixation and the use of a press fit approach, which led to inadequate integration and fixation of the polymer within bone. The second problem was associated with the sterilisation process, with small punctures noted in packaging after ethylene oxide sterilisation, suggesting that implants were not sterile during storage. Subsequently, these two errors led to a high failure rate of the

polyacetal-UHMWPE all-polymer TKR. Though evaluation was limited by the factors highlighted, it was observed that the all plastic articulation performed comparably to standard metal-on-UHMWPE implants, and only minor signs of wear reported in recovered prostheses. The mechanical fate of the femoral component at 10 years was investigated (Moore et al., 1998) as some prostheses were still functional at 10 years or over. At 10 years, there were 30 knees available for analysis (out of 63). There was also one retrieved all polymer knee available for histological analysis. The study showed that none of the polyacetal femoral components failed mechanically at 10 years and histological findings in a post mortem specimen at 9 years was unremarkable and wear reported as “slight”. Although the trial was considered unsuccessful, it did emphasize the possibility of a viable all polymer TKR based on observed low wear and mechanical integrity of the plastic femoral component.

### **1.5.2 Polyaryletherketone (PAEK)**

Polyaryletherketone (PAEK) is a group of semi-crystalline high temperature thermoplastic polymers that share a common molecular chain composed of an aromatic backbone interconnected with ether and ketone functional groups (Kurtz and Devine, 2007). Their chemical structure offers stability at temperatures exceeding 300°C and also stability to chemical and radiation damage. The ether and ketone ratio and sequence dictates the melting and glass transition temperatures and also affects its mechanical properties (Fuhrmann et al., 2014). Examples of PAEK plastic include polyetherketone (PEK), polyetherketoneketone (PEKK), polyetheretherketone (PEEK),

polyetheretherketoneketone (PEEKK) and polyetherketoneetherketoneketone (PEKEKK). The versatility of PAEK polymers is further enhanced by the ability to modify their modulus using reinforcing agents such as carbon or glass. The production of these polymers has been dependent on industrial needs. On a mass to mass basis, PAEK plastics exhibit greater specific strength compared to most metals, making PAEK a fascinating option for industrial applications especially aircraft and turbine blades. For reasons that are not clear in the literature and even following confirmation of their biocompatibility, use of this material in the fabrication of implants declined and was later abandoned for a period (Kurtz and Devine, 2007). Table 1.2 highlights mechanical and thermal properties of some biomaterials of clinical interest.

**Table 1.2:** Typical average mechanical and thermal properties of some clinically relevant materials

	Young's Modulus (GPa)	Poisson's Ratio	Ultimate Tensile strength (MPa)	Yield Strength (MPa)	Glass Transition Temp (°C)	Density (g/cm <sup>3</sup> )	Melting Point (°C)
CoCr***	200±10	0.3	2000±200	500	--	8.3	1330
CFRPEEK*	12	0.41	162	--	--	1.42	343
PEEK*	4	0.36	115	--	147	1.3	340
PEKK*	5.1	0.45	115	--	163	1.3	363
UHMWPE**	1.2±0.4	0.46	39-48	21-28	-80	0.93	125-138
Acetal**	2.6	0.35	67	67	-60	1.42	166
*Data from manufacturers' website/ datasheet. ** (Edidin and Kurtz, 2000). *** (Roach, 2007, Geringer et al., 2011b)							

#### **1.5.2.1 Clinical use of PAEK**

PEKEKK has previously been used in the design of a composite femoral hip stem. The Epoch hip stem (Zimmer, Warsaw, Inc) is a composite low stiffness extensively porous-coated femoral component that has an impressive track record in the published literature (Kurtz and Devine, 2007). The novel stem is made with an outer porous titanium fibre metal for fixation, a CoCrMo core and intervening PEKEKK polymer layer. In 1994, a prospective multicentre clinical trial involving 11 centres across the US was carried out. A similar clinical trial was conducted in 10 centres across Europe and Australia and a total of 366 people were enrolled globally (Glassman et al., 2001). The trial was carried out in accordance with the US Food and Drug Administration (FDA) under the approved Investigational Device Exemption (IDE) protocol, which mandated a minimum 2-year follow-up. A clinical review within the short to intermediate postoperative period demonstrated secure biological fixation and preservation of bone around the femoral prosthesis (Akhavan et al., 2006). Hartzband and his colleagues (Hartzband et al., 2010) conducted a review at 10 years follow-up however only 4 of the 11 US centres continued follow-up after the mandatory 2 year period. In this study, 102 patients with 106 Epoch stems were available for follow-up at 10 years (11 deaths and 5 lost to follow-up), representing 62% of enrolled individuals in the US study. All patients were judged to have excellent hip function as determined using the Harris hip score, which averaged 97.9 at 10 years. Dual-energy X-ray absorptiometry (DEXA) analysis was available in only one patient at long term review and when compared with the unoperated contralateral proximal femur, bone density appeared “nearly unchanged 12 years after receiving an Epoch femoral

prosthesis". Radiological examination showed bone ingrowth in all stems with initial endocortical-prosthesis contact maintained in all implants as determined at the last follow-up time-point. None of the femoral components had been revised.

### **1.5.3 Polyetheretherketone**

Polyetheretherketone is a semi-crystalline polymer with a crystalline and an amorphous phase. The crystalline content depends on the processing method and typically injection molded PEEK has a crystalline content of 30-35% (Green and Schlegel, 2001). The higher the crystallinity, the lower its ductility and higher the material stiffness. PEEK is used below its glass transition temperature of 143°C that is, in its "glassy" state, a feature of the amorphous phase permitting molecular mobility. Its melting point is 343°C. Ultrastructural examination of PEEK crystals shows very fine lamella which are organised into larger spherulites. The thickness of lamellae, dimensions and density of spherulites depend on the manufacturing process used. The chemical structure of PEEK explains its inherent resistance to thermal, chemical and radiation degradation. PEEK is inert in many simulated adverse conditions and is virtually insoluble in all conventional solvents except for sulphuric acid at room temperature (Kurtz and Devine, 2007).

Interest in PEEK for orthopaedic applications is based on its mechanical properties, versatility and observed success in load sharing when used in spinal applications. PEEK can be reinforced using carbon or glass to tailor its composite GPa to that of cortical bone (18GPa) or titanium. (Williams et al.,



1987, Cogswell and Hopprich, 1983). This versatility implies intricate options for researchers exploring PEEK as a new biomaterial in implant design (Kurtz and Devine, 2007). Carbon fibres in use are derived from two main parent materials, polyacrylonitrile (PAN) and mesophase-pitch (pitch) based fibres. Microstructural architecture shows that PAN based fibres have relatively larger and well oriented crystallites within its skin region and smaller and less well oriented crystallites in its core. Mesophase pitch based fibres show no difference in its microstructure across the fibre (Huang and Young, 1995).

### **1.5.3.1 Pre-Clinical Assessment of PEEK**

#### **1.5.3.1.1 Wear Assessment**

Simple preliminary assessment of various material combinations as a first step in evaluating and screening is commonplace. Scholes et al (Scholes and Unsworth, 2009) tested the wear performance of PEEK and CFR-PEEK against low carbon (Lc) and high carbon (Hc) CoCrMo for use as prosthetic bearing materials. A 4-station pin on plate device described by Joyce (Joyce et al., 2000) capable of rotational and reciprocating motion was used. The test was run over 2 million cycles at a frequency of 1Hz and stroke length of 25mm. A contact stress of approximately 2MPa was generated using a 40N load. New born calf serum was used as a lubricant and sodium azide added to inhibit bacterial growth. The set up was maintained at 37°C. Volumetric wear was calculated following gravimetric analysis based on material density and results showed that the PEEK-on-Lc/CoCrMo combination produced the greatest wear. After the running-in wear period, the pitch-based CFR-PEEK produced

slightly lower wear than the PAN-based against high carbon CoCrMo ( $0.129$  compared with  $0.177 \times 10^{-6} \text{N}^{-1} \text{M}^{-1}$ ). The CFR-PEEK/Lc CoCrMo demonstrated the lowest average wear ( $0.084 \times 10^{-6} \text{N}^{-1} \text{M}^{-1}$ ). To put these results into context, wear studies of UHMWPE versus stainless steel using a similar pin-on-plate apparatus was reported to produce an average wear of  $1.1 \times 10^{-6} \text{N}^{-1} \text{M}^{-1}$  (Joyce et al., 2000). It would appear that CFR PEEK (Pitch/PAN) produced less wear compared with UHMWPE versus stainless steel giving some confidence to its potential use as a bearing surface in Total Joint Arthroplasty.

In a more detailed test to further evaluate the suitability of PEEK composites as bearing surfaces in TJA, Wang et al (Wang et al., 1999) observed the tribological properties of composites as inserts under non-conforming high stress and conforming low stress contact conditions representative of total knee and total hip conditions respectively. In the high stress line contact set-up, 30% weight CFR PEEK produced the lowest wear rate compared with 10% or 50% weight samples. However, these composites wore significantly more than UHMWPE. In the hip simulator test, 30% CFR PEEK (Pitch) socket against zirconia ball produced the least wear rate (volume per million cycle), reported as  $1/30^{\text{th}}$  that of UHMWPE socket against similar balls. Wang concluded CFR-PEEK is not suitable for use as a tibial component in TKR. Historical wear testing of PEEK and PEEK composites described in this section investigated PEEK with a view to develop tibial inserts from PEEK in place of UHMWPE and in majority of cases, investigations were conducted at low stresses that replicate hip replacement stress levels.

#### 1.5.3.1.2 Biological Assessment

The need to ascertain the cellular response to PEEK wear particles and the bulk material *in vivo* has been of interest to researchers. The *in vitro* response of human osteoblast-like cells and macrophages to bulk CFR –PEEK composites has been previously investigated (Scotchford et al., 2003). Responses were judged by osteoblast attachment and proliferation and hydrogen peroxide production and beta glucuronidase activity by macrophages. Examination of osteoblast attachment and cell spreading using scanning electron microscopy on the composite surfaces after 2 hours of incubation demonstrated similar or greater cell process formation as compared with tissue culture plastic (TCP) and Ti6Al4v controls. Furthermore, osteoblast proliferation measured at various time points up to 11 days showed no significant difference when compared with controls. The macrophage response showed similar levels of beta glucuronidase activity on the composite surfaces however, hydrogen peroxide production was significantly increased when compared with the TCP and Ti6Al4v control groups. The investigators concluded that the composite surfaces demonstrated limited macrophage activation and similar osteoblast function when compared to Ti6Al4V surfaces. A study investigated the *in vitro* interaction of leachable substances extracted from PEEK and CFR-PEEK discs in line with British Standard BS5736 guidance. Impact of extracts on a 3T3 mouse fibroblast cell line and an immortalized rat osteoblast cell line was reported (Morrison et al., 1995). Intracellular levels of reduced glutathione, leakage of lactate dehydrogenase and MTT assay were used as markers of cellular cytotoxicity. Results showed that PEEK extracts exhibited no cytotoxic effect on both fibroblasts and

osteoblasts. Furthermore, it was observed that there was a stimulatory effect on osteoblast protein content suggesting that PEEK may enhance bone growth to its surface.

Wear particles generated at the bearing surface have been implicated in inducing a cellular response that leads to bone loss and implant failure (Purdue et al., 2007a). *In vitro* and *in vivo* assessments have been reported in literature (Revell et al., 1978, Matthews et al., 2000b, Utzschneider et al., 2010b). Macrophages are often used to study the particle induced biological response (Kandahari et al., 2016a) although many other cells may be involved in this process. *In vitro* assessment usually involves culturing phagocytic/inflammatory cells with particulate debris and assessment of cytokine production. *In vivo* evaluation normally entails the injection of particles into a defined cavity in suitable animal models, such as the rat air pouch model. The *in vivo* biological response of two different CFR PEEK (Pitch and PAN based) wear particles were evaluated alongside ultra-high molecular weight polyethylene (UHMWPE) (Utzschneider et al., 2010a). Wear particles generated from a knee simulator were characterized with regards shape and size. Using cryo-pulverisation, a replica of these characterized wear particles were generated, sterilised and injected into knee joint of female BALB/c mice. Seven days following injection, intravital fluorescence microscopy of synovial microcirculation and histological assessment of the synovial layer were performed. The parameters investigated were leukocyte adhesion to the endothelium and the fraction of rolling leucocytes giving that leukocyte influx is a rate limiting step in particle induced inflammation. Histological examination confirmed enhanced cellular infiltration in all synovial membranes challenged

with CFR-PEEK and UHMWPE, and this occurred to a similar extent with no significant difference in response among the different polymers investigated. No specific cell type was identified and based on this, it was concluded that CFR-PEEK appeared to be a suitable bearing material for use in orthopaedic applications.

#### **1.5.3.2 Uses of PEEK and PEEK Composites**

PEEK and PEEK based composite materials have been investigated as bearing surfaces in total hip arthroplasty. In 2001, an international, multicentre clinical study evaluated CFR-PEEK as a low wear bearing surface with the aim of investigating its use in extending the longevity of conventional THRs (Kurtz and Devine, 2007). Acetabular liner manufactured from PEEK reinforced with 30% pitch-based carbon fibres was investigated in the ABG II hip system (Stryker Orthopaedics, NJ). The liner articulated with an alumina head and at a mean 3 year follow-up period, results showed no cases of revision due to aseptic loosening (Pace et al., 2008). However, one of the 30 hips recruited in one of the centres was revised due to infection 26 months following the index operation. The patient had developed a haematoma following a traffic accident, which was drained and later became infected. Analysis of a retrieved CFR acetabular cup showed two distinct areas of wear. Firstly, a smooth worn region accounting for two-thirds of the cup surface was seen and secondly, a rougher, “unworn” area with original machine marks was also identified. Histological examination of the periprosthetic tissue was carried out to characterize particles and the inflammatory pattern. Two distinct periprosthetic

tissue types were reported; (i) a highly vascularised granulation tissue with abundant neutrophilic infiltration highly suggestive of an infective process, and (ii) a tissue pattern that showed perivascular inflammatory cells with extensive infiltration of lymphocytes and plasma cells. While this is suggestive of a chronic process prior to the onset of infection, a similar response has been described in hypersensitivity reactions (Willert et al., 2005). Examination using polarized light microscopy demonstrated macrophages containing three types of engulfed wear particles. Firstly, metal particles were seen as small black debris with sharp edges. Secondly, large black carbon particles were seen and lastly colourless grain from the PEEK matrix were observed, where these particles were found to be fewer in number when compared with the metal and carbon particles. As only a single hip was revised in this patient cohort, this success suggests the effectiveness of this implant design in the short-term follow-up period.

A rigid metal backed hemispherical acetabular component has been shown to distribute stress in a non-physiological manner (Manley et al., 2006) and this finding complements the development of a novel anatomical horse-shoe shaped acetabular resurfacing cup. This cup has been reported to reproduce the physiological distribution of stresses found in the natural acetabulum, which in turn reduces stress shielding adjacent to the implant (Brooks et al., 2004). A prototype horseshoe shaped acetabular cup, called the Cambridge cup was manufactured using a CFR-PBT (polybutyleneterephthalate) outer shell and a UHMWPE liner. This implant was investigated in 50 patients where 24 implants were uncemented and coated with a HA coating and the remaining 26 implants were uncoated and cemented in place. Three of the uncoated cups

were revised due to significant wear and migration within a 2-year follow-up period. None of the coated acetabular cups were revised over the same period. Using DEXA scanning, bone mineral density adjacent to the Cambridge cup was compared with bone density measured within the unoperated contralateral acetabulum. Results did not show a significant decrease in bone density suggesting that the Cambridge cup reduced stress shielding when used clinically and at 2 years follow up (Field and Rushton, 2005).

Based on the encouraging findings from the Cambridge cup study, CFR-PEEK was used in place of CFR-PBT and investigated in a flexible horseshoe acetabular resurfacing prosthesis (Latif et al., 2008) called the MITCH™ cup. Tribological testing was carried out against large ceramic heads in a five station hip simulator with maximum and minimum loads of 2800N and 250N respectively. Thirty percent stabilized calf serum was used as a lubricant and the test was run to 25 million cycles. Results showed that the mean wear measured was  $<1\text{mm}^3$  per million cycles (Latif et al., 2008) and based on these results, a prospective two centre clinical study commenced in 2007 where 25 MITCH cups were implanted. Over a 3-year period, 5 cases of acetabular implant migration were reported with 3 undergoing revision due to aseptic loosening. The cause of osteolysis was not clear from this study (Field et al., 2012).

## 1.6 WEAR TESTING OF BIOMATERIALS

The primary objective of *in vitro* wear testing is to simulate the likely wear performance of candidate materials when implanted in the body. New materials must meet certain criteria following mechanical evaluation and assessment of stability within the physiological environment among other things (Fisher, 1994). Tribological assessment is carried out prior to introducing new materials where evaluation of their wear and frictional properties are relevant. The design concept should ensure imposition of relevant physiological load using appropriate test component geometry and lubrication with load applied for a representative duration of time. Such tests vary in design and set-up and range from simple to complex simulation of the intended joint replacement. It follows that wear testing protocols should be adapted and designed for specific applications and striking a right balance in complexity has an impact on the test (Flannery et al., 2008). For instance, exclusion of any crucial element can make the model invalid as it no longer represents the intended joint. However, the more the set-up reproduces the physiological conditions, the costlier it becomes (Saikko, 1993). Invariably wear testing replicates *in vivo* performance at different levels of complexity however, even though each joint has its unique loading conditions, kinematics and geometry, it may be impossible that a single method of wear testing can be appropriate to evaluate new materials when considered for use in all joints.

The main benefit of a simplified wear testing procedure such as the pin on plate test, is in repeatable and reproducible screening and ranking of candidate materials in joint replacement. Furthermore, it may not be appropriate for wear



data to be generalised with different test set-ups as such results should only be considered in absolute quantities when the same set-up is used. However, prior to implantation in patients, candidate materials that are initially assessed using simplified test set-ups such as pin-on-plate tests, should be investigated in more physiologically relevant wear environments such as within a hip or knee simulating machine.

The components of a pin-on-plate wear testing set up are a simplified approximation of the complex geometry of the knee joint aimed at reproducing the point or line of contact conditions seen in TKRs. The femoral components are represented by a sphere or cylinder and the tibial component substituted by a flat polyethylene disc. Table 1.3 shows the geometrical representation and radius of some TKR designs currently in use (Hall et al., 2008, DesJardins et al., 2000).

**Table 1.3:** Showing femoral profile measurements of some prosthetic designs

Name of Implant	Sagittal Plane Radius at 60° of flexion (mm)
Insall-Burstein I (Zimmer)	20
NexGen Cruciate Retaining/ Cruciate Sacrificing (Zimmer)	20
Press-Fit Condylar (Sigma)	20
Scorpio (Howmedica)	24.5
Mobile Bearing Knee (Zimmer)	25

McKellop et al. previously developed a wear testing method, which has been adapted by the ASTM as a standard protocol for assessing candidate materials in total joint replacement surgery (McKellop, 1981). In this method, a flat polymeric pin was articulated against a reciprocated plate under low contact stresses of approximately 3.5MPa, which were more relevant in the hip (Walker et al., 1996) rather than the knee where stresses of approximately 30 – 60MPa has been estimated (D'Lima et al., 2008). Furthermore, when using this standard, applying a cyclic motion as described to the same portion of the polymer surface will not be representative of the cyclic loading applied during normal function in TKR. Therefore, mimicking the complex motion of the knee using a pin-on-plate wear test is a complicated endeavour. The kinematic variations within the gait cycle, especially with the main flexion-extension motion of the knee, includes a combination of rolling and sliding within a stationary or mobile contact (figure 1.6). It has previously been reported that sliding motion is the dominant kinematic condition as shown by the surface profile observed in an explanted UHMWPE tibial surface following TKR (Blunn et al., 1991). The sliding distance of components relative to each other and the contact stresses generated are considered the major factors influencing wear (D'Lima et al., 2008).

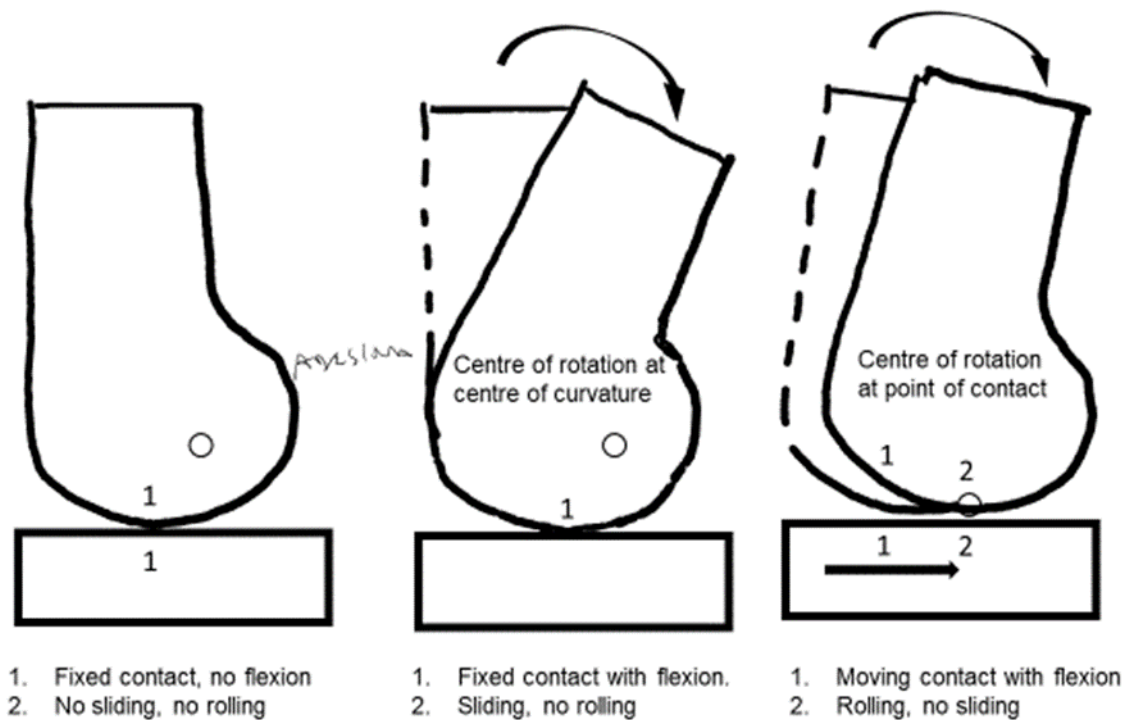


Figure 1.6: Rolling and sliding in knee joint adapted from Blunn et al, the dominance of cyclic sliding in producing wear in TKR. CORR 253-260.

## 1.7 AIM AND HYPOTHESIS

The overall aim of this research was to develop a metal-free, all polymer knee. Using unidirectional pin on plate testing, this study investigated the suitability of polyetheretherketone (PEEK), PEEK composites and polyacetal as bearing surfaces in all polymer Total Knee Replacement (TKR).

It was hypothesised that:

1. Under loads representative of the knee, the volumetric and gravimetric wear of PEEK, CFR-PEEK and polyacetal are reduced when compared with metal on polyethylene bearings.

2. A lower number of wear particles are generated from PEEK, CFR PEEK and polyacetal bearings when compared with metal-on-polyethylene bearings.
3. The inflammatory response to PEEK, CFR-PEEK and Acetal will be similar or less to that observed from polyethylene debris in a standard metal-on-polyethylene articulation.

The specific objectives of my research were:

1. To investigate the wear performance of PEEK, CFR-PEEK and polyacetal as bearing materials in TKR using a unidirectional pin on plate testing machine over 2 million cycles. Wear was assessed using gravimetric analysis, digital photography, surface profilometry and scanning electron microscopy (SEM).
2. To analyse and characterize the number and size of wear particles generated from each of the bearing combinations. Wear particles were isolated from lubricant fluid using an acid digestion method and observed and quantified using SEM and image analysis techniques.
3. To assess and compare the inflammatory response of wear particles generated from the pin-on-plate test by co-culturing particles with monocytes and quantifying cytokine production (TNF- $\alpha$ , IL-1 $\beta$  and IL-6) as measured using ELISA.

## 1.8 THESIS STRUCTURE

Chapter Two investigated the wear performance of PEEK, CFR-PEEK and polyacetal as alternative bearings in TKR using a unidirectional pin on plate testing device. The articulating materials were tested over 2 million cycles or until failure. Wear was assessed using gravimetric analysis, digital photography, surface profilometry and scanning electron microscopy (SEM).

Chapter Three characterized the wear particles generated from the pin on plate test from the various bearing combinations investigated. Wear particles were isolated from lubricant fluid using an acid digestion method originally described by Scott and also adopted in section 5.2.2 of ISO 17853:2011 standard (Scott et al., 2005).

In chapter Four, the inflammatory response to particles was investigated, by co-culturing particles with monocytes and cytokine production assessed using ELISA over a 24 hour period.

Chapter Five explores the main findings from my thesis and limitations of the study. Recommendations for future work and areas of possible clinical translation are highlighted.

## **Chapter 2: Wear Analysis**

### **2.1 INTRODUCTION**

Joint arthroplasty surgery remains one of the most successful orthopaedic procedures and is the treatment of choice for advanced degeneration of joints especially hips and knees (Carr et al., 2012) with over a million total knee replacements carried out annually worldwide and with a projected 10% increase per year (Walker et al., 2010). Presently the bearing components used for joint arthroplasty are manufactured from a hard material such as cobalt chromium (CoCr) or ceramic, articulated against either the same material or a softer polyethylene (PE). In total knee arthroplasty (TKA), hard-on-soft tribological couples are the norm with the majority of bearing couples utilising a CoCr femoral component bearing against PE.

Though contemporary TKA is successful, joint registry data suggests the observed early success rate is not maintained 10 – 15 years following surgery (Price et al., 2018), where a proportion will fail and require revision surgery. Between 2012 and 2030 the demand for revision TKA in England and Wales is predicted to increase by 332% (Patel et al., 2015). Similar estimates have also been reported in the USA (Bozic et al., 2010). One of the goals in TKA, therefore, is to improve survivorship, by investigating and potentially introducing new biomaterial combinations.

In spite of improvement in polyethylene technology, especially the emergence of highly cross-linked polyethylene (XLPE), which has resulted in a dramatic reduction in wear, aseptic loosening is still considered the leading cause of failure in TKA. Loosening is reported to account for up to 30% of revision

surgeries in the medium to long-term follow-up (Lombardi Jr et al., 2014, Schroer et al., 2013, Sharkey et al., 2014). Other factors such as instability, malalignment (Walker et al., 2010) and stress shielding (Karbowski et al., 1999, Petersen et al., 1996) may also contribute to failure. There is also debate around the possibility of metal ion release into surrounding tissues (Luetzner et al., 2007, Kretzer et al., 2014, Garrett et al., 2010), the incidence and effect of which remains uncertain. Recent retrieval data suggests a role for inflammatory cell induced corrosion (ICIC) as a mechanism of failure in TKA (Arnholt et al., 2016). Over recent years, there has been a considerable research interest in the use of polyetheretherketone (PEEK) as a biomaterial for orthopaedic implants. PEEK is a low modulus material that can be reinforced with carbon fibres to adapt its composite modulus to that of cortical bone, allowing for more intricate prospects in PEEK research. The use of a low modulus, low wearing biomaterial such as polyetheretherketone (PEEK) may be a suitable alternative to CoCr femoral components. The quest for a metal free articulation can be supported by the theoretical advantages which include, a more physiological stress distribution in the distal femur, better visualisation of the bone implant interface using plain radiographs, artefact free CT or MRI imaging and elimination of a biological reaction to metal, which may be one of the reasons for unexplained knee pain following TKA. Also, polymers can be injection molded at a relatively lower temperature and generally afford a cheaper option for the manufacture of prostheses due to lower energy consumption.

The concept of an all polymer TKA is not entirely new and the clinical evaluation of an all polymeric TKA made from polyacetal-on-polyethylene has

previously been investigated (Bradley et al., 1993, Moore et al., 1998). The outcome of the study, based solely on revision rate at 10 years, was similar to that of conventional cobalt chromium on polyethylene. In this series, fracture of the polyacetal femoral component or excessive wear was not observed as a cause of failure. Despite the drawbacks of the study, i.e. poor fixation of the femoral component and the likelihood of formaldehyde release from the polyacetal femoral component (McKellop et al., 1993), the study demonstrated the possibility of a viable all polymer TKA.

Interest in PEEK is based on its mechanical strength, resistance to radiation, chemical stability (Kurtz and Devine, 2007) and the encouraging results from clinical applications following use as cages in spinal fusion surgery and in disc replacement (Kersten et al., 2015, Chen et al., 2013). Low wear has been reported by various authors investigating carbon fibre reinforced PEEK (CFR PEEK) (Latif et al., 2008, Scholes and Unsworth, 2009).

In this study, the wear performance of PEEK, carbon reinforced PEEK (CFR-PEEK) and polyacetal as bearing materials was investigated using a reciprocating pin on plate test.

The hypothesis of this study was that less wear is generated from PEEK, polyacetal or CFR-PEEK bearings than with metal on polyethylene (MoP) bearings and that these combinations may provide a suitable alternative in TKA.



## 2.2 MATERIALS AND METHOD

A validated modification of the ASTM F732 (Appendix 1.1) described for assessing wear of material couples in total knee arthroplasty was used as the test protocol (Walker et al., 1996). Modifications were made to, specimen geometry, motion and applied load to ensure the test configuration was more representative of the loading and articulating conditions of the knee joint.

### 2.2.1 Test Specimen and Articulations

The principal aim of the study was to assess the suitability of PEEK and CFR-PEEK as bearing surfaces in all polymer TKA. It was also considered worthwhile to investigate the suitability of these biomaterials as ‘tibial inserts’ against CoCr pins. Twenty millimetre diameter cylindrical pins machined from cast medical grade CoCr (Orchid Orthopaedic Solutions, Sheffield, UK), PEEK (PEEK Optima, Invibio, Lancashire, UK), CFR-PEEK (PEEK Optima Wear Performance, Invibio, Lancashire, UK) and Acetal copolymer (Ensinger Ltd, Tonyrefail, UK) were axially loaded against flat circular plates made from either ultra-high molecular weight polyethylene (UHMWPE-GUR1050 Bacup, UK), highly cross-linked polyethylene (XLPE-GUR1020, Bacup, UK), PEEK, CFR-PEEK or polyacetal resulting in 12 material combinations. CoCr versus XLPE was used as a reference combination. The XLPE specimens were moderately cross-linked using 7.5MRad of gamma irradiation and free radicals extinguished by heat below the melting point of XLPE i.e. by annealing. Datasheets of test materials are included in Appendix 1.2

For ease of description and reporting, articulations are grouped based on pin material into 3 groups as described in Table 2.1.

**Table 2.1:** Articulations tested (Pin vs. Plate)

Group 1: (CFR-PEEK Pin Articulations)	Group 2: (PEEK and Acetal Pin Articulations)	Group 3: (CoCr Pin Articulations)
CFRPEEK vs. UHMWPE.	PEEK vs. UHMWPE	CoCr vs. UHMWPE
CFRPEEK vs. PEEK.	PEEK vs. XLPE	CoCr vs. XLPE
CFRPEEK vs. CFRPEEK.	PEEK vs. Acetal	CoCr vs. CFRPEEK
	PEEK vs. PEEK	CoCr vs. PEEK
	Acetal vs. XLPE	

Materials used in specimen fabrication were turned using a computerised numerical controlled (CNC) lathe and surface finishing of polymers carried out by fly cut milling while surface finishing of metals was by using a polishing mop.

The machined 20mm diameter cylindrical pins were spherically ended with a 25mm radius and the test plates measured 40 mm in diameter and were 6mm thick. Each plate had 2 orthogonal location slots on its under surface for accurate placement and alignment in the metallic holding jig while the pins had a shallow flat surface milled off the proximal aspect of its cylindrical end to serve the same purpose. All specimens were terminally sterilised by gamma radiation with 2.5Mrad in an inert environment before wear testing, except for specimens made from polyacetal (which is sensitive to gamma irradiation), which were sterilised using ethylene oxide. This specimen arrangement, illustrated in Figure 1, was considered representative of the typical condylar replacement (Walker et al., 1996).

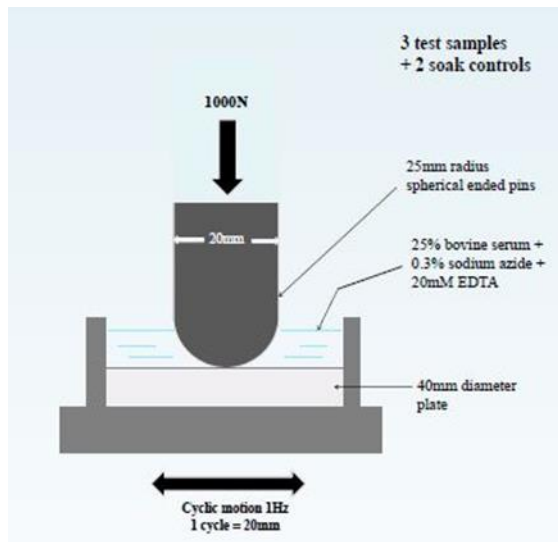


Figure 2.1- Schematic representation of pin on plate set up.

### 2.2.2 Test Set-Up

A customised rigid frame 6- station pin on plate test machine was used (figure 2.2). The machine used a servo hydraulic mechanism for axial load application on test pins and a motor-crank mechanism to produce reciprocating motion of the six metallic jigs holding the test plates.

Articulations were lubricated with 25% new born calf serum (Sera Laboratories International Ltd, UK) containing 0.3% sodium azide to retard bacterial growth and 20mM of ethylenediaminetetraacetic acid (EDTA) to prevent calcium deposition. Specimens were pre-soaked in lubricant for 48 hours, to allow for fluid saturation before commencing testing. Three sets of each bearing combination were tested for 2 million cycles (or until failure) at a frequency of 1Hz and cycle length of 20mm.



Figure 2.2 – Six station pin-on-plate testing device. Insert shows a single station.

Two passive soak controls, unloaded specimens with similar portions as test specimens exposed to lubricant fluid, were used concurrently with each articulation to correct for fluid absorption by the polymeric specimens. Each test and control station was enveloped with an elastic membrane to prevent lubricant contamination and the test was carried out at room temperature.

### 2.2.3 Contact Stresses

Tests were conducted under two different loading conditions. A constant load of either 50N and 1000N were applied to generate an initial contact stress of approximately 28MPa and 75MPa in the CoCr-on-PE articulation, representing stresses in high contact, conforming knee designs and a worst-case application of a low contact, non-conforming knee design respectively.

$$\text{Contact stress } (\sigma) \cong \frac{3F}{2\pi a^2} ;$$

$$\text{Where contact area of radius (a)} \cong \left(\frac{3RF}{2E}\right)^{\frac{1}{3}} \text{ and } \frac{1}{E'} = \frac{1}{2} \left(\frac{1-V_i^2}{E_i} + \frac{1-V_k^2}{E_k}\right)$$

$E_i$  = Elastic modulus (specimen 1)

$E_k$  = Elastic Modulus (specimen 2)

$V_i$  = Poisson ratio (specimen 1)

$V_k$  = Poisson ratio (specimen 2)

While applied load and geometry of test specimens were the same for each group of articulating couples, the calculated Hertzian contact stresses in each combination varied due to the different Poisson's ratio and elastic modulus of the materials used (Table 2.2). All articulation described in Table 2.1 were tested under high load (Table 2.3) while 4 articulations shown in table 2.4 were tested under low load condition.

**Table 2.2:** Typical average elastic modulus and Poisson's ratio of material tested

Material	Elastic Modulus (GPa)	Poisson's Ratio
PEEK	4	0.36
CFR-PEEK	12	0.41
UHMWPE	0.97	0.46
XLPE	0.97	0.46
Acetal	2.8	0.35

### High Loads

**Table 2.3:** Articulations and calculated contact stresses under a 1KN load

<b>Articulation</b>	<b>Initial Stresses (MPa)</b>
CoCr vs. UHMWPE	75
CoCr vs. XLPE	75
CoCr vs. PEEK	173
CoCr vs. CFR-PEEK	390
PEEK vs. UHMWPE	65
PEEK vs. XLPE	65
PEEK vs. PEEK	110
PEEK vs. Acetal	95
Acetal vs. XLPE	60
CFR-PEEK vs. UHMWPE	72
CFR-PEEK vs. PEEK	154
CFR-PEEK vs. CFR-PEEK	259

### Low Loads

**Table 2.4:** Articulations and calculated contact stresses using 50N load

<b>Articulation</b>	<b>Initial Stresses (MPa)</b>
CoCr vs. XLPE	28
PEEK vs. XLPE	24
PEEK vs. UHMWPE	24
CFR-PEEK vs XLPE	27

#### **2.2.4 Volumetric Wear Loss**

Tests were stopped at every 250,000 cycle interval for specimen cleaning, gravimetric analysis and photographic documentation of wear tracks as specified in ISO 14243-2 (ISO 14243-2, 2009) described for assessment of wear of tibial component of total knee prostheses (Appendix 1.3). Briefly, samples were allowed to vibrate in deionised water, then washed with 10% Decon 90 Solution (Decon Laboratories LTD, Hove, UK) in an ultrasonic bath, both for 10 minutes. Two further cycles of rinsing and sonication each for 10 minutes was carried out before drying in a vacuum drying chamber at minimum of 13.33 Pascal for 30 minutes. The specimens were then soaked in propanol for 5 minutes and desiccation in a vacuum drying chamber was carried out before weighing. The entire sample was weighed in rotation keeping the same sequence, within 90 minutes of removal from vacuum. Readings were taken until 2 values were within 100µg for the same specimen. Gravimetric analysis was carried out using an electronic balance with 0.01mg resolution. Wear of specimens was defined as weight difference of specimen after testing with addition of weight gained by soak controls assuming weight gains of test specimen and soak controls are the same. Volume loss of polymeric specimens was calculated using their material density (Table 2.5). Volumetric loss was plotted against number of cycles. The wear rate was defined as volume loss per million cycles (MC).

**Table 2.5:** Density of materials used

<b>Material</b>	<b>Density (g/cm<sup>3</sup>)</b>
PEEK	1.3
CFR-PEEK	1.42
UHMWPE	0.93
XLPE	0.93
Acetal	1.42

### **2.2.5 Surface Characterisation**

Prior to commencement of the wear test, metallic bearing surfaces were machined to have a surface finish of no rougher than 0.1µm and polymeric surfaces to have a surface roughness not greater than 2µm in accordance with ASTM F2083 which specifies surface finishing of prosthetic material for use in TKR in line with testing prerequisites and clinical use (ASTM International, 2012) – Appendix 1.4.

Photographic images of specimens were obtained at every 250,000 cycle interval, after component cleaning and weighing. Non-contact surface profile assessment was carried out using optical surface profilometry (Contour GT Scanning Scope, Bruker, USA) before commencement of each test, at one million cycles and the end of test. Surface roughness ( $R_a$ ) measurements were taken from the wear track of specimens. Depending on the size of the wear track, a minimum of 5  $R_a$  readings were taken. Average surface roughness ( $R_a$ ) with standard deviation was used to characterise each surface.



Scanning electron microscopy (SEM) was performed to further investigate the material surface following testing. SEM of failed articulations were examined to explain cause of failure and SEM images of best performing articulations were compared with those used in contemporary TKR to evaluate for similarities or differences in surface characteristics.

### **2.2.6 Statistical Analysis**

A minimum sample size of 3 was set, though a 0.8 level of statistical power was not assumed.

For each data set, Shapiro-Wilk test as carried out to assess for normality. When data is non-parametric i.e. not normally distributed and/ or  $n < 25$ , a non-parametric statistical test was indicated. Kruskal Wallis test – a non-parametric equivalent of the one-way ANOVA for independent samples and Mann Whitney test for 2 independent samples were used to calculate the level of statistical significance (p-value) associated with differences between the measured wear rates. When multiple comparisons were required, a Bonferroni correction ( $\alpha$ / number of comparisons) was made to adjust for inflation in type 1 error rate. Statistical tests were carried out using SPSS 22 for Windows (Chicago, USA).

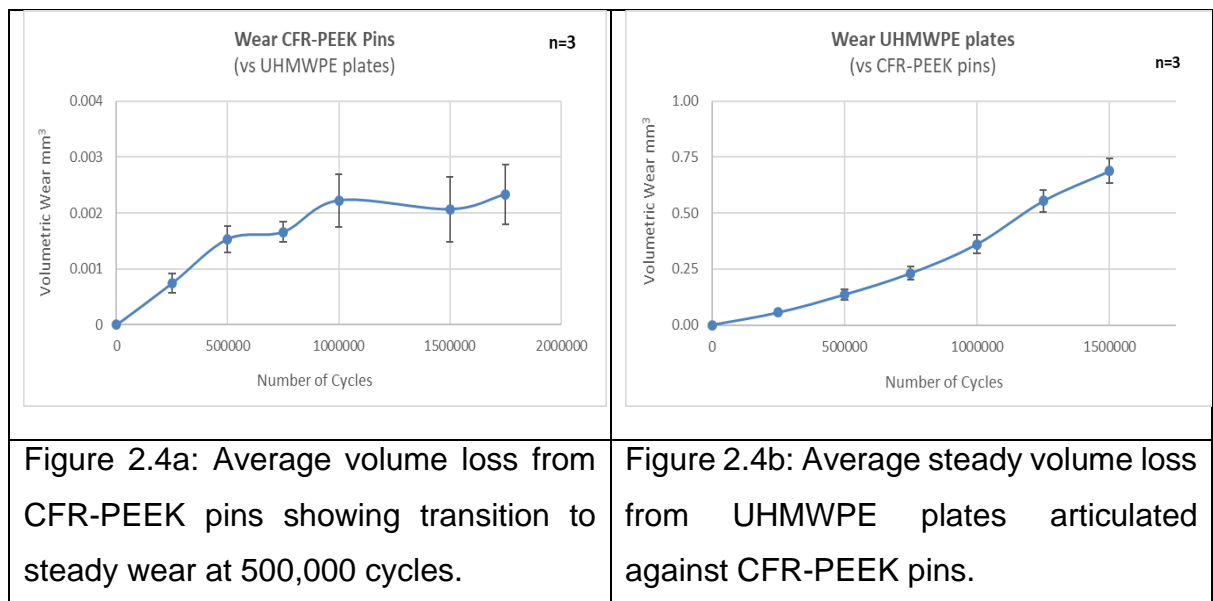
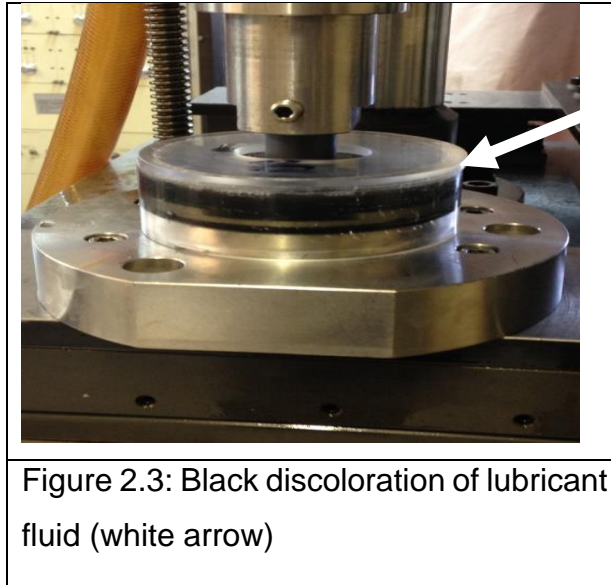
## 2.3 RESULTS (HIGH LOAD)

### 2.3.1 CFR-PEEK Pin Articulations

#### 2.3.1.1 Volumetric Wear Loss

All CFR-PEEK pin articulations were stopped either due to presumed high friction as implied by a loud squeaking sound from the articulated surfaces, black discoloration of lubricant fluid (Figure 2.3) or excessive wear of the counterfaces with CFR PEEK-on-UHMWPE. CFR PEEK versus CFR PEEK combinations were stopped at 3,656 cycles, CFR PEEK versus PEEK at 83,117 cycles and CFR-PEEK-on-UHMWPE tests were terminated after 1.65 Million cycles (Mc).

Figures 2.4a and 2.4b show graphical representation of the mean wear noted in CFR-PEEK pins and UHMWPE plates over the test duration. Running-in wear was noted in the CFR-PEEK pins up to 500,000 with a transition to a steady, relatively lower wear rate up to the termination of the test. UHMWPE plates showed a steady volume loss throughout the test period. A constant wear rate was noted in the UHMWPE counterface with a mean volume loss of  $4.6 \times 10^{-1} \pm 0.02 \text{ mm}^3/\text{MC}$  (Figure 2.4b).


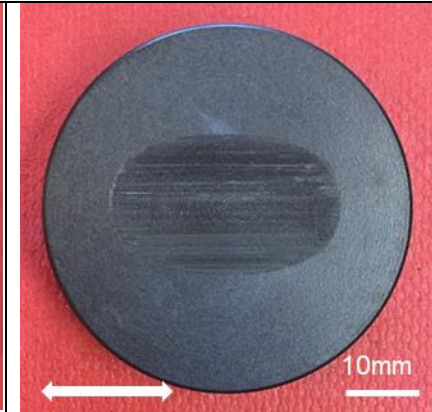
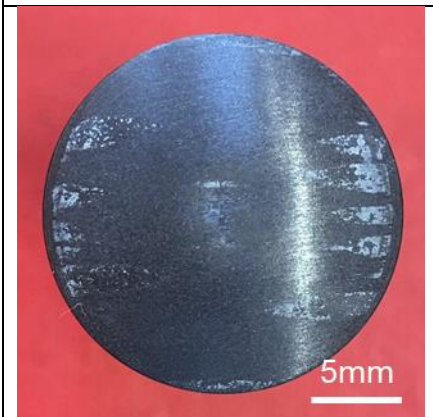
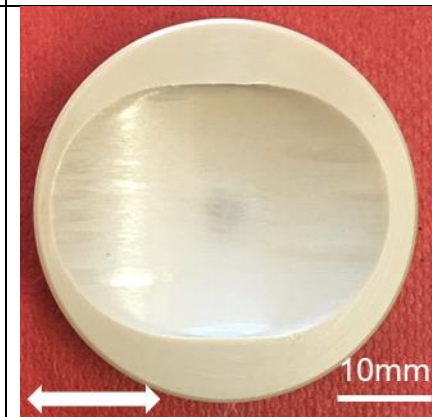


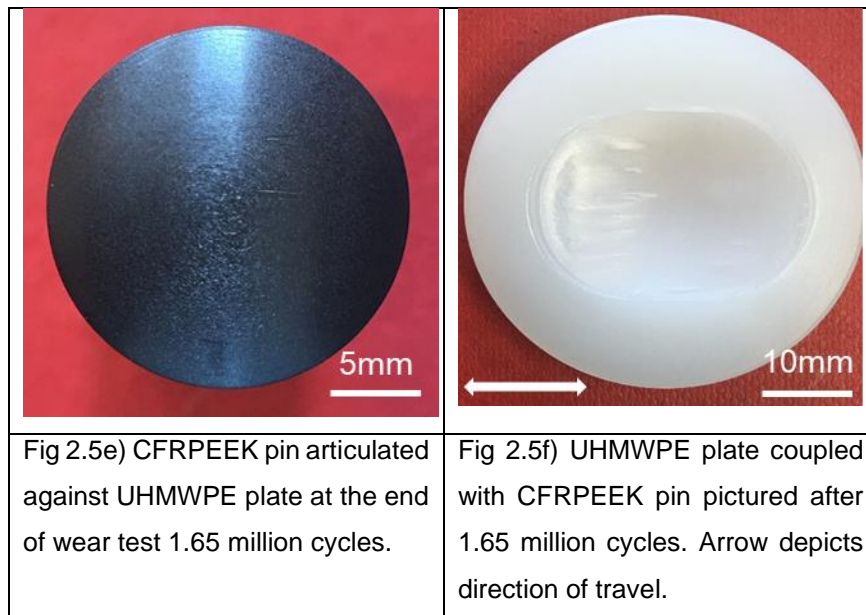
### 2.3.1.2 Surface Characterisation

#### 2.3.1.2.1 Qualitative Analysis:

Qualitative assessment of wear scars on test specimens as observed at the completion of wear tests are shown in Figure 2.5 (a – f). CFR-PEEK pins loaded against CFR-PEEK plates showed a grossly linear track along the direction of sliding (Figures 2.5a and 2.5b). Distinctive transfer films were

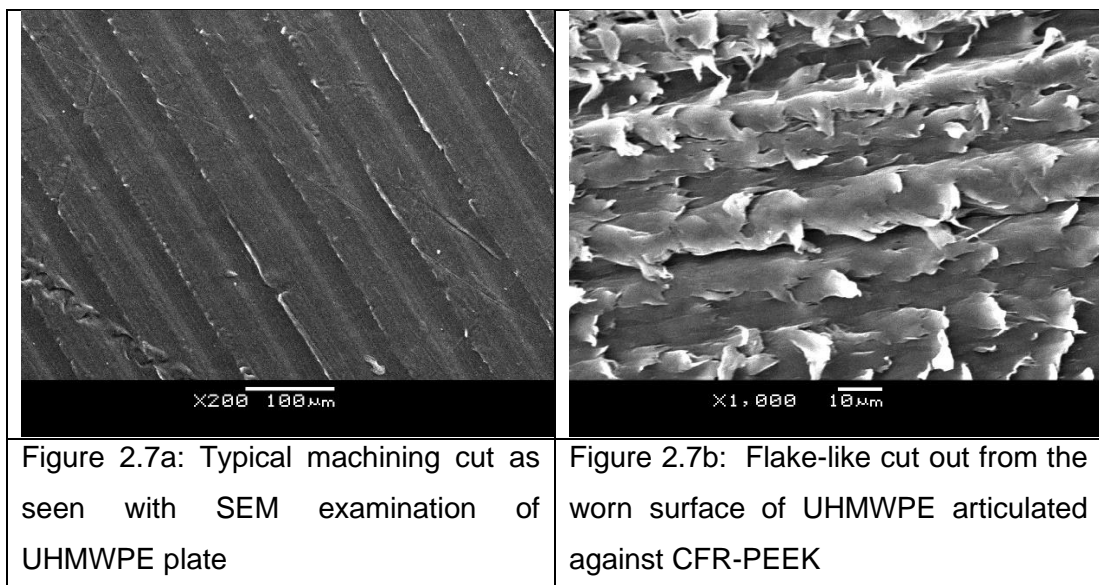
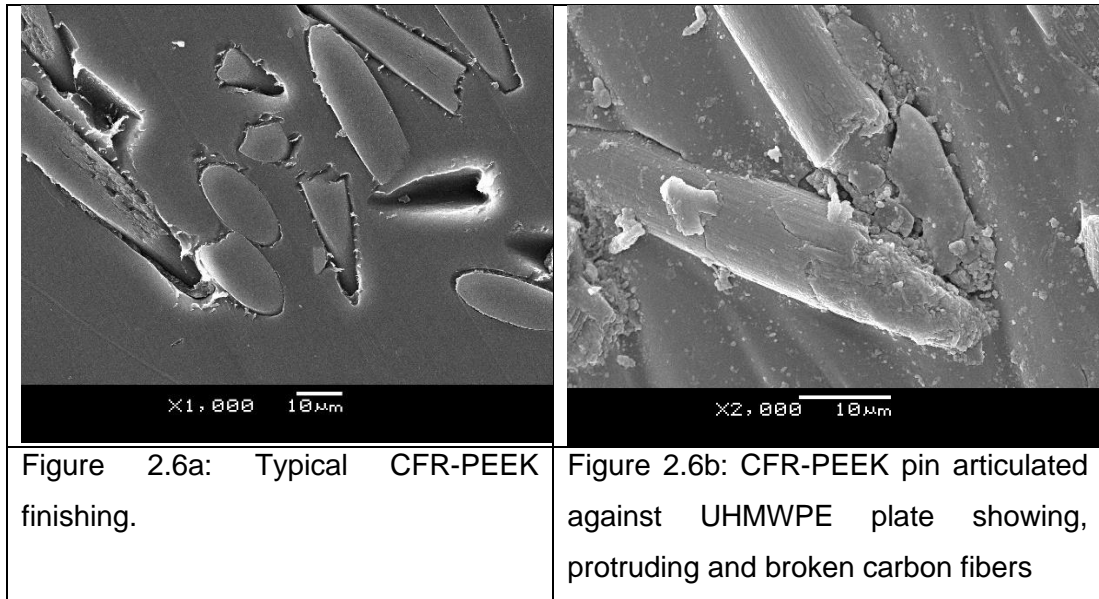
noted on the CFR-PEEK pins articulated against PEEK plates (figures 2.5c and 2.5d), the PEEK plates also showed areas of transfer. Deep troughs with cut out sharp edges were observed on PEEK and UHMWPE plates coupled with CFR-PEEK pins.

	
<p>Fig 2.5a) CFR-PEEK pin pictured after 3656 cycles coupled with CFR PEEK plate</p>	<p>Fig 2.5b) CFR PEEK plate coupled with CFR-PEEK pin pictured after 3656 cycles. Arrow depicts direction of travel.</p>
	
<p>Fig 2.5c) CFR PEEK pin coupled with PEEK plate pictured after 83117 cycles, transfer films noted on the test specimen.</p>	<p>Fig 2.5d) PEEK plate against CFR-PEEK pin shows corresponding area of transfer. Arrow depicts direction of travel.</p>



#### 2.3.1.2.2 Scanning Electron Microscopy:

Figure 2.6a depicts SEM images of a typical CFR-PEEK surface after machining and before wear testing. Figure 2.6b shows a worn CFR-PEEK pin coupled with a UHMWPE plate with detached and protruding shards of carbon fibre from the PEEK matrix and large granular particles which are likely disintegrated carbon particles, that may serve to propagate a third body wear within the counterfaces. Figure 2.7a and 2.7b show the SEM images of UHMWPE before wear and after testing with CFR-PEEK pins respectively. The post wear images demonstrate flake like cut-outs on the surface again illustrative of an aggressive wear mechanism.



### 2.3.2 PEEK Pin and Acetal Pin Articulations:

#### 2.3.2.1 Volumetric Wear Loss

All PEEK pins and polyacetal pin articulations were tested up to 2 million cycles without failure. Table 2.6 shows the mean volumetric wear loss of each

specimen and articulation ranked from the lowest wearing couple to the highest. Volume loss from the PEEK-on-XLPE articulation was mainly from the XLPE counterface with no appreciable wear loss from the PEEK pins. Wear loss from PEEK-on-XLPE articulations ( $1.3 \times 10^{-3} \text{ mm}^3$ ) was lower than observed from all other PEEK pin and acetal pin articulations ( $p < 0.001$ ). PEEK-on-UHMWPE ( $7.3 \times 10^{-3} \text{ mm}^3$ ) generated approximately 5 times combined volume loss when compared with the PEEK-on-XLPE articulation, with volume loss observed both from the PEEK pins and UHMWPE surfaces. PEEK-on-UHMWPE generated twice as much loss as measured from PEEK-on-acetal ( $3.3 \times 10^{-3} \text{ mm}^3$ )  $p = 0.021$ .

Acetal-on-XLPE ( $2.2 \times 10^{-2} \text{ mm}^3$ ) and PEEK-on-PEEK ( $4.9 \times 10^{-2} \text{ mm}^3$ ) each showed higher volume loss compared with other articulations in this group ( $p < 0.001$ ) with combined wear loss at least an order of magnitude higher than the mean wear rate noted for PEEK-on-XLPE ( $1.3 \times 10^{-3} \text{ mm}^3$ ), PEEK-on-acetal ( $3.3 \times 10^{-3} \text{ mm}^3$ ) and PEEK-on-UHMWPE ( $7.3 \times 10^{-3} \text{ mm}^3$ ) couples. Acetal-on-XLPE compared to PEEK-on-PEEK couples showed similar wear loss.

Figures 2.8 – 2.12 show the wear profile of test specimens. All polyethylene counterfaces showed a steady wear rate over the test period. The only acetal plate also showed a steady wear when coupled with PEEK. PEEK-on-PEEK articulations exhibited accelerated wear between 1,250,000 cycles to 1,750,000 cycles.

**Table 2.6:** Volume loss for PEEK and acetal pin articulations ranked from lowest to highest wearing couples

Combination	Material	Volume Loss: Mean $\pm$ SE (mm <sup>3</sup> )/ million cycle	Total volume loss/ couple
PEEK-on-XLPE	PEEK pins	-0.00009 $\pm$ (-0.00002)	1.3 x 10 <sup>-3</sup> mm <sup>3</sup>
	XLPE plates	(1.3 $\pm$ 0.4) x 10 <sup>-3</sup>	
PEEK-on-Acetal	PEEK pins	(6.6 $\pm$ 1.0) x 10 <sup>-4</sup>	3.3 x 10 <sup>-3</sup> mm <sup>3</sup>
	Acetal plates	(2.7 $\pm$ 0.3) x 10 <sup>-3</sup>	
PEEK-on-UHMWPE	PEEK pins	(2.4 $\pm$ 2.6) x 10 <sup>-4</sup>	7.3 x 10 <sup>-3</sup> mm <sup>3</sup>
	UHMWPE plates	(7.3 $\pm$ 1.1) x 10 <sup>-3</sup>	
Acetal-on-XLPE	Acetal pins	(1.6 $\pm$ 1.3) x 10 <sup>-3</sup>	2.2 x 10 <sup>-2</sup> mm <sup>3</sup>
	XLPE plates	(2.0 $\pm$ 0.9) x 10 <sup>-2</sup>	
PEEK-on-PEEK	PEEK pins	(1.5 $\pm$ 0.2) x 10 <sup>-2</sup>	4.9 x 10 <sup>-2</sup> mm <sup>3</sup>
	PEEK plates	(3.5 $\pm$ 0.4) x 10 <sup>-2</sup>	

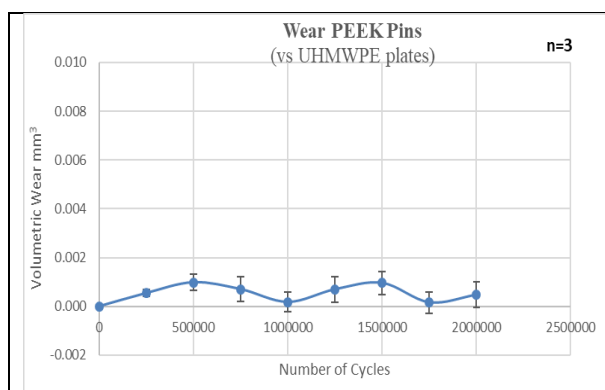


Figure 2.8a: Volume loss from PEEK pins articulated against UHMWPE plates

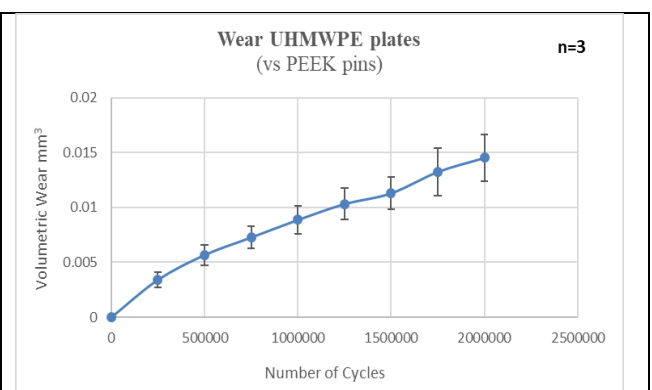
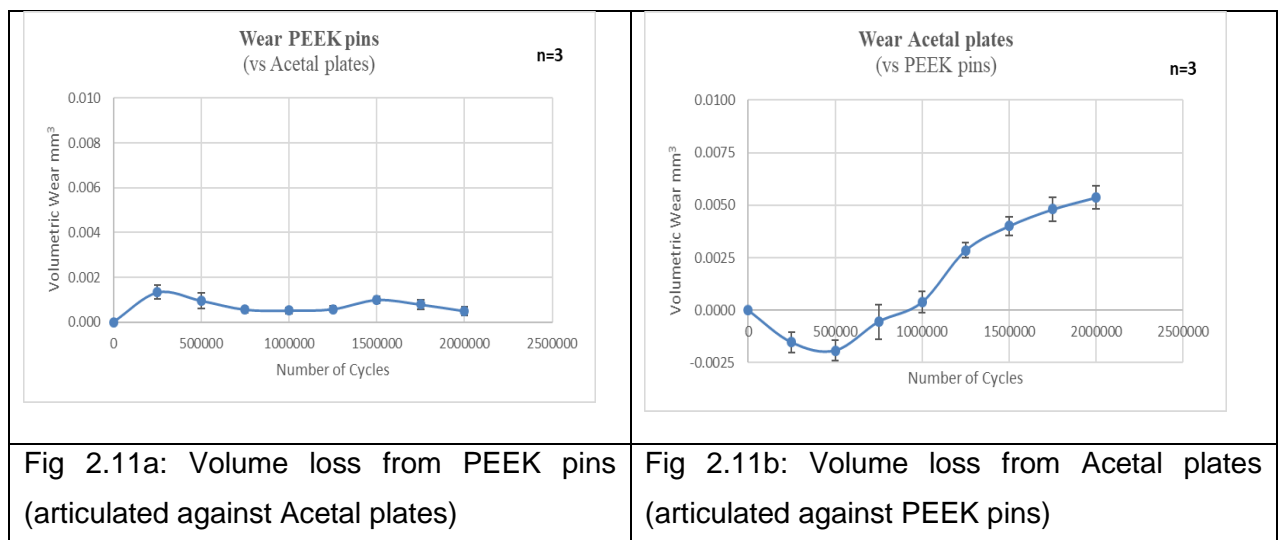
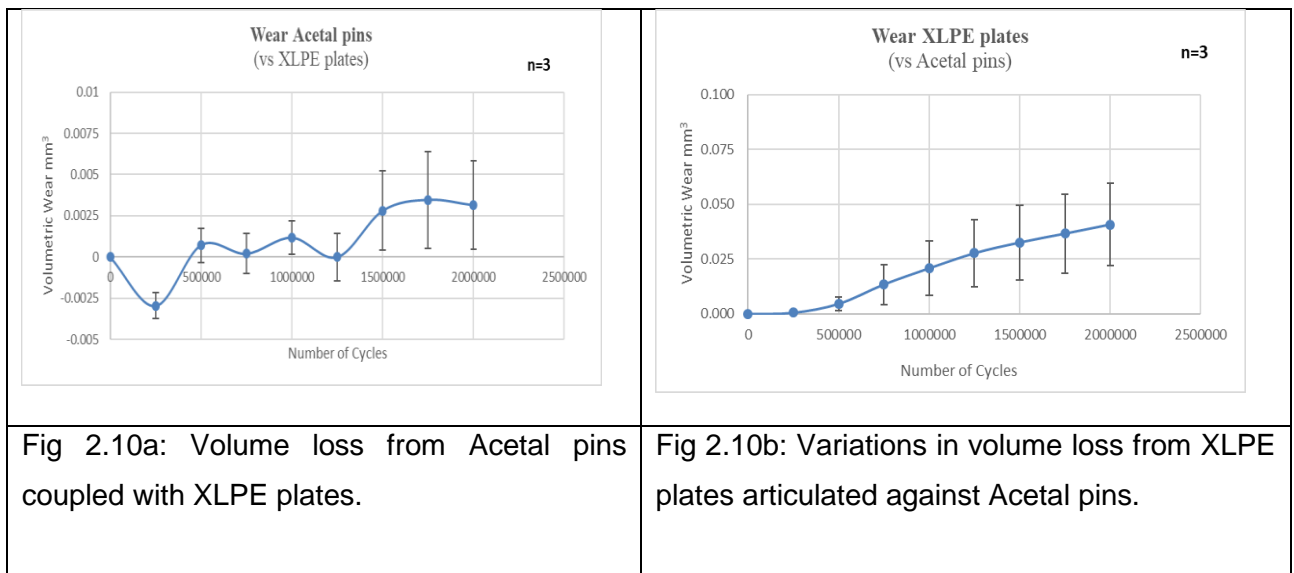
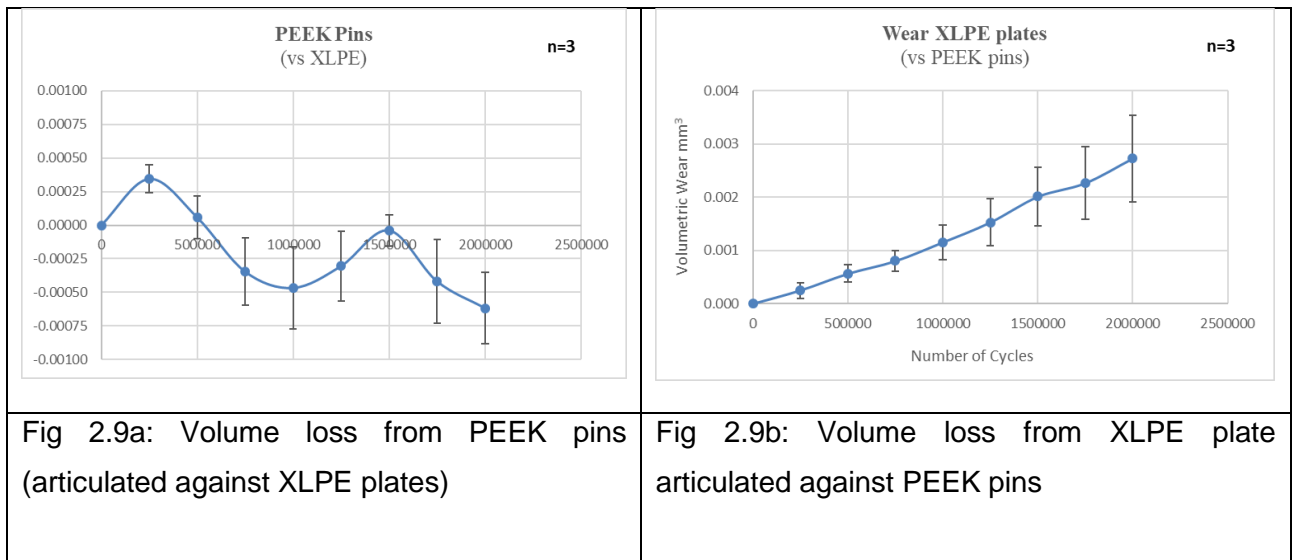
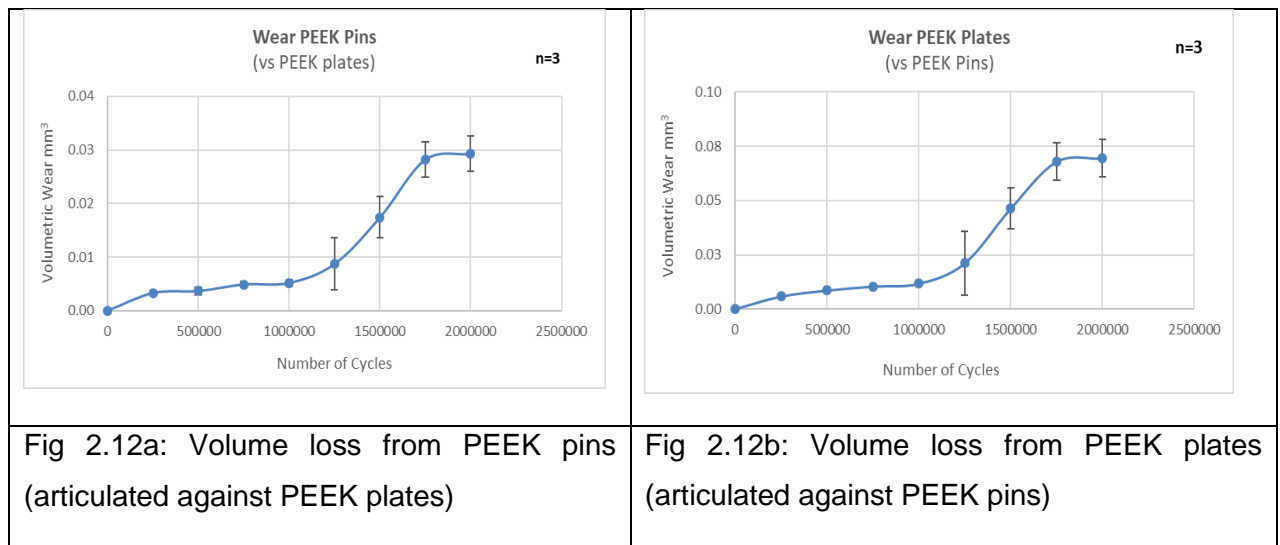


Figure 2.8b: Volume loss from UHMWPE plates articulated against PEEK pins.



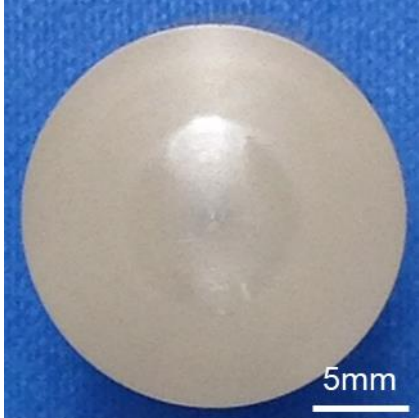
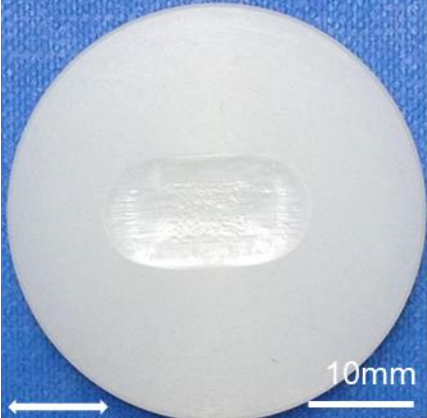
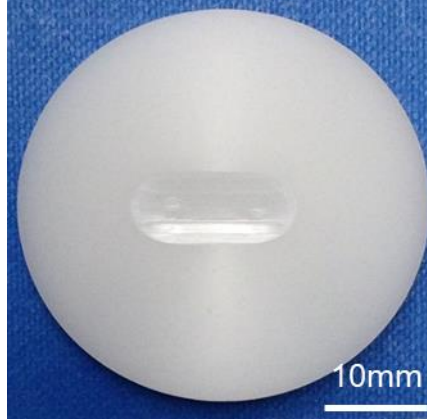
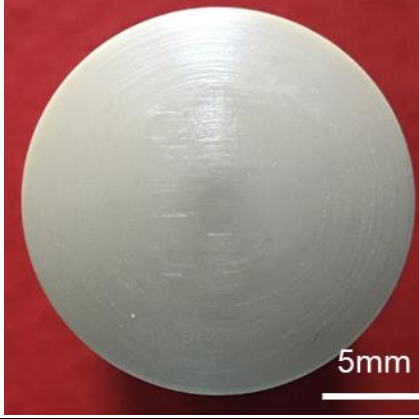



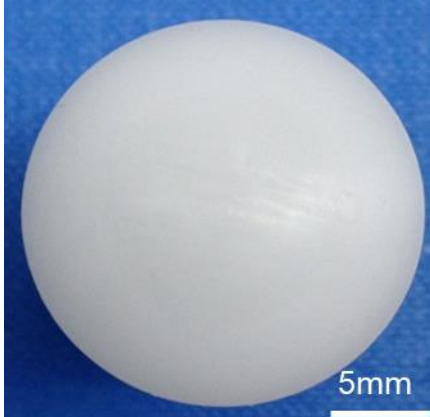
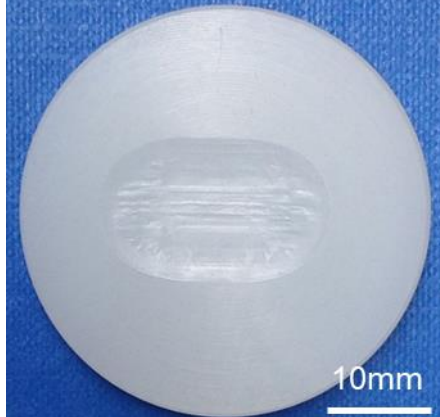
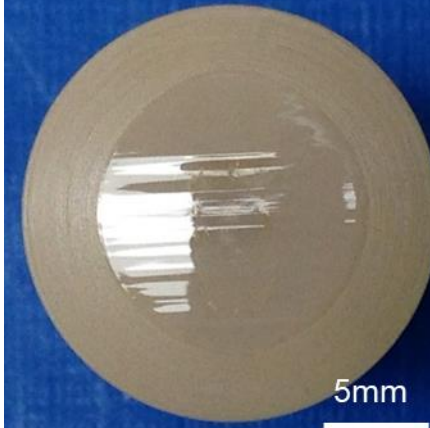
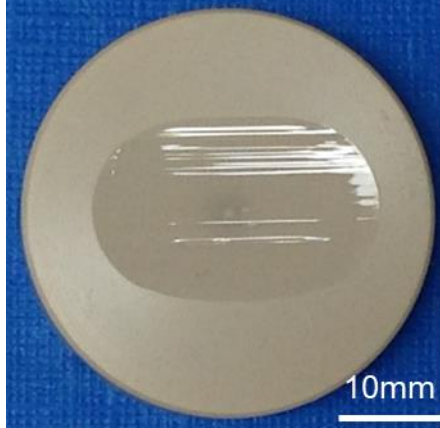



### 2.3.2.2 Surface Characterisation

#### 2.3.2.2.1 Qualitative Analysis

Figure 2.13 (a – k) shows the photographic images of all polymer-on-polymer specimens post wear testing. Light burnishing was observed on PEEK pins articulated against XLPE or UHMWPE. More prominent burnishing was observed on PEEK pins articulated against acetal plates. Rippling was observed in all plastic plates. Prominent burnishing and large wear scars were observed in PEEK-on-PEEK articulations with deep troughs in PEEK plates and flattening of the spherical ends of PEEK pins. The observed wear scar on acetal plates coupled with PEEK pins was smaller than scar observed on XLPE plates coupled with PEEK, though more wear was observed in the acetal plates. This observation is likely due to a more pronounced impact of creep i.e. time dependent deformation under constant load and plastic deformation under high stress in polyethylene counterfaces.

	
<p>Fig 2.13a). Light burnishing on PEEK pin articulated against XLPE plate at the end of wear test.</p>	<p>Fig 2.13b). XLPE plate coupled with PEEK pin pictured after 2 million cycles.</p>
	
<p>Fig 2.13c). PEEK pin articulated against acetal plate pictured after 2 million cycles</p>	<p>Fig 2.13d). Acetal plate coupled with PEEK pin pictured after 2 million cycles</p>
	
<p>Fig 2.13e). Light scratches observed on PEEK pins at the end of test with UHMWPE</p>	<p>Fig 2.13f). UHMWPE plate articulated with PEEK at the end of 2 million cycles</p>

	
<p>Fig 2.13g). Surface of acetal pin after a 2 million wear cycle coupled with XLPE</p>	<p>Fig 2.13h). XLPE plate coupled with acetal pin</p>
	
<p>Fig 2.13i). Large wear scar on PEEK pin coupled with PEEK plate, pictured after wear testing (2 million cycles)</p>	<p>Fig 2.13j). Corresponding wear scar on PEEK plate at the end of test.</p>
	
<p>Fig 2.13k). Flattening of PEEK pin coupled with PEEK plate (left). Comparison made with unused PEEK pins of similar dimensions.</p>	

### 2.3.2.2.2 Surface Profilometry:

The polymeric pins maintained their spherical configuration apart from PEEK pins articulated against PEEK plate which showed surface flattening. All PEEK pins investigated showed a reduction in surface roughness over the course of the test, and this was also seen on the articulating counterfaces. However, there was no significant change in the  $R_a$  values for the acetal pin on the XLPE counterface (Fig 2.14).

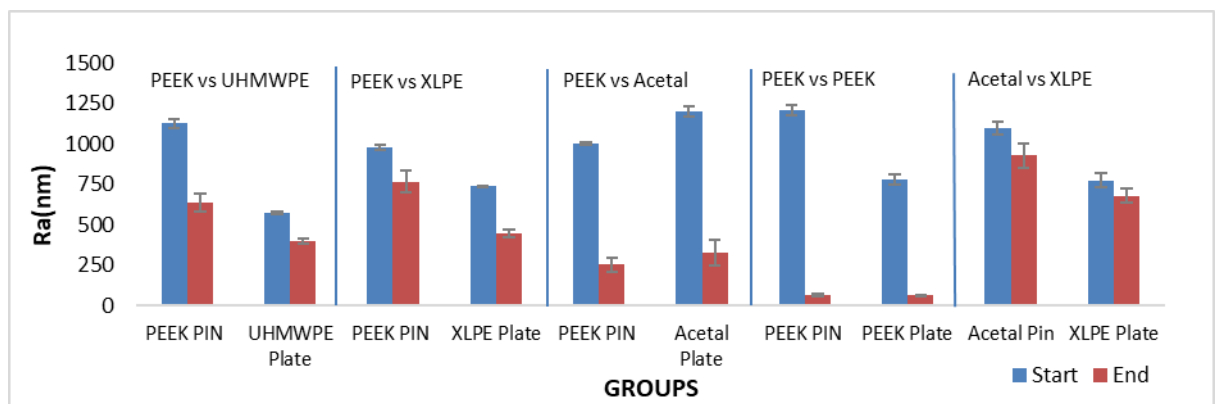


Figure 2.14:  $R_a$  values of all polymeric articulations (Mean ± SE) pre-test and post-test.

Results from the PEEK-on-UHMWPE articulations showed a significant reduction in  $R_a$  values of the PEEK pins from  $1127.32 \pm 30.18\text{nm}$  at the start of the test to  $638.43 \pm 54.98\text{nm}$  at the end of the test,  $p < 0.05$ . Likewise, a significant reduction in  $R_a$  was noted on the UHMWPE counterface from  $573.54 \pm 10.81\text{nm}$  pre-test to  $401.03 \pm 15.35$  post-test,  $p < 0.05$ . A different pattern was noted in PEEK-on-XLPE surface roughness, while a reduction was noted in the XLPE counterface from  $737.91 \pm 6.91\text{nm}$  at the start of testing to  $443.76 \pm 23.84\text{nm}$  at the end of testing,  $p < 0.05$ , no significant change was

noted in surface roughness of PEEK pins between the start ( $978.08 \pm 13.79\text{nm}$ ) and finish ( $768.05 \pm 70.07\text{nm}$ ) of testing.

When PEEK pins articulated against acetal plates, a significant reduction in  $R_a$  values was noted, in both the pins and plates, over the test period.  $R_a$  values of the PEEK pins reduced from  $1004.31 \pm 10.45\text{nm}$  at the start to  $254.50 \pm 42.73\text{nm}$  at the end ( $p < 0.001$ ), while  $R_a$  values of the acetal plates reduced from  $1201.52 \pm 28.67$  to  $327.72 \pm 82.02\text{nm}$  ( $p < 0.001$ ). Similar observations were noted in PEEK-on-PEEK articulations where surface roughness of PEEK pins reduced significantly from  $1213.2 \pm 31.40\text{nm}$  pre-test to  $64.67 \pm 7.23$  post-test ( $p < 0.001$ ) and surface roughness of the PEEK plates decreased from  $783.88 \pm 32.64\text{nm}$  pre-test to  $65.55 \pm 2.54\text{nm}$  post-test ( $p < 0.001$ ). However,  $R_a$  values of acetal pins and XLPE plates showed no significant change in pins or plates over course of test with values from  $1099.18 \pm 38.24$  to  $928.35 \pm 77.04\text{nm}$  for acetal pins and  $775.30 \pm 31.74\text{nm}$  to  $678.61 \pm 38.75\text{nm}$  for XLPE plates.

#### 2.3.2.2.3 Scanning Electron Microscopy

Pre-test surfaces and post wear SEM surface features of PEEK pins, PEEK and polyethylene plates are shown in Figures 2.15 – 2.19. Polishing of the PEEK pin when coupled with UHMWPE was noted at the end of the test (Fig 2.16). Flake-like cut outs were noted extensively on PEEK plate coupled with PEEK pins, similar features were observed on PEEK pins coupled with PEEK plates, this pattern may explain the accelerated wear noted in the PEEK-on-PEEK articulation. Areas of delamination and surface cracks perpendicular to direction of sliding was noted on XLPE plates coupled with PEEK pins (figure 2.20).



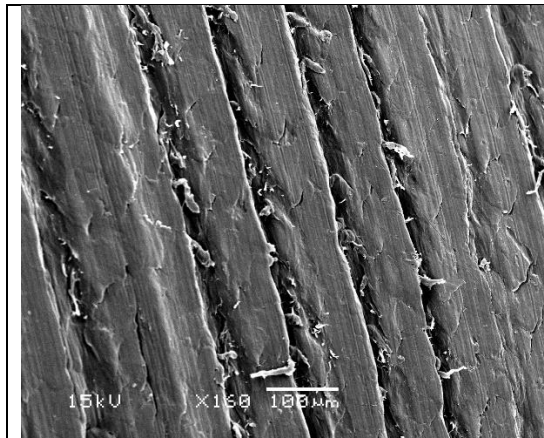


Figure 2.15: Typical machine finish of pre-test PEEK pin surfaces

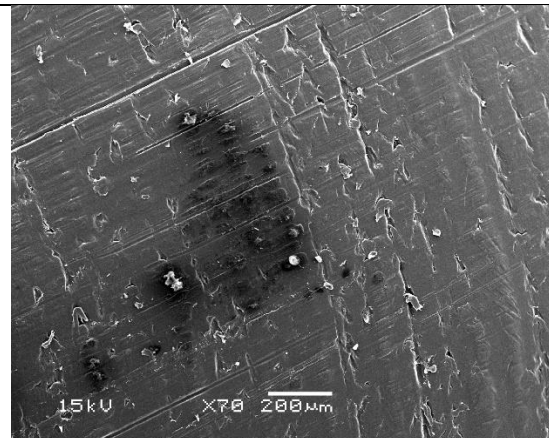


Figure 2.16: PEEK pin coupled with UHMWPE post testing

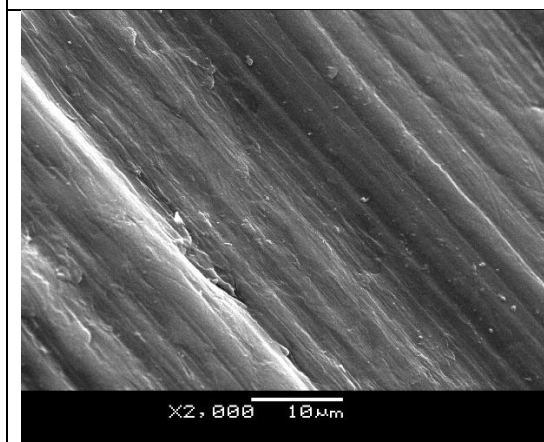


Figure 2.17: Typical machine surface finish of PEEK plate as seen before wear testing

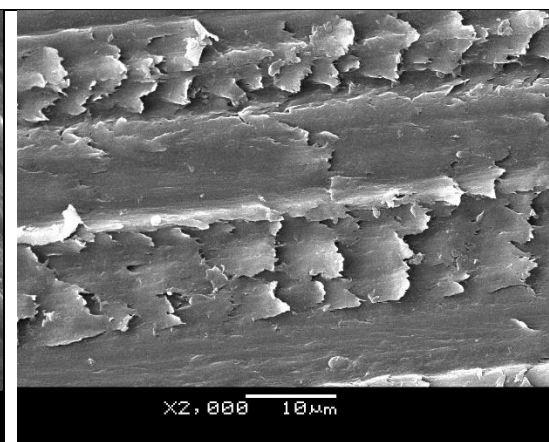


Figure 2.18: PEEK plate after wear test coupled with PEEK pin. Similar features observed on PEEK pin.

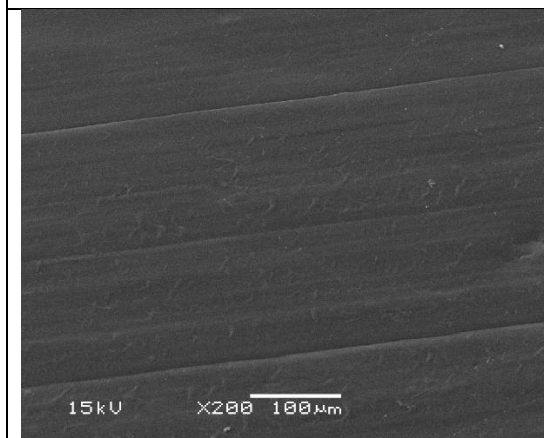


Figure 2.19: XLPE surface (coupled with PEEK) at low magnification

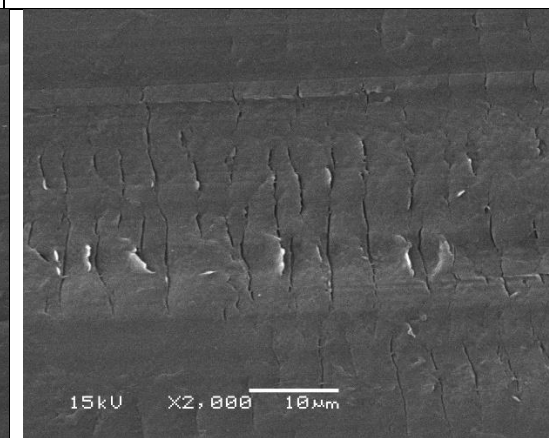


Figure 2.20: XLPE surface (coupled with PEEK) at high magnification with areas of delamination and surface cracks.

### 2.3.3 CoCr Pin Articulations:

#### 2.3.3.1 Volumetric Wear Loss

CoCr versus CFR-PEEK articulations were stopped after 63,768 cycles. Reasons for termination were similar to that described with CFR-PEEK pin articulations. CoCr-on-PEEK generated significantly more volume wear loss  $(2.3 \pm 1.6) \times 10^{-1} \text{ mm}^3/\text{MC}$  than the CoCr versus polyethylene ( $p < 0.0001$ ). CoCr versus UHMWPE and CoCr versus XLPE generated similar wear losses from the polymer counterface with observed mean loss of  $(1.7 \pm 0.6) \times 10^{-3} \text{ mm}^3/\text{MC}$  in the UHMWPE counterface and  $(1.5 \pm 0.2) \times 10^{-3} \text{ mm}^3/\text{MC}$  in the XLPE counterface. Table 2.7 shows the wear loss of specimen and articulations in a ranked order. The polymeric counterfaces tested to 2 million cycles generated steady volume loss over the course of wear test (figures 2.21 – 2.23).

**Table 2.7:** Volume loss for CoCr pin articulations ranked from lowest to highest wearing couples.

Combination	Material	Volume Loss: Mean $\pm$ SE ( $\text{mm}^3$ )/ million cycle	Total volume loss/ couple ( $\text{mm}^3$ )
CoCr-on-XLPE	CoCr pins	Assumed negligible	$(1.5 \pm 0.2) \times 10^{-3}$
	XLPE plates	$(1.5 \pm 0.2) \times 10^{-3}$	
CoCr-on-UHMWPE	CoCr pins	Assumed negligible	$(1.7 \pm 0.6) \times 10^{-3}$
	UHMWPE plates	$1.67 \times 10^{-3} \pm 0.00055$	
CoCr-on-PEEK	CoCr pins	Assumed negligible	$(2.3 \pm 1.6) \times 10^{-1}$
	PEEK plates	$(2.3 \pm 1.6) \times 10^{-1}$	
CoCr-on-CFRPEEK	CoCr pins	Assumed negligible	Stopped
	CFRPEEK plates		



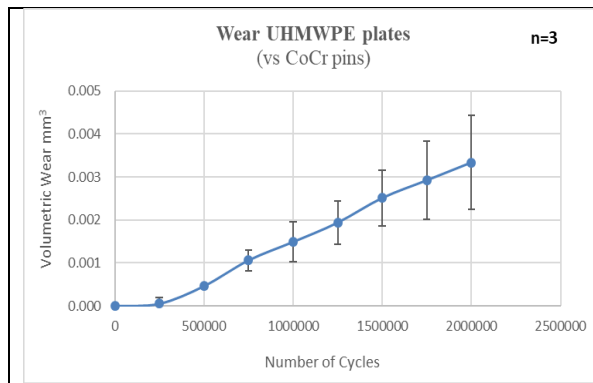


Figure 2.21: Volumetric wear loss generated from UHMWPE plates against CoCr Pins over the 2 million cycle period.

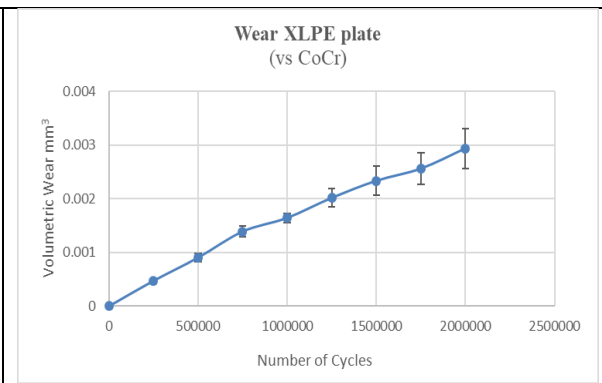


Figure 2.22: Volumetric wear from XLPE plates (against CoCr Pins).

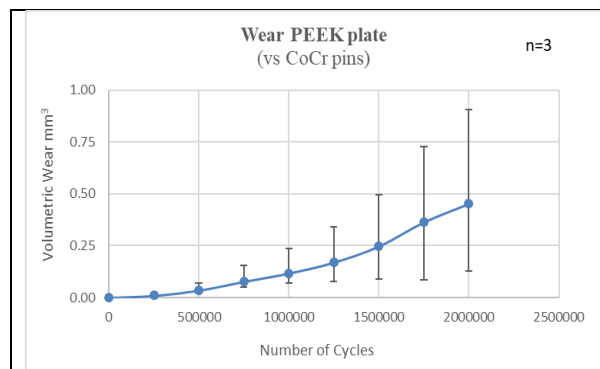
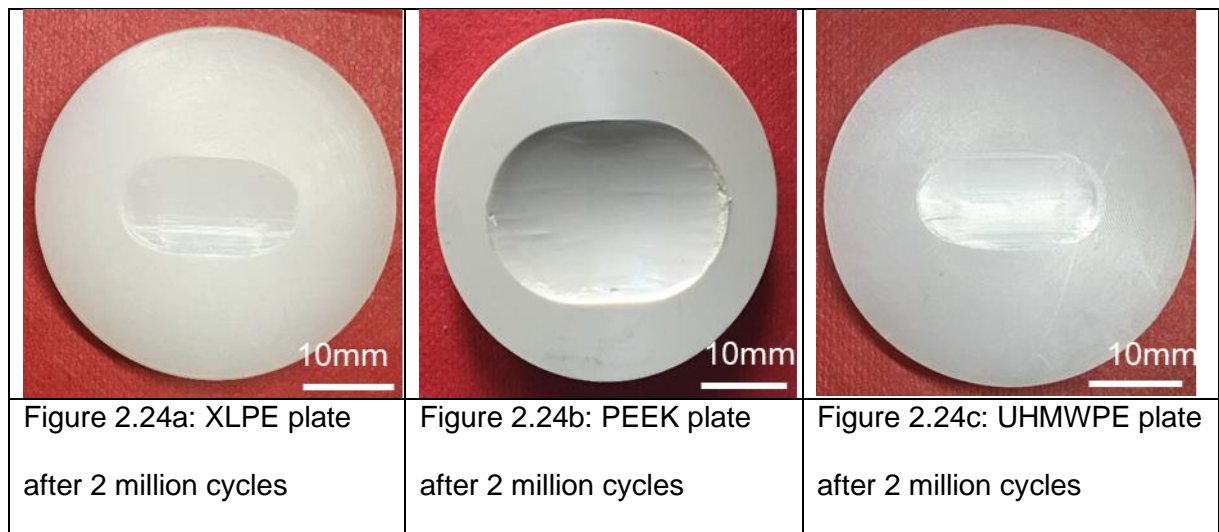


Figure 2.23: Volumetric wear from PEEK plates (against CoCr Pins).

### 2.3.3.2 Surface Characterisation

#### 2.3.3.2.1 Qualitative Analysis:

The most obvious macroscopic finding were the deep troughs noted on PEEK plates compared with the polyethylene plates (figure 2.24 a-c). This observation corresponded to the wear loss from PEEK plates relative to loss from polyethylene plates.



#### 2.3.3.2.2 Surface Profilometry:

A trend towards increased  $R_a$  values, from start to end of test, was noted in all CoCr pins (figure 2.25).  $R_a$  values of CoCr pins articulated against UHMWPE increased from  $14.70 \pm 3.05\text{nm}$  to  $27.15 \pm 2.66\text{nm}$  ( $p < 0.001$ ) and  $R_a$  values of CoCr pins articulated against XLPE increased from  $12.09 \pm 1.67\text{nm}$  to  $24.98 \pm 2.05\text{nm}$  ( $p < 0.001$ ). CoCr pins articulated against PEEK and CFR-PEEK also showed statistically significant increases in  $R_a$  at the end of the wear test, with  $R_a$  values of CoCr pins from CoCr-on-CFRPEEK articulations increasing from  $18.61 \pm 1.48\text{nm}$  to  $57.49 \pm 5.48\text{nm}$  ( $p < 0.001$ ) and  $R_a$  values of CoCr pins in CoCr-on-PEEK increasing from  $14.82 \pm 1.35\text{nm}$  to  $122.32 \pm 7.76\text{nm}$  ( $p < 0.001$ ).

All polymeric counterfaces showed a statistically significant reduction in  $R_a$  in all cases, except for CFR-PEEK plates where an increase in post-test  $R_a$  was measured.  $R_a$  values of UHMWPE counterface articulated with CoCr decreased from  $1342.82 \pm 6.58\text{nm}$  to  $787.15 \pm 23.89$  ( $p < 0.001$ ) while  $R_a$  values of XLPE counterfaces reduced from  $719.97 \pm 16.75\text{nm}$  to  $209.07 \pm 12.40\text{nm}$  ( $p < 0.001$ ). Measured  $R_a$  values of PEEK counterfaces decreased

from  $1218.74 \pm 52.12\text{nm}$  at the start of test to  $374.1 \pm 18.28\text{nm}$  at the end of the test ( $p<0.001$ ). The measured  $R_a$  of CFR-PEEK counterface increased from  $509.05 \pm 9.87\text{nm}$  to  $635.59 \pm 24.73\text{nm}$  ( $p<0.05$ ).

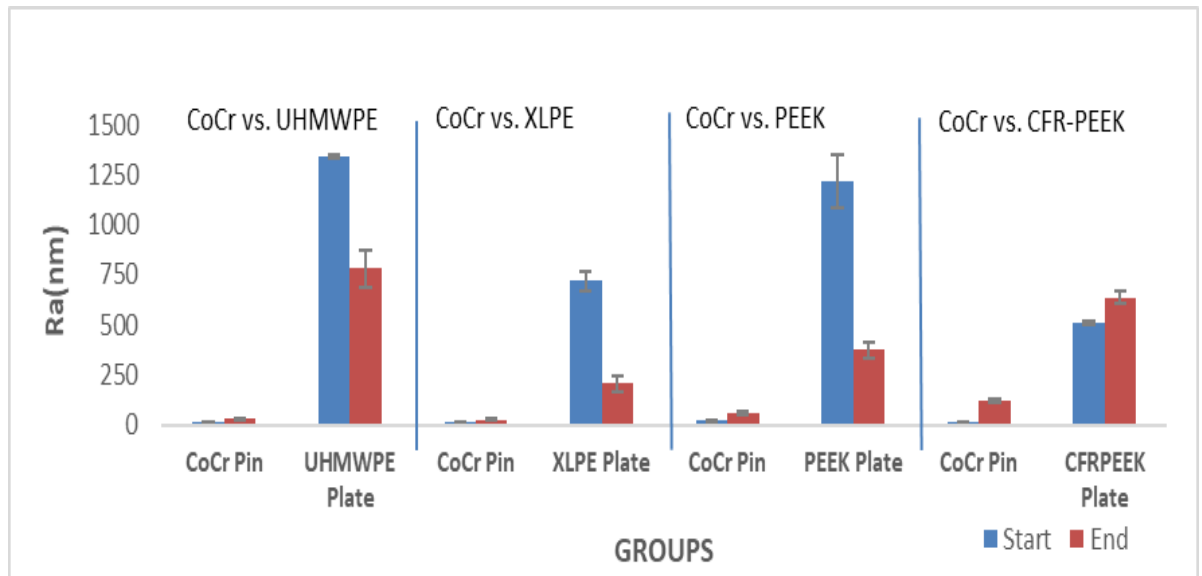
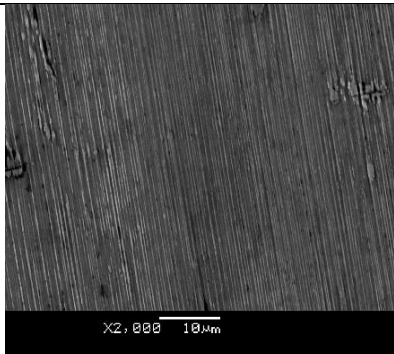
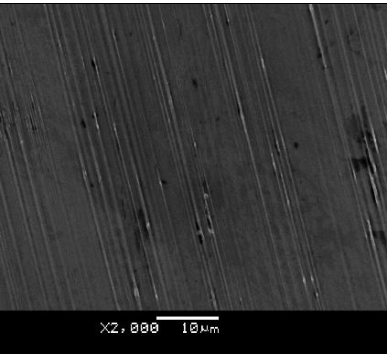
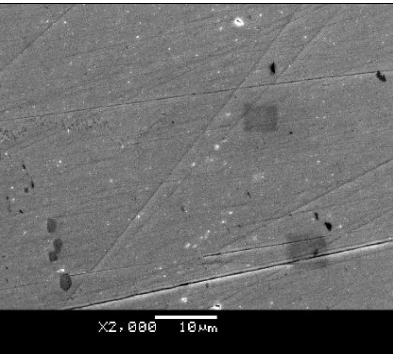
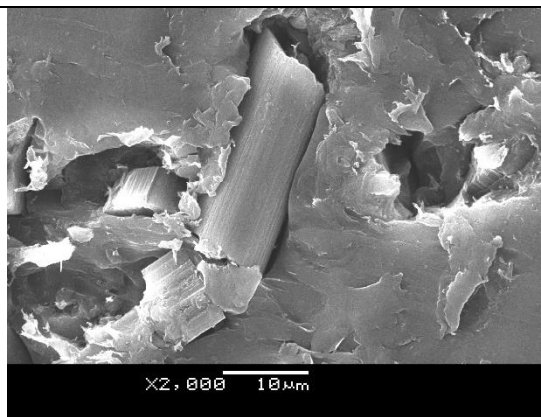
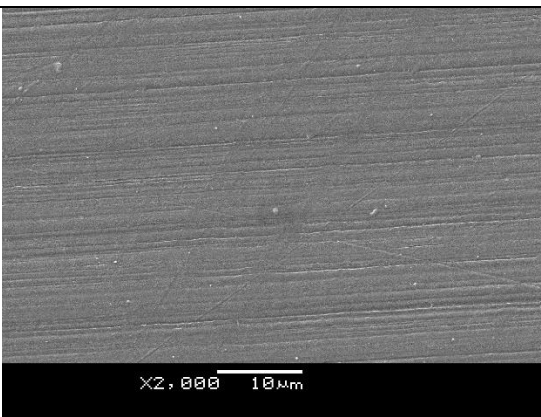


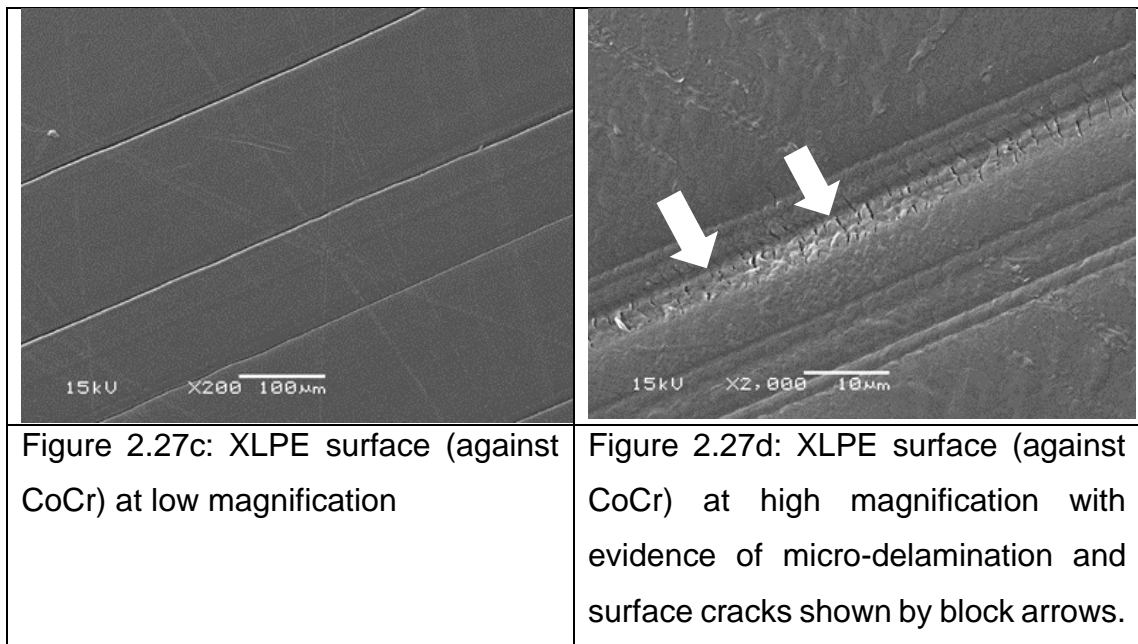
Figure 2.25:  $R_a$  values of CoCr pins (Mean  $\pm$  SE) articulated against various polymeric counterfaces pre-test and post-test.

#### 2.3.3.2.3 Scanning Electron Microscopy:

Figures 2.26a, b and c show SEM images of CoCr pins following articulation against CFR-PEEK, PEEK and polyethylene respectively. Deep scratches were noted on CoCr pins articulated with CFR-PEEK, a lighter degree of abrasion was noted on CoCr pins coupled with PEEK and polyethylene plates. Figures 2.27a, b, c and d show features of the polymeric counterfaces after wear testing.

		
<p>Fig 2.26a: Deep grooves (<math>R_a</math>-<math>635.59 \pm 9.87 \text{ nm}</math>) seen on CoCr pins coupled with CFR-PEEK</p>	<p>Fig 2.26b: Scratches seen on CoCr Pins coupled with PEEK</p>	<p>Fig 2.26c: Scratches on CoCr pins coupled with polyethylene.</p>

	
<p>Figure 2.27a: CFR-PEEK plate surface showing areas of carbon fibre detachment.</p>	<p>Figure 2.27b: PEEK surface showed a “polished” appearance post wear testing.</p>



A graph comparing volumetric wear of all articulations investigated in this study is presented in figure 2.28. With CoCr-on-XLPE (the most commonly used articulation in clinical practice) as reference, significantly higher volume loss was noted with PEEK-on-acetal ( $p<0.0001$ ), PEEK-on-UHMWPE ( $p<0.0001$ ), acetal-on-XLPE ( $p<0.0001$ ), PEEK-on-PEEK ( $p<0.0001$ ) and CoCr-on-PEEK ( $p<0.0001$ ) articulations. No significant differences were found when PEEK articulating against XLPE, CoCr against XPLE and CoCr against UHMWPE were compared.

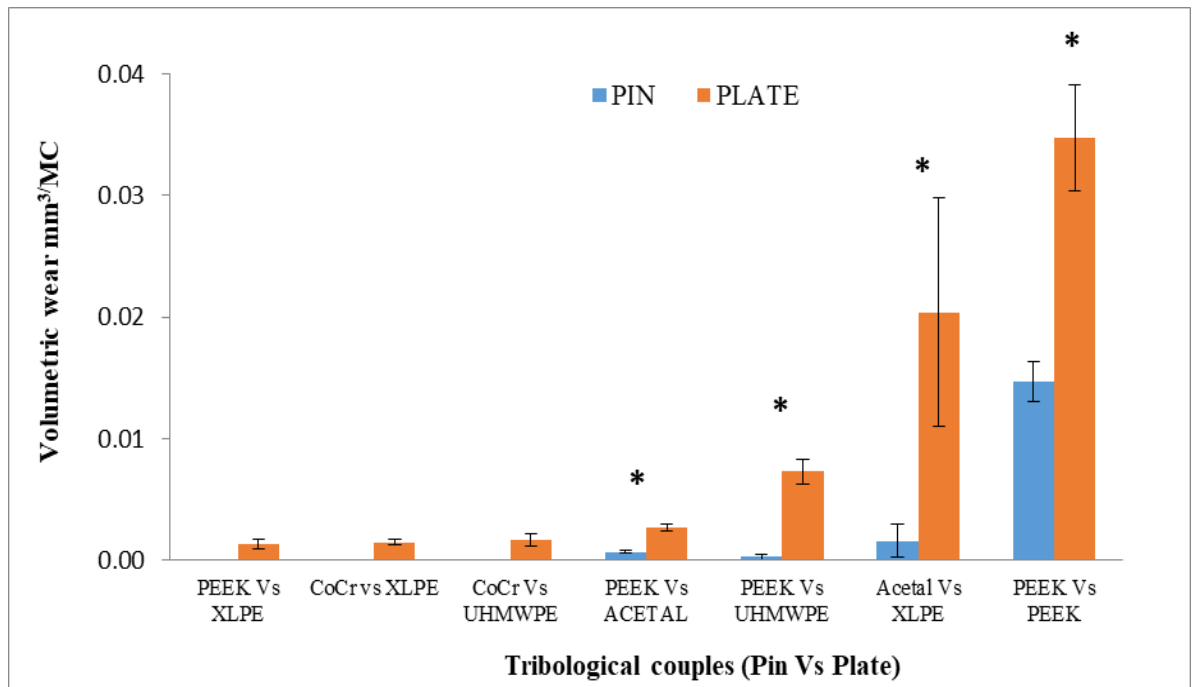


Figure 2.28: Average wear ( $\pm$  SD) of materials tested to 2MC, PEEK-on-Acetal, PEEK-on-UHMWPE, Acetal-on-XLPE and PEEK-on-PEEK generating 2x, 5x, 13x and 30x more wear respectively compared to CoCr-on-XLPE.

A further observation from this study was that while CoCr-on- XLPE and CoCr-on-UHMWPE produced statistically similar wear, PEEK-on-XLPE and PEEK-on-UHMWPE produced statistically different volume loss as shown in Figure 2.29, with loss from PEEK-on-UHMWPE approximately 5 times more than measured from PEEK-on-XLPE articulation, suggesting differences in the tribology of PEEK-on-XLPE and PEEK-on-UHMWPE.

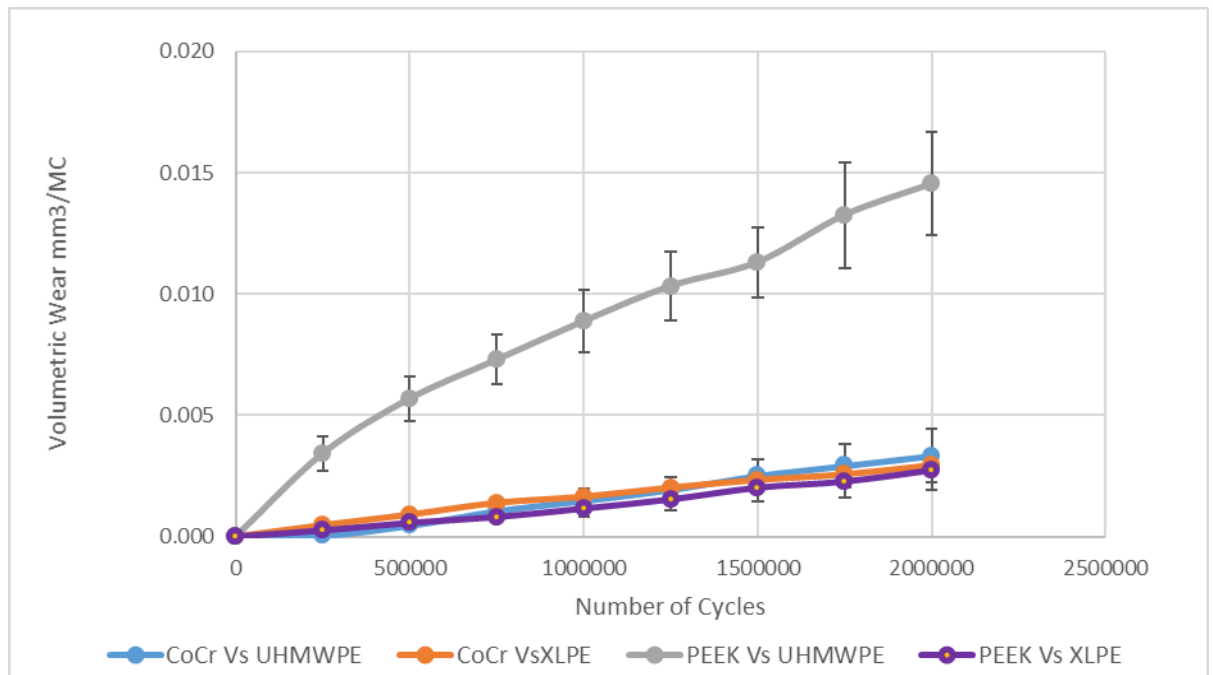


Fig 2.29: Wear rate of CoCr-on-UHMWPE, CoCr-on-XLPE, PEEK-on-XLPE and PEEK-on-UHMWPE

## 2.4 RESULTS (LOW LOAD)

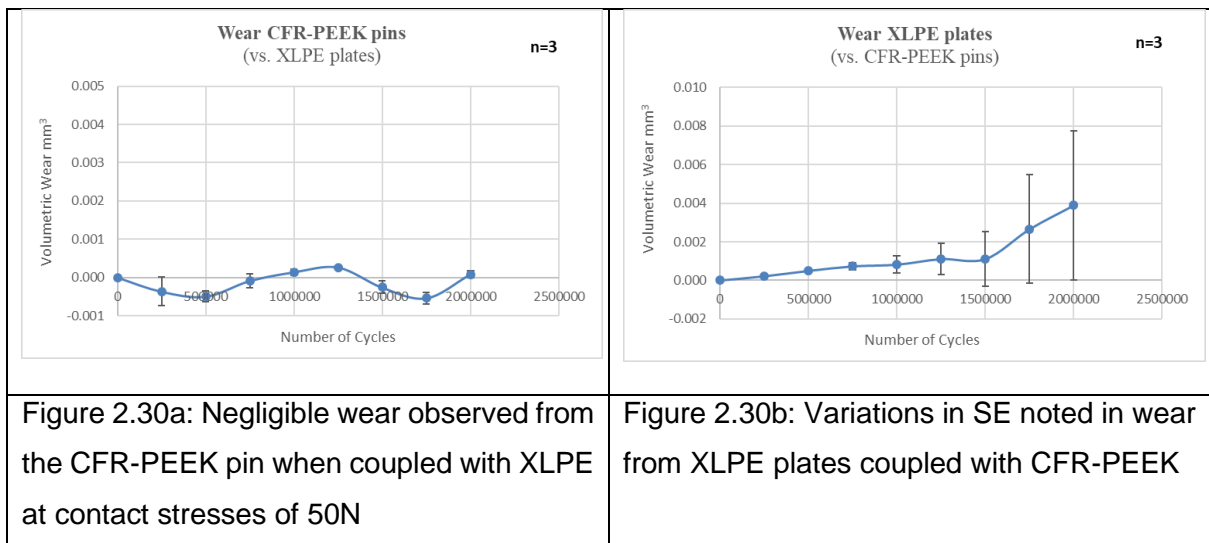
Four articulations were tested with a 50N load to investigate the best and worst articulations from the tests carried out under high stress (worst case scenario) under more normal physiological loading conditions. For ease of description, similar categories as described for high stress testing is used (Table 2.8)

**Table 2.8:** Articulations tested at low stresses (Pin versus Plate)

CFR-PEEK pin articulation	PEEK pin articulations	CoCr pin articulation
CFR-PEEK vs XLPE	PEEK vs UHMWPE  PEEK vs XLPE	CoCr vs XLPE

#### 2.4.1 CFR-PEEK Pin Articulation:

CFR PEEK-on-XLPE articulations were tested to 2 million cycles without failure. No appreciable wear was measured in the CFR-PEEK pins, with a mean volumetric loss per million cycle of  $(4.0 \pm 3.0) \times 10^{-5} \text{mm}^3/\text{MC}$  (figure 2.30a). High variation was noted in the amount of wear measured on the XLPE counterface with values ranging from  $2.5 \times 10^{-4} \text{mm}^3$  –  $4.1 \times 10^{-3} \text{mm}^3$  (fig 2.30b) and differences of up to one order of magnitude observed, the measured average volumetric wear from the XLPE counterface was  $(1.9 \pm 1.1) \times 10^{-3} \text{mm}^3$ / million cycle.

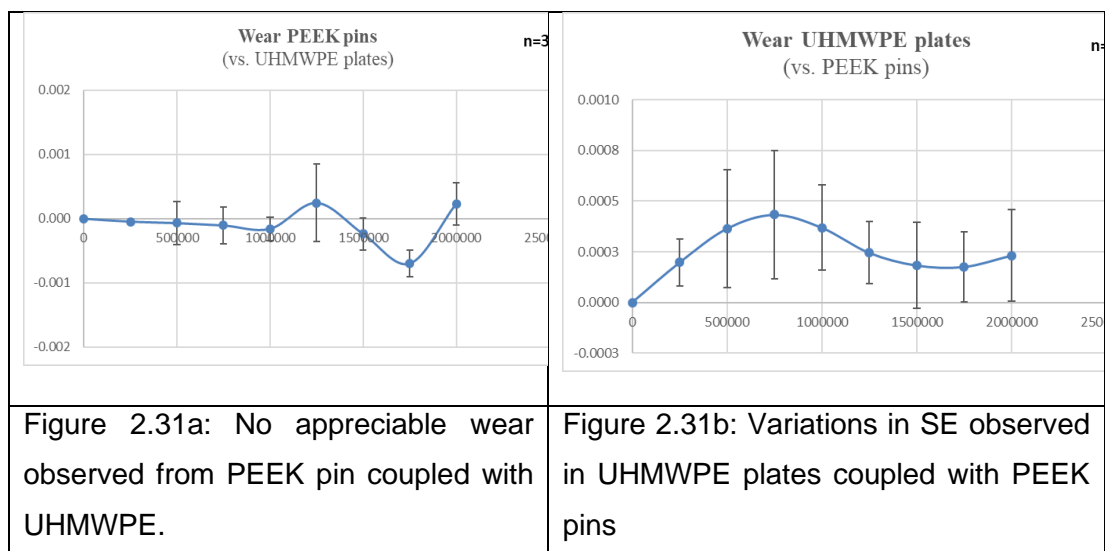


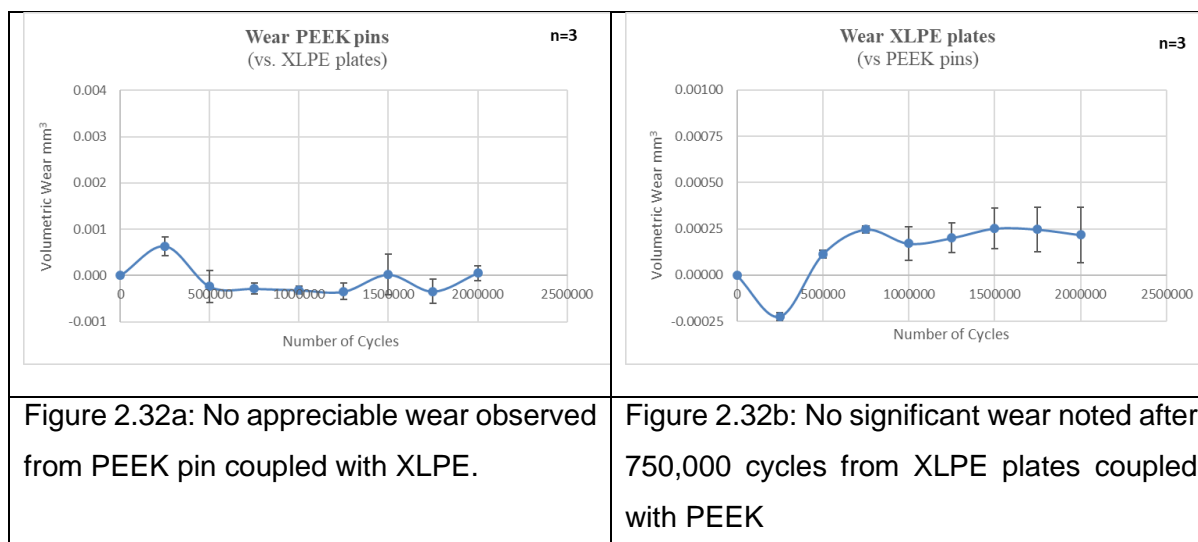


## 2.4.2 PEEK Pin Articulations:

At low stresses, wear of PEEK pins and polyethylene counterfaces is shown in figures 2.31 and 2.32. The wear from the polyethylene counterfaces did not follow a linear pattern as observed with high stress articulations. Negligible wear was observed from the PEEK pins coupled against UHMWPE ( $1.2 \pm 1.0$ )  $\times 10^{-4} \text{mm}^3/\text{MC}$  and PEEK pins from PEEK-on-XLPE articulations ( $0.1 \pm 1.7$ )  $\times 10^{-4} \text{mm}^3/\text{MC}$ .

UHMWPE and XLPE exhibited a period of running-in wear up to 750,000 cycles, after this the wear graph gradient approached zero, suggesting wear in the UHMWPE and XLPE plates was negligible after 750,000 cycles. Over the 2 million test period, the mean wear from UHMWPE articulated against PEEK was  $(1.2 \pm 0.7) \times 10^{-4} \text{mm}^3/\text{MC}$ , while average loss from XLPE was  $(1.1 \pm 0.4) \times 10^{-4} \text{mm}^3/\text{MC}$





### 2.4.3 CoCr Pin Articulation:

In its steady state, after 500,000 cycles, wear in the XLPE plate as deduced from the gradient of the graph was negligible (fig 2.33). The measured average wear from XLPE plates articulated against CoCr pins over the 2 million cycles was  $(3.0 \pm 3.0) \times 10^{-5} \text{mm}^3/\text{MC}$ .

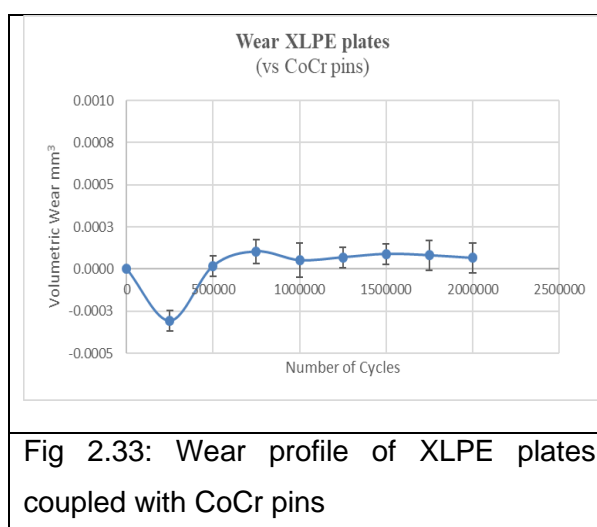


Fig 2.33: Wear profile of XLPE plates coupled with CoCr pins

Table 2.9 shows the volumetric wear of each articulation tested at low stresses. Figures 2.34 and 2.35 show the average wear from these articulations. Mann Whitney U test show no statistical difference in PEEK-on-XLPE or PEEK-on-UHMWPE when compared with CoCr-on-XLPE. CFR-PEEK-on-XLPE generated statistically significant volume loss compared to CoCr-on-XLPE articulation ( $p=0.008$ ).

**Table 2.9:** Volume loss for articulations tested at with 50N load

Combination	Material	Volume Loss: Mean $\pm$ SE ( $\text{mm}^3$ )/ million cycle	Total volume loss/ couple ( $\text{mm}^3$ )
CoCr-on-XLPE	CoCr pins	Assumed negligible	$(3.0 \pm 3.0) \times 10^{-5}$
	XLPE plates	$(3.0 \pm 3.0) \times 10^{-5}$	
PEEK-on-UHMWPE	PEEK pins	$(1.2 \pm 1.0) \times 10^{-4}$	$(2.4 \pm 1.7) \times 10^{-4}$
	UHMWPE plates	$(1.2 \pm 0.7) \times 10^{-4}$	
PEEK-on-XLPE	PEEK pins	$(1.0 \pm 17) \times 10^{-5}$	$(1.2 \pm 0.6) \times 10^{-4}$
	XLPE plates	$(1.1 \pm 0.4) \times 10^{-4}$	
CFR-PEEK-on-XLPE	CFR-PEEK pins	$(4.0 \pm 3.0) \times 10^{-5}$	$(1.9 \pm 1.1) \times 10^{-3}$
	XLPE plates	$(1.9 \pm 1.1) \times 10^{-3}$	

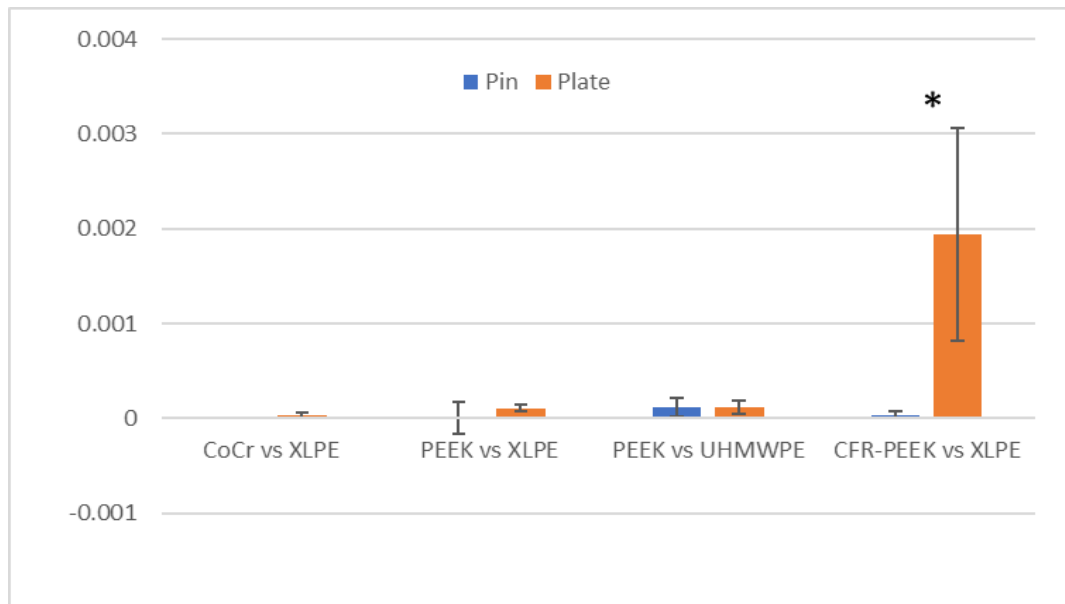


Figure 2.34: Average wear ( $\pm$  SD) of materials tested to 2MC at low stresses. Asterisk depicts significance when compared to volumetric wear loss of CoCr vs. XLPE articulation.

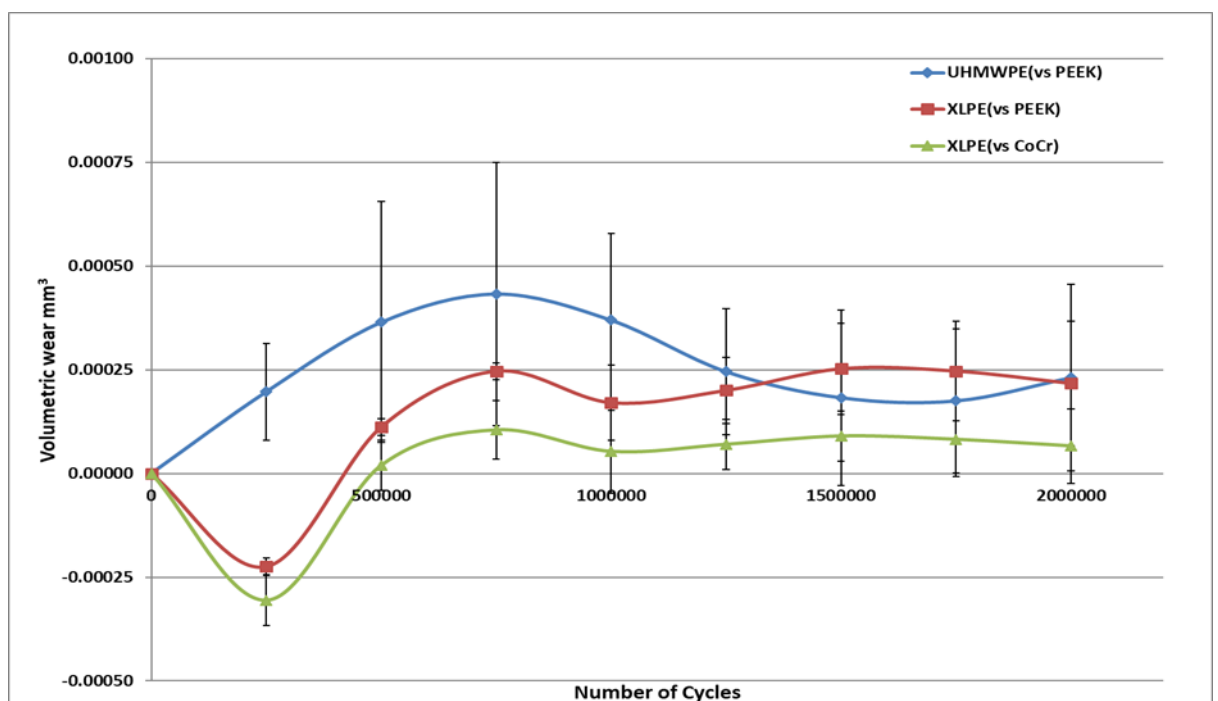


Figure 2.35: Graphical Representation comparing wear in CoCr vs. XLPE, PEEK vs. XLPE, PEEK vs. UHMWPE.

## 2.5 DISCUSSION

The main objective of this study was to evaluate the wear performance of PEEK, CFR-PEEK and acetal as bearing surfaces in a metal free TKA. The wear performance of an established MoP tribological coupling was compared with various physiologically relevant polymeric couples under test conditions representative of TKA. Using high load test conditions, PEEK-on-XLPE bearing couples produced similar wear loss compared to metal on polyethylene couples. PEEK-on-acetal, PEEK-on-UHMWPE, acetal-on-XLPE, PEEK-on-PEEK and CoCr-on-PEEK articulations all produced significantly higher volume loss when compared to CoCr-on-XLPE articulations. At low stresses, PEEK-on-XLPE and PEEK-on-UHMWPE articulations produced similar wear loss to CoCr-on-XLPE couples while CFR-PEEK-on-XLPE articulations generated significantly higher volume loss relative to CoCr-on-XLPE articulations. These results did not support the initial hypothesis that reduced wear is generated from polymeric bearings when compared with MoP bearings. However, it does suggest PEEK-on-XLPE may be a suitable alternative to MoP articulations based on comparable wear loss observed at high and low stresses.

All articulations tested at high stresses, with CFR-PEEK as pin or plate were stopped either due to excessive wear or high friction. CFR-PEEK-on-UHMWPE articulations generated a 400-fold mean wear loss ( $458.5 \times 10^{-3} \text{ mm}^3/\text{MC}$ ) compared with CoCr-on-UHMWPE ( $1.7 \times 10^{-3} \text{ mm}^3/\text{MC}$ ). The abrasive nature of CFR-PEEK is believed to be due to shards of carbon fibres protruding from the PEEK matrix, it is also possible for these shards of chopped carbon fibres to break off under high stresses such as in this study,

causing third body wear. Given the high carbon fibre/PEEK matrix interfacial strength, >70MPa (Meyer et al., 1994, Zhang and Piggott, 2000), carbon filler detachment may occur mainly under high stresses and possibly a long term phenomenon in low stress articulations due to fatigue at the carbon fibre-PEEK junction. Another indicator of the abrasive characteristic of CFR-PEEK was the surface profile of CoCr pins when articulated against CFR-PEEK plates, increasing 10-fold after 63,768 cycles when the test was stopped. The SEM features of specimens articulated against CFR-PEEK also alludes to an aggressive wear pattern likely secondary to abrasion.

Another observation from tests conducted at high stresses was that while CoCr-on- XLPE and CoCr-on-UHMWPE produced similar wear, PEEK-on-UHMWPE generated fivefold more wear loss than PEEK-on-XLPE, suggesting differences in the tribology of PEEK-on-XLPE and PEEK-on-UHMWPE. Though cross shear was not applied in our test setup, Baykal et al (2016) reported that cross shear did not affect the wear rate of PEEK-on-XLPE articulations even when component arrangement was changed. However, the rate of UHMWPE wear was affected under such conditions showing that the wear performance of PEEK-on-XLPE and PEEK-on-UHMWPE may vary even under similar conditions. Cross linking of UHMWPE improves wear resistance, with concomitant reduction in elastic modulus, ultimate true strain and ultimate stress with increasing radiation density (Gomoll et al., 2002). Malito and colleagues, examined the impact of cross-linking dosage, UHMWPE base resin (GUR 1020 and GUR 1050) and antioxidant processes on 12 resultant UHMWPE formulations of clinical relevance (Malito et al., 2018). It was observed that cross-linking alters the microstructure and mechanical

properties of polyethylene across its range with changes observed in constitutive behaviour with both tension and compression testing. Poisson's ratio for GUR 1020 was noted to approach 0.5 as radiation dosage increased while all GUR 1050 base resin formulations had Poisson's ratio exceeding 0.5, these values are higher than 0.46 which is widely quoted in literature (Edidin and Kurtz, 2000, Geringer et al., 2011a). Yield values and moduli noted in compression, though not the same values as observed in tension, followed similar trends among the various formulations. Observed variations in elastic modulus ranged widely from 521MPa to 1130MPa noted in GUR 1020 (radiated at 75K Gy, remelted) and GUR 1020 (radiated at 80K Gy with Covernox<sup>TM</sup> antioxidant) respectively. Importantly, the cross-linked formulation with the lowest elastic modulus is similar in part to the XLPE material used in this thesis – same base resin and crosslinking dosage though not remelted. For a given radiation dose, it was noted that submelt annealing exhibited higher crystallinity compared to remelting. Increased crystallinity has been associated with an increase in elastic modulus and higher contact stress (Ries and Pruitt, 2005). Reduced modulus in XLPE may partly explain reduction in wear as there is a corresponding reduction in calculated Hertzian stresses which is dependent on Young's modulus and Poisson's ratio. This reduction in wear as a function of reduced contact stress may explain the reduced wear observed in PEEK-on-XLPE compared with PEEK-on-UHMWPE but does not fully explain the differential volumetric wear observed when compared to differences from CoCr on polyethylene counterfaces.

The initial contact stresses in high load articulations were 2.5 – 3 times higher than stresses in tests conducted with low loads. Importantly, under high

loading conditions, the polyethylene counterface operated at stress levels above its yield stress of 23MPa. Plastic deformation is expected to occur at such high stresses. Polyethylene has been reported to undergo strain hardening i.e. molecular alignment in the direction of cyclic loading following plastic deformation (Alotta et al., 2018). This is a feature of the amorphous phase of viscoelastic materials, results in increased material stiffness and propensity for large plastic deformation before failure i.e. ductile fracture. Wear is believed be dependent on plastic flow parameters and operating stress levels of the polymeric counterface(Kurtz et al., 1998). Accumulation of inelastic strain until a critical strain is reached under area of contact in low stress (below yield stress) conditions or delamination due to severe shear stresses with fatigue fracture in high yield stress conditions are mechanisms of wear generation and polymer failure (Wang et al., 1995, Pascaud et al., 1997). In this study, four material couples – out of twelve tested at high loads were tested at low loads. The main finding from the low stress articulations was that PEEK-on-XLPE, PEEK-on-UHMWPE and CoCr-on-XLPE produced similar wear results with a pattern of initial running-in wear followed by a period of negligible wear over the remainder of the test period except for the CFR-PEEK-on-XLPE articulation where continued steady wear was observed. This observation may be related to a change in mode of lubrication, with deformation of the wear track either secondary to material loss from wear or due to time-dependent deformation under constant load i.e. creep, there is an increase in contact area between specimens and decrease in contact stresses, with a possible transition towards a fluid filled lubrication profile. Aside the negligible wear noted in the low stress articulations, negative wear was an



observed feature of most low wearing specimens either from low stress articulations or high stress articulations, at least for the first 500,000 cycles. The accuracy of measurements from gravimetric analysis is dependent on weight gain of controls being small in comparison to wear loss in test specimens and the assumption that fluid absorption is consistent and identical among specimens (Clarke et al., 1985). When wear is relatively low, even relatively small variations in fluid absorption may manifest as “negative wear” i.e. apparent overall gain in weight of test samples as observed in low wearing specimens in this study. Also, hygroscopic materials are likely to produce variations in fluid absorption and produce negative wear (Flannery et al., 2010).

In the high stress group, the study showed a trend towards a reduction in the Ra of polymeric surfaces when tested up to 2 million cycles. This observation may be due to the relatively high surface roughness measurements of polymeric surfaces due to the machining procedure and a subsequent reduction due to surface polishing during wear testing. While previous experimental studies have shown that relatively high surface roughness of the CoCr counterface cause a significant increase in polyethylene wear volume in CoCr-on-PE articulations (Fisher et al., 1995, Muratoglu et al., 2004), suggesting a predominantly abrasive process, breaking of adhesive welds under load is a more likely event in all polymer articulations. Therefore, except for CFR-PEEK, particles generated from all polymer articulations are likely related to size of surface asperities rather than a “gouging” action of the counterface, this may have implications for a particulate immune response *in vivo*.

East (East et al., 2015a) examined the wear performance of unfilled PEEK pins and PEEK filled with carbon fibres aligned either predominantly axially (along the pin) or tangentially (to the reciprocating surfaces), similar conclusions were reached with regards the suitability of PEEK as a possible alternative to CoCr in an all polymeric joint based on wear comparison to historical data using the same pin on plate test set up. They also reported poor wear performance of CFR-PEEK on UHMWPE articulations regardless of the carbon fibre orientation used in the test.

Baykal also studied the tribology of PEEK in all polymeric articulations (Baykal et al., 2016). Ten different bearing couples comprised of three CoCr versus polyethylene articulations (UHMWPE or XLPE or UHMWPE infused with vitamin E) and seven polymeric articulations consisting of PEEK (unfilled PEEK, PEEK filled with barium sulphate or carbon fibre) versus polyethylene for up to 2 million cycles using a multidirectional pin-on-plate tester at 2MPa contact stress level. The authors noted that apart from CFR-PEEK articulations, all polymeric articulations generated similar wear loss to conventional bearings and that PEEK-on-XLPE articulations ( $0.9 \pm 1.1\text{mm}^3/\text{MC}$ ) showed a comparable wear performance to CoCr-on-XLPE ( $1.6 \pm 2.0\text{mm}^3/\text{MC}$ ).

The two studies described above used contact stresses of 2MPa, this level of contact is lower than what is observed in most joints (Scholes and Unsworth, 2010). Furthermore, the real benefit of all polymer articulation is in knee arthroplasty where stresses are significantly higher than 2MPa (East et al., 2015b).

Conducting a simple wear test, before an elaborate joint simulator test, to assess the wear performance of candidate bearing materials suitable in joint replacement is commonplace. Various experimental setups have been described for examining wear performance of likely materials for joint replacement. A common requirement of such tests is to replicate in vivo features and produce wear mechanisms identical to those observed in retrieved specimens. Contact stresses of up to 60 MPa has previously been reported in TKA especially with deep flexion or sudden thrust (D'Lima et al., 2008, Bartel et al., 1995). Furthermore, kinematic conditions have been noted to be determinants of the wear profile from CoCr-on-polyethylene articulation under constant loading (Cornwall et al., 2001). Based on these, a simple test with considerations for the kinematic conditions of the knee, loading conditions and contact stresses may be appropriate in the initial assessment of wear couples for TKA.

One of the commonly used protocols in pin-on-plate setups is the American Society for Testing and Materials (ASTM International) F732. With this protocol, flat polymeric pins are axially loaded against reciprocating metallic plates. Consequently, the relatively low contact stresses (3.5MPa) are kept constant throughout the test. Furthermore, the same area of polymeric pin is loaded as the plastic travels back and forth on the metal wear track despite the alternating directions of frictional shear stress. These attributes are dissimilar to the observations in the knee. For example, stresses in the knee are significantly higher than 3.5MPa and polymeric inserts are cyclically loaded rather than in constant fashion. It is therefore not uncommon to use experimental jigs and setup different from the one described in the ASTM

protocol. Wang and colleagues (Wang et al., 1999) in assessing the suitability of CFR-PEEK as inserts in TKR utilised a high stress line contact tester in which 72mm rings made of CoCr or ceramic were loaded against CFR-PEEK plates under 1150N load. Authors of the ASTM F732 pointed out that no one method is appropriate for preliminary assessment in all joints. The significance of this can further be highlighted by the different morphology, size and distribution of wear debris generated in disparate joints such as the knee and hip (Walker et al., 1996).

In this study, a method of preliminary evaluation of tribological couples for TKA described by Walker and co-workers (Walker et al., 1996) was used as test protocol. The principal kinematic conditions of the knee were replicated with a setup that used a 25mm spherical ended 'femoral' components axially loaded against flat 'tibial' inserts. These simplified geometries are largely illustrative of the variety of complex geometries utilised in contemporary condylar replacement. Using the same experimental setup, Blunn and co-workers (Blunn et al., 1991) observed that the pattern of surface wear of UHMWPE plates was similar to what was observed in TKA explants. 'Worst case' loading conditions were applied in this current study, with initial peak stresses in the setup of approximately 75MPa for the CoCr-on-PE test couples. Fracture of test specimens was not observed under this loading condition. However, it must be noted that with material loss and deformation of the polyethylene counter face especially under high stresses, an increase in contact area of the articulating surfaces was observed, subsequently resulting in decreased contact pressures with time i.e. keeping the contact stresses constant during this test was not possible. This is similar to observation in joint simulation tests

and retrieval studies where creep, deformation and penetration on polyethylene surfaces play a part (Muratoglu et al., 2003).

This study provides a first step towards the tribological evaluation of PEEK and PEEK composites as materials for all polymeric TKA using an experimental setup that reproduces *in vivo* mechanisms of TKA. Under these test conditions, PEEK-on-XLPE wear couples out performed other all polymeric tribological couples and generated wear loss similar to CoCr-on-XLPE couples. An important next step in the tribological assessment of PEEK for all polymeric TKA will be the evaluation of PEEK-on-XLPE couples in a knee simulator test to assess the likely long-term performance of this combination in a more 'physiological' setting. If this wear simulator test is successful, it may be possible to replace CoCr in TKA with PEEK which may be beneficial because of the low elastic modulus, artefact free imaging with better visualisation of bone-implant interface and reduction of biological activity associated with metal alloy *in vivo*. Additionally, CFR PEEK was found to be unsuitable as a bearing surface for an all polymer TKA.

## **Chapter 3: Wear Particle Analysis**

### **3.1 INTRODUCTION**

Articulating surfaces, irrespective of material combination and design generate wear debris of various sizes, shapes and quantity (Shanbhag et al., 2000). These particulate debris have been implicated in aseptic loosening (Harris, 2001, Purdue et al., 2007b). It has been noted that volumetric wear alone is insufficient in assessing the clinical performance of articulating couples (Tipper et al., 2006), but also the concentration of wear loss within the critical size range for macrophage stimulation (Ingham and Fisher, 2000). Quantification and characterisation of wear debris is therefore considered an important aspect in the preclinical evaluation of candidate biomaterials considered for joint replacement, particularly in speculating a role in inflammatory response, aseptic loosening and failure (Endo et al., 2002).

Wear particle analysis depends largely on accurate examination of particles after a meticulous and effective isolation protocol (Baxter et al., 2009). Various protocols, based on acid, alkaline or enzymatic sample digestion methods have been described (Niedzwiecki et al., 2001). The general theme of the isolation processes involves sample digestion, protein and lipid extraction and debris purification and isolation (Billi et al., 2012a).

Particles from wear test described in Chapter 2 were isolated for characterisation. Acetal containing articulations i.e. acetal pins vs XLPE plates and PEEK pins vs acetal plates were excluded in the study as acetal is not stable but dissolvable with HCl. Also, articulations stopped before the first 250,000 interval were not included, i.e. CFR-PEEK vs CFR-PEEK, CFR-PEEK

vs PEEK and CoCr vs CFR-PEEK. Though negligible wear was measured from the PEEK pin surfaces over the 2 million test cycle, it is speculated that higher volume loss will occur from the PEEK surface in the long-term. Based on this, developing a method for separating PEEK from polyethylene particles was deemed necessary as the particle fractions may vary in size and morphology.

The aim of this chapter was to analyse and characterize the number and morphology of wear particles generated from each of the bearing combinations reported in Chapter 2. The hypothesis was that a lower number of wear particles will be generated from the best performing all polymer articulation (PEEK vs XLPE) when compared with metal-on-polyethylene bearings. Additionally, a protocol for separating PEEK particles from XLPE particles was developed, such a protocol will aid morphological assessment and speculation on the inflammatory potential of each particle fraction.

## 3.2 MATERIALS AND METHODS

### 3.2.1 Specimen Parameters

Proteinaceous test lubricant fluid, containing particles, from high stress articulations described in Chapter 2 was used for particle analysis. Each chamber contained approximately 50ml of lubricant fluid which was collected at approximately 250,000-interval and stored at -25°C. The test lubricant was composed of 25% new born calf serum (Sera Laboratories International Ltd, UK) which contained 20mM ethylene diamine tetra-acetic acid (EDTA) and 0.3% sodium azide. Samples were digested within 6 months of storage.

### 3.2.2 Purification of Reagents

Deionised water and methanol were filtered through 0.1 µm polycarbonate filter membrane to generate particle-free reagents. This step also eliminated other contaminants especially bacteria and spores, if present. Concentrated (37% w/w) hydrochloric acid (HCl) was used as received.

### 3.2.3 Articulations Tested

Wear particles were retrieved from the seven articulations listed in Table 3.1.

**Table 3.1:** List of articulations used in wear debris analysis

CoCr vs XLPE	PEEK vs XLPE
CoCr vs UHMWPE	PEEK vs UHMWPE
CoCr vs PEEK	PEEK vs PEEK
CFR-PEEK vs UHMWPE	

### 3.2.4 Sample Digestion/ Isolation of Particles

Wear particles were isolated from lubricant fluid using an acid digestion method (Appendix 1.5) originally described by Scott (Scott et al., 2001) and also adopted in section 5.2.2 of ISO 17853:2011 (ISO 17853, 2011). This acid digestion method using HCl was found most efficient after consideration for time, cost and efficacy of the technique.

Eight serum samples were collected per articulation over the 2 million cycles. Samples at 3 stoppage intervals (500,000, 1,250,000 and 1,750,000 cycles)



were pooled for analysis. Ten (10) ml of representative lubricant fluid was digested in 40ml of hydrochloric (HCl) acid 37% volume fraction at 50 °C - 60°C for 1 hour. Following this, an aliquot of the digested lubricant was added to 100ml of methanol and filtered through a 0.05µm pore filter (Nucleopore track etched Whatman, NJ, USA) under vacuum. Volume of digested lubricant added to methanol was adjusted for each articulation to permit for even distribution of particles on the filter membrane (Section 3.3.1).

### 3.2.5 Scanning Electron Microscopy (SEM)

Each polycarbonate filter membrane was mounted on a smooth-surfaced aluminum stub using double-sided adhesive carbon tape (Agar Scientific, Stansted, UK). The samples were coated with gold-palladium using a sputter coater (Emitech K550, Quorum Technologies, Laughton, UK) before examination using an SEM (JSM 5500, JEOL, UK). A minimum of 10 fields were imaged per membrane, using recommended magnifications as suggested by ASTM F1877-05 (2010) i.e. magnifications of 100x, 1000x and 10,000x for a particle size range of 10-100µm, 1-10µm and 0.1-1.0µm respectively. A minimum of 400 particles were counted for analysis per articulation.

### 3.2.6 Characterisation of Wear Particles

Wear particles were characterized using ImageJ analysis software (NIH, Maryland, USA). SEM images of particles as displayed on filter membranes were used as inputs for the ImageJ program and the subsequent automated image analysis sequence. SEM micrograph images were calibrated and a threshold of grayscale pixels was estimated interactively and set between 0 and 255, with zero representing completely black pixels and 255 assigned to completely white pixels. Based on the set threshold, a binary result was obtained with pixels above the set threshold assigned white and pixels below the threshold assigned black. This process distinguished the particles from the filter membrane and allowed for automated analysis of particles. Area, perimeter, roundness and aspect ratio (AR) measurements of each of the analyzed particle were generated and equivalent circle diameter and form factor deduced.

These parameters are defined in the ASTM F1877-05 (ASTM International, 2010) . Equivalent circle diameter (ECD) is defined as the diameter of a circle with equivalent area as the area of particle being analyzed, while the AR is defined as the ratio of the longest line between any 2 points on the particle ( $d_{max}$ ) and longest perpendicular line to the  $d_{max}$  assigned  $d_{min}$ . The particle roundness is a measure of resemblance to a circle and the form factor (FF) relates the perimeter (P) of the particle to its area. ECD was used as a measure of size while AR, roundness and form factor were used as morphology descriptors. Mathematically, these factors are expressed as:

$$ECD = 2. \sqrt{Area/\pi} \quad (1)$$

$$AR = d_{(max)}/d_{(min)} \quad (2)$$

$$Roundness = (4. Area)/(\pi. d_{max}^2) \quad (3)$$

$$Form\ factor = 4. \pi. Area /P^2 \quad (4)$$

### 3.2.7 Quantification of Wear Particles

The approximate quantity of particles generated after a million cycles was determined based on the average number of particles viewed, the area of filter membrane viewed, volume of serum digested, and estimated volume of serum harvested over a million cycles. The number of particles counted per unit area should correspond to the total number of particles retrieved from the representative digested lubricant over the area of the filter membrane if particles are evenly distributed with no particle overlaps. i.e.:

$$\frac{\text{Average number counted}}{\text{Area of filter viewed}} = \frac{\text{Total number of particles}}{\text{Area of filter membrane}}$$

It was assumed that 1ml of digested lubricant fluid represented 0.2ml of the lubricant serum prior digestion. This assumption was made since 10ml of the lubricant serum was digested in 40ml of HCl acid (1 in 5 dilution).

$$n_{(T)} = \frac{\text{area of filter} \times \text{average number counted}}{0.2 \times \text{area of filter viewed}}$$

Approximately 50ml of lubricant fluid was harvested at each test stoppage from each articulating test couples. To normalise for the varying aliquot of digested lubricant fluid analysed and area of view, the estimated total number of particles ( $n_{(T)}$ ) in the 200ml of representative lubricant fluid digested and harvested over a million cycle was determined using the formula:

$$n_{(T)} = 200 \times A_{Filter} \times \frac{\text{average number counted}}{\text{area of filter viewed}} \times \frac{1}{(0.2) \text{ vol of lubricant aliquot}} \times 10^6$$

(5)

where  $A_{Filter}$  is the area of the filter membrane (mm<sup>2</sup>) and area of view (μm<sup>2</sup>) was determined from ImageJ.

### 3.2.8 Protocol for Separating PEEK from XLPE Particles

Results from chapter 2 showed similar volume loss in PEEK-on-XLPE and CoCr-on-polyethylene articulations. A method of separating each particle fraction from PEEK-on-XLPE wear debris using proprietary supplied PEEK (VESTAKEEP 1000 UFP10, Evonik, Germany) and UHMWPE (Ceridust 3715, Clariant, Germany) was developed and described in this section. The separation technique which was based on the different densities of PEEK (1.3g/cm<sup>3</sup>) and polyethylene (0.93g/cm<sup>3</sup>), employed a density gradient created by the water based digested lubricant fluid and chloroform: methanol mixture to segregate the particle fractions.

500mg each of PEEK and Ceridust was added to 50ml of freshly prepared 25% new born calf serum containing EDTA and sodium azide. 10ml of the

mixture was digested using the HCl acid digestion method described above, 2ml of digested serum was layered over 10ml of chloroform: methanol mixture (2:1) and centrifugation carried out at 2000rpm for 5 minutes. Particles at the water-chloroform interface and particles that settled beneath the chloroform: methanol column were collected separately. Ice cold acetone was added to each collected particle solution in a 5:1 ratio, vortexed and left for 1 hour at -20°C. The particle solution was then spun down for 2 minutes at 2000rpm, supernatant decanted and particles reconstituted in methanol and collected on 0.05 filter membrane after vacuum filtration. FT-IR spectroscopy (FT/IR-4200, JASCO, Germany) of the isolated particles were analysed and compared with spectra from the proprietary acquired neat particles.

### 3.2.9 Statistical Analysis

Following particle characterisation, the mean, median, range and standard deviation were presented. Data was analysed using SPSS, version 22 for Windows (Chicago, USA). Following test for normality, non-parametric analysis using a Kruskal Wallis and Mann Whitney U tests were conducted as appropriate, to assess for significant differences ( $p < 0.05$ ) between groups. Bonferroni correction was applied to reduce familywise error rate.

## 3.3 RESULTS

### 3.3.1 Qualitative Analysis

Figures 1 and 2 show contrasting images based on displayed number of particles. A large number of particles were observed generated from the CoCr-

on-PEEK articulation (figure 3.1) when 1ml of digested lubricant was added to 100ml of methanol before vacuum filtration as described in the digestion protocol used in this study. Using the same volume of digested lubricant (1ml), a very scanty number of particles was isolated from CoCr-on-XLPE articulations (figure 3.2). Based on this observation the volume of lubricant fluid added to methanol was adjusted to permit a more uniform display of particles that ensured ease of individual particle characterisation. Following this adjustment, particle analysis using SEM showed a more uniform distribution of particle types on the polycarbonate filter membrane with most particles round in appearance and of <1 micron in size. Occasional agglomerates were observed, but this was minimal. Figure 3.3 – 3.9, shows typical SEM images of particles in each articulation and the corresponding ImageJ outline used for automated analysis.

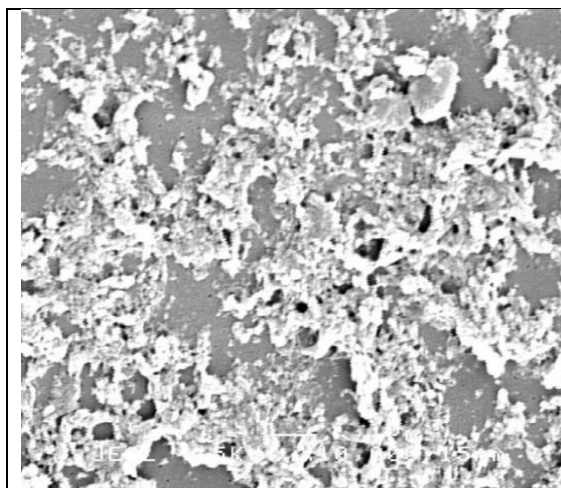
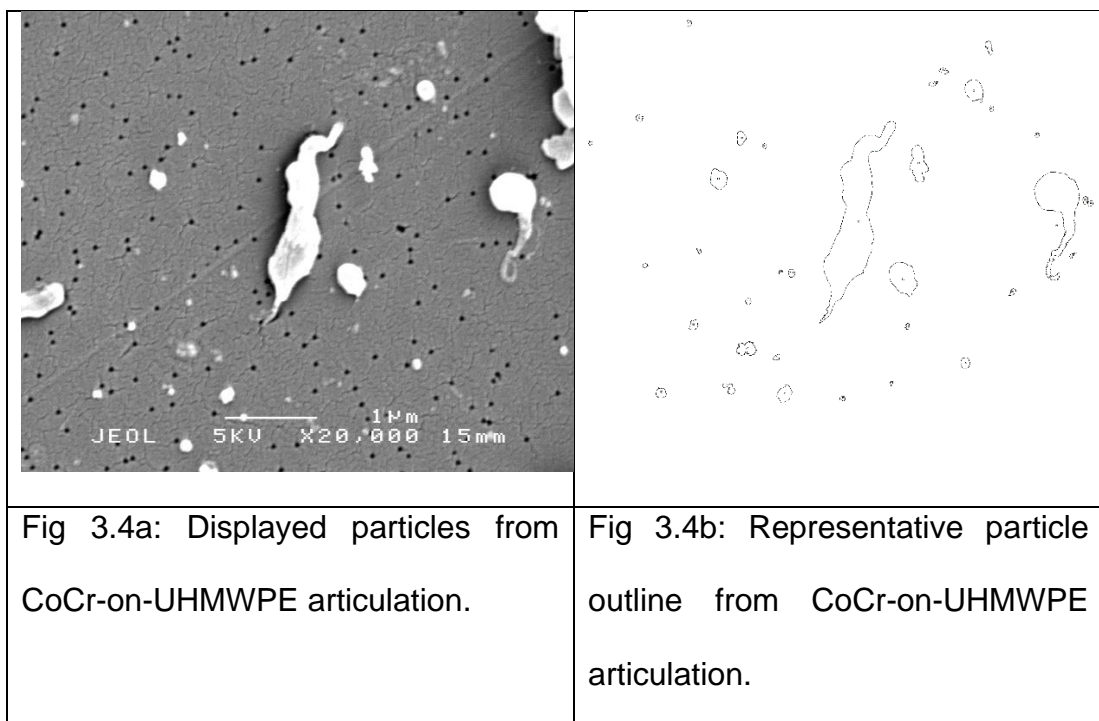
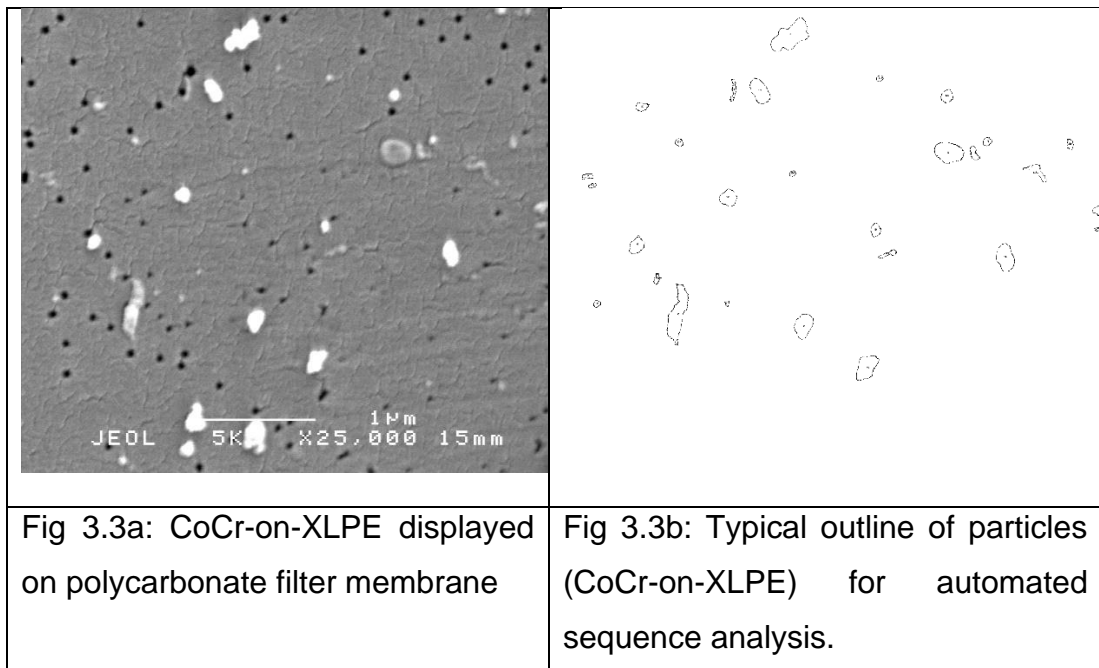


Fig 3.1: Particle laden filter membrane showing particles from the CoCr vs PEEK articulation



Fig 3.2: Few particles were obtained from CoCr vs XLPE articulations



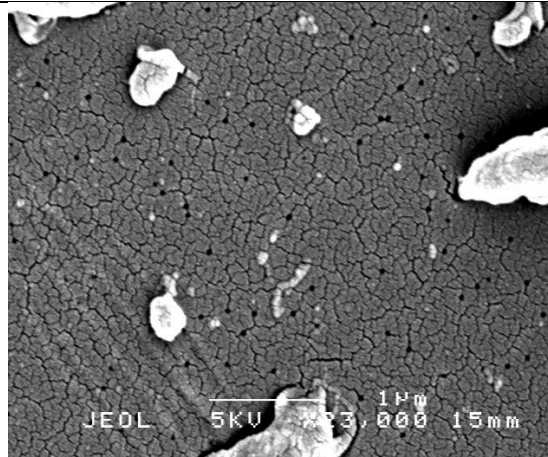


Fig 3.5a: SEM image of PEEK particles from CoCr-on-PEEK articulation.

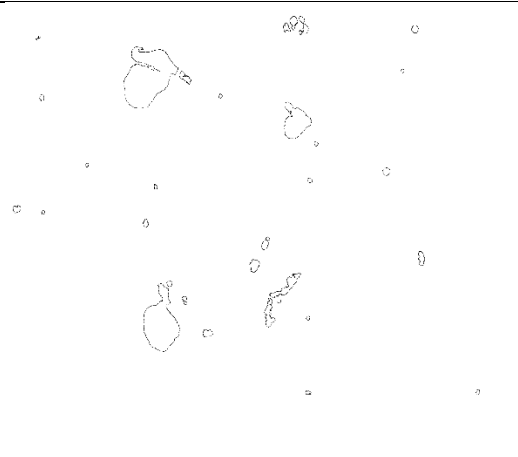


Fig 3.5b: ImageJ rendered outline of PEEK particles from CoCr-on-PEEK articulations.

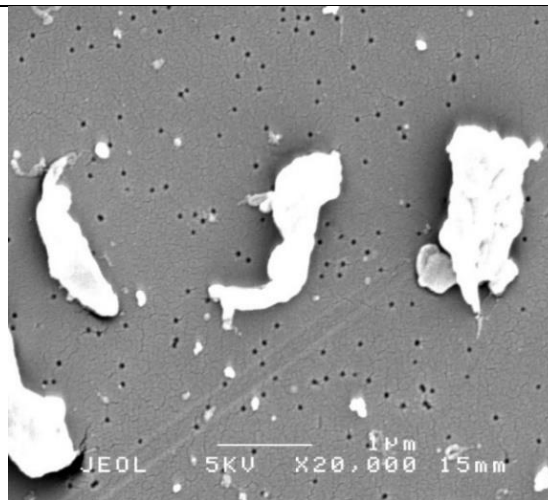


Fig 3.6a: Particles from CFR-PEEK-on-UHMWPE articulation as viewed by SEM

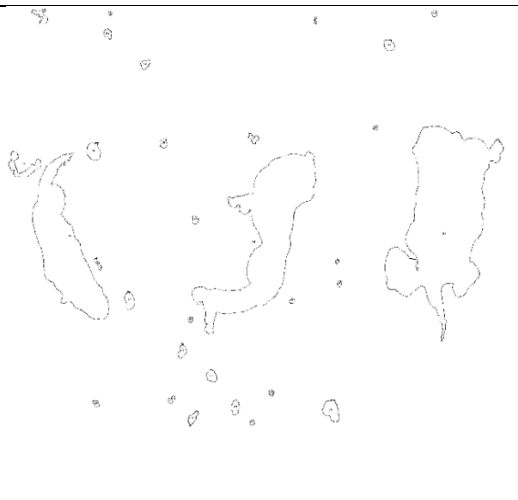
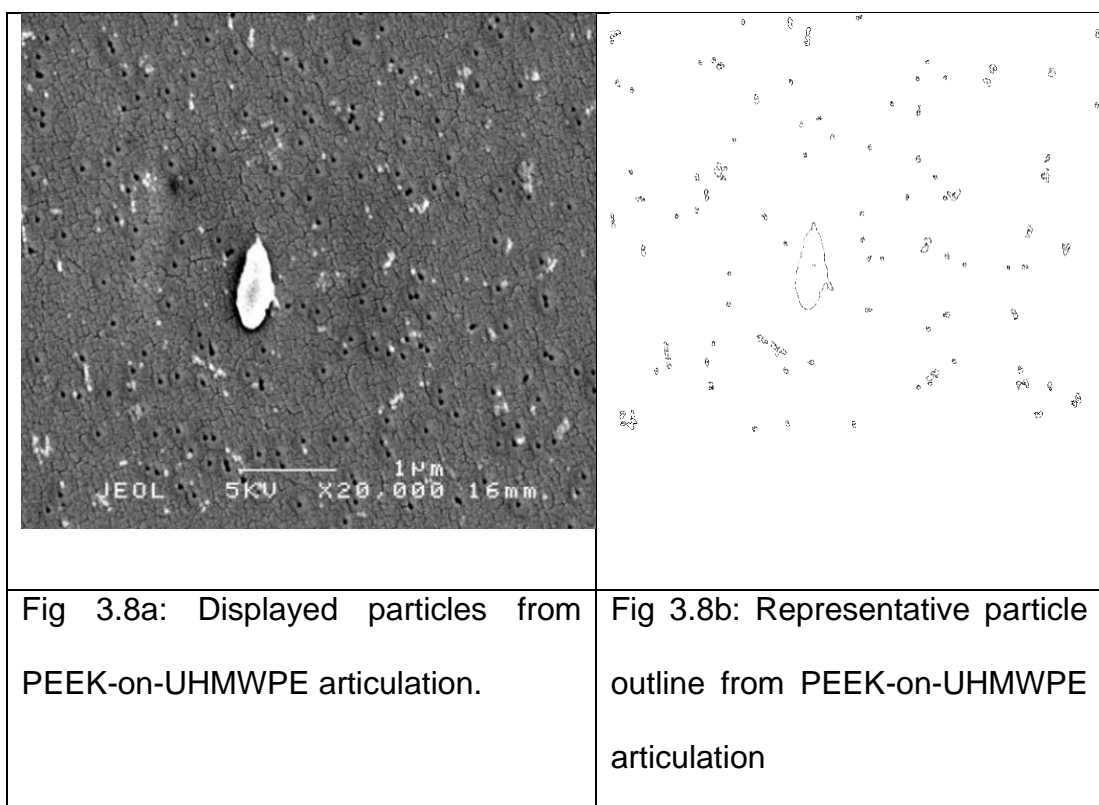
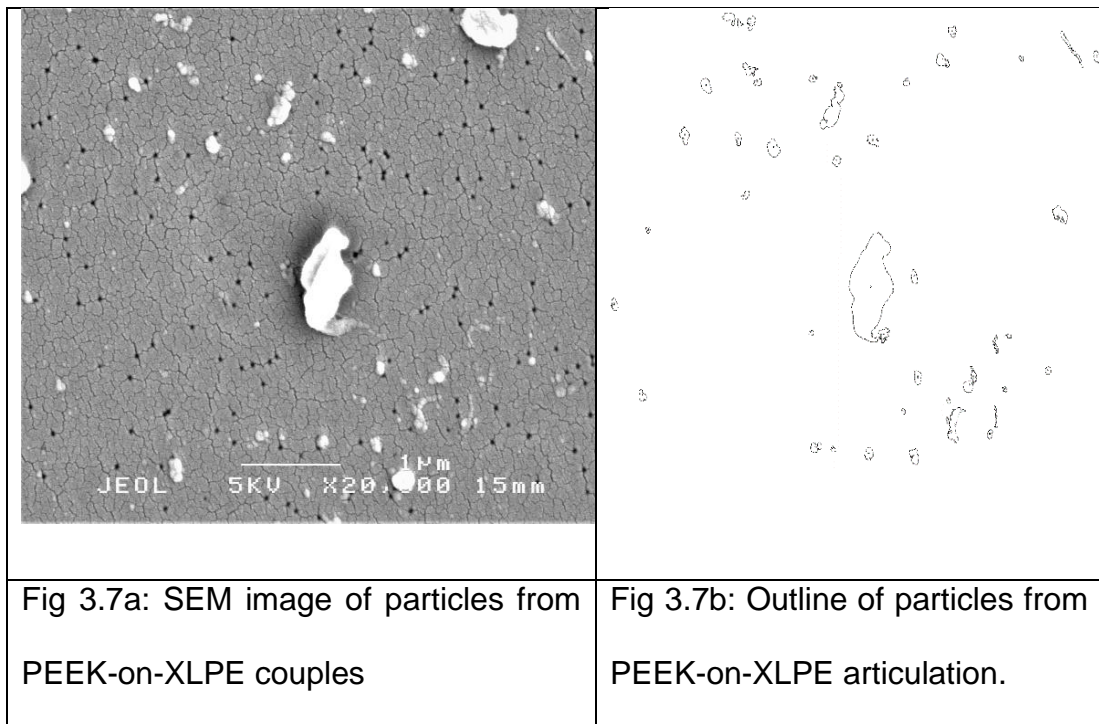
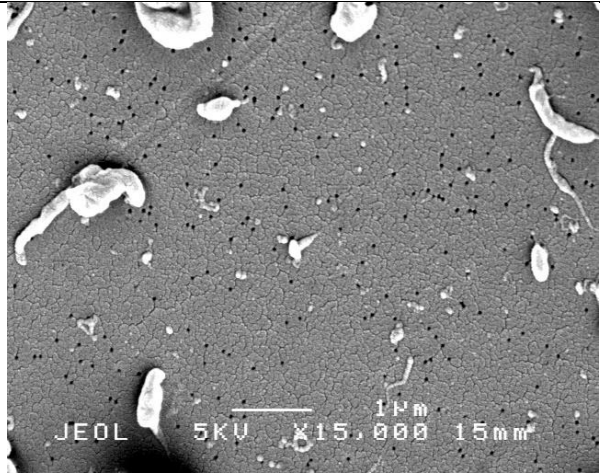
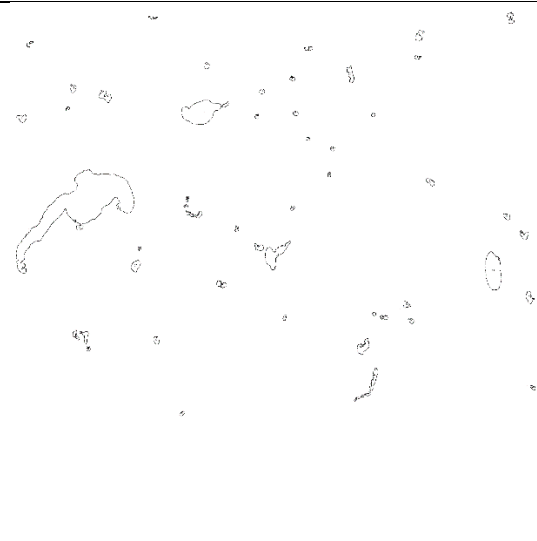


Fig 3.6b: ImageJ rendered outline of particles from CFR-PEEK-on-UHMWPE articulations.





	
<p>Fig 3.9a: Displayed particles from PEEK vs PEEK articulation.</p>	<p>Fig 3.9b: Representative particle outline from PEEK-on-PEEK articulation</p>

### 3.3.2 Particle Size Analysis

Table 3.2 lists the 7 articulations in descending order with regards to ECD. Twenty-one possible permutation of particle types were compared, and the trend was that particles from CoCr-on-UHMWPE ( $0.26\mu\text{m} \pm 0.19\mu\text{m}$  median=  $0.22\mu\text{m}$ ) were significantly larger than all other particle size ( $p < 0.0001$  in all cases), but similar in size to PEEK particles from PEEK-on-PEEK ( $0.24\mu\text{m} \pm 0.19\mu\text{m}$ , median=  $0.20\mu\text{m}$ ) articulations. CoCr-on-PEEK ( $0.20\mu\text{m} \pm 0.16\mu\text{m}$ , median=  $0.16\mu\text{m}$ ) particles were significantly larger than PEEK-on-XLPE ( $0.17\mu\text{m} \pm 0.12\mu\text{m}$ , median=  $0.11\mu\text{m}$ ) particles ( $p < 0.0001$ ) and PEEK-on-UHMWPE ( $0.19\mu\text{m} \pm 0.29\mu\text{m}$ , median=  $0.09\mu\text{m}$ ) particles ( $p < 0.0001$ ). The smallest particles observed were CoCr vs XLPE ( $0.18\mu\text{m} \pm 0.17\mu\text{m}$ , median=  $0.11\mu\text{m}$ ) particles and they were comparable in size to CFR-PEEK vs

UHMWPE ( $0.21\mu\text{m} \pm 0.23\mu\text{m}$ , median=  $0.12\mu\text{m}$ ) particles. Importantly, particles generated from PEEK-on-XLPE articulations were larger than particles from CoCr-on-XLPE ( $p=0.006$ ), but smaller than CoCr-on-UHMWPE articulations ( $p<0.0001$ ). The particle size distribution also varied between particles generated from PEEK-on-XLPE and PEEK-on-UHMWPE articulations, with particles generated from the PEEK-on-UHMWPE articulations being smaller ( $p<0.0001$ ).

Figure 3.10 shows histograms depicting the particle size distribution of the seven analysed articulations with at least 40% of particles from each articulation having an equivalent circle diameter of less than 0.2 micron.

**Table 3.2:** Particle sizes (ECD) of various articulations in descending order

Particle Size				
Articulations	Mean ECD ( $\pm$ SD) $\mu\text{m}$	Median ECD $\mu\text{m}$	Range $\mu\text{m}$	Number of particles
CoCr vs UHMWPE	0.26 ( $\pm$ 0.19)	0.22	0.06 – 1.34	440
PEEK vs PEEK	0.24 ( $\pm$ 0.19)	0.20	0.11 – 2.86	585
CoCr vs PEEK	0.20 ( $\pm$ 0.16)	0.16	0.08 – 1.74	770
PEEK vs XLPE	0.17 ( $\pm$ 0.12)	0.11	0.11 – 0.97	417
PEEK vs UHMWPE	0.19 ( $\pm$ 0.29)	0.09	0.05 – 2.19	431
CFR-PEEK vs UHMWPE	0.21 (0.23)	0.12	0.04 – 1.42	452
CoCr vs XLPE	0.18 ( $\pm$ 0.17)	0.11	0.08 – 1.50	474

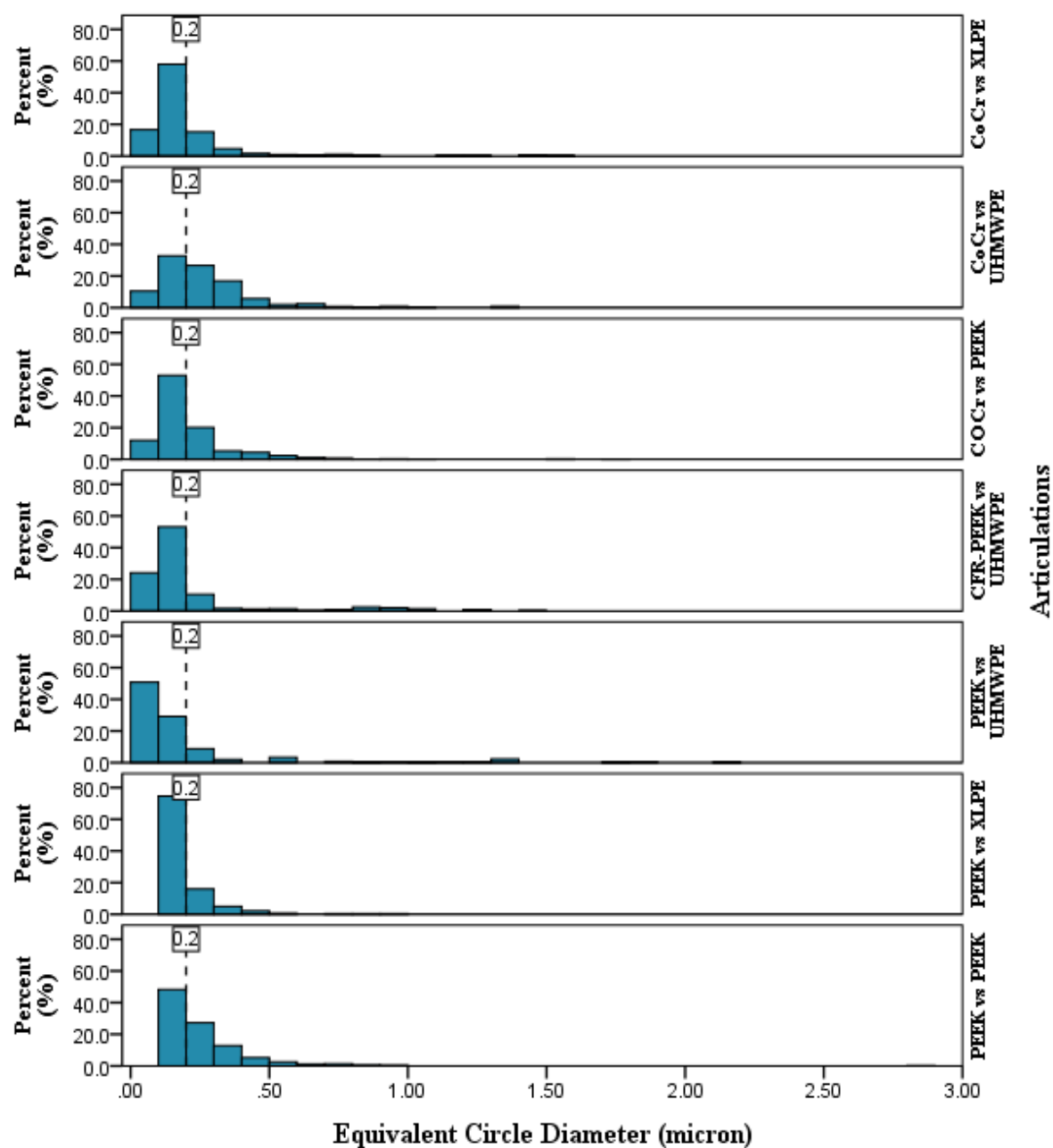


Figure 3.10: Particle sizes (ECD) of analysed wear particles from seven articulations.

### 3.3.3 Particle Morphology

Particles isolated from CoCr-on-polyethylene articulations differed in AR with particles from CoCr-on-XLPE ( $1.70 \pm 0.69$ , median 1.56) articulations being more circular than particles from CoCr-on-UHMWPE ( $1.87 \pm 0.67$ , median 1.67) articulations ( $p < 0.0001$ ). PEEK-on-XLPE ( $1.82 \pm 0.71$ , median 1.62) particles had similar aspect ratio compared to CoCr-on-XLPE and CoCr-on-UHMWPE particles. Particles from CoCr-on-UHMWPE articulations generated the biggest numerical aspect ratio implying more elongated, less circular particles compared to particles from all other articulations ( $p < 0.001$ ) apart from particles from PEEK-on-PEEK ( $1.84 \pm 0.79$ , median 1.62) and PEEK-on-XLPE ( $1.82 \pm 0.71$ , median 1.62) articulations to which they are comparable. Table 3.3 shows the aspect ratio of particles from articulations in a descending order from elongated morphology to a near circular outline.

Analysis of the roundness profile of particles showed a similar trend to AR but in reverse order (Table 3.4). In context, a roundness measure of 1 implies a perfect circle and with deformation of the particle the value of roundness decreases while the aspect ratio increases. Therefore, AR may be seen as a surrogate measure of roundness and vice versa. Of the 21 comparisons possible, the trend was for particles from articulations to differ in form factor in all but 4 comparisons, i.e. CoCr-on-XLPE particles ( $0.56 \pm 0.30$ , median 0.53) versus CoCr-on-UHMWPE particles ( $0.53 \pm 0.21$ , median 0.52), PEEK-on-XLPE ( $0.63 \pm 0.28$ , median 0.62) versus PEEK-on-PEEK ( $0.66 \pm 0.26$ , median 0.65) particles, CoCr-on-PEEK ( $0.42 \pm 0.18$ , median 0.42) versus CFR-PEEK-on-UHMWPE ( $0.41 \pm 0.19$ , median 0.42) particles and CoCr-on-PEEK ( $0.42 \pm$

0.18, median 0.42) versus PEEK-on-UHMWPE ( $0.46 \pm 0.23$ , median 0.39) particles.

Importantly, particles generated from PEEK-on-XLPE were noted to have different form factors compared to the particles from metal on polyethylene articulation ( $p < 0.0001$ ). Table 3.5 depicts the form factor characteristics of each articulation while figure 3.11 highlights the morphological characteristics of each articulation.

**Table 3.3:** Aspect ratio of wear debris, showing mean  $\pm$  SD, median and range

Aspect Ratio				
Articulations	Mean AR ( $\pm$ SD)	Median AR	Range	Number of particles
CoCr vs UHMWPE	1.87 ( $\pm 0.67$ )	1.67	1.01 – 4.70	440
PEEK vs XLPE	1.82 ( $\pm 0.71$ )	1.62	1.04 – 7.62	417
PEEK vs PEEK	1.84 ( $\pm 0.79$ )	1.62	1.02 – 7.36	585
CoCr vs XLPE	1.70 ( $\pm 0.69$ )	1.56	1.03 – 5.54	474
CoCr vs PEEK	1.74 ( $\pm 0.64$ )	1.55	1.03 – 5.67	770
CFR-PEEK vs UHMWPE	1.76 ( $\pm 0.87$ )	1.51	1.03 – 7.76	452
PEEK vs UHMWPE	1.67 ( $\pm 0.68$ )	1.47	1.02 – 5.39	431

**Table 3.4:** Analysis of particle roundness from different bearing couples.

Roundness				
Articulations	Mean Roundness ( $\pm$ SD)	Median Roundness	Range	Number of particles
PEEK vs UHMWPE	0.66 ( $\pm$ 0.17)	0.68	0.19 – 0.98	431
CFR-PEEK vs UHMWPE	0.64 ( $\pm$ 0.19)	0.66	0.13 – 0.97	452
CoCr vs PEEK	0.63 ( $\pm$ 0.17)	0.65	0.18 – 0.97	770
CoCr vs XLPE	0.63 ( $\pm$ 0.18)	0.65	0.18 – 0.97	474
PEEK vs PEEK	0.61 ( $\pm$ 0.18)	0.62	0.13 – 0.99	585
PEEK vs XLPE	0.61 ( $\pm$ 0.19)	0.62	0.13 – 0.97	417
CoCr vs UHMWPE	0.60 ( $\pm$ 0.18)	0.60	0.21 – 0.99	440

**Table 3.5:** Form factor description from each articulation

Form Factor				
Articulations	Mean Form factor ( $\pm$ SD)	Median Form factor	Range $\mu$ m	Number of particles
PEEK vs PEEK	0.66 ( $\pm$ 0.26)	0.65	0.14 – 1.72	585
PEEK vs XLPE	0.63 ( $\pm$ 0.28)	0.62	0.11 – 1.72	417
CoCr vs XLPE	0.56 ( $\pm$ 0.30)	0.53	0.07 – 1.72	474
CoCr vs UHMWPE	0.53 ( $\pm$ 0.21)	0.52	0.13 – 1.00	440
CFR-PEEK vs UHMWPE	0.41 ( $\pm$ 0.19)	0.42	0.07 – 1.15	452
CoCr vs PEEK	0.42 ( $\pm$ 0.18)	0.42	0.02 – 0.98	770
PEEK vs UHMWPE	0.46 ( $\pm$ 0.23)	0.39	0.10 – 1.08	431

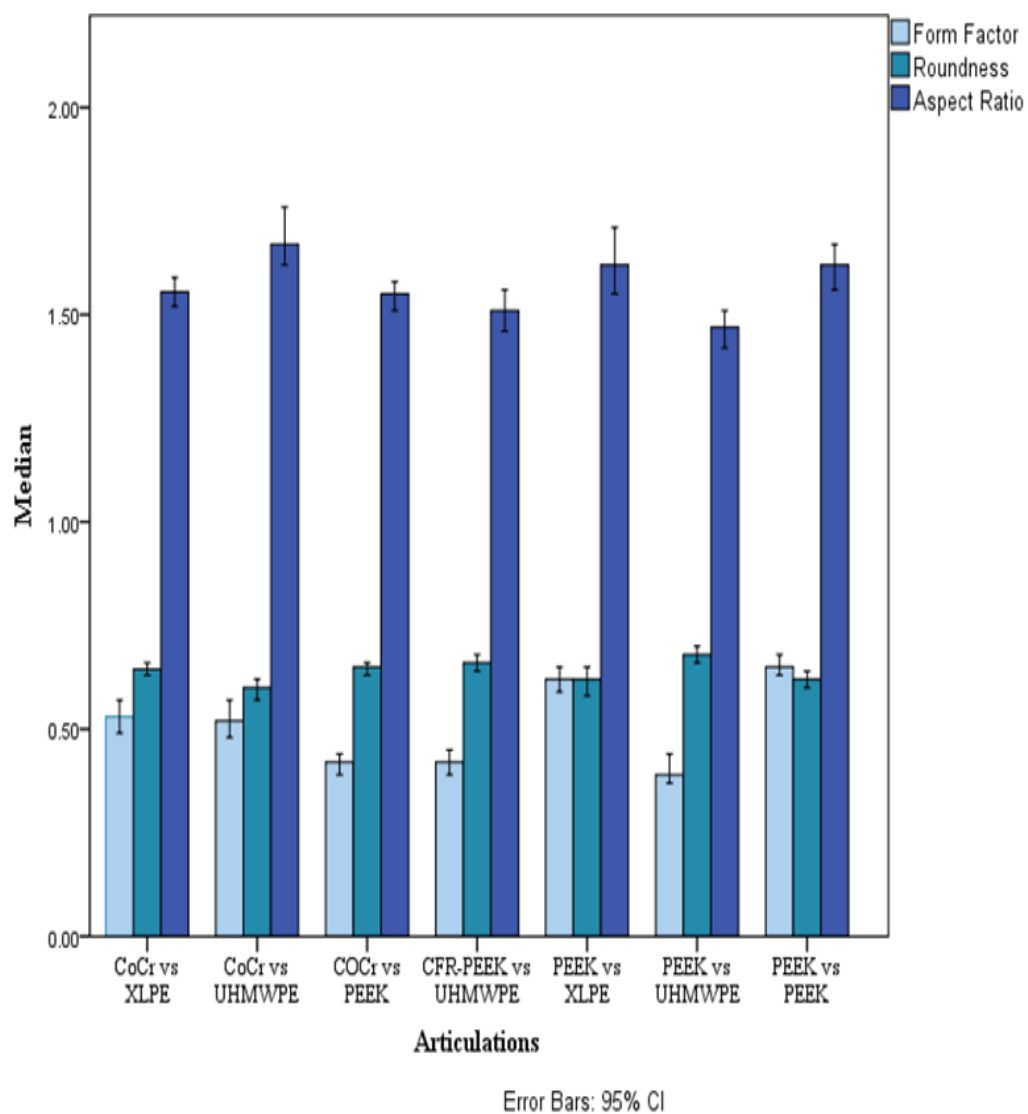


Figure 3.11: Summary of the morphological characteristics of the different articulations.



### 3.3.4 Particle Quantification

Table 3.6 shows the estimated number of particles generated after one million cycles in ascending order based on articulation.

**Table 3.6:** CoCr-on-UHMWPE, PEEK-on-XLPE and CoCr-on-XLPE generated a statistically similar number of wear particles. Asterisks highlight combinations that are statistically different to CoCr-on-XLPE articulations.

Articulations	Lubricant vol. added to methanol (ml)	Estimated number of Particles/ $10^6$ cycles (Mean $\pm$ SD) $\times 10^x$
CoCr vs UHMWPE	2	$187.6 \pm 103.9 \times 10^9$
PEEK vs XLPE	2	$195.7 \pm 80.2 \times 10^9$
CoCr vs XLPE	2	$200.4 \pm 61.2 \times 10^9$
PEEK vs UHMWPE	1	$302.7 \pm 128.4 \times 10^9$ *
PEEK vs PEEK	1	$737.1 \pm 189 \times 10^9$ *
CFR-PEEK vs UHMWPE	0.15	$18.1 \pm 3.7 \times 10^{12}$ *
CoCr vs PEEK	0.05	$20.8 \pm 9.9 \times 10^{12}$ *

PEEK-on-XLPE couples, CoCr-on-XLPE and CoCr-on-UHMWPE showed a statistically similar particle count per million cycles. CoCr-on-XLPE generated more particles compared to CoCr-on-UHMWPE couples, but this did not reach statistical significance. CoCr-on-PEEK and CFR-PEEK-on-UHMWPE generated a statistically similar number of particles and a significantly

increased number compared to other articulations  $p<0.0001$ . PEEK-on-PEEK generated statistically higher number of particles compared to PEEK-on-UHMWPE couples,  $p<0.0001$ .

### 3.3.5 PEEK-XLPE Particle Separation Protocol

Figures 3.12 and 3.13 show SEM images of the proprietary polyethylene (Ceridust 3715) and PEEK (VESTAPEEK UP10) particles respectively. The ceridust particles are viewed as granular, approximately 10 $\mu$ m as supplied. The PEEK particles were also of similar size range, but more irregular compared to the Ceridust particles.

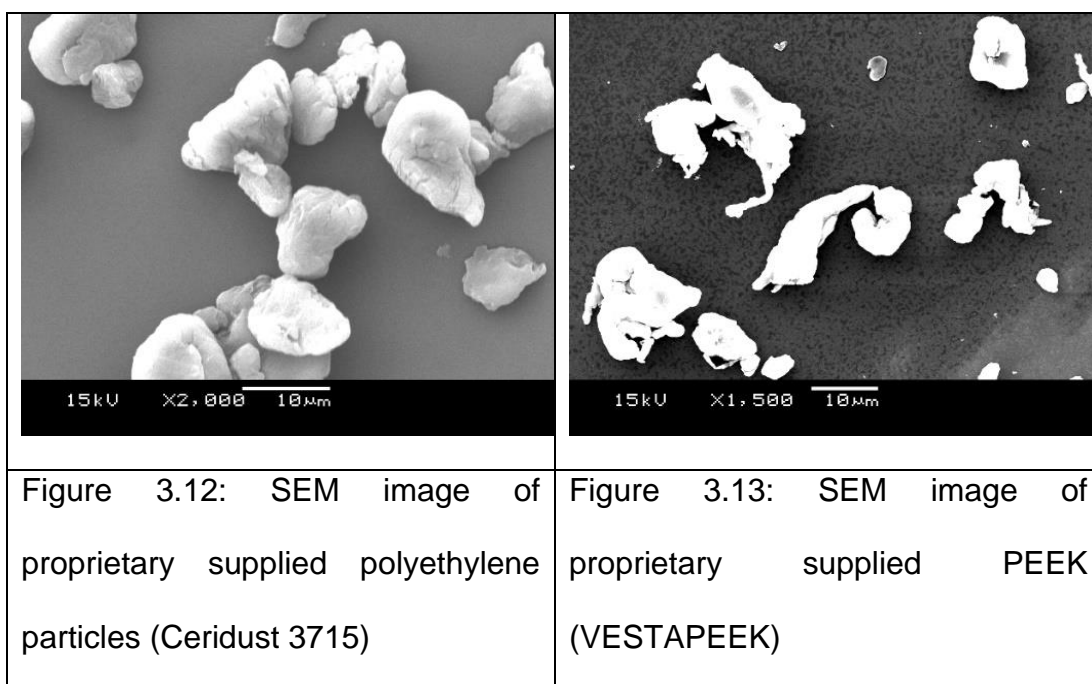


Figure 3.14 shows digested serum containing particles. The serum was reconstituted in a similar fashion to the lubricant fluid used for wear testing described in chapter 2, contained Ceridust and PEEK particles and subjected to the same acid digestion protocol described earlier in this chapter. Figure

3.15 shows digested lubricant layered over chloroform: methanol (ratio 2:1) mixture while Figure 3.16 shows successful separation of particles into 2 distinct portions, after centrifugation. The particle portions were displayed on a polycarbonate filter membrane (Fig 3.17) after careful particle collection, acetone treatment, reconstitution in methanol and vacuum filtration.



Figure 3.14: Digested lubricant containing Ceridust and PEEK powder.



Figure 3.15: Digested lubricant layered over chloroform: methanol mixture (2:1).

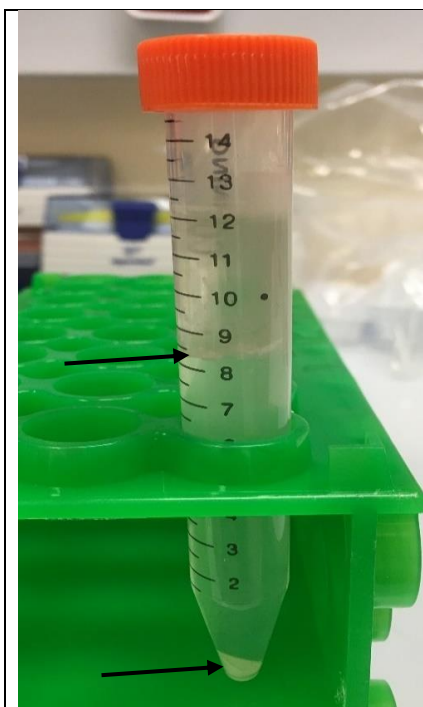


Figure 3.16: Separation into layers after centrifugation



Figure 3.17: Particles collected on to 0.05micron pore filter membrane.

Figures 3.18 and 3.19 show the FT-IR tracing of retrieved ceridust 3715 and plain as received proprietary ceridust 3715 while Figures 3.20 and 3.21 show the FT-IR spectra of retrieved VESTAPEEK and plain as received proprietary VESTAPEEK particles for comparison. With clear similarities in the spectra of samples retrieved after separation and samples of neat polymers as received.

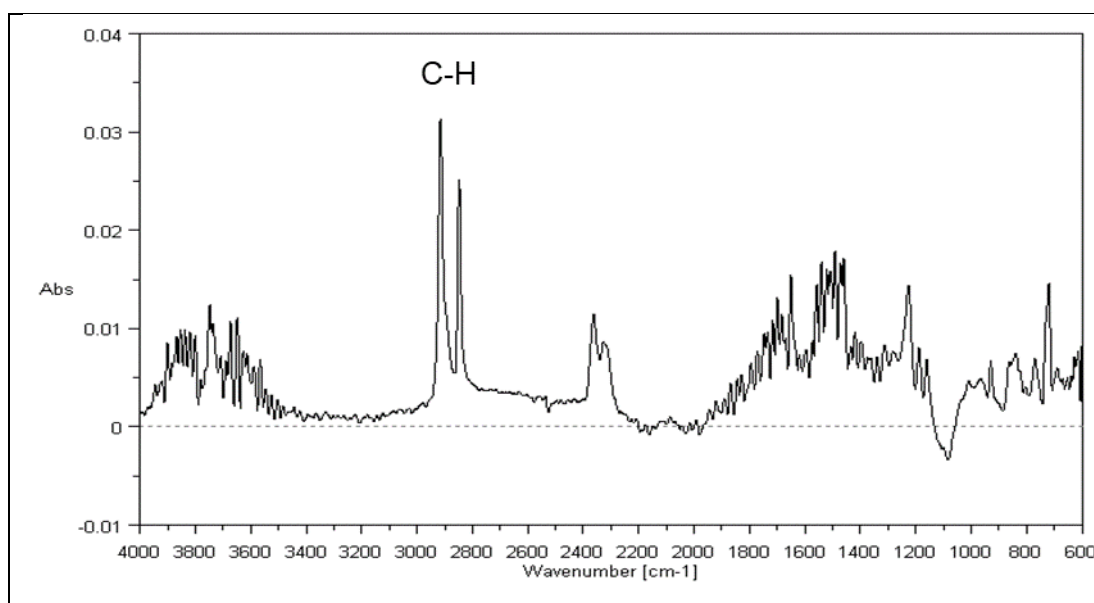


Figure 3.18: Retrieved ceridust with described separation protocol. The double peak at approximately  $2900\text{cm}^{-1}$  is characteristic of the hydrocarbon bond of polyethylene (C-H).

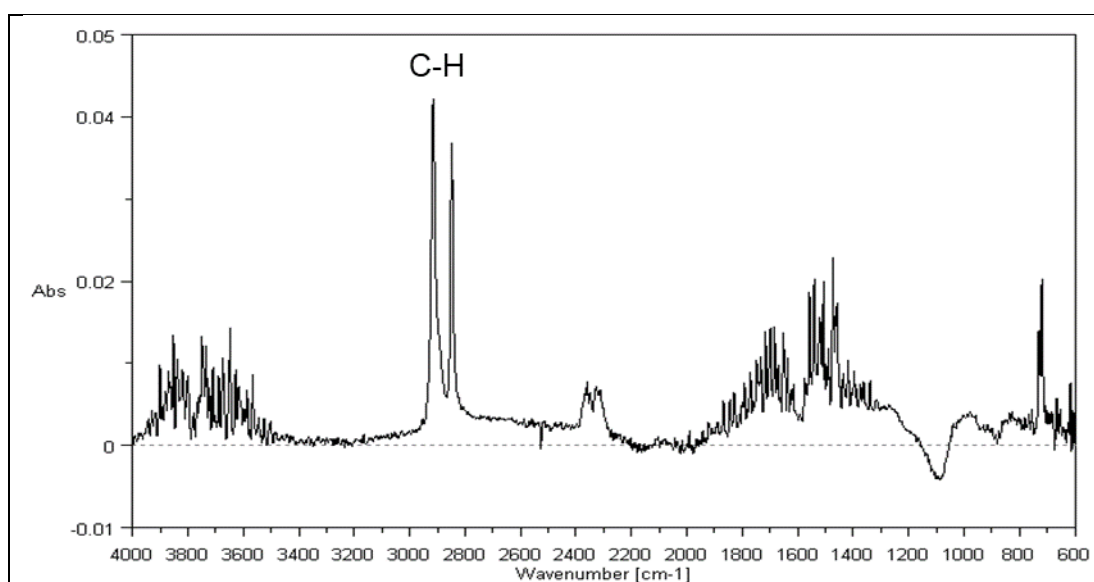


Figure 3.19: FT-IR spectrum of plain ceridust showing similarities to the tracing of retrieved ceridust after separation.

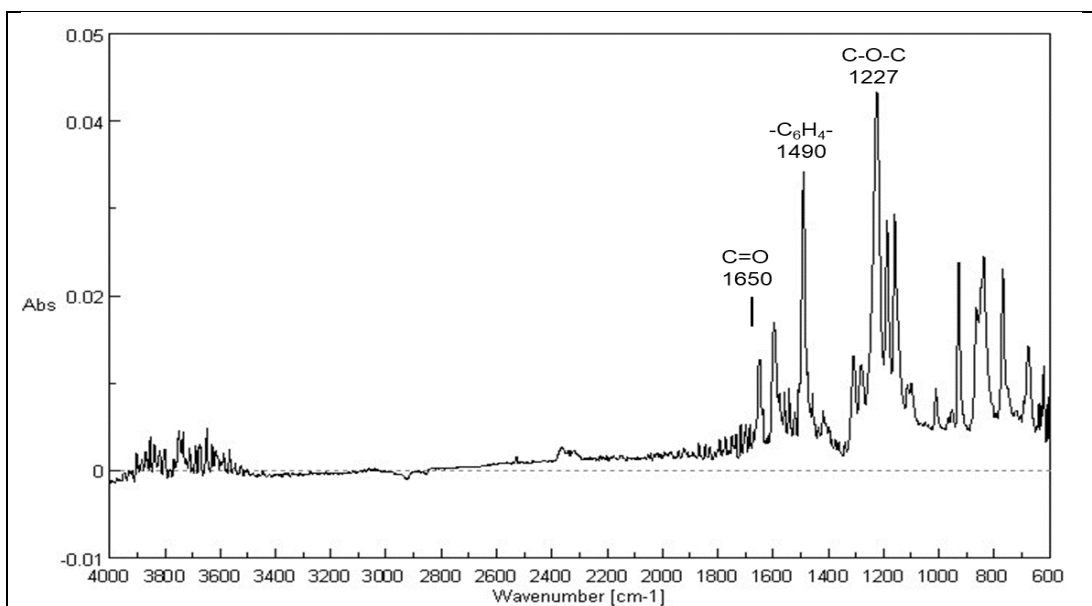


Figure 3.20: FT-IR spectrum of retrieved VESTAPEEK particles after separation. Distinctive features of PEEK spectra exhibited mainly in the fingerprint region showing carbonyl bond (C=O), ether bond (C-O-C) and aromatic benzene ring (-C<sub>6</sub>H<sub>4</sub>-) (Nguyen and Ishida, 1986)

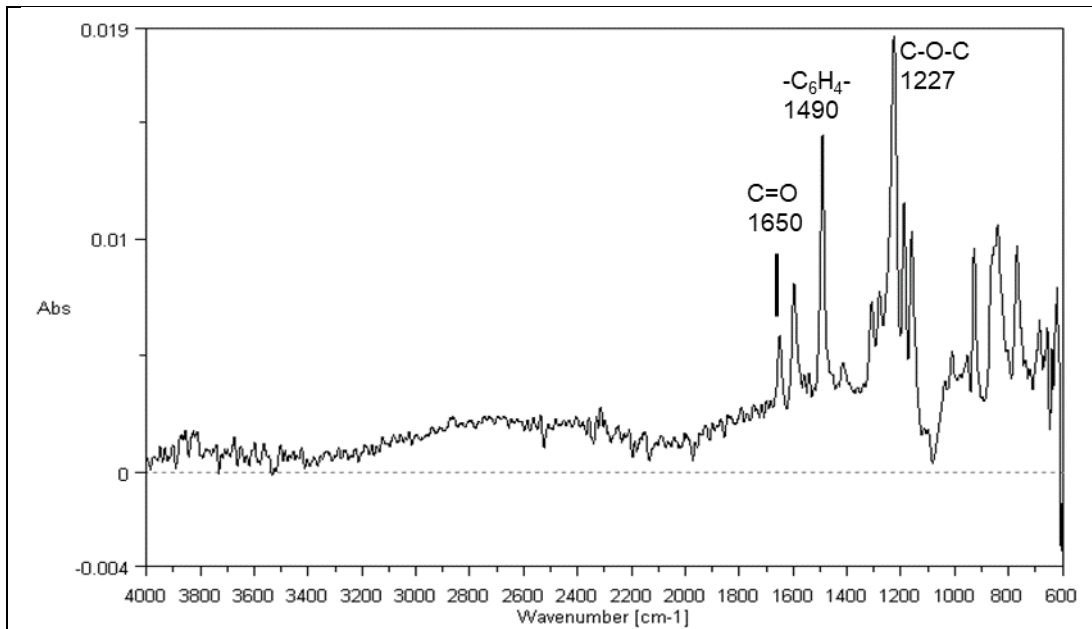


Figure 3.21: FT-IR spectrum of proprietary received VESTAPEEK showing carbonyl bond (C=O), ether bond (C-O-C) and aromatic benzene ring.

### 3.4 DISCUSSION

The findings of the wear debris examination showed significant variations among the different bearing couples with regards to size and shape. These variations may have implications on the inflammatory response to the generated particles. However, one important observation was that particles from PEEK-on-XLPE couples had similar roundness and aspect ratio to particles from metal on polyethylene articulations. Also, the number and size of generated particles from PEEK-on-XLPE articulations were noted to be similar to those from metal on polyethylene articulations. While these observations did not support the hypothesis of lower number of particles from PEEK-on-XLPE articulations it suggests similar biological stimulation of inflammatory cells by particles generated from PEEK-on-XLPE and metal-on-polyethylene articulations, based on similarities in particle number / unit volume and morphology.

The method of isolation of particles as described by Scott was modified for this study (Scott et al., 2005). The quantity of retrieved particles noted for the CoCr-on-polyethylene articulation is similar to what has been reported in the literature. Kretzer reported an estimated  $263 \times 10^9$  particles per million cycles in fixed bearing unicondylar knee designs and  $336 \times 10^9$  in mobile bearing unicondylar designs with conventional low cross-linked ( $\sim 30$ KGy) polyethylene inserts (Kretzer et al., 2011). Using a bicondylar knee design, Williams reported an estimated  $205 \times 10^9$  particles and  $50 \times 10^9$  particles per million cycles with conventional ( $\sim 35$  KGy) and with highly cross-linked ( $\sim 75$ KGy) tibial inserts respectively (Williams et al., 2010). These values are in agreement with numbers reported in this study.

Wear from CoCr surfaces is considered negligible in CoCr-on-polyethylene couples, but some degree of volume loss is expected from the articulating counterfaces in all polymer articulations especially in the long-term. A method was described in this study and the rationale for this separation technique was based on the differential densities of PEEK ( $1.3\text{g/cm}^3$ ) and polyethylene ( $0.93\text{g/cm}^3$ ). Chloroform (density  $1.48\text{g/cm}^3$ ) was mixed with methanol (density  $0.79\text{g/cm}^3$ ) to provide an appropriate medium that permitted differential travel of the 2 particle types with centrifugation. The density of the chloroform: methanol (2:1) mixture is approximately  $1.33\text{g/cm}^3$  (Kijevčanin et al., 2007), higher than that of polyethylene thereby creating dissimilar friction drag for travel down the separating chloroform: methanol column, permitting further excursion of the denser PEEK particles down the column. The distinctive spectrum feature of each particle fraction and the matching similarities between the recovered and respective neat particle fraction confirmed complete separation. Importantly, characterisation of polyethylene using FT-IR identifies a double peak at approximately  $2900\text{cm}^{-1}$  (Shanbhag et al., 1994b, East et al., 2015a), while peaks around  $1655\text{cm}^{-1}$  representing carbonyl stretching vibration and a shoulder at  $1252\text{cm}^{-1}$  are characteristic features of PEEK FT-IR spectrum (Nguyen and Ishida, 1986, Al Lafi, 2014) . One limitation in the development of this technique was that the proprietary particles used for protocol development were larger than the wear particles generated from the wear test signifying the likelihood of more rapid separation of particles based on a higher centrifugal force exerted on the particles. For particles of the size range isolated from the previously described wear test a



higher centrifugation force and duration may be required for particle separation.

Statistically significant variations were noted in morphological characteristics and size measurements among the different articulations investigated. It is not entirely clear whether these small numerical variations, though statistically significant will have clinical relevance. The large sample size (3552 particles in total) offers high statistical power that permits small differences in size and morphological values to be interpreted as significant (Bell, 2018). Green (Green et al., 1998) in determining particle sizes of critical importance in stimulating cellular response examined polyethylene particles with average sizes of 0.21, 0.49, 4.3 and 7.2 $\mu\text{m}$ . An important observation from Green's study was that the particles of size range  $0.21 \pm 0.07\mu\text{m}$  failed to stimulate macrophages to elaborate cytokines significantly above levels noted in controls, likewise the particles in the 7.2 $\mu\text{m}$  size range. This contrasted with the effect noted in particle sizes in the  $0.49 \pm 0.11\mu\text{m}$  and  $4.3 \pm 1.89 \mu\text{m}$  size range, which showed significant effect on cytokine elaboration. The lower range, non-stimulatory particle sizes noted in Green's study are similar to most particles in this study with 72.6% within this size category i.e. below 0.21 $\mu\text{m}$ . In a review (Ingham and Fisher, 2000), polyethylene size range 0.2-0.8 $\mu\text{m}$  was deemed the critical size range necessary for macrophage stimulation. Based on this, it is possible subsets of particle sizes within the 0.2-0.8 $\mu\text{m}$  critical range, may show statistical significance as observed in this study, without necessarily demonstrating differential stimulation of inflammatory cells. Also, Sieving and colleagues (Sieving et al., 2003) investigated the impact of particle shape especially AR and texture on inflammatory response using a rat air

pouch model (Gelb et al., 1994, Ren et al., 2002). Synovial cavity mimicking pouches were created by injecting sterile air at the back of mice. Following injection of particles into these pouches, the number of cellular infiltrates and cytokine levels (TNF- $\alpha$  and IL1 $\beta$ ) as assessed by ELISA were used as measures of cellular response and activity. Particles with AR between 1 – 2.39 were defined as round/ granular while elongated/ fibula shaped particles are defined as particles with AR of between 2.4 – 5. This implies that using Sieving's classification, 85.6% of particles reported in this study would be considered round. The study showed that elongated wear particles elicited substantially higher cytokine levels and cellular infiltrates when compared to the effect of smooth, globular shaped wear particles. While the AR of CoCr-on-XLPE ( $1.70 \pm 0.64$ , median= 1.56) was noted to be statistically different from that of CoCr-on-UHMWPE ( $1.87 \pm 0.67$ , median=1.67), both particle types would be considered as round particles based on Sieving's classification and expected to elicit similar cellular and inflammatory response.

Central to accurate analysis of particulate wear debris is a digestion scheme that effectively isolates wear particles without altering the morphological features of the wear particle. Traditionally, isolation of tissue from retrievals or *in vitro* lubricant fluid is carried out using acid, base or enzymatic digestion followed by SEM analysis of particles (Niedzwiecki et al., 2001, Scott et al., 2005). Enzyme based digestion methods are reported as being ideal for metal particles, as base and acid digestion protocols can affect the morphology of metal particles (Doorn et al., 1998). Polyethylene particles are generally reported as stable to acid, base or enzymatic digestion procedures (Niedzwiecki et al., 2001). Over 40 digestion techniques have been reported

in literature (Baxter et al., 2009) and preference for any particular method depends on effectiveness, cost implications, ease of use and possible effect on particles. Following meticulous particle isolation, image analysis software has also been extensively used to provide precise size and morphological characterisation. Brown (Brown et al., 2011) suggested that SEM analysis may be prone to sampling bias and reported the use of a light scattering technique which permits analysis of the entire sample with particles in suspension. The results of light scattering technique and SEM characterisation were however noted to be comparable.

Some steps in particle characterisation have been reported to have impact on the observed size and morphology. It has been previously reported that filtration through a 0.05µm pore size filter membrane compared to a 0.2µm filter membrane isolated more particles especially of lower size range (Scott et al., 2001), implying larger size filter pores resulted in partial loss of particles. Nanoparticles have been isolated and reported in simulator studies, this feature previously seen in hard on hard bearing (Billi et al., 2012b) has been associated with new approaches and technological novelty, one of such being field emission gun SEM that allows higher magnification and resolution (Tipper et al., 2006, Schroder et al., 2013). Schroder investigated the effect of some of the inherent processes in particle characterisation such as lubricant fluid storage, pore size of filtration membranes, duration of sputter coating and magnification of SEM used in analysis to identify possible pitfalls (Schroder et al., 2013). Magnification was reported as having the greatest effect on measured ECD with mode of wear size distribution decreasing at higher magnification and larger particle size range noted at low magnification.

Furthermore, storage of lubricant especially in the frozen state (-20°C) for 6 months increased ECD and lowered particle roundness compared to lubricant analysed for particles straight out of the wear simulator or particles stored at room temperature for 6 months. A longer duration of sputter coating was also reported to increase particle size however, a recommendation as to an ideal coating time was difficult as too short sputtering time may hinder necessary magnification due to conductivity of the particles.

In conclusion, wear particle analysis is a complex systematic process that can be used to postulate the biological activity of particles. Many factors may influence the wear debris characterisation process. The results from this study are consistent with other tests that have shown that the majority of retrieved particles are less than 1µm in size with a trend towards XLPE particles being smaller compared to UHMWPE particles generated from CoCr-on-polyethylene wear articulations (Fisher et al., 2004, Utzschneider et al., 2009). The reported morphology descriptors and ECD are similar to data reported in the published literature relating to knee simulator tests (Kretzer et al., 2011, Schroder et al., 2013, Utzschneider et al., 2009). Though the ECDs correspond better to the lower end of reported values in the published literature. The wear particles analysed in this study were generated using a unidirectional pin on plate test device with kinematics tailored to that of the knee joint. The similarities between the results from published data and observation from this study confer validity to the study protocol and design. Based on this, it would appear that the biological activity of PEEK-on-XLPE articulation will be similar to those from metal on polyethylene couples.

## **CHAPTER 4: Inflammatory Response to PEEK, XLPE and UHMWPE Particles**

### **4.1 INTRODUCTION**

Polyethylene debris has been shown to instigate a cascade of events culminating in aseptic loosening of implants. Macrophages engulf particulate debris shed into surrounding tissue generated mainly from the articulating surfaces (Shanbhag et al., 1995) and in a bid to breakdown inert polymeric debris, macrophages become activated releasing pro-inflammatory cytokines such as TNF- $\alpha$  and interleukins for example, IL-6, IL-8 and IL-1 $\beta$  (Ingham and Fisher, 2005). These cytokines are osteoclast stimulating resulting in a discrepancy in normal periprosthetic bone metabolism favouring bone breakdown, ultimately leading to implant loosening. Furthermore, wear debris has been shown to have a direct and deleterious effect on mesenchymal stem cells impairing their differentiation into effective osteoblasts (Wang et al., 2002), inhibiting collagen production (Vermes et al., 2001) and initiating osteoblast apoptosis (Pioletti et al., 2002).

The introduction of low wearing alternative bearing surfaces such as metal-on-metal (MoM) and ceramic with a view to reduce debris induced osteolysis has been fraught with other problems; adverse tissue reaction in MoM articulations led to a high failure rate (Haddad et al., 2011), while cost precludes the widespread use of ceramics (Carnes et al., 2016). Presently, data from Joint Registries show that the metal on polyethylene bearing continues to be the most widely used biomaterial combination in joint replacement procedures (National Joint Registry, 2018).

Many *in vitro* and *in vivo* studies have demonstrated the inflammatory potential of particle debris resultant from wear. Histological assessment and grading of observed phagocytic cell reactions in explanted tissue (Revell et al., 1978), *in vitro* cellular responses of phagocytic cells to particulate matter with quantification of liberated soluble cell products (Green et al., 1998) and injection of particle solutions into body cavities of test animals followed by immunohistochemical analysis (Utzschneider et al., 2010b) are among described methodologies published in the literature. Previous assessment of the osteolytic potential of polyethylene particles has shown that particulate material in the phagocytosable size range are most stimulatory of osteoclastogenesis. The generally held belief is that particles less than  $<10\mu\text{m}$  impact a pro-inflammatory effect *in vitro* (Matthews et al., 2000b, Green et al., 2000) with particles in  $0.1\text{-}1.0\mu\text{m}$  size range most stimulatory (Ingham and Fisher, 2005). Particles in the nanometre size range are internalised by pinocytosis and may not activate inflammatory cells to elicit a paracrine effect on osteoclasts (Liu et al., 2015). While there is some agreement about the impact of particle size on the inflammatory cells, there is debate about the ideal particle dose to elicit the observed pro-inflammatory response. Cells respond to particle aspect ratio, surface area and topography as such, using number as a sole method of dosing cells in a cell-particle challenge is not appropriate (Matthews et al., 2000b). Shanbhag proposed the concept of “surface area ratio” i.e. ratio of particle total surface area to cell surface area as a method of standardising dosage (Shanbhag et al., 1994a). One other method proposed by Green and his colleagues suggested a particle volume in the range between

10-100 microns to a cell is effective for monocyte stimulation (Green et al., 1998).

Furthermore, the impact of different material chemistry even if in a similar group e.g. polymeric debris is also controversial. Different polymeric particles may elicit a different reactivity to inflammatory cells. It has been previously suggested that polyurethane particles may be less inflammatory when compared with UHMWPE (Smith and Hallab, 2010, Smith et al., 2010). Size, composition, surface morphology and particle area are factors that have been reported to affect cell reactivity to polymers. Based on this, the cellular response to PEEK particles may vary to that observed in established conventional orthopaedic polymers, notably polyethylene.

Previous studies have assessed the inflammatory response of monocytes challenged with PEEK, UHMWPE and XLPE particles fabricated by cryopulverisation. Cryopulverized particles have sharp edges and the surface chemistry may be different and as such, may not have similar inflammatory effects when compared to particles generated and retrieved from explants or wear testers (Shanbhag et al., 1995). Results from the wear test described in chapter 2 showed that PEEK-on-XLPE bearing couples produced similar wear loss compared to contemporary MoP bearing surfaces. While the majority of wear was noted on the XLPE counterface, it is appropriate to examine the impact of PEEK particles of phagocytosable size generated at a PEEK XLPE bearing as the PEEK particles are likely going to be contributory to the inflammatory response seen if such articulation were used *in vivo*.

The aim of this study was to evaluate the biological response of PEEK particles generated from the wear test carried out in chapter 2 when cultured with human monocytes isolated from peripheral blood. It was hypothesised that PEEK particles will be less inflammatory to human derived monocytes on a particle volume to cell number basis compared to XLPE and UHMWPE derived from a similar source.

The objectives of this study were to:

1. Isolate PEEK, XLPE and UHMWPE particles (0.1-1.0 $\mu$ m size range) and characterise by measuring their form, roundness and aspect ratio using SEM and image analysis techniques.
2. To confirm isolation of monocytes by measuring CD14 cell surface expression using flow cytometry.
3. To remove endotoxin and assess the biological impact of these particles at challenges of 100:1 and 10:1 (particle volume: cell volume) by quantifying the release of pro-inflammatory cytokines IL-1 $\beta$ , IL-6 and TNF $\alpha$  at 12 and 24 hours post particle challenge, comparing monocyte metabolic activity (Alamar Blue Assay at 24 hours) and cell viability using a live/dead assay at 36 hours.

## 4.2 MATERIALS AND METHODS

### 4.2.1 Particle Preparation and characterisation

Lubricant fluid collected immediately after the wear test and stored at -25°C was digested using an acid digestion protocol as described in Chapter 2. An



extra step was added to the digestion protocol to enhance particle collection; equal volumes of the digested lubricant and chloroform: methanol solution (2:1) was agitated over a 12-hour period in 50 ml falcon tubes (Sigma Aldrich, Dorset, UK). The mixture was then centrifuged at 2000 rpm for 5 minutes. Particles were collected at the interface between the water miscible methanol with lubricant layer and the immiscible chloroform layer. The particle layer was carefully collected by aspiration, washed and resuspended in methanol. Particles were then sequentially filtered through a 10 $\mu$ m pore membrane (Cyclopore track etched Whatman, NJ, USA) and a 1 $\mu$ m filter membrane (Cyclopore track etched Whatman, NJ, USA) and collected on a 0.1 $\mu$ m pore filter membrane (Nucleopore track etched Whatman, NJ, USA). SEM images (JSM 5500, JEOL, UK) of particles were characterised using image analysis software (ImageJ, NIH, Maryland, USA). Minimum of 10 random regions were imaged per group. Particle morphology was assessed using form factor (FF), aspect ratio (AR) and roundness (R), while equivalent circle diameter (ECD) was used as a measure of particle size.

#### **4.2.2 Depyrogeneration of Particles**

Glassware used at this stage of the experiment were treated with dry heat at 250°C for 30 minutes to eliminate absorbed pyrogen (Hecker et al., 1994). Filter membranes were pre-weighed using a balance with resolution of 0.01mg and autoclaved for sterilisation and procedures were carried out in class II laminar flow hoods. The depyrogenation method as described by Girot and associates (Girot et al., 1990) was modified for particle depyrogenation.

Particles collected on filter membrane were agitated in endotoxin free glass jars containing 30ml of endotoxin free water (LAL reagent water, Lonza, UK) for 1 hour, after which filters were dried and prepared for SEM examination to confirm complete removal of particles from the filter membrane into solution. Seventy (70) mls of absolute ethanol was then added to the endotoxin free water to make 70% ethanol. Sodium hydroxide (NaOH) pellets were added to this solution to make a 0.2M solution. The 70% ethanol-0.2M NaOH solution containing particles was agitated for 3 hours in an ultrasonic shaker. The particle containing solution was then neutralised using 0.2M hydrochloric acid (HCl) prior to filtration as the membrane filters are not resistant to NaOH treatment. Particles were washed with copious volumes of endotoxin free PBS (Gibco DPBS, Life Technologies, UK) until the pH of the effluent fluid measured between 7.3-7.4. Particles collected on the membrane filter were then left to dry for a 6-hour period and then weighed. The weight of sterile, endotoxin free particles on filter membrane was then determined by subtraction. Particles were then suspended in monocyte culture medium in appropriate particle volume to cell number ratio as described in section 4.2.5.

#### **4.2.3 Endotoxin testing using Gel Clot Limulus Amoebocyte Lysate (LAL) Assay**

The gel clot Limulus Amoebocyte Lysate assay (LAL Pyrogen Plus, Lonza, USA) with sensitivity of 0.06EU/ml was used to verify the presence or absence of endotoxin in solution containing particles at the concentration to be applied to monocyte culture. The gel clot technique is one of the methods of bacterial

endotoxin testing based on the formation of a clot when lysate reagent and endotoxin interact. Tests were conducted to confirm the sensitivity of labelled lysate, validity of the test (Table 4.1) and to assess for the possibility of interfering factors as part of preparatory testing before performing the LAL testing (Table 4.2). The labelled sensitivity of the lysate is defined as the minimum endotoxin concentration required to clot the reconstituted lysate under standard conditions, while the test is considered valid if the lowest concentration of standard endotoxin dilutions show a negative result in all repeat tests.

**Table 4.1:** Showing set-up for assessment of test sensitivity and validity

Endotoxin Standard (EU/ml)	Diluent	Replicates
1.0	LAL Reagent Water	2
0.5	LAL Reagent Water	2
0.25	LAL Reagent Water	2
0.12 (2 $\times$ )	LAL Reagent Water	2
0.06 ( $\times$ )	LAL Reagent Water	2
0.03 (0.5 $\times$ )	LAL Reagent Water	2
0.015 (0.25 $\times$ )	LAL Reagent Water	2

**Table 4.2:** Setup for evaluating test interference.

Test	Diluent	Replicates
2λ	Sample 1 (PEEK 100:1)	2
2λ	Sample 2 (PEEK 10:1)	2
2λ	Sample 3 (XLPE 100:1)	2
2λ	Sample 4 (XLPE 10:1)	2
2λ	Sample 5 (UHMWPE 100:1)	2
2λ	Sample 6 (UHMWPE 10:1)	2

Equal volumes (100μL) of particle stock solution and reconstituted LAL were incubated at 37°C ± 1°C in a heating block for 60 minutes. After this, test tubes were inverted through 180 degrees to assess the integrity of formed gel, if any. A firm clot at the base of the tube that maintains its integrity upon inversion of the tube is indicative of a positive result, any other observation is considered a negative result (Appendix 1.6).

#### **4.2.4 Cells**

Human monocytes were used to assess the biological response to particles. Intravenous blood was obtained from 3 healthy volunteers. Blood samples were collected following UCL Ethics Committee approval and informed consent was obtained prior to venepuncture. The peripheral blood

mononuclear cell (PBMC) fraction was isolated (Appendix 1.7) by layering diluted whole blood over Ficoll-Paque density gradient media (Sigma Aldrich, Dorset, UK) using SepMate™ tubes (Stemcell™ Technologies, Cambridge, UK). The isolated PBMCs were resuspended in monocyte culture medium. The monocyte medium used contained RPMI 1640 without L-glutamine (Sigma Aldrich, Dorset, UK), 10% v/v heat treated foetal calf serum (First Link Ltd, UK), 100u/ml penicillin/streptomycin (Invitrogen Corporation, Paisley, UK), 2mM Glutamine and 15mM HEPES. After 2 hours of incubation in a 75cm<sup>2</sup> vented cell culture flask (Corning, USA) kept at 37°C in a humidified incubator with 5% (v/v) CO<sub>2</sub> in air, non-adherent cells were washed off using Hank's balanced salt solution (Sigma Aldrich, Dorset, UK). This process eliminated non-adherent PBMCs (lymphocytes) and non-viable monocytes. Adherent monocytes were then retrieved using non-enzymatic cell dissociation solution (Sigma Aldrich, Dorset, UK). A Trypan Blue exclusion viability assay was carried out to establish cell yield, viability of monocytes and count for culture.

#### **4.2.4.1 Flow Cytometry – Analysis of cells for CD14+ Expression**

Aliquots of the isolated cells were analysed for their surface expression of CD14+ using flow cytometry (Appendix 1.8). Approximately 20,000 cells isolated from each of the volunteers were analysed. The cells were labelled with Anti-Human CD14 APC (Affymetrix eBioscience, Vienna, Austria) and Mouse IgG1 kappa isotype APC (Affymetrix eBioscience, Vienna, Austria) as isotype control. The CD expression was compared to the isotype control. For flow cytometric examination, cells were fixed in 4% formaldehyde for 15

minutes at room temperature, then washed with 0.5% Bovine serum albumin (BSA), stained with the conjugated primary antibody or isotype control for 1 hour at room temperature in the dark. After an hour, the cells were washed with 0.5% BSA, resuspended in PBS and analysed with a flow cytometer (Cytoflex, Beckman Coulter) based on their side and forward scatter features, and their allophycocyanin (APC) fluorescence.

#### **4.2.5 Particle Preparation for Cell-Particle Challenge**

Two cell-particle challenges were investigated in this chapter and these were a (1) 100:1 and (2) a 10:1 particle volume to monocyte number ratio. In order to obtain a cell concentration of  $1 \times 10^5$  cells/well, a particle volume of  $1.0 \times 10^7 \mu\text{m}^3$  or  $1.0 \times 10^6 \mu\text{m}^3$  was required for each well in a 100:1 or 10:1 particle volume to cell number ratio respectively. The required mass of particles per well was estimated based on particle density. The density of UHMWPE and XLPE is approximately  $0.93 \mu\text{g}/\mu\text{m}^3$  while the density of PEEK is  $1.3 \mu\text{g}/\mu\text{m}^3$ . The required mass of wear particulate debris per well was estimated using the following equation based on density and volume.

Mass of wear debris (UHMWPE or XLPE) = Density x particle volume

For 100:1 UHMWPE or XLPE concentration =  $1.0 \times 10^7 \mu\text{m}^3 \times 0.93 \mu\text{g}/\mu\text{m}^3 \times 10^{-6}$

=  $9.3 \mu\text{g}/\text{well}$

For 10:1 UHMWPE or XLPE concentration =  $1.0 \times 10^6 \mu\text{m}^3 \times 0.93 \mu\text{g}/\mu\text{m}^{-3} \times 10^{-6}$

$$= 0.93 \mu\text{g}/\text{well}$$

Mass of wear debris (PEEK) = Density x Particle volume

For 100:1 PEEK concentration =  $1.0 \times 10^7 \mu\text{m}^3 \times 1.3 \mu\text{g}/\mu\text{m}^{-3} \times 10^{-6}$

$$= 13.0 \mu\text{g}/\text{well}$$

For 10:1 PEEK concentration =  $1.0 \times 10^6 \mu\text{m}^3 \times 1.34 \mu\text{g}/\mu\text{m}^{-3} \times 10^{-6}$

$$= 1.30 \mu\text{g}/\text{well}$$

0.5% percent (weight/volume) agarose (low melting point, Sigma Aldrich, UK) was prepared by autoclaving 500mg agarose in 100mls of monocyte culture medium at 121°C for 15 minutes. Following the estimation of mass of polymer needed per well as described above, stock solutions of particles were prepared such that 133μL contained the mass of particles needed in each well. 67μL of sterile 0.5% agarose was then mixed with the required particle stock/well to make a 200μL of agarose particle mixture per well. The particle-agarose mixture was added to 48 well plate in duplicates (Table 4.3).

#### **4.2.6 Monocyte-Particle challenge.**

Monocytes ( $1 \times 10^5$ ) were seeded into non-tissue culture treated sterile 48 well plates (Corning, USA) containing 200μL of agarose-particle mixture at a concentration of 100:1 and 10:1 (particle volume  $\mu\text{m}^3$ : cell number). Wells

treated with 0.1ng/ml LPS were used as positive controls and cells seeded on agarose gel without particles were negative controls (Table 4.3).

#### Experimental set-up:

**Table 4.3:** Test setup in sterile 48 well plate, colour coding represents each participant.

	1	2	3	4	5	6	7	8
A	100:1 PEEK. (12.24)		100:1 UHMWP. (12.24)		Negative control		10:1 XLPE. (12.24)	
B	100:1 PEEK. (12.24)		100:1 UHMWP. (12.24)		Negative control		10:1 XLPE. (12.24)	
C	100:1 PEEK. (12.24)		100:1 UHMWP. (12.24)		Negative control		10:1 XLPE. (12.24)	
D	100:1 XLPE. (12.24)		Positive control		10:1 PEEK. (12.24)		10:1 UHMWP. (12.24)	
E	100:1 XLPE. (12.24)		Positive control		10:1 PEEK. (12.24)		10:1 UHMWP. (12.24)	
F	100:1 XLPE. (12.24)		Positive control		10:1 PEEK. (12.24)		10:1 UHMWP. (12.24)	

The control groups investigated were:

1. Culture medium + Agarose (no particles) + LPS + cells – positive control.
2. Culture medium + Agarose (no particles) + cells – negative control.

The culture plate was then incubated in humidified 5% (v/v) CO<sub>2</sub> in air at 37°C. Supernatant from cell culture plates were collected at 12 hours and 24 hours and stored at -20°C prior cytokine evaluation.



## **4.2.7 Assessment of Cell Activity**

### **4.2.7.1 Monocyte Metabolic Activity**

An Alamar Blue Assay (Bio-Rad Antibodies, Kidlington, UK) was used to measure cell metabolism on completion of the particle challenge test (Appendix 1.9). 10% Alamar Blue in monocyte culture medium was added to each well, following a 12-hour incubation period excitation at 560nm and emission at 590nm were measured using a Tecan plate reader (Tecan, Infinite Pro Series, Switzerland).

### **4.2.7.2 Monocyte Viability**

Wells containing agarose gel and cells were washed with phosphate buffered saline (PBS) thrice. Cells on agarose gel within the wells were then incubated with a solution of 2 $\mu$ M Calcein AM and 4 $\mu$ M Ethidium homodimer-1 (Live/Dead Viability kit, Invitrogen Molecular Probes™) for 30 minutes in the dark. Gel was then smeared on glass slides for cell visualisation using a widefield fluorescence microscope (Apotome, Zeiss, Germany).

### **4.2.7.3 Cytokine Analysis**

Tumour necrosis factor alpha (TNF- $\alpha$ ), interleukin six (IL-6), and interleukin one beta (IL-1 $\beta$ ) levels were determined using an enzyme-linked immunosorbent assay (ELISA) – protocol included (Appendix 1.10). Absorbance was read at 450nm and cytokine concentration expressed as pg/ml.

#### 4.2.7.4 Phagocytosis and Particle Uptake

After 24 hours of particle co-culture with monocytes, cells were retrieved from gel surfaces, stained with Trypan blue to identify viable cells. The viable cells were then examined using polarised light to determine the presence of particles within viable cells. Polarised light examination was based on the birefringent properties of PEEK and polyethylene particles.

#### 4.2.8 Statistical Analysis.

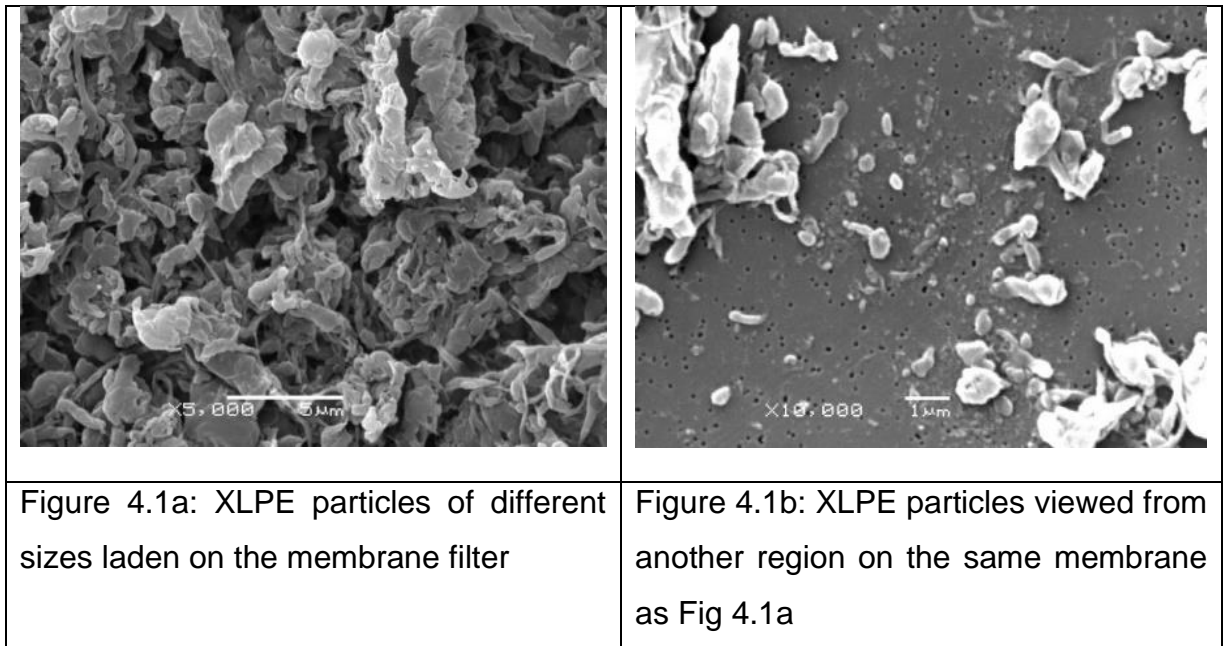
Data was analysed using SPSS, version 22 for Windows (Chicago, USA). The data did not fit the assumptions for parametric testing based on a Kolmogorov-Smirnov test ( $p < 0.05$ ). Non-parametric analysis using a Kruskal Wallis test was conducted to assess for differences between groups. When significance was noted analysis using the Mann-Whitney U test with a post hoc Bonferroni adjustment was carried out. This was necessary because as the number of comparisons increased there was an inflation in type 1 error (increase false positive result). A 5% false discovery rate was used and threshold for significance reduced for every paired comparison. Data was presented as mean  $\pm$  standard deviation.

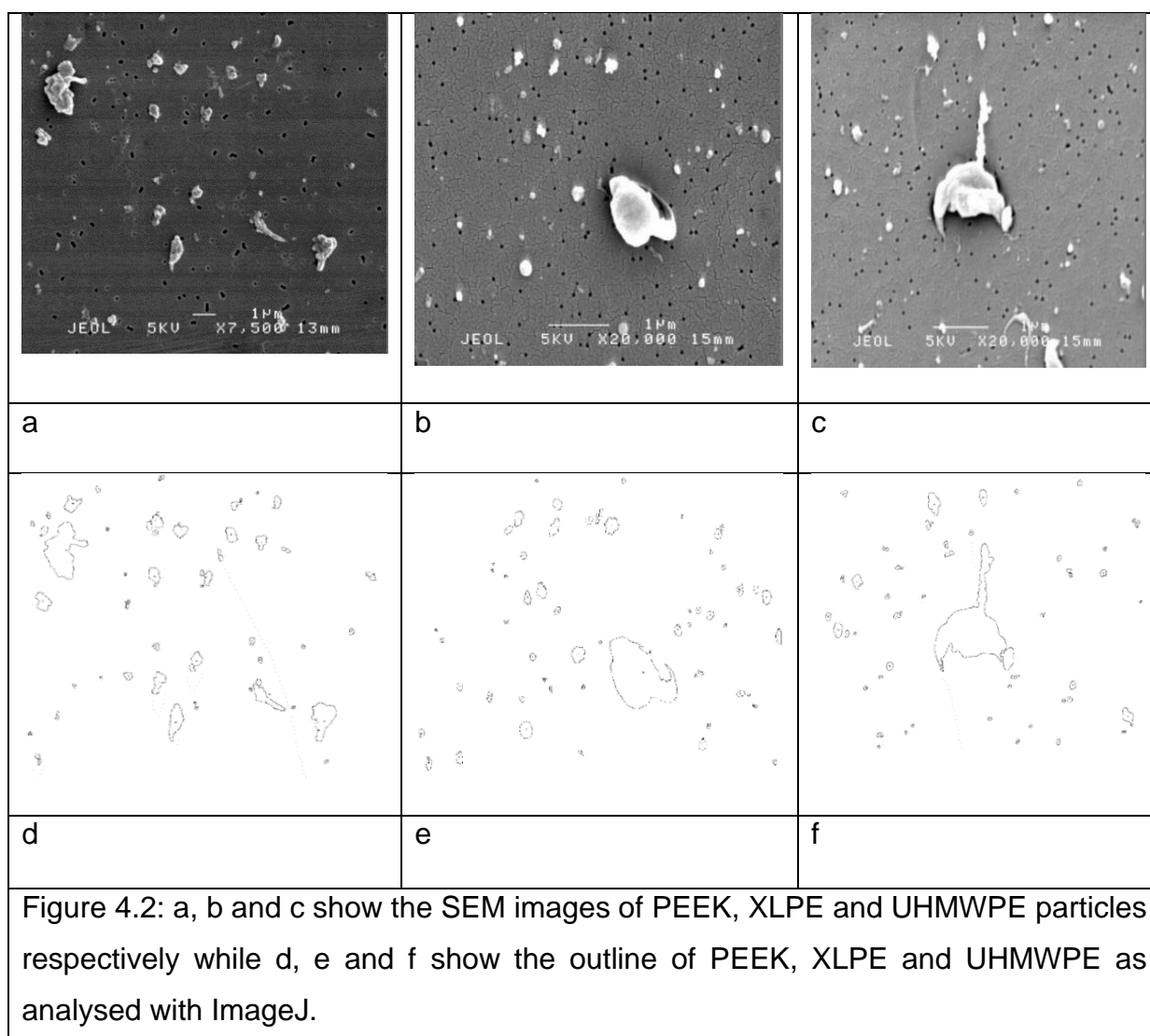
### 4.3 RESULTS

#### 4.3.1 Particle Isolation and Characterisation

Images of particles collected as demonstrated in Figure 4.1 (a and b) shows the effectiveness of the acid digestion test developed and used in this chapter.

This technique was found particularly useful in collecting large quantities of particles as the original description entailed diluting 1ml of digested lubricant in 100ml of methanol. For this test over 1 litre of digested lubricant fluid was used for each particle type. Figure 4.2 shows particle distribution after sequential filtration through 10 micron and 1 micron pore filter membranes.





### 4.3.2 Particle Size Distribution

The size distribution and morphology of analysed particles is shown in figure 4.3 and figure 4.4 respectively. A minimum of 200 particles were characterised by ImageJ (NIH, Maryland, USA) after images of the particles were taken using SEM. More than 80% of each particle type measured less than 0.5micron (Fig 3). These sizes are of within the phagocytosable range and considered those with the most inflammatory potential.

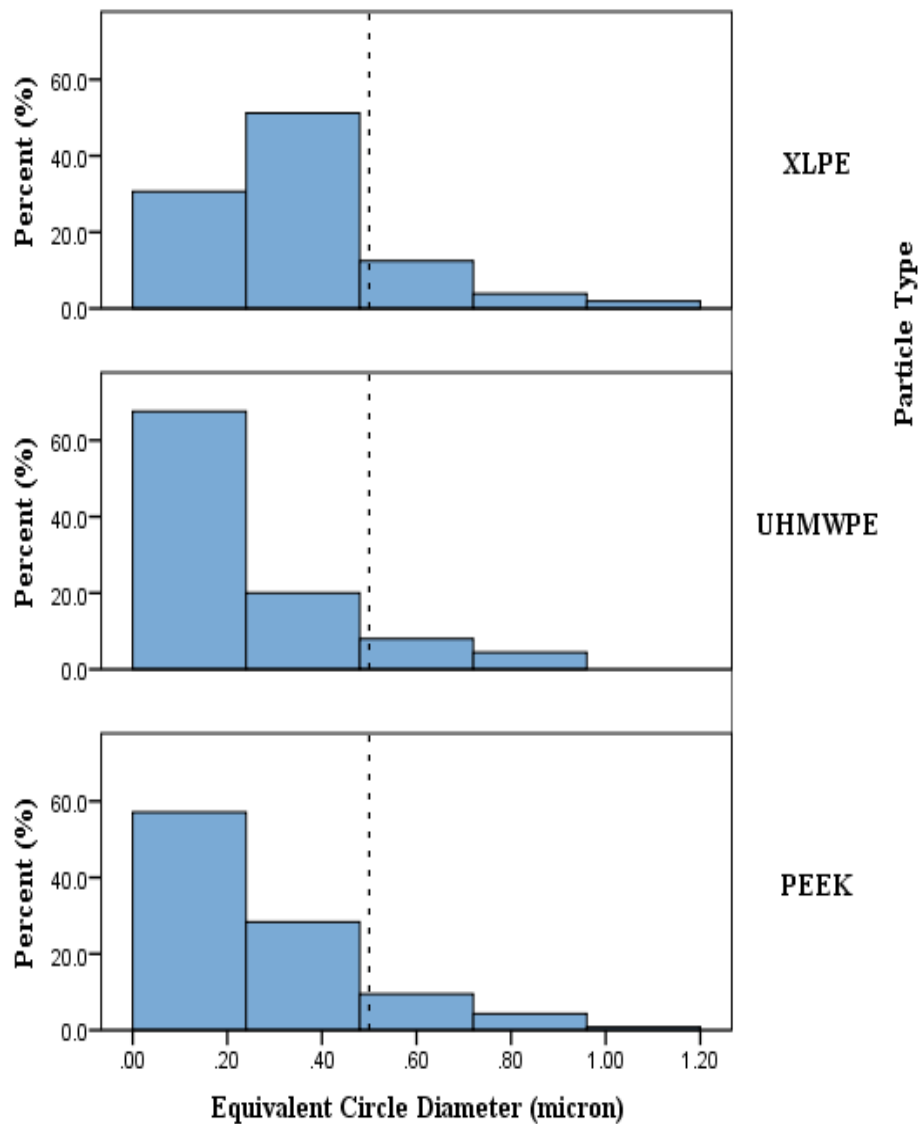


Figure 4.3: Histograms showing the particle size range for XLPE, UHMWPE and PEEK.

The size range of particles were  $0.11\mu\text{m} - 1.02\mu\text{m}$  for PEEK,  $0.11\mu\text{m} - 0.92\mu\text{m}$  for UHMWPE and  $0.11\mu\text{m} - 1.04\mu\text{m}$  for XLPE. The observed mean particle size for PEEK, UHMWPE and XLPE particles after filtration through a micron pore filter membrane was  $0.28\mu\text{m} \pm 0.19\mu\text{m}$ ,  $0.25\mu\text{m} \pm 0.18\mu\text{m}$ ,  $0.34\mu\text{m} \pm 0.19\mu\text{m}$  respectively. A statistically significant difference was noted in particle

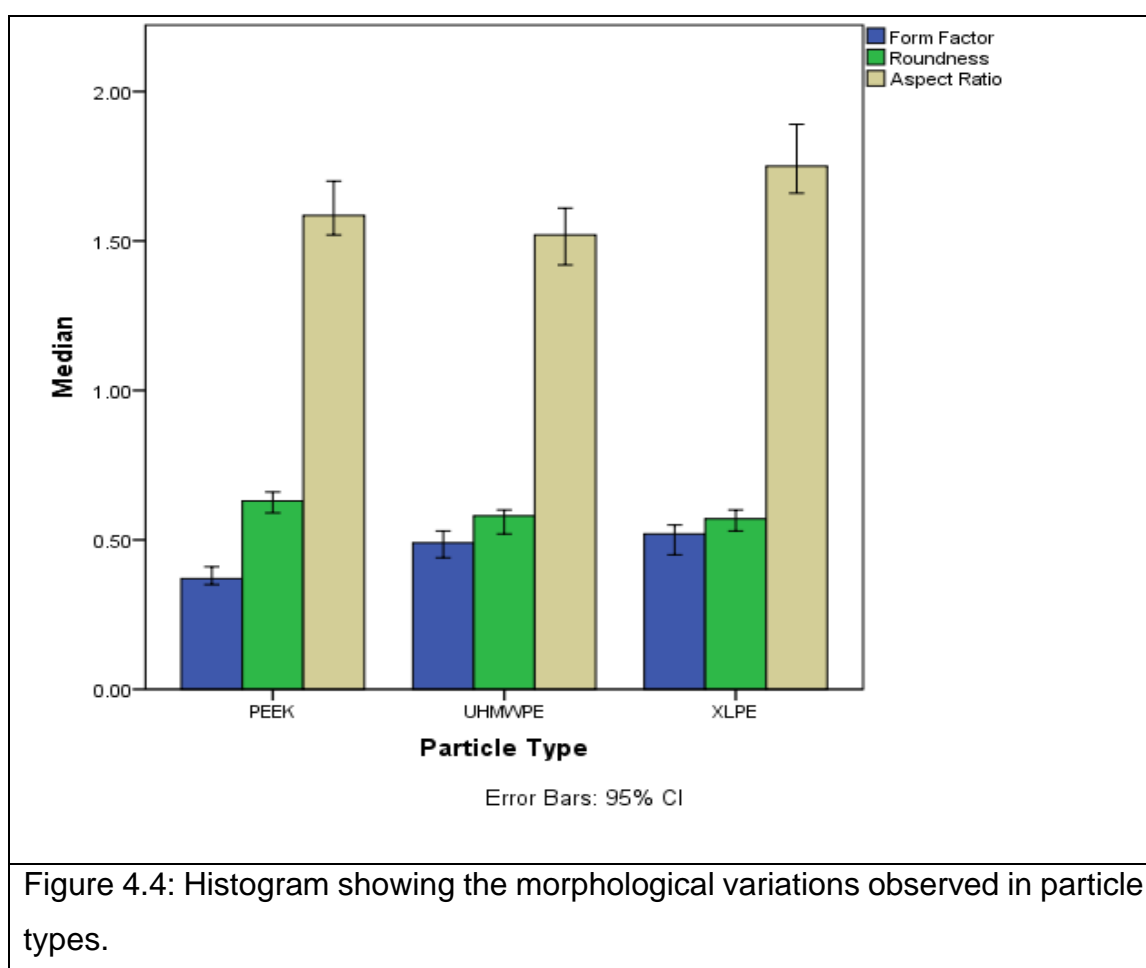
size distribution between groups with XLPE particles larger than UHMWPE and PEEK particles ( $p < 0.0001$ ).

With regards aspect ratio, XLPE particles ( $2.11\mu\text{m} \pm 1.03\mu\text{m}$ ) exhibited a statistically more elongated profile compared to UHMWPE particles ( $1.56\mu\text{m} \pm 0.8\mu\text{m}$ ) and PEEK particles ( $1.82\mu\text{m} \pm 0.8\mu\text{m}$ ) with  $p$  values of  $<0.0001$  and  $0.001$  respectively. PEEK particles were also longer than UHMWPE particles,  $p=0.017$ .

The roundness analysis showed that PEEK particles ( $0.62\mu\text{m} \pm 0.19\mu\text{m}$ ) were more circular compared to UHMWPE particles ( $0.55\mu\text{m} \pm 0.24\mu\text{m}$ ),  $p=0.003$  and XLPE particles ( $0.56\mu\text{m} \pm 0.2\mu\text{m}$ ),  $p=0.001$  while UHMWPE and XLPE particles were observed to have similar roundness values.

The form factor of PEEK particles ( $0.42\mu\text{m} \pm 0.23\mu\text{m}$ ) differed significantly to form factors of UHMWPE ( $0.74\mu\text{m} \pm 0.7\mu\text{m}$ ) and XLPE particles ( $0.5\mu\text{m} \pm 0.21\mu\text{m}$ ),  $p<0.0001$ . However, XLPE and UHMWPE showed similar form factors.

Essentially, the distribution of PEEK morphological parameters was statistically different to those observed in the polyethylene subtypes and the polyethylene subtypes were similar in all but aspect ratio where XLPE particles were noted to be longer than UHMWPE particles.



### 4.3.3 Endotoxin testing

Results of endotoxin testing are shown in Tables 4.4 and 4.5. Validity was confirmed as the lowest dilution of endotoxin standard incubated with LAL lysate showed negative results in test replicates. The sensitivity of the test kit was also confirmed as the minimum required endotoxin standard needed to clot the lysate corresponded to the labelled sensitivity of 0.06EU/ml ( $\lambda$ ).

**Table 4.4:** Endotoxin standard incubated with lysate

Endotoxin Standard (EU/ml)	Diluent	Replicates	Result 1	Result 2
1.0	LAL Reagent Water	2	Positive	Positive
0.5	LAL Reagent Water	2	Positive	Positive
0.25	LAL Reagent Water	2	Positive	Positive
0.12 (2 $\times$ )	LAL Reagent Water	2	Positive	Positive
0.06 ( $\times$ )	LAL Reagent Water	2	Positive	Negative
0.03 (0.5 $\times$ )	LAL Reagent Water	2	Negative	Negative
0.015 (0.25 $\times$ )	LAL Reagent Water	2	Negative	Negative

**Table 4.5:** Positive product control (PPC) incubated with lysate

Test	Diluent	Replicates	Result 1	Result 2
2 $\times$	Sample 1 (PEEK 100:1)	2	Positive	Positive
2 $\times$	Sample 2 (PEEK 10:1)	2	Positive	Positive
2 $\times$	Sample 3 (XLPE 100:1)	2	Positive	Positive
2 $\times$	Sample 4 (XLPE 10:1)	2	Positive	Positive
2 $\times$	Sample 5 (UHMWPE 100:1)	2	Positive	Positive
2 $\times$	Sample 6 (UHMWPE 10:1)	2	Positive	Positive



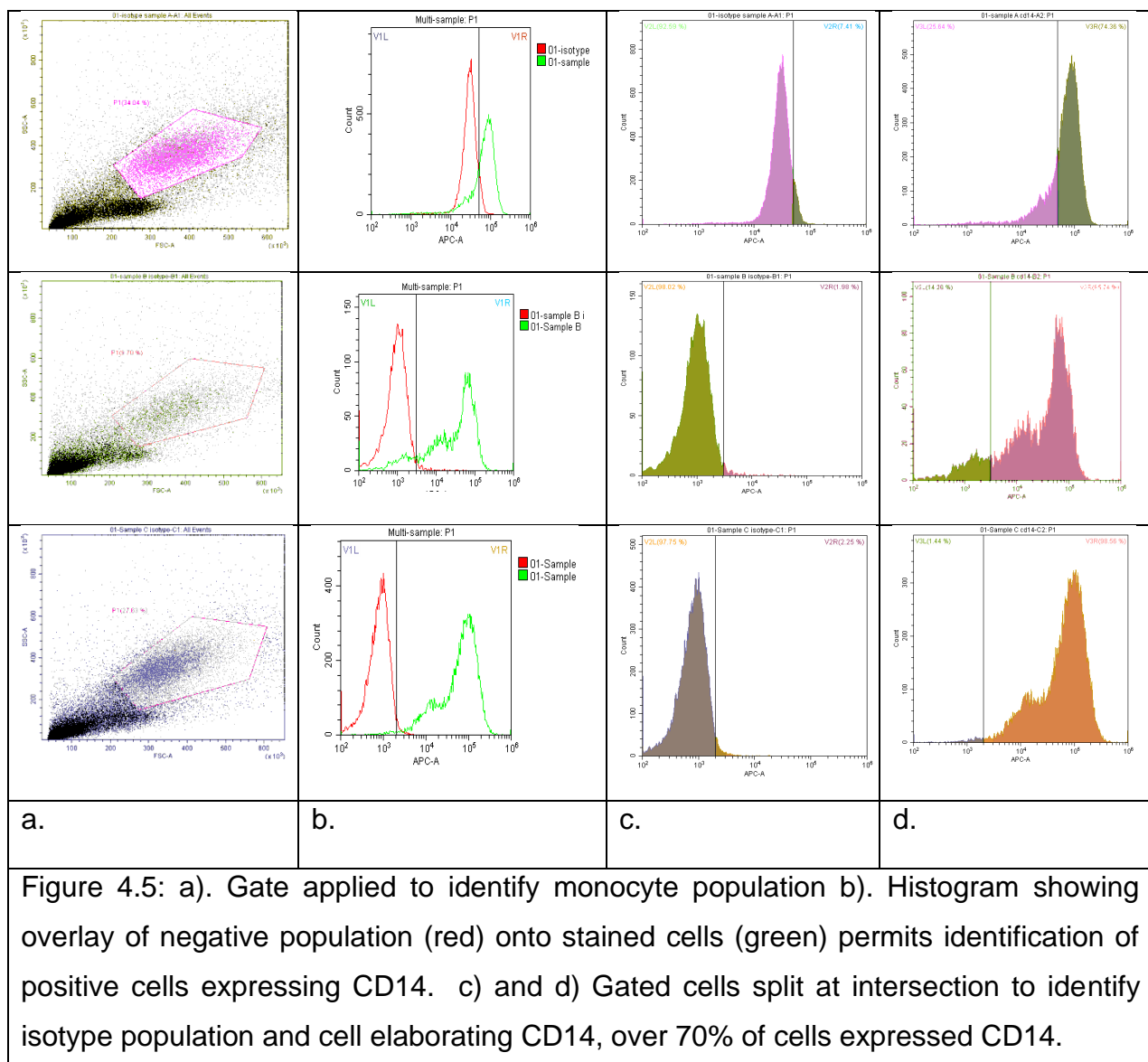
Table 4.5 shows the results of test solution with endotoxin concentration twice the label sensitivity of test kit diluted with particle stock solution (positive product control). These solutions produced positive results after incubation with reconstituted lysate. A negative test would have suggested an interference such as pH which may need to be adjusted. Table 4.6 outlines the results of the gel clot-based endotoxin testing of PEEK, XLPE and UHMWPE particle stock solution. The results show that the particle solutions have endotoxin level less than the labelled sensitivity of the test kit at <0.06EU/ml. This confirms the effectiveness of the depyrogenation technique.

**Table 4.6:** Results of LAL testing using gel clot method

Test	Diluent	Replicates	Result 1	Result 2
Sample 1 (PEEK 100:1)	None	2	Negative	Negative
Sample 2 (PEEK 10:1)	None	2	Negative	Negative
Sample 3 (XLPE 100:1)	None	2	Negative	Negative
Sample 4 (XLPE 10:1)	None	2	Negative	Negative
Sample 5 (UHMWPE 100:1)	None	2	Negative	Negative
Sample 6 (UHMWPE 10:1)	None	2	Negative	Negative
Negative control	LAL Reagent Water	2	Negative	Negative

#### **4.3.4 Flow Cytometry**

Flow cytometric analysis of cells confirmed the presence of CD14+ cells. Figure 4.5 shows the the results obtained where over 70% of analysed cells expressed CD14. CD14 is expressed mainly by monocytes/ macrophages, though granulocytes and immature monocytic bone marrow cells may also express CD14, though to a lesser extent (Xu et al., 2005). Given that the cells were harvested from peripheral blood, monocytes which are precursors of tissue macrophages are the most likely cells identified with flow cytometry, possibly with contaminating granulocytes.



### 4.3.5 Biological Activity of Cells

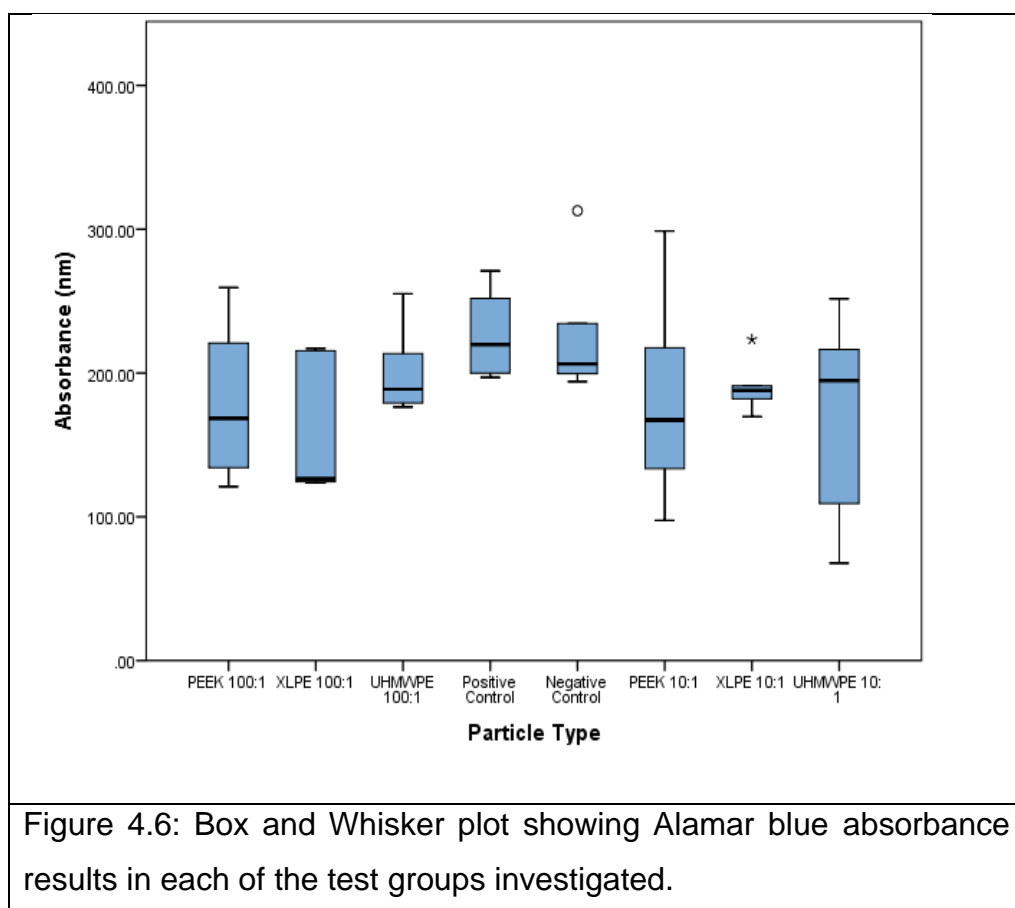
#### 4.3.5.1 Cell Metabolic Activity

The mean absorbance levels obtained from the Alamar blue assay (shown in Table 4.7) were similar for all test groups and showed no statistical difference after 12 hours of particle-monocyte incubation when compared with negative controls. Phagocytosis of particles by cells at 100:1 and 10:1 particle volume

to cell number did not affect monocyte metabolic activity based on absorbance results compared with negative controls. Figure 4.6 shows a box and whisker plot displaying the different absorbance range measured with varying stimulation from particles of different concentration.

**Table 4.7:** Alamar blue test results – Kruskal Wallis (Absorbance)  $p=0.182$ .

<b>Particle Type and Concentration</b>	<b>Median absorbance values (95% confidence interval)</b>
PEEK 100:1	168.5 (120.2 – 237.3)
XLPE 100:1	126.5 (106.2 – 204.8)
UHMWPE 100:1	188.7 (168.7 – 231.7)
Positive Control	219.7 (195.7 – 257.3)
Negative Control	206.3 (178.2 – 272.9)
PEEK 10:1	167.3 (106.4 – 254.3)
XLPE 10:1	188.0 (171.5 – 209.2)
UHMWPE 10:1	194.7 (99.3 – 245.5)



#### 4.3.5.2 Cell Viability

Calcein AM and ethidium homodimer-1 (Live/Dead) assay (Fisher Scientific, Loughborough, UK) was used to confirm viability of the phagocytic cells following the introduction of particles. Live cells were stained green while dead cells stained red. Results showed that a particle stock at 100:1 did not affect cell viability after 24 hours of incubation. Images demonstrated no red stained cells in any group (figure 4.7) suggesting a similar impact of polyethylene particles on monocytes as PEEK particles.

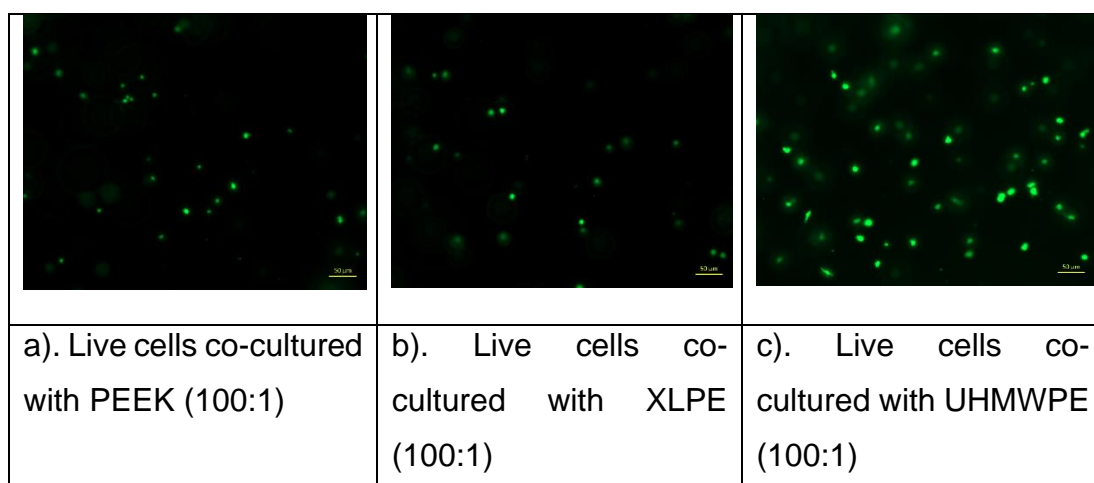
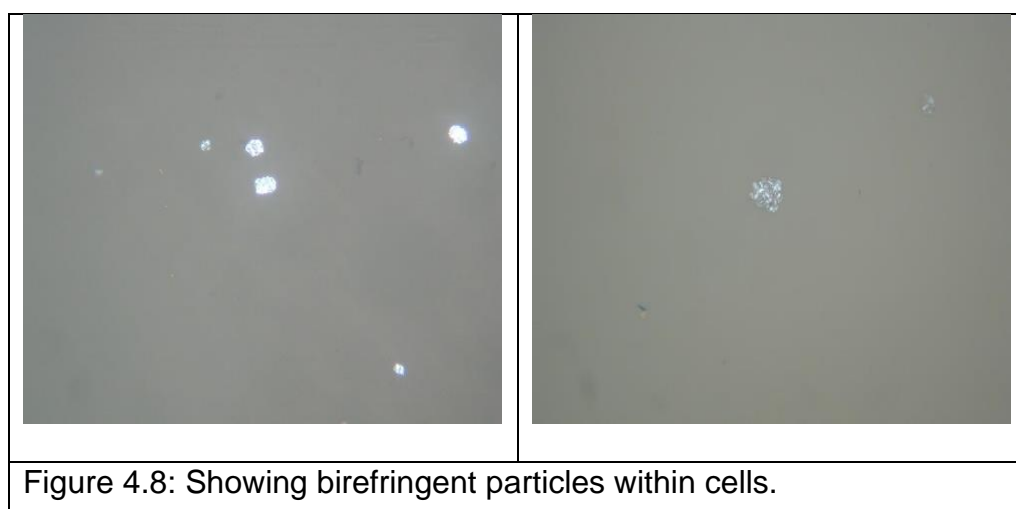


Figure 4.7 (a, b & c): Live/Dead staining of cells after test as observed with a widefield fluorescence microscope (Apotome, Zeiss, Germany)

#### 4.3.5.3 Particle Uptake

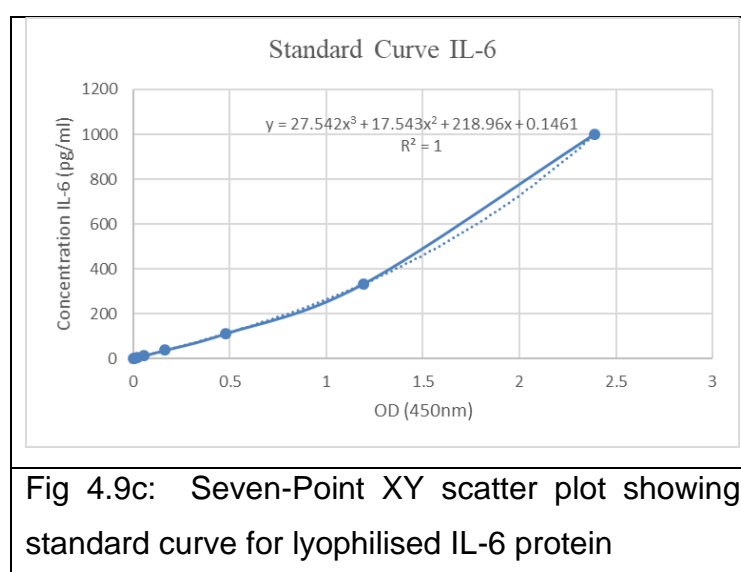
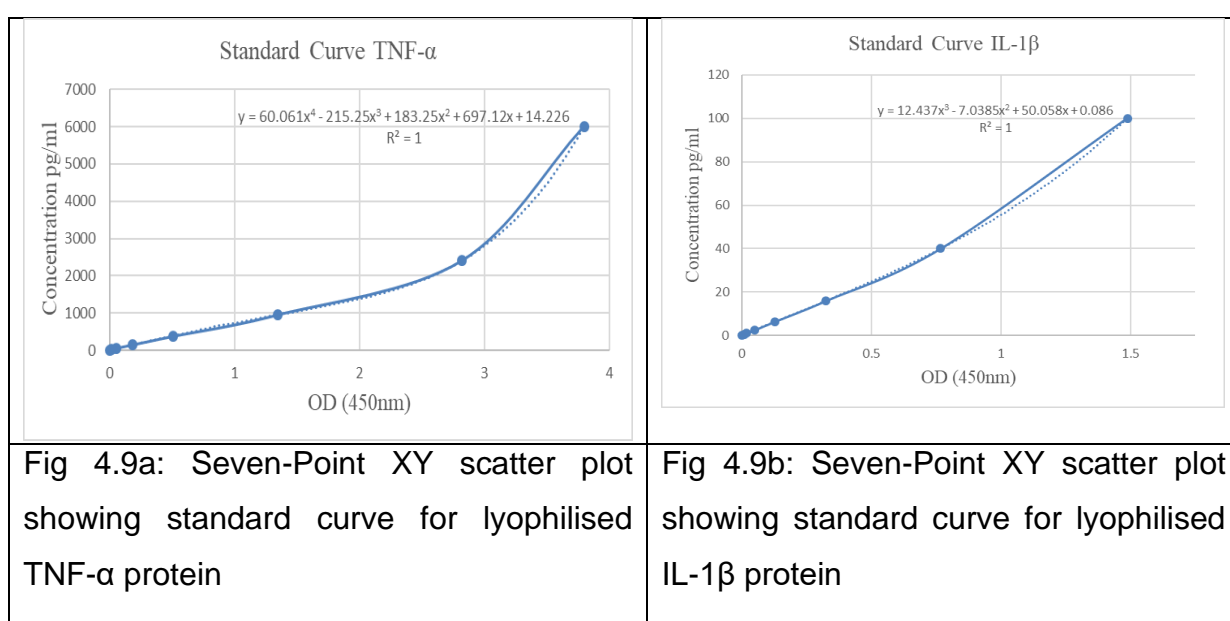
Very few cells were retrieved on agarose gel after treatment with Non-Enzymatic Cell Dissociation Solution (Sigma Aldrich, Dorset, UK) however, polarised light examination demonstrated birefringent particles located within the cytoplasm of monocytes suggesting active phagocytosis of the particles (Figure 4.8).



#### 4.3.5.4 Enzyme Linked Immunosorbent Assay (ELISA)

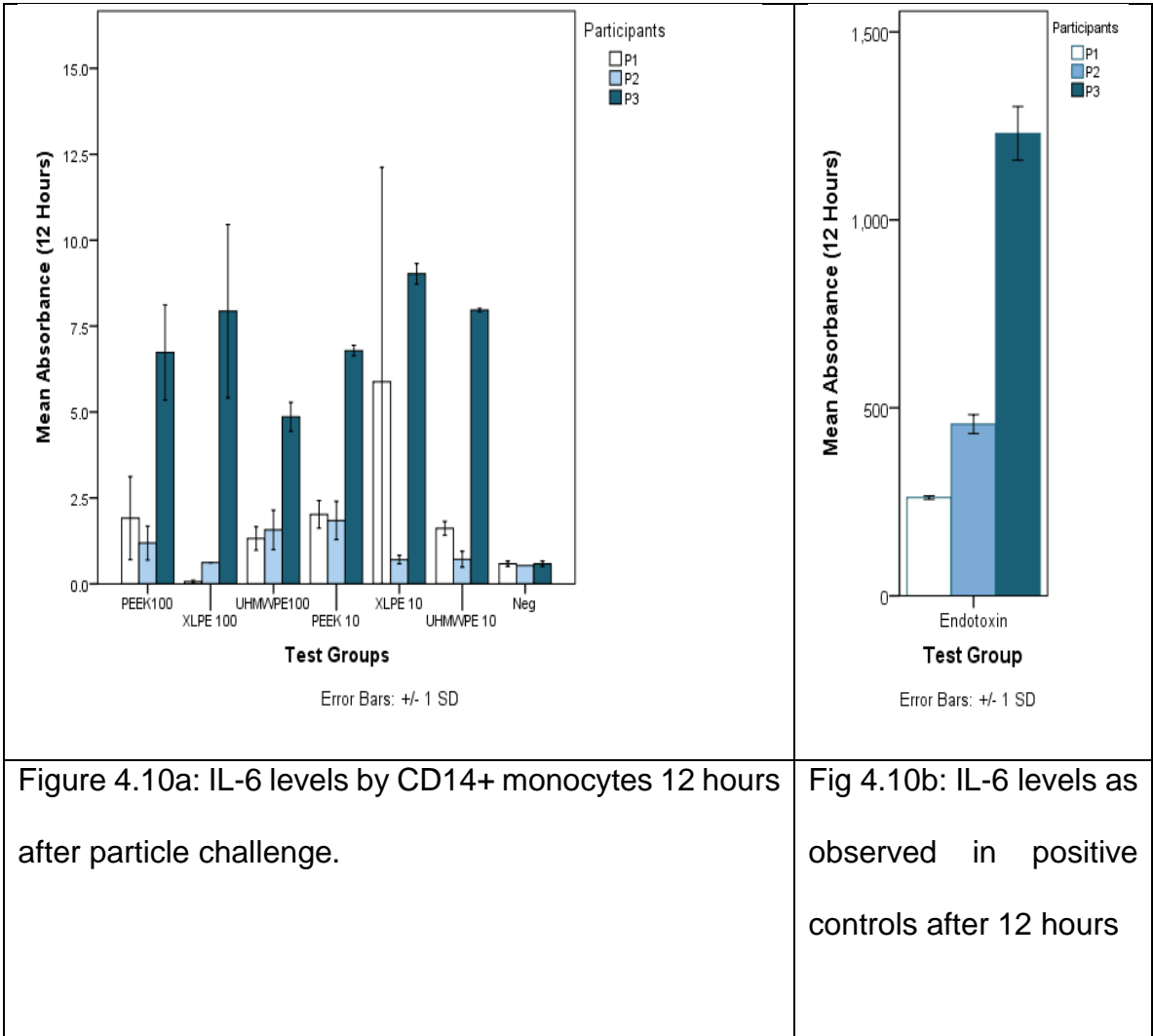
##### 4.3.5.4.1 Standard Curves

Standard curves were constructed from known concentrations of cytokine after serial dilution of lyophilised cytokine was plotted against measured optical density (Fig 4.9). The concentration of unknown cytokines was then deduced.

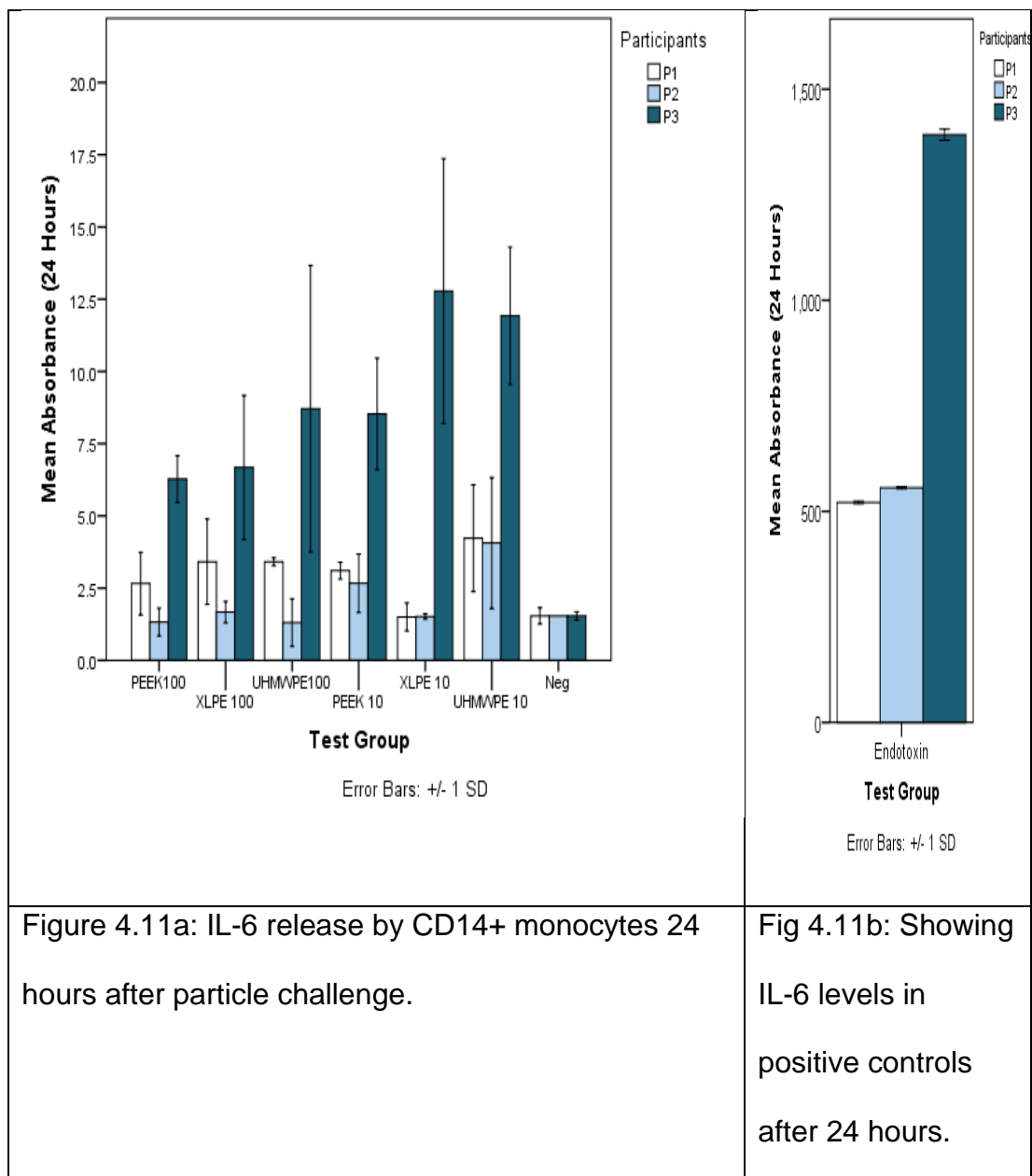


#### 4.3.5.4.2 IL-6 Assay

IL-6 levels released by monocytes is shown in Figure 4.10 and 4.11. At both 12 and 24 hours, monocytes from one of the 3 participants consistently released significantly higher IL-6 levels compared to negative controls (without particles) when compared with the other 2 participants. Monocytes from the other 2 participants released similar IL-6 levels compared to controls. Table 4.8 shows the mean IL-6 levels from the 3 participants at 12 and 24 hours.







**Table 4.8:** Kruskal Wallis IL-6 concentration compared with negative control at 12 and 24 hours; p= 0.585 and 0.310 respectively.

<b>Particle Type and Concentration</b>	<b>Mean IL-6 concentration at 12 hours pg/ml. (± standard deviation)</b>	<b>Mean IL-6 concentration at 24 hours pg/ml. (± standard deviation)</b>
PEEK 100:1	3.28 (± 2.83)	3.42 (± 2.38)
XLPE 100:1	2.87 (± 4.09)	3.92 (± 2.62)
UHMWPE 100:1	2.58 (± 1.80)	4.48 (± 4.08)
Positive Control	829.8 (± 110.25)	1196.21 (± 92.38)
Negative Control	0.57 (± 0.06)	1.54 (± 0.16)
PEEK 10:1	3.55 (± 2.53)	4.77 (± 3.08)
XLPE 10:1	5.20 (± 4.68)	5.27 (± 6.18)
UHMWPE 10:1	3.43 (± 3.54)	6.74 (± 4.36)

#### 4.3.5.4.3 IL-1Beta and TNF-alpha

Absorbance readings from IL-1 beta and TNF- alpha showed no clear pattern with over 50% of wells showing negative absorbance values, as such no clear conclusion could be drawn from these assay analyses.

#### 4.4 DISCUSSION

The main aim of this chapter was to examine the inflammatory potential of PEEK and polyethylene particles generated from my pin on plate wear test using Enzyme Linked Immunoassay (ELISA). However, based on the inability to obtain absorbance signals above the minimum reading detectable in 2 of the 3 cytokines investigated, it was not possible to accept or reject my hypothesis on the effect of these three groups of polymer particles on human monocytes.

One critical step in the ELISA test is adjusting the concentration of target protein and determining an optimal dilution factor so that the concentration of the target protein falls within the measurable range for the particular test kit. High volume of monocyte culture medium in the culture wells may lead to excessive dilution of the target protein and conversely a low volume of culture medium may lead to concentrated cytokine content within the culture wells. Based on this, a concentrated sample with values outside the measurable range will need diluting and desiccation of the sample may be appropriate in the diluted sample. With this consideration, samples were desiccated after repeated analyses and use of neat, as harvested supernatant failed to yield any detectable cytokines, even though the positive control clearly confirmed monocyte stimulation by way of cytokine generation in all three tests. After desiccation, only IL-6 showed positive absorbance signals above the minimum reading for the test kit. A plausible explanation for observed results in this test would be that a relatively excessive amount of culture medium had been dispensed per well and this led to an excessive dilution of cytokines. Perhaps,

further desiccation was required to be able to demonstrate cytokine release in all tests.

Monocytes from one of the 3 participants released significantly higher IL-6 levels compared to cell only negative controls after 12 and 24 hours. Monocytes from the other 2 participants released IL-6 levels similar to that seen in the negative control groups. Heterogeneity in the response of individuals to biological stimulation has previously been observed and reported (Matthews et al., 2000b), and similar results were noted by (Liu et al., 2015) with regards to monocyte response to micrometre sized UHMWPE particles, similar to the particle size range used in this study. Differential cytokine production in individuals has been suggested as a contributory factor in determining the survivorship of implants (Matthews et al., 2000b, Matthews et al., 2000c). Distinctive immunological responsiveness by individuals to different orthopaedic biomaterials with emphasis on exaggerated release of pro-inflammatory cytokines may stimulate osteoclastic activity and tilt the homeostatic balance in favour of bone resorption. This effect has been attributed to the function of cytokine promoter gene polymorphisms (Daser et al., 1996) and this genetic difference may in part explain why not all individuals receiving a prosthetic joint replacement experience significant periprosthetic bone loss leading to loosening, despite the generation of wear debris. In this study, the IL-6 results obtained showed variation in cytokine response among individuals, with the concentration of released cytokine measured as sometimes 5 times higher between different donors.

Using the same samples, the TNF-alpha and IL-1beta assessment resulted in low signals in more than 50% of wells making it virtually impossible to describe

a trend or conclude on the impact of these particles on the monocytes tested in this study. Many possible factors were adduced to explain these findings and attempts made at adjusting variables and optimise test conditions. As part of the preliminary evaluation and test variable optimisation, considerations were given to the particle size distribution, particle depyrogenation technique, timing of supernatant collection/ termination of tests, dosing of monocytes and methods of keeping monocytes and phagocytes in the same plane as these factors have been previously shown to affect results.

The plate adherence method is an established technique used for isolating PBMCs and culturing monocytes (Bennett and Cohn, 1966, Johnson et al., 1977) and was the method used for the particle challenge study investigated in this chapter. Flow cytometry was used to confirm monocytic lineage, especially as heavy granulocyte or lymphocyte contamination without viable monocytes may explain the inability of cells to release cytokines. Granulocytes and lymphocytes do not have the same phagocytic ability as the monocyte/ macrophage cell lines however, flow cytometry confirmed the expression of the pan-monocyte marker CD14 in cells used in this study.

The particles used in this study were generated using a modification of the acid digestion method described by Scott (Scott et al., 2005). Size range was determined by filtration, using a micron pore size filter. The sub micrometre size range has been previously shown to be the size range isolated in a clinical retrieval study (Campbell et al., 1995) and is the size considered to initiate the most significant biological response (Green et al., 1998). While the method of generation will not explain the inability to measure any cytokine release, the quantity of particles used when challenging the cells is a very important factor

in this test. The optimal dose when investigating cell-particle interactions has been a significant subject of discourse with no universally acceptable method. The number of particles per cell (Hallab et al., 2012), weight percent (Glant et al., 1993), particle volume per cell number (Green et al., 1998) or surface area ratio (Shanbhag et al., 1994a) are previously described methods of dosing cells. None of these methods is devoid of limiting factors and correcting for these limiting factors allows for a more uniform cell-particle challenge. For example, the number of particles without consideration for size, volume or density of the particles may make it difficult to explain the observed effect. Also, sole utilisation of particle weight as a method of dosing without adjusting for particle size distribution or density may produce a similar dilemma with interpretation. In my study, the particle volume per cell number ratio was used to provide uniformity in cell particle interaction, a particular size range was employed with particles of submicron size selected.

While troubleshooting the experimental processes to explain the possible reason for undetectable cytokine levels, the one concern was the possibility of particles not being phagocytosed by cells. To address this concern, supersaturation of agarose with particles and a different study design with PEEK particles and monocyte without agarose was tried. None of these two approaches addressed this concern as cytokines were barely detectable. For phagocytosis of particles and subsequent activation of monocytes to occur, particles and cells must be in the same plane and in close proximity. UHMWPE and XLPE particles have a density of approximately  $0.93\text{g/cm}^3$  and will therefore float in culture medium. Importantly, monocytes are adherent cells and will attach to the base of well plates, creating a differential plane which

may preclude phagocytosis of polyethylene particles. Though PEEK particles have a density of  $1.3\text{g/cm}^3$  and will therefore sink in culture medium a similar test methodology was used for all particles to ensure uniformity in the test design. For this test, an agarose gel technique previously described by Harada et al (Harada et al., 1994) was used to hold the particles in the same plane to facilitate phagocytosis. Other methods have been described to ensure that the particles and cells remain in close proximity for cell-particle interaction to occur. For example culturing adherent cells on coverslips and inverting over particles floating in culture medium (Matthews et al., 2000c), culturing cells on the underside of inserts and placing the inserts in wells with culture medium to ensure contact with floating particles (Horowitz and Gonzales, 1997), culturing cells within collagen embedded with particles (Atkins et al., 2009), and particles have been held in collagen with cells seeded on the embedding collagen gel (Endres et al., 2008).

One observation from my study was that the positive control groups where monocytes stimulated with endotoxin produced a large increase in the concentration of cytokines measured while the negative controls released significantly lower levels in all ELISA groups. These observations suggest viability of cells and ability to secrete cytokines with appropriate stimulation. Another observation, based on the Alamar blue and live-dead assay results showed that cell metabolic activity and viability were not impaired by PEEK, UHMWPE or XLPE particles. It therefore suggests that the cells are viable and should carry out phagocytic activity necessary for activation and cytokine release.

Bacterial endotoxin/ lipopolysaccharide (LPS) located on the cell wall of Gram negative bacteria strongly evokes a series of events that culminate in the production of inflammatory mediators from monocytes and macrophages. LPS is ubiquitous and may readily contaminate particles presenting a confounding factor in the monocyte-particle challenge (Cho et al., 2002). To eliminate this, a depyrogenation step is essential especially if particles have not been generated using an endotoxin free set-up (Matthews et al., 2000b) . Previous studies have shown that lubricant fluid digested by an acid method as engaged in this experiment may still have contaminating endotoxin despite treatment with concentrated hydrochloric acid and heat (Paulus et al., 2012) . Numerous methods of depyrogenation have been described, and Hitchins (Hitchins and Merritt, 1999) showed that particles contaminated with endotoxin can be successfully depyrogenated with 48 hour incubation in 70% ethanol. Followed by a subsequent phosphate buffer saline (PBS) wash, combination treatment with alternating cycles of nitric acid ( $\text{HNO}_3$ ) and NaOH with ethanol has also been previously reported (Ragab et al., 1999). The use of ultracentrifugation has also been described (Paulus et al., 2012). The effectiveness of the protocol used in depyrogenation in this experiment is evident by the negative LAL result from the particle stock solutions.

Following termination of the test, an attempt was made to harvest cells, treat with trypan blue and examine retrieved cells under polarised light with the view to demonstrate particles within viable cells. The problem with this approach was that cell yield after trypsinisation was very low, monocytes were noted to be extremely adherent after prolonged culture and cell scraping was not an alternative, as agarose gel is difficult to handle. Examination of the few



retrieved cells showed evidence of birefringent particles within cells, suggesting phagocytosis of particles.

Within the limitations of this study, two outcomes are apparent. First, PEEK and polyethylene particles had a similar effect on cell metabolism and viability. Secondly, IL-6 as measured using ELISA showed individual variation in response similar to studies that have been previously reported. It is thought that desiccation of samples might have resulted in the detection of measurable cytokines. However, cost and time restraints precluded further repeats of this test.

## Chapter 5: GENERAL DISCUSSIONS AND CONCLUSIONS

### 5.1 GENERAL DISCUSSIONS

This chapter outlines the main findings and conclusions of my thesis and suggests future work. The overall aim of my thesis was to investigate the suitability of PEEK, CFR-PEEK and acetal as an alternative bearing in an all polymer total knee replacement. **The main finding and contribution to knowledge was that using a pin on plate device designed to simulate a simplified knee couple, PEEK pins representing femoral components articulated against moderately cross-linked polyethylene tibial inserts (an all poly TKA) exhibited comparable wear loss and inflammatory potential to the contemporary metal on polyethylene articulations. Additionally, CFR-PEEK was found unsuitable as a bearing surface in an all polymer TKA.**

Chapter one of my thesis reviewed the literature pertaining to the kinematics, biomaterials and loading of the knee joint as a basis for understanding and choosing an appropriate method of initial wear testing. Movement along the sagittal plane resulting in flexion and extension of the knee produced the largest degree of freedom with sliding and rolling being the main components of this motion. Sliding has been reported as of dominant importance in producing the wear pattern noted in tibial inserts (Blunn et al., 1991). Hence, the wear test device applied mainly sliding motion on component materials with geometry similar to knee designs (Walker et al., 1996). Also, the chapter reviewed and established the likely cause of failure in a previously described acetal on polyethylene all polymeric knee articulation, failure of which may be

related to the method of implant fixation rather than component material or design (McKellop et al., 1993, Moore et al., 1998). This observation suggested the viability of an all polymer design in a large, weight bearing joint such as the knee. Progress in developing an all polymer knee joint has trailed MoP couples possibly because of the continued success observed in MoP articulation and the introduction of XLPE, which has reduced wear significantly. With the theoretical benefits of a metal free knee; physiological stress transfer around the implant (de Ruiter et al., 2017a, de Ruiter et al., 2017b) resulting in maintenance of an adequate periprosthetic bone stock, artefact free MRI or CT imaging allowing improved analysis of the bone-implant interface and elimination of a biological reaction to metal, it was appropriate to re-investigate the suitability of the all polymer knee concept.

In chapter 2 of this thesis, biomaterial couples including various combinations of PEEK, PEEK composite and acetal were tested and compared with established MoP articulations using a pin on plate wear testing machine under two loading conditions. The aim was to identify a polymeric bearing couple that may be a suitable candidate in a metal-free knee design and potentially be investigated further. PEEK-on-XLPE was noted to have similar volume loss to contemporary MoP couples. This was the case in both the high and low stress experiments. The 2 million cycle wear test showed no significant surface loss from the PEEK surface in PEEK-on-XLPE articulation. The implication of this is that the inflammatory contribution of the wear particles from PEEK-on-XLPE articulations if based solely on quantity and volume, will be from the particles generated from the XLPE counterface. It is however postulated that in the long-

term, more wear is expected from the PEEK counterface and the inflammatory impact from the relatively few PEEK particles is at present unclear.

In order to assess the inflammatory cell stimulating properties of the different particles, chapter 3 investigated, characterised and quantified particles generated from the wear test described and reported in chapter 2 under high stress conditions. Quantity and morphological features of particles from articulations differed in size and shape with statistical significance seen in many groups. The importance of this observation was discussed based on previous published work within the literature, as statistical differences may not necessarily imply clinical relevance. The number, shape and size of particles from PEEK-on-XLPE articulations were similar to particles from MoP articulations, though the relative quantity of particles analysed was small compared to the overall estimated quantity of particles shed from the articulating couples over the test period. Importantly, a method of separating PEEK and polyethylene particle fractions from PEEK-on-Polyethylene couples was developed and effective separation confirmed using FTIR. This novel separation method was based on differential densities of the particle fractions.

*In vitro* assessment of the inflammatory potential of wear particles using wear test generated debris was conducted in chapter 4. Particles of the most stimulatory size-range ( $< 1 \mu\text{m}$ ) were co-cultured with human derived primary monocytes and the release of pro-inflammatory cytokines (IL-1 $\beta$ , IL-6 and TNF $\alpha$ ) were quantified using ELISA. Results primarily from IL-6 quantification showed no significant difference among groups however variations were observed in individual reactivity to the particles.

The overall hypothesis of this study was that, under stresses representative of the knee, the volumetric wear and quantity of particles from PEEK, CFR-PEEK and acetal bearings are reduced when compared with MoP bearings. It was also hypothesized that these particles will exhibit similar or less inflammatory potential when compared with polyethylene debris from a standard MoP articulation. The results from this study did not support the hypothesis of reduced volumetric wear or decreased particle count from polymeric bearings, it however shows similar volumetric loss and particle quantity between PEEK-on-XLPE and CoCr-on-XLPE bearings. Also, similarities in the inflammatory potential of PEEK and polyethylene particles were observed. The findings from the series of tests conducted in my thesis have provided preliminary information and strongly suggest the suitability of using PEEK in knee replacement design, especially as a candidate material for femoral components in a metal-free knee. It has also raised interesting areas and ideas for future work before clinical translation.

To further progress the investigation of PEEK in an all polymer knee replacement and against the back drop of the already highlighted benefits, it would be useful to investigate PEEK-on-XLPE in a more rigorous environment to assess the long term profile.

## 5.2 FUTURE DIRECTIONS

### 5.2.1 Further Tribological Testing

Following use of a pin on plate device, a joint simulator test is the usual next step as it is helpful in predicting long term wear of the proposed new

biomaterial couple (Walker et al., 1997) in a more physiological environment using actual prostheses. Two main modes of knee simulator designs are used, either the force-controlled or displacement-controlled test philosophies where the different protocols are highlighted by the International Organization for Standardization (ISO 14243-1, 2009, ISO 14243-3, 2009). Briefly, both viewpoints in knee simulator testing agree that flexion-extension motion of the simulated knee joint is predetermined i.e. displacement controlled. However, the main difference in the force-controlled and displacement-controlled philosophies is that anterior-posterior movement and torsional movement of the tested knee is determined by the applied load in a force-controlled set-up but pre-set and generated by the simulator in displacement-controlled devices. Force-controlled designs are more complex to design and reproduce *in vivo* motion more accurately while a displacement-controlled set-up may have limited use in testing constrained prosthetic designs (Kaddick C, 2014). From the standpoint of an all polymer joint test, where coefficient of friction may be higher than MoP articulations (Cowie et al., 2019), adhesive wear may be the significant mode of surface loss, and a force controlled design may be a more appropriate approach to testing. In hypothetical terms, with a high friction articulation, loaded plastics are “sticky” and if displacement of the articulating surfaces is pre-determined, it might follow the path of least resistance. However, if force controls AP and torsion, high adhesive force and wear at the articulating interface may ensue and based on this, wear in force-controlled and displacement-controlled designs may differ when investigating all plastic articulations. Furthermore, a recent test used a displacement-controlled device

to test PEEK-on-UHMWPE couples (Cowie et al., 2016) and a force-controlled test may complement such a study or come to a different conclusion.

Apart from choice of joint simulator, other considerations in wear testing include the use of injection moulded femoral implants, which reduces surface roughness and may impact on the wear volume generated. The PEEK pins used in this study were fashioned from extruded rods and surfaces prepared using a fly cutter resulting in an initial surface roughness (Ra) of ~1000nm. Injection moulded PEEK surfaces have been observed to have surface roughness (Ra) as low as ~40nm (Cowie et al., 2019). Increasing surface roughness of CoCr in MoP articulations has been shown to increase wear of the polyethylene counterface (Fisher et al., 1995, Muratoglu et al., 2004), it is not clear whether such an effect will be observed in “soft-on-soft” bearings like PEEK-on-XLPE. Based on this, it may be appropriate to investigate the optimal surface parameters for PEEK in all polymer articulations. Sectioning through the worn, weight-bearing segment of the plastic femoral component with subsequent macroscopic, microscopic and ultra-structural examination to determine the presence of material failure may contribute to assessment of the long-term suitability of PEEK as a bearing component in TKR.

It would also be interesting to investigate the impact of further cross-linking on volume loss using highly crosslinked polyethylene. My thesis employed the use of a first generation moderately cross-linked polyethylene (PEEK-on-XLPE) similar to the marketed XLPE – Crossfire (Stryker Orthopaedics), with evidence of a reduction in wear when compared to PEEK-on-UHMWPE, however it is not clear whether this trend will continue, or further cross-linking will produce no further impact on wear. A large mix of XLPE implants do exist

due to manufacturing differences (especially radiation protocol and method of free radical elimination) and may have impact on performance within the cross-linked polyethylene subgroup. This was highlighted in a recent population based registry study (Boyer et al., 2018). Using the joint simulator wear test to investigate wear performance of PEEK articulated against a variety of second generation XLPE tibial inserts such as sequentially annealed X3™ (Stryker Orthopaedics) and Vitamin E stabilised E1 (Biomet, Warsaw, IN, USA) tibial inserts, may be essential to achieve best wear outcome.

#### 5.2.2 Further Investigation of Inflammatory Potential

Though bulk PEEK is inert and has been used in spinal implants with success (Kurtz and Devine, 2007), the additional challenge in arthroplasty is wear and response to generated debris.

It will be fascinating to compare particles from a knee simulator test with particles described in my thesis. Particles generated from MoP knee simulators as reported in literature are similar to ones isolated and described in this study. Whether increasing the degrees of freedom with introduction of cross-shear will change the shape or size of particles is unknown in all plastic joints. Cross-shear has been shown to increase particle number in pin on plate devices using MoP articulations (Joyce et al., 2000). Separating particle fractions to identify variation in morphology and subsequent use of such particles for an *in vivo* inflammatory test also appears an interesting prospect.

In addition to the SEM based and automated analysis technique employed for particle analysis in my thesis, the use of technologies such as the light



scattering technique is advocated. This technique is capable of analysing a large volume of particles while in suspension in a non-destructive fashion (Elfick et al., 2000). The non-destructive method of analysis allows for supplementation by SEM examination, providing a detailed analysis of the particles.

Investigating particles obtained from a simulator test in an *in vivo* setting will add to the robustness of preclinical evaluation of a PEEK-on-XLPE knee. ASTM International standard F1904 (ASTM International (F1904), 2014) describes methods for *in vivo* testing of particles. A rat pouch model has been described to create a synovial cavity type space. Particle testing by pouch infiltration and subsequent assessment of particle challenged pouches for exudate production, cytokine analysis, histochemistry and histological analyses are part of the components of inflammatory assessment. Also, particles may be generated *in vivo* from implanted prostheses and inflammatory response to these particles investigated using histological assessment of capsular membrane and implant-periarticular junction for osteolysis, particles may also be retrieved for further analysis. An example of this approach had previously been described by Coathup and colleagues (Coathup et al., 2005) using large sheep model. *In vivo* testing has the added advantage of offering different approaches to evaluating the inflammatory potential of particles, allowing for multiple test components aside from cytokine analysis alone by ELISA and would add to the overall robustness of the study. Furthermore, the identification of particles within inflammatory cells using immunochemical techniques coupled with confocal microscopy can be used to

demonstrate particles within the cells increasing the confidence in the experimental methodology.

### 5.2.3 Limitations of the study

A sample size analysis was not conducted in this study and the number of repeats used in the wear test was limited to three ( $n=3$ ). This is considered a limitation of the study, while the number of test station per group may be appropriate for statistical analysis, it may not represent appropriate level of power needed in the study. Regardless, the measured volumetric loss from each articulation show only minimal variation and increasing the number of repeats may probably produce similar mean wear rates. A second limitation may be the loads applied during tests conducted at low, near physiological stress levels. Given the inherent reduction in contact stress levels expected in the articulation secondary to creep and material loss from the polyethylene counterface, it does appear the contact stress levels dropped appreciably during testing reflecting as wear rate graphs with near zero gradient especially after approximately 500,000 cycles of testing. Load applied for high stress articulation may be open to debate. However, highly demanding environment is required to test new bearing material to give credence to its suitability. Furthermore, similar high loads have been applied previously in assessment of PEEK as a tibial inserts (Wang et al., 1999). Conducting a frictional test as part of this study would have been an ideal component of the tribological assessment of PEEK and CFR-PEEK articulations. This is mainly due to the fact that high frictional force may lead to increased wear (Hall et al., 2001) and

probably more importantly increased torque at the bone-implant interface leading to mechanical loosening (Latif et al., 2008, Cowie et al., 2019). Quantifying and comparing the co-efficient of friction of PEEK-on-XLPE and CoCr-on-XLPE articulations would have added invaluable details to the assessment conducted in this study. A further limitation of this work is given by the inability to conclusively demonstrate the impact of particle phagocytosis on cytokine production in all but IL-6. This limitation was extensively discussed in chapter 4 of my work and may be related to the volume of culture medium per well used to incubate human derived monocytes during testing.

PEEK and XLPE have both been used in clinical applications, however comprehensive evaluation of the bearing components in a fashion directed for TKR application is necessary before translation to clinical use, this will offer confidence for suitability and safety of the articulation. From the results presented in my thesis, it may be possible to replace CoCr in TKR with PEEK. The notions of an all polymer TKR are intended to realise physiological stress distribution in the periprosthetic bone, reduce stress shielding with bone loss and eliminate biological activity to metal alloy. If achieved, this conceptual goal of obtaining long term, near natural periprosthetic stress domain around the knee may offer benefit in a group of individuals undergoing total knee replacement.

## **APPENDIX**

### **1. LABORATORY PROTOCOLS**

#### **1.1 Wear Test Set-up (Section 2.2).**

Extracts from Section 7, ASTM: F732 – 00 (Reapproved 2011) Standard Test Method for Wear Testing of Polymeric Materials Used in Total Joint Prostheses

1. Make any initial measurements required to determine the subsequent amount of wear of the polymeric specimen.
2. Place the control soak specimen(s) in a soak chamber of test lubricant, such that the total surface area exposed to the lubricant is equal to that of the wear specimens when mounted in the test chambers. Maintain the soak chamber lubricant temperature at the same nominal temperature as the test chambers. This temperature shall be  $37\pm3^{\circ}\text{C}$  unless justification can be provided that use of a different temperature will not affect the results.
3. Place the wear test specimens in their test chambers, add the lubricant, and activate load(s) and motion(s).
4. As testing is commenced, monitor the specimens for signs of erratic behaviour that might require early termination of the test.
5. Remove the wear and soak specimens at desired intervals, wash, rinse, concurrently. It is important that both the wear and soak components be treated identically to ensure that they have the same exposure to the wash, rinse, and drying fluids. This will provide the most accurate correction for fluid sorption by the wear specimens, and correction for any other factors which could affect wear measurements.

6. After rinsing and drying, conduct wear measurements.
7. Thoroughly rinse all test assembly surfaces which have contacted bovine serum using deionized water.
8. Inspect the bearing surfaces of the test specimens and note the characteristics of the wear process. Visual, microscopic, profilometric, replication, or other inspection techniques can be used. Care must be taken, however, that the surfaces do not become contaminated or damaged by any substance or technique that might affect the subsequent wear properties. If contamination occurs, thoroughly reclean the specimens prior to restarting the wear test.
9. Replace the wear specimens, maintaining original couples and orientation, and soak control(s) in fresh lubricant and continue wear cycling.
10. The appropriate wear test duration depends on the objective of the specific test, the duration of run-in effects, the linearity of wear rates, and the potential for wear mechanism transitions. The minimum duration shall be two million wear cycles. The minimum number of wear measurements, subsequent to the initial measurement shall be four.

## 1.2: Datasheets of Test Materials

### TECAFORM AH natural - Stock Shapes (rods, plates, tubes)

**Chemical Designation**  
POM-C (Polyacetal (Copolymer))

**Colour**  
white opaque

**Density**  
1.41 g/cm<sup>3</sup>

**Main features**  
→ high strength  
→ resistant to cleaning agents  
→ stiff  
→ high toughness  
→ very good electrical insulation  
→ good machinability  
→ good slide and wear properties  
→ difficult to bond

**Target Industries**  
→ mechanical engineering  
→ automotive industry  
→ aircraft and aerospace technology  
→ electronics  
→ food technology  
→ oil and gas industry

Mechanical properties	parameter	value	unit	norm	comment
Modulus of elasticity (tensile test)	1mm/min	2800	MPa	DIN EN ISO 527-2	1) (1) For tensile test specimen type 1b
Tensile strength	50mm/min	67	MPa	DIN EN ISO 527-2	(2) For flexural test: support span 64mm, norm specimen.
Tensile strength at yield	50mm/min	67	MPa	DIN EN ISO 527-2	(3) Specimen 10x10x10mm
Elongation at yield	50mm/min	9	%	DIN EN ISO 527-2	(4) Specimen 10x10x50mm, modulus range between 0.5 and 1% compression.
Elongation at break	50mm/min	32	%	DIN EN ISO 527-2	(5) For Charpy test: support span 64mm, norm specimen.
Flexural strength	2mm/min, 10 N	91	MPa	DIN EN ISO 178	(6) Specimen in 4mm thickness
Modulus of elasticity (flexural test)	2mm/min, 10 N	2600	MPa	DIN EN ISO 178	n.b. = not broken
Compression strength	1% / 2% / 5% 5mm/min, 10 N	20/35/68	MPa	EN ISO 604	(3)
Compression modulus	5mm/min, 10 N	2300	MPa	EN ISO 604	(4)
Impact strength (Charpy)	max. 7.5J	n.b.	kJ/m <sup>2</sup>	DIN EN ISO 179-1eU	(5)
Notched impact strength (Charpy)	max. 7.5J	8	kJ/m <sup>2</sup>	DIN EN ISO 179-1eA	(6)
Ball indentation hardness		165	MPa	ISO 2039-1	(6)
Thermal properties	parameter	value	unit	norm	comment
Glass transition temperature		-60	°C	DIN EN ISO 11357	1) (1) Found in public sources.
Melting temperature		166	°C	DIN EN ISO 11357	(2) Found in public sources.
Service temperature	short term	140	°C		Individual testing regarding application conditions is mandatory.
Service temperature	long term	100	°C		
Thermal expansion (CLTE)	23-60°C, long.	13	10 <sup>-5</sup> K <sup>-1</sup>	DIN EN ISO 11359-1;2	
Thermal expansion (CLTE)	23-100°C, long.	14	10 <sup>-5</sup> K <sup>-1</sup>	DIN EN ISO 11359-1;2	
Specific heat		1.4	J/(g*K)	ISO 22007-4:2008	
Thermal conductivity		0.39	W/(K*m)	ISO 22007-4:2008	
Electrical properties	parameter	value	unit	norm	comment
surface resistivity	Silver electrode, 23°C, 12% r.h.	10 <sup>14</sup>	Ω	DIN IEC 60093	1) (1) Specimen in 20mm thickness
volume resistivity	Silver electrode, 23°C, 12% r.h.	10 <sup>13</sup>	Ω*cm	DIN IEC 60093	(2) Specimen in 1mm thickness
Dielectric strength	23°C, 50% r.h.	49	kV/mm	ISO 60243-1	(2)
Resistance to tracking (CTI)	Platin electrode, 23°C, 50% r.h., solvent A	600	V	DIN EN 60112	
Other properties	parameter	value	unit	norm	comment
Water absorption	24h / 96h (23°C)	0.05 / 0.1	%	DIN EN ISO 62	1) (1) Ø ca. 50mm, h=13mm
Resistance to hot water/ bases		(+)	-	-	(2) (+) limited resistance
Resistance to weathering		-	-	-	(3) - poor resistance
Flammability (UL94)	corresponding to	HB	-	DIN IEC 60695-11-10;	(4) (4) Corresponding means no listing at UL (yellow card). The information might be taken from resin, stock shape or estimation. Individual testing regarding application conditions is mandatory.

Our information and statements reflect the current state of our knowledge and shall inform about our products and their applications. They do not assure or guarantee chemical resistance, quality of products and their merchantability in a legally binding way. Our products are not defined for use in medical or dental implants. Existing commercial patents have to be observed. The corresponding values and information are no minimum or maximum values, but guideline values that can be used primarily for comparison purposes for material selection. These values are within the normal tolerance range of product properties and do not represent guaranteed property values. Therefore they shall not be used for specification purposes. Unless otherwise noted, these values were determined by tests at reference dimensions (typically rods with diameter 40-60 mm according to DIN EN 15860) on extruded and machined specimen. As the properties depend on the dimensions of the semi-finished products and the orientation in the component (esp. in reinforced grades), the material may not be used without a separate testing under individual circumstances. The customer is solely responsible for the quality and suitability of products for the application and has to test usage and processing prior to use. Data sheet values are subject to periodic review, the most recent update can be found at [www.ensingerplastics.com](http://www.ensingerplastics.com). Technical changes reserved.

Ensinger Ltd  
Wilfried Way  
Torynrefail, Mid Glamorgan CF39 8JQ  
Great Britain

Phone (01443) 678400  
Fax (01443) 675777  
[ensingerplastics.com](http://ensingerplastics.com)

Date: 2020/05/04

Version: AE



## MOTIS™ Polymer Typical Material Properties

Granular Form\* materials required

Property	Method	Units	MOTIS Grade	
			MOTIS G	MOTIS LV
Color			Black	Black
Melt Viscosity	Capillary Rheometer*	kNs/m <sup>2</sup>	0.73	0.37
Density	ISO 1183	g cm <sup>-3</sup>	1.42	1.42
Tensile Strength	ISO 527	MPa	155	155
Tensile Elongation (Break)	ISO 527	%	2.2	2
Tensile Modulus	ISO 527	GPa	15	15
Flexural Modulus	ISO 178	GPa	12.5	12.5
Flexural Strength	ISO 178	MPa	240	230
Shear Strength	ASTM D732	MPa	95	94
Shear Modulus	ISO 15310	GPa	2.2	2.2
Compressive Strength	ISO 604	MPa	200	200
Compressive Modulus	ISO 604	GPa	12	12
Poisson's Ratio	ASTM D638	N/A	0.41	0.41
Rockwell Hardness	ASTM D785	M Scale	104	105
Izod Impact (Unnotched)	ISO 180	kJm <sup>-2</sup>	33	30
Izod Impact (Notched)	ISO 180	kJm <sup>-2</sup>	5.7	5.5
Water Absorption (24 hrs)	ISO 62	Wt. %	0.5	0.5
Melt Temperature	DSC	°C (°F)	343 (649)	343 (649)
Mold Shrinkage	In Flow Direction. Mold temp. 210°C (410°F)	%	0.3	0.1
	Across Flow Direction. Mold temp. 210°C (410°F)		0.7	0.9
Coefficient of Thermal Expansion	ASTM D696	10 <sup>-5</sup> °C <sup>-1</sup>	0.8	1.2
			1.5	1.5

Mechanical properties as molded

\*Melt Viscosity measurement carried out according to internal Invibio test method

### Rod Forms

Property	Method	Units	MOTIS Rod
Tensile Strength	ISO 527	MPa	98
Tensile Elongation (Break)	ISO 527	%	2.8
Flexural Modulus	ISO 178	GPa	6.4
Flexural Strength	ISO 178	MPa	164
Izod Impact (Unnotched)	ISO 180	kJm <sup>-2</sup>	30
Izod Impact (Notched)	ISO 180	kJm <sup>-2</sup>	3.6







## PEEK-OPTIMA® Polymer Typical Material Properties

**Granular Form\*** materials required

Property	Method	Units	PEEK-OPTIMA Grade	
			LT1	LT3
Color			Natural	Natural
Melt Viscosity	*Capillary Rheometer	kNs/m <sup>2</sup>	0.44	0.16
Density	ISO 1183	G cm <sup>-3</sup>	1.3	1.3
Tensile Strength (Yield)	ISO 527	MPa (ksi)	100	108
Tensile Elongation (Break)	ISO 527	%	40	25
Flexural Modulus	ISO 178	GPa	4.1	4.2
Flexural Strength	ISO 178	MPa	165	170
Shear Strength	ASTM D732	MPa	90	88
Shear Modulus	ISO 15310	GPa	1.15	1.00
Compressive Strength	ISO 604	MPa	135	135
Poisson's Ratio	ASTM D638	N/A	0.36	0.36
Rockwell Hardness	ASTM D785	M Scale	99	99
Izod Impact (Unnotched)	ISO 180	kJm <sup>-2</sup>	No break	No break
Izod Impact (Notched)	ISO 180	kJm <sup>-2</sup>	7.5	4.5
Relative Thermal Index	UL 746 B	°C (°F)	260 (500)	260 (500)
Water Absorption (24 hours)	ISO 62	Wt. %	0.5	0.5
Melt Temperature	DSC	°C (°F)	340 (644)	340 (644)
Mold Shrinkage in flow direction	Mold temp. 210°C (410°F)	%	1.2	1.3
Coefficient of Thermal Expansion	ASTM D696	10 <sup>-5</sup> °C <sup>-1</sup>		
			Below T <sub>g</sub> 4.7 Above T <sub>g</sub> 10.8	Below T <sub>g</sub> 4.7 Above T <sub>g</sub> 10.8

Mechanical properties as molded

\*Melt viscosity measurement carried out according to internal Invibio test method

### Rod Forms

Property	Method	Units	PEEK-OPTIMA Rod
Tensile Strength (Yield)	ISO 527	MPa (ksi)	115
Tensile Elongation (Break)	ISO 527	%	20
Flexural Modulus	ISO 178	GPa	4
Flexural Strength	ISO 178	MPa	170
Izod Impact (Unnotched)	ISO 180	kJm <sup>-2</sup>	Does not break
Izod Impact (Notched)	ISO 180	kJm <sup>-2</sup>	4.7





Accredited to  
ISO/IEC 17025:2005

# TEST CERTIFICATE



**ORTHOPLASTICS**

*Science making a material difference*

## Orthoplastics PUR - 1050 Medical Grade UHMWPE

CERTIFICATE ACCORDING TO ISO 5834-2 2011 This material also meets the requirements of ASTM F648-10a

Batch No **12017M** ISO Type **2** Powder Lot No **0000516475** Polymer Grade GUR **1050**  
This Material Has Been Processed By **Ram Extrusion** Country of Origin - **UK**

Customer **UCL** Order Number **HQ972496** Orthoplastics Ref **018010/1**  
Address **[REDACTED]** Size **40mm dia x 1m**  
Centre for Biomedical Engineering Part Number **RDT0040S4/CUS**  
Institute of Orthopaedics Number off Rod/Slab ref. #'s  
Brockley Hill **2 off. rod #91.**  
Stanmore, Middlesex **HA7 4LP**

MATERIAL SUPPLIED AGAINST THIS CERTIFICATE HAS BEEN ANNEALED IN ACCORDANCE WITH ORTHOPLASTICS QUALITY PROCEDURES  
SECTION VII OMU 002. NO NON-FUSED FLAKES (LIGHT PATCHES) OR PARTICLES >300 µm WERE FOUND ON TEST.

Certificate Number **018010/1-12017M-1**

Date of Test **3/8/12**

Property	ISO	Units	Requirements	Test Result
Density	5834-2 2011	kg/m <sup>3</sup>	927/944	932
Ash*	3451-1 2008	mg/kg	≤ 150	43
Particle Count <300 µm	5834-2 2011	Number	≤ 10	0
Light Patch <300 µm	N/A	Number	≤ 10	0
Charpy Impact Strength	5834-2 2011	kJ/m <sup>2</sup>	≥ 90	146
Tensile Stress at Yield	5834-2 2011	MPa	≥ 19	21.8
Ultimate Tensile Strength	5834-2 2011	MPa	≥ 27	51
Elongation at Break	5834-2 2011	%	≥ 300	404
Morphology Index	5834-2 2011	Number		0
Customer specific tests - limits and methods per specification				
Izod Impact Strength	5834-2 2011	kJ/m <sup>2</sup>	≥ 73	110

\* Test carried out by external subcontractor not covered by Orthoplastics' accreditations

This certificate does not affect the obligation to perform an incoming goods inspection. This certificate relates to semi-finished material. Printed

20-Nov-12

Signed **[REDACTED]** Date **20/11/2012**  
LIAM DAY - INSPECTOR Version **1.11** for Orthoplastics

Orthoplastics Ltd., Unit A, Beech Industrial Estate, Bacup, Lancashire, OL13 9EL, England.  
Telephone: +44 (0)1706 874171 Fax: +44 (0)1706 870826

<b>1.3: Method of specimen cleaning and weighing (Section 2.2.4):</b> <b>Extracts from ISO 14243 – 2 (2009)</b>		
	4.4 Preparation of test specimen for gravimetric measurements (pre-soaking)	CONDITIONING BY SOAKING
1	4.4.1 Soak the test specimen and control specimen in the fluid test medium (4.2.1) for 48 h $\pm$ 4h.	<b>Soak in test fluid (for 48h)</b>
2	4.4.2 Remove the test specimen and control specimen from the fluid test medium (4.2.1) and clean in the ultrasonic cleaner (4.3.2).	
	A typical cleaning regime in the ultrasonic cleaner is as follows:	
	a) Vibrate for 10 min in deionized water;	10 min in deionized water
	b) Rinse in deionized water;	Rinse in deionized water
	c) Vibrate for 10 min in a mixture of ultrasonic cleaning detergent in deionized water at the concentration recommended by the detergent manufacturer;	10 min 10% Decon90/deionised solution

	d) Rinse in deionized water;	Rinse in deionized water
	e) Vibrate for 10 min in deionized water;	10 min in deionized water
	f) Rinse in deionized water;	Rinse in deionized water
	g) Vibrate for 3 min in deionized water;	3 min in deionised water
	h) Rinse in deionized water;	Rinse in deionized water
	i) Dry in a vacuum drying chamber (4.3.3).	Vacuum dry
	Care should be taken to avoid abrasion in the ultrasonic cleaner which could lead to change in mass.	
	4.4.3 Dry the test specimen and control specimen with a jet of inert gas (4.3.4).	Dry with inert gas
	4.4.4 Soak the test specimen and control specimen in propan-2-ol (4.2.3) for 5 min $\pm$ 15s.	Soak 5 min $\pm$ 15 s in propan-2-ol

	4.4.5 Dry the test specimen and control specimen with a jet of filtered inert gas (4.3.4), then dry further in a vacuum of better than 13,33 Pa $\pm$ 0, 13 pa for at least 30 min.	Dry with inert gas
		30 min Vacuum dry
	4.4.6 Dry the test specimen and control specimen on the balance twice in rotation within 90 min of removal from the vacuum. If the two readings per specimen are not identical within 100 $\mu$ g, continue taking readings in rotation until at least two readings per specimen are identical within 100 $\mu$ g. Store the test specimen and control specimen in a sealed dust-free container between weighings.	Take weight twice within 90 min
		Repeat if required
		Store in a sealed container
	4.4.7 Repeat 4.4.2 to 4.4.6 at intervals until incremental mass change of the specimen over 24 hrs is less than 10% of the previous cumulative mass change.	Repeat from 4.4.2 to 4.4.6
	4.4.8 Record the average gain in mass of the control specimen	Record initial control weight

#### **1.4 Finishing and Marking of Specimen Surfaces (Section 2.2.5)**

(Extracts from ASTM: F2083 – 12. Standard Specification for Knee Replacement Prosthesis)

1. Metallic components conforming to this specification shall be finished and marked in accordance with Practice F86, where applicable.
2. *Metallic Bearing Surface*—The main bearing surfaces shall have a surface finish no rougher than 0.10- $\mu\text{m}$  (4- $\mu\text{in.}$ ) roughness average,  $R_a$ , when measured in accordance with the principles given in ANSI/ASME B46.1.
3. *Polymeric Bearing Surface*—The main bearing surface of a UHMWPE component shall have a surface roughness no greater than 2- $\mu\text{m}$  (80- $\mu\text{in.}$ ) roughness average,  $R_a$ , when measured in accordance with the principles given in ANSI/ ASME B46.1.

When inspected with normal or corrected vision, the bearing surface shall be free from scale, embedded particles, scratches, and score marks other than those arising from the finishing process.

#### **1.5: Method of Particle Isolation (Section 3.2.4):**

Extract from BS ISO 17853:2011 section 5.2 –Wear of implant materials – Polymer and metal wear particles – Isolation and characterization.

## **Procedure for polymer materials — For example UHMWPE and polyetheretherketone (PEEK)**

### **1. Serum digestion with hydrochloric acid**

The following method has been published by Scott et al. and was originally used for UHMWPE materials only. The isolation of other materials such as PEEK and ceramics has been found to be successful with the acid digestion method, but resistance to hydrochloric acid should be investigated carefully for all materials other than UHMWPE.

- a) Add 10 ml of the serum sample to 40 ml of hydrochloric acid (37 % volume fraction).
- b) Mix with a stirrer bar for approximately 1 h at 50 °C. The fluid turns a slightly purple colour.
- c) Add 100 ml of methanol to 0.5 ml of the digestion solution.

### **2. Collection of particles**

The particles are collected by filtering through a 0.05µm polycarbonate filter membrane. Smaller pore sizes such as 0.015µm might be necessary for materials known to generate nanometre-sized particles. Alternatively, a sequence of progressively smaller filter sizes, e.g. 10µm, 1µm and 0.015µm, should be used for heavily loaded simulator lubricants to enable observation of individual particles.

Relevant aspects of ASTM F1877-05 (2010) standard practice for characterisation of particles was adequately described in chapter 3 (section 3.2.6).

## 1.6 (Section 4.2.3)

### LAL Assay Protocol (Quick guide published by Lonza®)

Pharma&Biotech

**Lonza**

## Traditional Gel Clot Limulus Amebocyte Lysate (LAL) Assay Procedure Quick Guide

This is a step by step guide depicting how to perform a traditional gel clot LAL assay. Prior to initiating the assay procedure, allow reagent vials to equilibrate to room temperature.

### Step 1

Reconstitute Control Standard Endotoxin (CSE) with LAL Reagent Water (LRW).



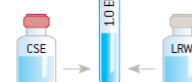
### Step 2

Vortex for 15 minutes.



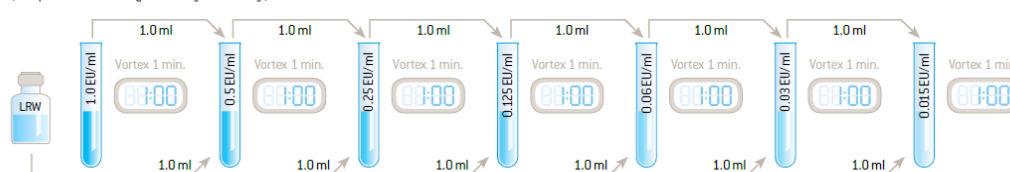
### Step 3

Dilute endotoxin with LRW to a concentration of 1.0 EU/ml using the endotoxin potency identified on the Certificate of Analysis (CoA).



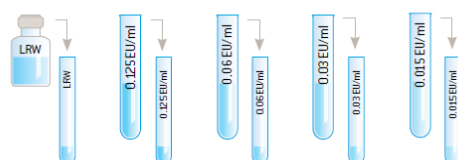
### Step 4

Label the tubes with the appropriate endotoxin concentration and add 1.0 ml of LRW to each. Using the 1.0 EU/ml solution, prepare serial 2-fold dilutions to bracket lysate sensitivity. (Example based on a test using 0.06 EU/ml lysate sensitivity.)



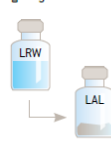
### Step 5

Add 100 µl of endotoxin standards and negative control (LRW) into each appropriately labeled 10×75 mm reaction tube.



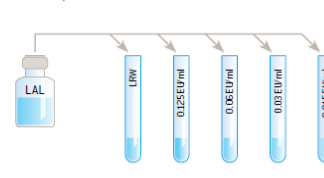
### Step 6

Immediately prior to use, reconstitute LAL and gently swirl.



### Step 7

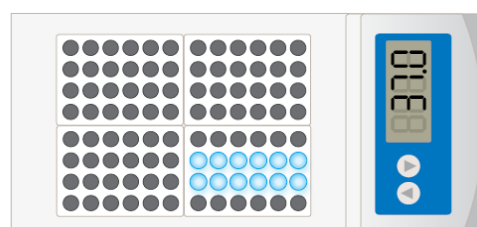
Add 100 µl reconstituted LAL into each reaction tube.



### Step 8

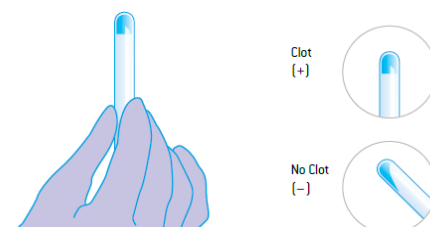
Place tubes in 37°C ± 1°C non-circulating water bath or heating block for 60 minutes.

Note: Water or dry bath should be located in the lab away from all sources of vibration that could disturb clot formation.



### Step 9

After 60 minutes (± 2 minutes) of incubation, carefully remove each tube and invert 180°. Record the reaction in each tube as either positive or negative.



Step by step guide to performing traditional Gel clot assay (Described in Lonza product brochure).

## **1.7 Procedure for isolation of mononuclear cells using SepMate™ tubes**

### **(Section 4.2.4)**

1. Add 15ml Ficoll-Paque gradient medium to the 50ml SepMate™ tube by carefully pipetting it through the central hole of the SepMate™ insert.
2. Prepare sample by adding equal volumes of blood sample to equal volume of Hanks balanced salt solution. Mix gently by pipetting.
3. Keeping the SepMate™ tube vertical, pipette 15ml of the diluted blood sample down the side of the tube.
4. Centrifuge at 1200 x g for 10 minutes at room temperature, with the brake on.
5. Pour off the top layer, which contains the enriched Mononuclear cells, into a new tube. Do not hold the SepMate™ tube in the inverted position for longer than 2 seconds.
6. Wash enriched mononuclear cells with Hanks balanced salt solution. Repeat wash. Centrifuging at 300 x g for 8 minutes at room temperature, with the brake on, is recommended.

## **1.8 Flow Cytometry Protocol (Section 4.2.4.1)**

### Cell fixation

1. Collect cells by centrifugation and aspirate supernatant.
2. Resuspend cells in 0.5- 1ml 1X PBS. Add appropriate volume of formaldehyde to obtain a final concentration of 4%.
3. Fix for 10 min in a 37°C water bath.
4. Chill tubes on ice for 1 min.



## Immunostaining

1. Aliquot  $0.5\text{--}1 \times 10^6$  cells into each assay tube.
2. Add 2ml incubation buffer to each tube and wash by centrifugation.  
Repeat.
3. Resuspend cells in 100 $\mu$ l of diluted primary antibody prepared in incubation buffer at the recommended dilution.
4. Incubate for 1 hour at room temperature.
5. Wash by centrifugation in 2ml incubation buffer.
6. Using a fluorochrome-conjugated primary antibody, resuspend cells in 0.5 ml 1x PBS and analyse on flow cytometer.

### **1.9 Cell viability protocol (Alamar Blue) – Section 4.2.7.1**

1. Warm the cell viability reagent to room temperature before use.
2. Add 1/10th volume of cell viability reagent directly to cells in culture medium.
3. Incubate for 1–4 hours at 37°C in a cell culture incubator, protected from direct light.

Note: Sensitivity of detection increases with longer incubation times. For samples with fewer cells, use longer incubation times of up to 24 hours.

4. Record results using the following fluorescence or absorbance values:
  - Fluorescence: Read fluorescence using a fluorescence excitation wavelength of 560 nm (excitation range is 540–570 nm) and an emission of 590 nm (emission range is 580–610–nm).

- Absorbance: Monitor the absorbance of reagent at 570 nm, using 600 nm as a reference wavelength (normalized to the 600-nm value).

### **1.10 ELISA Protocol (Section 4.2.7.3)**

(Based on technical document for Sandwich ELISA provided by Sigma Aldrich, UK)

1. Bring all reagents and samples to room temperature (18 - 25°C) before use. It is recommended that all standards and samples be run at least in duplicate.
2. Add 100 µl of each standard and sample into appropriate wells. Cover wells and incubate for 2.5 hours at room temperature or overnight at 4°C with gentle shaking.
3. Discard the solution and wash 4 times with 1X Wash Solution. Wash by filling each well with Wash Buffer (300 µl) using a multi-channel Pipette or autowasher. Complete removal of liquid at each step is essential to good performance. After the last wash, remove any remaining Wash Buffer by aspirating or decanting. Invert the plate and blot it against clean paper towels.
4. Add 100 µl of 1x prepared Detection Antibody to each well. Cover wells and incubate for 1 hour at room temperature with gentle shaking.
5. Discard the solution. Repeat the wash procedure as in step 3.
6. Add 100 µl of prepared Streptavidin solution to each well. Cover wells and incubate for 45 minutes at room temperature with gentle shaking.
7. Discard the solution. Repeat the wash as in step 3.

8. Add 100  $\mu$ l of TMB One-Step Substrate Reagent (Item H) to each well.  
Cover wells and incubate for 30 minutes at room temperature in the dark with gentle shaking.
9. Add 50  $\mu$ l of Stop Solution (Item I) to each well. Read absorbance at 450 nm immediately.

## CHAPTER TWO STATISTICS

**Volume loss comparison from PEEK pin and acetal pin articulations conducted at high stresses. Kruskal Wallis H test  $p < 0.0001$**

	PEEK-on-Acetal	PEEK-on-XLPE	PEEK-on-PEEK	PEEK-on-UHMWPE	Acetal-on-XLPE
PEEK-on-Acetal		<0.0001	0.001	0.021	<0.0001
PEEK-on-XLPE			<0.0001	<0.0001	<0.0001
PEEK-on-PEEK				0.015	0.409
PEEK-on-UHMWPE					<0.0001
Acetal-on-XLPE					

Table 1: Analysis of volume loss comparison from PEEK pin and acetal pin articulations. P values from Mann Whitney U tests shown. Comparisons with statistical significance highlighted in red (adjusted  $\alpha$  value: 0.01)

**Analysis volume loss comparing CoCr pin articulations conducted at high stresses. Kruskal Wallis H test  $p < 0.0001$**

	CoCr-on-PEEK	CoCr-on-UHMWPE	CoCr-on-XLPE
CoCr-on-PEEK		<0.0001	<0.0001
CoCr-on-UHMWPE			0.307
CoCr-on-XLPE			

Table 2: Analysis of volume loss comparison from CoCr pin articulations. P values from Mann Whitney U tests shown. Comparisons with statistical significance highlighted in red (adjusted  $\alpha$  value: 0.015).

**Direct Comparison of Articulations with CoCr-on-XLPE (High stress articulations)**

CoCr-on-XLPE	PEEK-on-XLPE	0.364
CoCr-on-XLPE	CoCr-on-UHMWPE	0.307
CoCr-on-XLPE	PEEK-on-Acetal	<0.0001
CoCr-on-XLPE	PEEK-on-UHMWPE	<0.0001
CoCr-on-XLPE	Acetal-on-XLPE	<0.0001
CoCr-on-XLPE	PEEK-on-PEEK	<0.0001
CoCr-on-XLPE	CFR-PEEK-on-UHMWPE	<0.0001
CoCr-on-XLPE	CoCr-on-PEEK	<0.0001

Table 3: Direct comparison of volume loss from each articulation with reference combination, CoCr-on-XLPE, statistically significant combinations are highlighted in red

### Volume loss in all articulations tested low stress articulations

	CoCr-on-XLPE	PEEK-on-XLPE	PEEK-on-UHMWPE	CFR-PEEK-on-XLPE
CoCr-on-XLPE		0.902	0.650	0.008
PEEK-on-XLPE			0.695	0.005
PEEK-on-UHMWPE				0.032
CFR-PEEK-on-XLPE				

Table 4: Analysis of volume loss comparison from all articulations tested at low stresses. Comparisons with statistical significance highlighted in red.

Other statistics including analysis of surface profilometry for PEEK pin, acetal pin and CoCr pin articulations was discussed in Chapter 2.

# STATISTICS CHAPTER 3

## Equivalent Circle Diameter. Particles from articulations (Section 3.3.2): Kruskal Wallis $p = <0.0001$

	CoCr-on-XLPE	CoCr-on-UHMWPE	CoCr-on-PEEK	CFR-PEEK-on-UHMWPE	PEEK-on-XLPE	PEEK-on-UHMWPE	PEEK-on-PEEK
CoCr-on-XLPE		<0.0001*	<0.0001*	0.680	0.006*	<0.0001*	<0.0001*
CoCr-on-UHMWPE			<0.0001*	<0.0001*	<0.0001*	<0.0001*	0.013
CoCr-on-PEEK				<0.0001*	<0.0001*	<0.0001*	<0.0001*
CFR-PEEK-on-UHMWPE					0.005*	<0.0001*	<0.0001*
PEEK-on-XLPE						<0.0001*	<0.0001*
PEEK-on-UHMWPE							<0.0001*
PEEK-on-PEEK							

Table 5: Comparison of articulations, asterisks depicts significance. Adjusted  $\alpha$  value – 0.007.

**Aspect Ratio: Particles from articulations: (3.3.3) Kruskal Wallis  $p = <0.0001$**

	CoCr-on-XLPE	CoCr-on-UHMWPE	CoCr-on-PEEK	CFR-PEEK-on-UHMWPE	PEEK-on-XLPE	PEEK-on-UHMWPE	PEEK-on-PEEK
CoCr-on-XLPE		<0.0001*	0.753	0.244	0.106	0.015	0.04
CoCr-on-UHMWPE			<0.0001*	<0.0001*	0.099	<0.0001*	0.084
CoCr-on-PEEK				0.147	0.109	0.001*	0.043
CFR-PEEK-on-UHMWPE					0.010	0.232	0.003*
PEEK-on-XLPE						<0.0001*	0.889
PEEK-on-UHMWPE							<0.0001*
PEEK-on-PEEK							
Table 6: Comparison of articulations, asterisks depicts significance. Adjusted $\alpha = 0.007$							



**Roundness. Particles from articulations: (Section 3.3.3). Kruskal Wallis p= 0.001**

	CoCr-on-XLPE	CoCr-on-UHMWPE	CoCr-on-PEEK	CFR-PEEK-on-UHMWPE	PEEK-on-XLPE	PEEK-on-UHMWPE	PEEK-on-PEEK
CoCr-on-XLPE		<0.0001*	0.757	0.234	0.092	0.015	0.037
CoCr-on-UHMWPE			<0.0001*	<0.0001*	0.120	<0.0001*	0.102
CoCr-on-PEEK				0.135	0.098	0.002*	0.038
CFR-PEEK-on-UHMWPE					0.008	0.241	0.002*
PEEK-on-XLPE						<0.0001*	0.895
PEEK-on-UHMWPE							<0.0001*
PEEK-on-PEEK							
Table 7: Comparison of articulations. Asterisks depicts significance. Adjusted $\alpha$ = 0.007							

**Form Factor. Particles from articulations (Section 3.3.3): Kruskal Wallis  $p < 0.0001$**

	CoCr-on-XLPE	CoCr-on-UHMWPE	CoCr-on-PEEK	CFR-PEEK-on-UHMWPE	PEEK-on-XLPE	PEEK-on-UHMWPE	PEEK-on-PEEK
CoCr-on-XLPE		0.560	<0.0001*	<0.0001*	<0.0001*	<0.0001*	<0.0001*
CoCr-on-UHMWPE			<0.0001*	<0.0001*	<0.0001*	<0.0001*	<0.0001*
CoCr-on-PEEK				0.153	<0.0001*	0.058	<0.0001*
CFR-PEEK-on-UHMWPE					<0.0001*	0.008	<0.0001*
PEEK-on-XLPE						<0.0001*	0.106
PEEK-on-UHMWPE							<0.0001*
PEEK-on-PEEK							
Table 8: Comparison of articulations, asterisks depicts significance. Adjusted $\alpha$ value = 0.007							

**Particle Quantification (Section 3.3.4). Kruskal Wallis  $p < 0.0001$**

	CoCr-on-XLPE	CoCr-on-UHMWPE	CoCr-on-PEEK	CFR-PEEK-on-UHMWPE	PEEK-on-XLPE	PEEK-on-UHMWPE	PEEK-on-PEEK
CoCr-on-XLPE		0.174	<0.0001*	<0.0001*	0.671	<0.0001*	<0.0001*
CoCr-on-UHMWPE			<0.0001*	<0.0001*	0.372	<0.0001*	<0.0001*
CoCr-on-PEEK				0.438	<0.0001*	<0.0001*	<0.0001*
CFR-PEEK-on-UHMWPE					<0.0001*	<0.0001*	<0.0001*
PEEK-on-XLPE						<0.0001*	<0.0001*
PEEK-on-UHMWPE							<0.0001*
PEEK-on-PEEK							
Table 9: Comparison of articulations using Mann Whitney U test. Asterisks depicts significance, adjusted $\alpha = 0.007$ .							

## STATISTICS CHAPTER 4

### 4.1 Particle Morphology (section 4.3.2)

#### 4.1.1 Aspect Ratio

	PEEK	XLPE	UHMWPE
PEEK		0.001	0.017
XLPE			0.000
UHMWPE			
Table 10: p values after statistical analysis, significance displayed in red, adjusted $\alpha$ value of 0.017.			

#### 4.1.2 Equivalent Circle Diameter

	PEEK	XLPE	UHMWPE
PEEK		0.000	0.024
XLPE			0.000
UHMWPE			
Table 11: p values after statistical analysis, significance displayed in red, adjusted $\alpha$ value of 0.017.			

#### 4.1.3 Form factor

	PEEK	XLPE	UHMWPE
PEEK		0.000	0.000
XLPE			0.243
UHMWPE			
Table 12: p values after statistical analysis, significance displayed in red, adjusted $\alpha$ value of 0.017.			

#### 4.1.4 Roundness

	PEEK	XLPE	UHMWPE
PEEK		0.001	0.003
XLPE			0.927
UHMWPE			
Table 13: p values after statistical analysis, significance displayed in red, adjusted $\alpha$ value of 0.017.			

## BIBLIOGRAPHY

1. AKHAVAN, S., MATTHIESEN, M. M., SCHULTE, L., PENOYAR, T., KRAAY, M. J., RIMNAC, C. M. & GOLDBERG, V. M. 2006. Clinical and histologic results related to a low-modulus composite total hip replacement stem. *J Bone Joint Surg Am*, 88, 1308-14.
2. AL LAFI, A. G. 2014. FTIR spectroscopic analysis of ion irradiated poly (ether ether ketone). *Polymer Degradation and Stability*, 105, 122-133.
3. ALOTTA, G., BARRERA, O. & PEGG, E. C. 2018. Viscoelastic material models for more accurate polyethylene wear estimation. *The Journal of Strain Analysis for Engineering Design*, 53, 302-312.
4. ANDERSEN, M. R., WINTHER, N. S., LIND, T., SCHRODER, H. M. & MORK PETERSEN, M. 2018. Bone Remodeling of the Distal Femur After Uncemented Total Knee Arthroplasty-A 2-Year Prospective DXA Study. *J Clin Densitom*, 21, 236-243.
5. ARNHOLT, C. M., MACDONALD, D. W., MALKANI, A. L., KLEIN, G. R., RIMNAC, C. M., KURTZ, S. M., KOCAGOZ, S. B., GILBERT, J. L. & COMMITTEE, I. R. C. W. 2016. Corrosion damage and wear mechanisms in long-term retrieved CoCr femoral components for total knee arthroplasty. *The Journal of arthroplasty*, 31, 2900-2906.
6. ASTM INTERNATIONAL 2010. F1877-5(2010) Standard Practice for Characterization of Particles. Pennsylvania, USA: ASTM International.

7. ASTM INTERNATIONAL 2012. ASTM F2083 - 12. Standard Specification for Knee Replacement Prosthesis. Pennsylvania, USA: ASTM International.
8. ASTM INTERNATIONAL (F1904) 2014. Standard Practice for Testing the Biological Responses to Particles *In vivo*. Pennsylvania, USA.
9. ATKINS, G. J., WELLDON, K. J., HOLDING, C. A., HAYNES, D. R., HOWIE, D. W. & FINDLAY, D. M. 2009. The induction of a catabolic phenotype in human primary osteoblasts and osteocytes by polyethylene particles. *Biomaterials*, 30, 3672-3681.
10. BARATZ, M. E., FU, F. H. & MENGATO, R. 1986. Meniscal tears: the effect of meniscectomy and of repair on intraarticular contact areas and stress in the human knee. A preliminary report. *Am J Sports Med*, 14, 270-5.
11. BARTEL, D. L., RAWLINSON, J., BURSTEIN, A., RANAWAT, C. & FLYNN, J. W. 1995. Stresses in polyethylene components of contemporary total knee replacements. *Clinical Orthopaedics and Related Research*, 76-82.
12. BAXTER, R. M., STEINBECK, M. J., TIPPER, J. L., PARVIZI, J., MARCOLONGO, M. & KURTZ, S. M. 2009. Comparison of periprosthetic tissue digestion methods for ultra-high molecular weight polyethylene wear debris extraction. *J Biomed Mater Res B Appl Biomater*, 91, 409-18.
13. BAYKAL, D., SISKEY, R. S., UNDERWOOD, R. J., BRISCOE, A. & KURTZ, S. M. 2016. The biotribology of PEEK-on-HXLPE bearings is

comparable to traditional bearings on a multidirectional Pin-on-disk tester.

*Clinical Orthopaedics and Related Research*®, 474, 2384-2393.

14. BELL, M. L. 2018. New guidance to improve sample size calculations for trials: eliciting the target difference. *Trials*, 19, 605.
15. BENNETT, W. E. & COHN, Z. A. 1966. The isolation and selected properties of blood monocytes. *Journal of Experimental Medicine*, 123, 145-160.
16. BILLI, F., BENYA, P., KAVANAUGH, A., ADAMS, J., EBRAMZADEH, E. & MCKELLOP, H. 2012a. The John Charnley Award: an accurate and sensitive method to separate, display, and characterize wear debris: part 1: polyethylene particles. *Clin Orthop Relat Res*, 470, 329-38.
17. BILLI, F., BENYA, P., KAVANAUGH, A., ADAMS, J., MCKELLOP, H. & EBRAMZADEH, E. 2012b. The John Charnley Award: an accurate and extremely sensitive method to separate, display, and characterize wear debris: part 2: metal and ceramic particles. *Clin Orthop Relat Res*, 470, 339-50.
18. BLUNN, G. 2013. (iii) Bearing surfaces. *Orthopaedics and Trauma*, 27, 85-92.
19. BLUNN, G. W., WALKER, P. S., JOSHI, A. & HARDINGE, K. 1991. The dominance of cyclic sliding in producing wear in total knee replacements. *Clinical Orthopaedics and Related Research*, 273, 253-260.
20. BOYER, B., BORDINI, B., CAPUTO, D., NERI, T., STEA, S. & TONI, A. 2018. Is Cross-Linked Polyethylene an Improvement Over Conventional



Ultra-High Molecular Weight Polyethylene in Total Knee Arthroplasty? *J Arthroplasty*, 33, 908-914.

21. BOZIC, K. J., KURTZ, S. M., LAU, E., ONG, K., CHIU, V., VAIL, T. P., RUBASH, H. E. & BERRY, D. J. 2010. The epidemiology of revision total knee arthroplasty in the United States. *Clinical Orthopaedics and Related Research*, 468, 45-51.
22. BRACCO, P. & ORAL, E. 2011. Vitamin E-stabilized UHMWPE for total joint implants: a review. *Clin Orthop Relat Res*, 469, 2286-93.
23. BRADLEY, G. W., FREEMAN, M. A., TUKE, M. A. & MCKELLOP, H. A. 1993. Evaluation of wear in an all-polymer total knee replacement. Part 2: clinical evaluation of wear in a polyethylene on polyacetal total knee. *Clin Mater*, 14, 127-32.
24. BROOKS, R. A., JONES, E., STORER, A. & RUSHTON, N. 2004. Biological evaluation of carbon-fibre-reinforced polybutyleneterephthalate (CFRPBT) employed in a novel acetabular cup. *Biomaterials*, 25, 3429-38.
25. BROWN, T., BAO, Q. B., AGRAWAL, C. M. & HALLAB, N. J. 2011. An in vitro assessment of wear particulate generated from NUBAC: a PEEK-on-PEEK articulating nucleus replacement device: methodology and results from a series of wear tests using different motion profiles, test frequencies, and environmental conditions. *Spine (Phila Pa 1976)*, 36, E1675-85.
26. BUCKWALTER, J. A., EINHORN, T. A. & SIMON, S. R. 2000. *Orthopaedic basic science: biology and biomechanics of the musculoskeletal system*, Amer Academy of Orthopaedic.

27. BUECHEL, F. F. & PAPPAS, M. 1986. The New Jersey Low-Contact-Stress Knee Replacement System: biomechanical rationale and review of the first 123 cemented cases. *Archives of Orthopaedic and Trauma Surgery*, 105, 197-204.
28. CALCE, S. E., KURKI, H. K., WESTON, D. A. & GOULD, L. 2018. The relationship of age, activity, and body size on osteoarthritis in weight-bearing skeletal regions. *International Journal of Paleopathology*, 22, 45-53.
29. CAMPBELL, P., MA, S., YEOM, B., MCKELLOP, H., SCHMALZRIED, T. & AMSTUTZ, H. 1995. Isolation of predominantly submicron-sized UHMWPE wear particles from periprosthetic tissues. *Journal of Biomedical Materials Research Part A*, 29, 127-131.
30. CARNES, K. J., ODUM, S. M., TROYER, J. L. & FEHRING, T. K. 2016. Cost Analysis of Ceramic Heads in Primary Total Hip Arthroplasty. *J Bone Joint Surg Am*, 98, 1794-1800.
31. CARR, A. J., ROBERTSSON, O., GRAVES, S., PRICE, A. J., ARDEN, N. K., JUDGE, A. & BEARD, D. J. 2012. Knee replacement. *The Lancet*, 379, 1331-1340.
32. CHEN, Q. & THOUAS, G. A. 2015. Metallic implant biomaterials. *Materials Science and Engineering: R: Reports*, 87, 1-57.
33. CHEN, Y., WANG, X., LU, X., YANG, L., YANG, H., YUAN, W. & CHEN, D. 2013. Comparison of titanium and polyetheretherketone (PEEK) cages in the surgical treatment of multilevel cervical spondylotic myelopathy: a

prospective, randomized, control study with over 7-year follow-up. *European Spine Journal*, 22, 1539-1546.

34. CHO, D. R., SHANBHAG, A. S., HONG, C.-Y., BARAN, G. R. & GOLDRING, S. R. 2002. The role of adsorbed endotoxin in particle-induced stimulation of cytokine release. *Journal of Orthopaedic Research*, 20, 704-713.
35. CHRISTIANSEN, T. 1969. A new hip prosthesis with trunnion-bearing. *Acta Chir Scand*, 135, 43-6.
36. CHRISTIANSEN, T. 1974. A combined endo- and total hip prosthesis with trunnion-bearing. The Christiansen prosthesis. *Acta Chir Scand*, 140, 185-8.
37. CHUMMY, S. S. & SINNATAMBY, F. 1999. Last's Anatomy; Regional and Applied. Churchill Livingstone.
38. CLARKE, I., STARKEBAUM, W., HOSSEINIAN, A., MCGUIRE, P., OKUDA, R., SALOVEY, R. & YOUNG, R. 1985. Fluid-sorption phenomena in sterilized polyethylene acetabular prostheses. *Biomaterials*, 6, 184-188.
39. COATHUP, M. J., BLACKBURN, J., GOODSHIP, A. E., CUNNINGHAM, J. L., SMITH, T. & BLUNN, G. W. 2005. Role of hydroxyapatite coating in resisting wear particle migration and osteolysis around acetabular components. *Biomaterials*, 26, 4161-4169.
40. COBELLI, N., SCHARF, B., CRISI, G. M., HARDIN, J. & SANTAMBROGIO, L. 2011. Mediators of the inflammatory response to joint replacement devices. *Nature Reviews Rheumatology*, 7, 600.

41. COGSWELL, F. & HOPPRICH, M. 1983. Environmental resistance of carbon fibre-reinforced polyether etherketone. *Composites*, 14, 251-253.
42. COLLIER, J. P., CURRIER, B. H., KENNEDY, F. E., CURRIER, J. H., TIMMINS, G. S., JACKSON, S. K. & BREWER, R. L. 2003. Comparison of cross-linked polyethylene materials for orthopaedic applications. *Clin Orthop Relat Res*, 289-304.
43. CORNWALL, G., BRYANT, J. & HANSSON, C. 2001. The effect of kinematic conditions on the wear of ultra-high molecular weight polyethylene (UHMWPE) in orthopaedic bearing applications. *Proceedings of the Institution of Mechanical Engineers, Part H: Journal of Engineering in Medicine*, 215, 95-106.
44. COTTINO, U., ABDEL, M. P., PERRY, K. I., MARA, K. C., LEWALLEN, D. G. & HANSSEN, A. D. 2017. Long-Term Results After Total Knee Arthroplasty with Contemporary Rotating-Hinge Prostheses. *J Bone Joint Surg Am*, 99, 324-330.
45. COWIE, R. M., BRISCOE, A., FISHER, J. & JENNINGS, L. M. 2016. PEEK-OPTIMA() as an alternative to cobalt chrome in the femoral component of total knee replacement: A preliminary study. *Proc Inst Mech Eng H*, 230, 1008-1015.
46. COWIE, R. M., BRISCOE, A., FISHER, J. & JENNINGS, L. M. 2019. Wear and Friction of UHMWPE-on-PEEK OPTIMA. *J Mech Behav Biomed Mater*, 89, 65-71.

47. D'LIMA, D. D., FREGLY, B. J., PATIL, S., STEKLOV, N. & COLWELL, C. W., JR. 2012. Knee joint forces: prediction, measurement, and significance. *Proc Inst Mech Eng H*, 226, 95-102.
48. D'LIMA, D. D., STEKLOV, N., FREGLY, B. J., BANKS, S. A. & COLWELL, C. W. 2008. In vivo contact stresses during activities of daily living after knee arthroplasty. *Journal of Orthopaedic Research*, 26, 1549-1555.
49. DASER, A., MITCHISON, H., MITCHISON, A. & MULLER, B. 1996. Non-classical-MHC genetics of immunological disease in man and mouse. The key role of pro-inflammatory cytokine genes. *Cytokine*, 8, 593-7.
50. DE RUITER, L., JANSSEN, D., BRISCOE, A. & VERDONSCHOT, N. 2017a. The mechanical response of a polyetheretherketone femoral knee implant under a deep squatting loading condition. *Proc Inst Mech Eng H*, 231, 1204-1212.
51. DE RUITER, L., JANSSEN, D., BRISCOE, A. & VERDONSCHOT, N. 2017b. A preclinical numerical assessment of a polyetheretherketone femoral component in total knee arthroplasty during gait. *J Exp Orthop*, 4, 3.
52. DESJARDINS, J. D., WALKER, P. S., HAIDER, H. & PERRY, J. 2000. The use of a force-controlled dynamic knee simulator to quantify the mechanical performance of total knee replacement designs during functional activity. *Journal of Biomechanics*, 33, 1231-1242.
53. DIEPPE, P. A. & LOHMANDER, L. S. 2005. Pathogenesis and management of pain in osteoarthritis. *Lancet*, 365, 965-73.

54. DOORN, P. F., CAMPBELL, P. A., WORRALL, J., BENYA, P. D., MCKELLOP, H. A. & AMSTUTZ, H. C. 1998. Metal wear particle characterization from metal on metal total hip replacements: transmission electron microscopy study of periprosthetic tissues and isolated particles. *J Biomed Mater Res*, 42, 103-11.
55. DUMBLETON, J. H., D'ANTONIO, J. A., MANLEY, M. T., CAPELLO, W. N. & WANG, A. 2006. The basis for a second-generation highly cross-linked UHMWPE. *Clinical orthopaedics and related research*, 453, 265-271.
56. DUMBLETON, J. H., MANLEY, M. T. & EDIDIN, A. A. 2002. A literature review of the association between wear rate and osteolysis in total hip arthroplasty. *J Arthroplasty*, 17, 649-61.
57. EAST, R. H., BRISCOE, A. & UNSWORTH, A. 2015a. Wear of PEEK-OPTIMA(R) and PEEK-OPTIMA(R)-Wear Performance articulating against highly cross-linked polyethylene. *Proc Inst Mech Eng H*, 229, 187-93.
58. EAST, R. H., BRISCOE, A. & UNSWORTH, A. 2015b. Wear of PEEK-OPTIMA® and PEEK-OPTIMA®-Wear Performance articulating against highly cross-linked polyethylene. *Proceedings of the Institution of Mechanical Engineers, Part H: Journal of Engineering in Medicine*, 229, 187-193.

59. EDIDIN, A. A. & KURTZ, S. M. 2000. Influence of mechanical behavior on the wear of 4 clinically relevant polymeric biomaterials in a hip simulator. *J Arthroplasty*, 15, 321-31.
60. EFTEKHAR, N. 1983. Total knee-replacement arthroplasty. Results with the intramedullary adjustable total knee prosthesis. *JBJS*, 65, 293-309.
61. ELFICK, A. P., GREEN, S. M., PINDER, I. M. & UNSWORTH, A. 2000. A novel technique for the detailed size characterization of wear debris. *J Mater Sci Mater Med*, 11, 267-71.
62. ENDO, M., TIPPER, J. L., BARTON, D. C., STONE, M. H., INGHAM, E. & FISHER, J. 2002. Comparison of wear, wear debris and functional biological activity of moderately crosslinked and non-crosslinked polyethylenes in hip prostheses. *Proc Inst Mech Eng H*, 216, 111-22.
63. ENDRES, S., BARTSCH, I., STÜRZ, S., KRATZ, M. & WILKE, A. 2008. Polyethylene and cobalt–chromium molybdenum particles elicit a different immune response in vitro. *Journal of Materials Science: Materials in Medicine*, 19, 1209-1214.
64. FELSON, D. T. 1988. Epidemiology of hip and knee osteoarthritis. *Epidemiologic reviews*, 10, 1-28.
65. FELSON, D. T., NAIMARK, A., ANDERSON, J., KAZIS, L., CASTELLI, W. & MEENAN, R. F. 1987. The prevalence of knee osteoarthritis in the elderly. the framingham osteoarthritis study. *Arthritis & Rheumatism*, 30, 914-918.

66. FIELD, R. E., RAJAKULENDRAN, K., ESWARAMOORTHY, V. K. & RUSHTON, N. 2012. Three-year prospective clinical and radiological results of a new flexible horseshoe acetabular cup. *Hip Int*, 22, 598-606.
67. FIELD, R. E. & RUSHTON, N. 2005. Five-year clinical, radiological and postmortem results of the Cambridge Cup in patients with displaced fractures of the neck of the femur. *J Bone Joint Surg Br*, 87, 1344-51.
68. FISHER, J. 1994. Wear of ultra high molecular weight polyethylene in total artificial joints. *Current Orthopaedics*, 8, 164-169.
69. FISHER, J., FIRKINS, P., REEVES, E., HAILEY, J. & ISAAC, G. 1995. The influence of scratches to metallic counterfaces on the wear of ultra-high molecular weight polyethylene. *Proceedings of the Institution of Mechanical Engineers, Part H: Journal of Engineering in Medicine*, 209, 263-264.
70. FISHER, J., MCEWEN, H. M., TIPPER, J. L., GALVIN, A. L., INGRAM, J., KAMALI, A., STONE, M. H. & INGHAM, E. 2004. Wear, debris, and biologic activity of cross-linked polyethylene in the knee: benefits and potential concerns. *Clin Orthop Relat Res*, 114-9.
71. FITZGERALD, R. H., KAUFER, H. & MALKANI, A. L. 2002. *Orthopaedics*, Gulf Professional Publishing.
72. FLANNERY, M., JONES, E. & BIRKINSHAW, C. 2010. Compliant layer knee bearings. Part II: Preliminary wear assessment. *Wear*, 269, 331-338.



73. FLANNERY, M., MCGLOUGHLIN, T., JONES, E. & BIRKINSHAW, C. 2008. Analysis of wear and friction of total knee replacements: Part I. Wear assessment on a three station wear simulator. *Wear*, 265, 999-1008.
74. FREEMAN, M. & PINSKEROVA, V. 2005. The movement of the normal tibio-femoral joint. *Journal of biomechanics*, 38, 197-208.
75. FREEMAN, M., SAMUELSON, K. & BERTIN, K. 1985. Freeman-Samuelson total arthroplasty of the knee. *Clinical orthopaedics and related research*, 192, 46-58.
76. FREEMAN, M. A., SWANSON, S. A. & TODD, R. C. 1973. Total replacement of the knee using the Freeman-Swanson knee prosthesis. *Clin Orthop Relat Res*, 153-70.
77. FUHRMANN, G., STEINER, M., FREITAG-WOLF, S. & KERN, M. 2014. Resin bonding to three types of polyaryletherketones (PAEKs)—Durability and influence of surface conditioning. *Dental Materials*, 30, 357-363.
78. GARINO, J. P. & BEREDJIKLIAN, P. K. 2007. *Adult reconstruction and arthroplasty*, Elsevier Health Sciences.
79. GARRETT, S., JACOBS, N., YATES, P., SMITH, A. & WOOD, D. 2010. Differences in metal ion release following cobalt-chromium and oxidized zirconium total knee arthroplasty. *Acta Orthopaedica Belgica*, 76, 513.
80. GELB, H., SCHUMACHER, H. R., CUCKLER, J., DUCHEYNE, P. & BAKER, D. G. 1994. In vivo inflammatory response to polymethylmethacrylate particulate debris: effect of size, morphology, and surface area. *J Orthop Res*, 12, 83-92.

81. GERINGER, J., TATKIEWICZ, W. & ROUCHOUSE, G. 2011a. Wear behavior of PAEK, poly (aryl-ether-ketone), under physiological conditions, outlooks for performing these materials in the field of hip prosthesis. *Wear*, 271, 2793-2803.
82. GERINGER, J., TATKIEWICZ, W. & ROUCHOUSE, G. 2011b. Wear behavior of PAEK, poly(aryl-ether-ketone), under physiological conditions, outlooks for performing these materials in the field of hip prosthesis. *Wear*, 271, 2793-2803.
83. GIROT, P., MOROUX, Y., DUTEIL, X. P., NGUYEN, C. & BOSCHETTI, E. 1990. Composite affinity sorbents and their cleaning in place. *Journal of Chromatography A*, 510, 213-223.
84. GLANT, T. T., JACOBS, J. J., MOLNÁR, G., SHANBHAG, A. S., VALYON, M. & GALANTE, J. O. 1993. Bone resorption activity of particulate-stimulated macrophages. *Journal of Bone and Mineral Research*, 8, 1071-1079.
85. GLASSMAN, A. H., CROWNINSHIELD, R. D., SCHENCK, R. & HERBERTS, P. 2001. A low stiffness composite biologically fixed prosthesis. *Clin Orthop Relat Res*, 128-36.
86. GOLDBLATT, J. P. & RICHMOND, J. C. 2003. Anatomy and biomechanics of the knee. *Operative Techniques in Sports Medicine*, 11, 172-186.
87. GOLDRING, M. B. & GOLDRING, S. R. 2007. Osteoarthritis. *J Cell Physiol*, 213, 626-34.

88. GOMOLL, A., WANICH, T. & BELLARE, A. 2002. J-integral fracture toughness and tearing modulus measurement of radiation cross-linked UHMWPE. *Journal of Orthopaedic Research*, 20, 1152-1156.
89. GRANCHI, D., CENNI, E., TIGANI, D., TRISOLINO, G., BALDINI, N. & GIUNTI, A. 2008. Sensitivity to implant materials in patients with total knee arthroplasties. *Biomaterials*, 29, 1494-1500.
90. GREEN, S. & SCHLEGEL, J. 2001. A polyaryletherketone biomaterial for use in medical implant applications. *Polym for the Med Ind Proc, Brussels*, 14-15.
91. GREEN, T., FISHER, J., STONE, M., WROBLEWSKI, B. & INGHAM, E. 1998. Polyethylene particles of a 'critical size' are necessary for the induction of cytokines by macrophages in vitro. *Biomaterials*, 19, 2297-2302.
92. GREEN, T. R., FISHER, J., MATTHEWS, J. B., STONE, M. H. & INGHAM, E. 2000. Effect of size and dose on bone resorption activity of macrophages by in vitro clinically relevant ultra high molecular weight polyethylene particles. *Journal of Biomedical Materials Research Part A*, 53, 490-497.
93. GUNSTON, F. H. 1971. Polycentric knee arthroplasty. *Bone & Joint Journal*, 53, 272-277.
94. HADDAD, F. S., THAKRAR, R. R., HART, A. J., SKINNER, J. A., NARGOL, A. V., NOLAN, J. F., GILL, H. S., MURRAY, D. W., BLOM, A.

- W. & CASE, C. P. 2011. Metal-on-metal bearings: the evidence so far. *J Bone Joint Surg Br*, 93, 572-9.
95. HALL, J., COPP, S. N., ADELSON, W. S., D'LIMA, D. D. & COLWELL, C. W. 2008. Extensor mechanism function in single-radius vs multiradius femoral components for total knee arthroplasty. *The Journal of arthroplasty*, 23, 216-219.
96. HALL, R. M., BANKES, M. J. K. & BLUNN, G. 2001. Biotribology for joint replacement. *Current Orthopaedics*, 15, 281-290.
97. HALLAB, N. J., MCALLISTER, K., BRADY, M. & JARMAN-SMITH, M. 2012. Macrophage reactivity to different polymers demonstrates particle size-and material-specific reactivity: PEEK-OPTIMA® particles versus UHMWPE particles in the submicron, micron, and 10 micron size ranges. *Journal of Biomedical Materials Research Part B: Applied Biomaterials*, 100, 480-492.
98. HAMILTON, W. J. 1982. *Textbook of human anatomy*, Springer.
99. HARADA, Y., DOPPALAPUDI, V., WILLIS, A., JASTY, M., HARRIS, W. & GOLDRING, S. Human macrophage response to polyethylene particles in vitro: A new experimental model. *Proceedings of the 40th Annual Meeting of the Orthopaedic Research Society*, 1994.
100. HARRIS, W. H. 2001. Wear and periprosthetic osteolysis: the problem. *Clin Orthop Relat Res*, 66-70.
101. HARTZBAND, M. A., GLASSMAN, A. H., GOLDBERG, V. M., JORDAN, L. R., CROWNINSHIELD, R. D., FRICKA, K. B. & JORDAN, L. C. 2010.

- Survivorship of a low-stiffness extensively porous-coated femoral stem at 10 years. *Clin Orthop Relat Res*, 468, 433-40.
- 102.HECKER, W., WITTHAUER, D. & STAERK, A. 1994. Validation of dry heat inactivation of bacterial endotoxins. *PDA J Pharm Sci Technol*, 48, 197-204.
- 103.HITCHINS, V. & MERRITT, K. 1999. Decontaminating particles exposed to bacterial endotoxin (LPS). *Journal of Biomedical Materials Research Part A*, 46, 434-437.
- 104.HOROWITZ, S. M. & GONZALES, J. B. 1997. Effects of polyethylene on macrophages. *Journal of orthopaedic research*, 15, 50-56.
- 105.HOWIE, D., VERNON-ROBERTS, B., OAKESHOTT, R. & MANTHEY, B. 1988. A rat model of resorption of bone at the cement-bone interface in the presence of polyethylene wear particles. *JBJS*, 70, 257-263.
- 106.HUANG, Y. & YOUNG, R. 1995. Effect of fibre microstructure upon the modulus of PAN-and pitch-based carbon fibres. *Carbon*, 33, 97-107.
- 107.HWANG, H. S. & KIM, H. A. 2015. Chondrocyte Apoptosis in the Pathogenesis of Osteoarthritis. *Int J Mol Sci*, 16, 26035-54.
- 108.ILALOV, K., COHN, R. M. & SLOVER, J. 2013. High-performance total knee replacement. *Bull Hosp Jt Dis (2013)*, 71, 79-88.
- 109.INGHAM, E. & FISHER, J. 2000. Biological reactions to wear debris in total joint replacement. *Proc Inst Mech Eng H*, 214, 21-37.
- 110.INGHAM, E. & FISHER, J. 2005. The role of macrophages in osteolysis of total joint replacement. *Biomaterials*, 26, 1271-1286.

- 111.INSALL, J., SCOTT, W. N. & RANAWAT, C. S. 1979. The total condylar knee prosthesis. A report of two hundred and twenty cases. *JBJS*, 61, 173-180.
- 112.INSALL, J. N., LACHIEWICZ, P. & BURSTEIN, A. 1982. The posterior stabilized condylar prosthesis: a modification of the total condylar design. Two to four-year clinical experience. *JBJS*, 64, 1317-1323.
- 113.ISO 14243-1 2009. Implants for surgery-Wear of total joint prostheses - Part 1: Loading and displacement parameters for wear testing machines with load control and corresponding environmental conditions for test. London: International Organization for Standardization.
- 114.ISO 14243-2 2009. Implants for surgery - Wear of total joint prostheses, Part 2: Methods of measurement.
- 115.ISO 14243-3 2009. Implants for surgery -- Wear of total knee-joint prostheses -- Part 3: Loading and displacement parameters for wear-testing machines with displacement control and corresponding environmental conditions for test. International Organization for Standardization.
- 116.ISO 17853 2011. Wear of implant materials - Polymer and metal wear particles - Isolation and characterization. London.
- 117.IWAKI, H., PINSKEROVA, V. & FREEMAN, M. 2000. Tibiofemoral movement 1: the shapes and relative movements of the femur and tibia in the unloaded cadaver knee. *Bone & Joint Journal*, 82, 1189-1195.

118. JIANG, Y., JIA, T., WOOLEY, P. H. & YANG, S.-Y. 2013. Current research in the pathogenesis of aseptic implant loosening associated with particulate wear debris. *Acta Orthop Belg*, 79, 1-9.
119. JOHNSON, W., MEI, B. & COHN, Z. A. 1977. The separation, long-term cultivation, and maturation of the human monocyte. *Journal of Experimental Medicine*, 146, 1613-1626.
120. JOYCE, T., MONK, D., SCHOLLES, S. & UNSWORTH, A. 2000. A multi-directional wear screening device and preliminary results of UHMWPE articulating against stainless steel. *Bio-medical materials and engineering*, 10, 241-249.
121. KADDICK C 2014. *Simulator Testing of Total Knee Replacements*. In: Knahr K. (eds) *Tribology in Total Hip and Knee Arthroplasty*, Berlin, Heidelberg Springer.
122. KANDAHARI, A. M., YANG, X., LAROCHE, K. A., DIGHE, A. S., PAN, D. & CUI, Q. 2016a. A review of UHMWPE wear-induced osteolysis: the role for early detection of the immune response. *Bone Res*, 4, 16014.
123. KANDAHARI, A. M., YANG, X., LAROCHE, K. A., DIGHE, A. S., PAN, D. & CUI, Q. 2016b. A review of UHMWPE wear-induced osteolysis: the role for early detection of the immune response. *Bone research*, 4, 16014.
124. KANISAWA, I., BANKS, A. Z., BANKS, S. A., MORIYA, H. & TSUCHIYA, A. 2003. Weight-bearing knee kinematics in subjects with two types of anterior cruciate ligament reconstructions. *Knee Surgery, Sports Traumatology, Arthroscopy*, 11, 16-22.

- 125.KARBOWSKI, A., SCHWITALLE, M., ECKARDT, A. & HEINE, J. 1999. Periprosthetic bone remodelling after total knee arthroplasty: early assessment by dual energy X-ray absorptiometry. *Archives of orthopaedic and trauma surgery*, 119, 324-326.
- 126.KEAN, W. F., KEAN, R. & BUCHANAN, W. W. 2004. Osteoarthritis: symptoms, signs and source of pain. *Inflammopharmacology*, 12, 3-31.
- 127.KERSTEN, R. F. M. R., VAN GAALEN, S. M., DE GAST, A. & ÖNER, F. C. 2015. Polyetheretherketone (PEEK) cages in cervical applications: a systematic review. *The Spine Journal*, 15, 1446-1460.
- 128.KIJEVČANIN, M. L., DJURIŠ, M. M., RADOVIĆ, I. R., DJORDJEVIĆ, B. D. & ŠERBANOVIĆ, S. P. 2007. Volumetric properties of the binary methanol+ Chloroform and Ternary Methanol+ Chloroform+ Benzene Mixtures at (288.15, 293.15, 298.15, 303.15, 308.15, and 313.15) K. *Journal of Chemical & Engineering Data*, 52, 1136-1140.
- 129.KOMISTEK, R. D., DENNIS, D. A. & MAHFOUZ, M. 2003. In vivo fluoroscopic analysis of the normal human knee. *Clinical orthopaedics and related research*, 410, 69-81.
- 130.KOMISTEK, R. D., KANE, T. R., MAHFOUZ, M., OCHOA, J. A. & DENNIS, D. A. 2005. Knee mechanics: a review of past and present techniques to determine in vivo loads. *Journal of biomechanics*, 38, 215-228.
- 131.KRETZER, J. P., JAKUBOWITZ, E., REINDERS, J., LIETZ, E., MORADI, B., HOFMANN, K. & SONNTAG, R. 2011. Wear analysis of unicondylar



mobile bearing and fixed bearing knee systems: a knee simulator study. *Acta Biomater*, 7, 710-5.

- 132.KRETZER, J. P., REINDERS, J., SONNTAG, R., HAGMANN, S., STREIT, M., JEAGER, S. & MORADI, B. 2014. Wear in total knee arthroplasty—just a question of polyethylene? *International orthopaedics*, 38, 335-340.
- 133.KUROSAWA, H., WALKER, P., ABE, S., GARG, A. & HUNTER, T. 1985. Geometry and motion of the knee for implant and orthotic design. *Journal of Biomechanics*, 18, 487493-491499.
- 134.KURTZ, S. M. 2004. Chapter 1 - A Primer on UHMWPE. *The UHMWPE Handbook*. San Diego: Academic Press.
- 135.KURTZ, S. M. & DEVINE, J. N. 2007. PEEK biomaterials in trauma, orthopedic, and spinal implants. *Biomaterials*, 28, 4845-69.
- 136.KURTZ, S. M., MAZZUCCO, D., RIMNAC, C. M. & SCHROEDER, D. 2006. Anisotropy and oxidative resistance of highly crosslinked UHMWPE after deformation processing by solid-state ram extrusion. *Biomaterials*, 27, 24-34.
- 137.KURTZ, S. M., MURATOGLU, O. K., EVANS, M. & EDIDIN, A. A. 1999. Advances in the processing, sterilization, and crosslinking of ultra-high molecular weight polyethylene for total joint arthroplasty. *Biomaterials*, 20, 1659-1688.
- 138.KURTZ, S. M., PRUITT, L., JEWETT, C. W., CRAWFORD, R. P., CRANE, D. J. & EDIDIN, A. A. 1998. The yielding, plastic flow, and fracture behavior

of ultra-high molecular weight polyethylene used in total joint replacements. *Biomaterials*, 19, 1989-2003.

139.KUSTER, M. S., WOOD, G. A., STACHOWIAK, G. W. & GACHTER, A. 1997. Joint load considerations in total knee replacement. *J Bone Joint Surg Br*, 79, 109-13.

140.LAFORTUNE, M., CAVANAGH, P., SOMMER, H. & KALENAK, A. 1992. Three-dimensional kinematics of the human knee during walking. *Journal of biomechanics*, 25, 347-357.

141.LATIF, A. M., MEHATS, A., ELCOCKS, M., RUSHTON, N., FIELD, R. E. & JONES, E. 2008. Pre-clinical studies to validate the MITCH PCR Cup: a flexible and anatomically shaped acetabular component with novel bearing characteristics. *J Mater Sci Mater Med*, 19, 1729-36.

142.LIU, A., RICHARDS, L., BLADEN, C. L., INGHAM, E., FISHER, J. & TIPPER, J. L. 2015. The biological response to nanometre-sized polymer particles. *Acta biomaterialia*, 23, 38-51.

143.LOMBARDI JR, A., BEREND, K. & ADAMS, J. 2014. Why knee replacements fail in 2013: patient, surgeon, or implant? *The bone & joint journal*, 96, 101-104.

144.LUETZNER, J., KRUMMENAUER, F., LENGEL, A. M., ZIEGLER, J. & WITZLEB, W.-C. 2007. Serum metal ion exposure after total knee arthroplasty. *Clinical Orthopaedics and Related Research®*, 461, 136-142.

- 145.MAGUIRE, J. K., JR., COSCIA, M. F. & LYNCH, M. H. 1987. Foreign body reaction to polymeric debris following total hip arthroplasty. *Clin Orthop Relat Res*, 213-23.
- 146.MALITO, L. G., AREVALO, S., KOZAK, A., SPIEGELBERG, S., BELLARE, A. & PRUITT, L. 2018. Material properties of ultra-high molecular weight polyethylene: Comparison of tension, compression, nanomechanics and microstructure across clinical formulations. *J Mech Behav Biomed Mater*, 83, 9-19.
- 147.MANLEY, M. T., ONG, K. L. & KURTZ, S. M. 2006. The potential for bone loss in acetabular structures following THA. *Clin Orthop Relat Res*, 453, 246-53.
- 148.MAQUET, P. G., VAN DE BERG, A. J. & SIMONET, J. C. 1975. Femorotibial weight-bearing areas. Experimental determination. *J Bone Joint Surg Am*, 57, 766-71.
- 149.MATTHEWS, J. B., BESONG, A. A., GREEN, T. R., STONE, M. H., WROBLEWSKI, B. M., FISHER, J. & INGHAM, E. 2000a. Evaluation of the response of primary human peripheral blood mononuclear phagocytes to challenge with in vitro generated clinically relevant UHMWPE particles of known size and dose. *J Biomed Mater Res*, 52, 296-307.
- 150.MATTHEWS, J. B., BESONG, A. A., GREEN, T. R., STONE, M. H., WROBLEWSKI, B. M., FISHER, J. & INGHAM, E. 2000b. Evaluation of the response of primary human peripheral blood mononuclear phagocytes to challenge with in vitro generated clinically relevant UHMWPE particles of

known size and dose. *Journal of Biomedical Materials Research Part A*, 52, 296-307.

151. MATTHEWS, J. B., GREEN, T. R., STONE, M. H., WROBLEWSKI, B. M., FISHER, J. & INGHAM, E. 2000c. Comparison of the response of primary human peripheral blood mononuclear phagocytes from different donors to challenge with model polyethylene particles of known size and dose. *Biomaterials*, 21, 2033-2044.
152. MCKELLOP, H. 1981. Wear of Artificial Joint Materials II: Twelve-Channel Wear-Screening Device: Correlation of Experimental and Clinical Results. *Engineering in Medicine*, 10, 123-136.
153. MCKELLOP, H. A., ROSTLUND, T. & BRADLEY, G. 1993. Evaluation of wear in an all-polymer total knee replacement. Part 1: laboratory testing of polyethylene on polyacetal bearing surfaces. *Clin Mater*, 14, 117-26.
154. MEYER, M. R., FRIEDMAN, R. J., DEL SCHUTTE JR, H. & LATOUR JR, R. A. 1994. Long-term durability of the interface in FRP composites after exposure to simulated physiologic saline environments. *Journal of biomedical materials research*, 28, 1221-1231.
155. MIDDLETON, S. & TOMS, A. 2016. Allergy in total knee arthroplasty: a review of the facts. *Bone Joint J*, 98-B, 437-41.
156. MILLER, M. D. & THOMPSON, S. R. 2016. *Miller's Review of Orthopaedics*, Elsevier Health Sciences.

- 157.MIRRA, J. M., MARDER, R. A. & AMSTUTZ, H. C. 1982. The pathology of failed total joint arthroplasty. *Clinical Orthopaedics and Related Research*, 175-183.
- 158.MOBASHERI, A. 2012. Osteoarthritis year 2012 in review: biomarkers. *Osteoarthritis Cartilage*, 20, 1451-64.
- 159.MOORE, D. J., FREEMAN, M. A., REVELL, P. A., BRADLEY, G. W. & TUKE, M. 1998. Can a total knee replacement prosthesis be made entirely of polymers? *J Arthroplasty*, 13, 388-95.
- 160.MORRISON, C., MACNAIR, R., MACDONALD, C., WYKMAN, A., GOLDIE, I. & GRANT, M. H. 1995. In vitro biocompatibility testing of polymers for orthopaedic implants using cultured fibroblasts and osteoblasts. *Biomaterials*, 16, 987-92.
- 161.MORRISON, J. 1970. The mechanics of the knee joint in relation to normal walking. *Journal of biomechanics*, 3, 51-61.
- 162.MURATOGLU, O. K., BURROUGHS, B. R., BRAGDON, C. R., CHRISTENSEN, S., LOZYNSKY, A. & HARRIS, W. H. 2004. Knee simulator wear of polyethylene tibias articulating against explanted rough femoral components. *Clinical Orthopaedics and Related Research (1976-2007)*, 428, 108-113.
- 163.MURATOGLU, O. K., PERINCHIEF, R. S., BRAGDON, C. R., O'CONNOR, D. O., KONRAD, R. & HARRIS, W. H. 2003. Metrology to quantify wear and creep of polyethylene tibial knee inserts. *Clinical Orthopaedics and Related Research®*, 410, 155-164.

164. NATIONAL JOINT REGISTRY 2018. 15th Annual Report National Joint Registry for England, Wales, Northern Ireland and the Isle of Man. 2018 ed.
165. NELSON, A. E., ALLEN, K. D., GOLIGHTLY, Y. M., GOODE, A. P. & JORDAN, J. M. 2014. A systematic review of recommendations and guidelines for the management of osteoarthritis: The Chronic Osteoarthritis Management Initiative of the U.S. Bone and Joint Initiative. *Seminars in Arthritis and Rheumatism*, 43, 701-712.
166. NGUYEN, H. X. & ISHIDA, H. 1986. Molecular analysis of the melting behaviour of poly(aryl-ether-ether-ketone). *Polymer*, 27, 1400-1405.
167. NIEDZWIECKI, S., KLAPPERICH, C., SHORT, J., JANI, S., RIES, M. & PRUITT, L. 2001. Comparison of three joint simulator wear debris isolation techniques: acid digestion, base digestion, and enzyme cleavage. *J Biomed Mater Res*, 56, 245-9.
168. O'CONNOR, J., SHERCLIFF, T., BIDEN, E. & GOODFELLOW, J. 1989. The geometry of the knee in the sagittal plane. *Proceedings of the Institution of Mechanical Engineers, Part H: Journal of Engineering in Medicine*, 203, 223-233.
169. ORAL, E., MALHI, A. S. & MURATOGLU, O. K. 2006. Mechanisms of decrease in fatigue crack propagation resistance in irradiated and melted UHMWPE. *Biomaterials*, 27, 917-25.
170. ORAL, E. & MURATOGLU, O. K. 2011. Vitamin E diffused, highly crosslinked UHMWPE: a review. *International orthopaedics*, 35, 215-223.

- 171.PACE, N., MARINELLI, M. & SPURIO, S. 2008. Technical and Histologic Analysis of a Retrieved Carbon Fiber–Reinforced Poly-Ether-Ether-Ketone Composite Alumina-Bearing Liner 28 Months After Implantation. *The Journal of Arthroplasty*, 23, 151-155.
- 172.PASCAUD, R., EVANS, W., MCCULLAGH, P. & FITZPATRICK, D. 1997. Influence of gamma-irradiation sterilization and temperature on the fracture toughness of ultra-high-molecular-weight polyethylene. *Biomaterials*, 18, 727-735.
- 173.PATEL, A., PAVLOU, G., MÚJICA-MOTA, R. & TOMS, A. 2015. The epidemiology of revision total knee and hip arthroplasty in England and Wales: a comparative analysis with projections for the United States. A study using the National Joint Registry dataset. *The bone & joint journal*, 97, 1076-1081.
- 174.PAULUS, A. C., SCHRÖDER, C., SIEVERS, B., FRENZEL, J., JANSSON, V. & UTZSCHNEIDER, S. 2012. Evaluation of different methods to eliminate adherent endotoxin of polyethylene wear particles. *Wear*, 294, 319-325.
- 175.PENICK, K. J., SOLCHAGA, L. A., BERILLA, J. A. & WELTER, J. F. 2005. Performance of polyoxymethylene plastic (POM) as a component of a tissue engineering bioreactor. *J Biomed Mater Res A*, 75, 168-74.
- 176.PETERSEN, M. M., LAURITZEN, J. B., PEDERSEN, J. G. & LUND, B. 1996. Decreased bone density of the distal femur after uncemented knee

arthroplasty: A1-year follow-up of 29 knees. *Acta Orthopaedica Scandinavica*, 67, 339-344.

177. PIOLETTI, D. P., LEONI, L., GENINI, D., TAKEI, H., DU, P. & CORBEIL, J. 2002. Gene expression analysis of osteoblastic cells contacted by orthopedic implant particles. *Journal of Biomedical Materials Research Part A*, 61, 408-420.
178. PRICE, A. J., ALVAND, A., TROELSEN, A., KATZ, J. N., HOOPER, G., GRAY, A., CARR, A. & BEARD, D. 2018. Knee replacement. *The Lancet*, 392, 1672-1682.
179. PURDUE, P. E., KOULOUVARIS, P., POTTER, H. G., NESTOR, B. J. & SCULCO, T. P. 2007a. The cellular and molecular biology of periprosthetic osteolysis. *Clinical orthopaedics and related research*, 454, 251-261.
180. PURDUE, P. E., KOULOUVARIS, P., POTTER, H. G., NESTOR, B. J. & SCULCO, T. P. 2007b. The cellular and molecular biology of periprosthetic osteolysis. *Clin Orthop Relat Res*, 454, 251-61.
181. RAGAB, A. A., VAN DE MOTTER, R., LAVISH, S. A., GOLDBERG, V. M., NINOMIYA, J. T., CARLIN, C. R. & GREENFIELD, E. M. 1999. Measurement and removal of adherent endotoxin from titanium particles and implant surfaces. *Journal of Orthopaedic Research*, 17, 803-809.
182. RAMSEY, D. K. & WRETENBERG, P. F. 1999. Biomechanics of the knee: methodological considerations in the in vivo kinematic analysis of the tibiofemoral and patellofemoral joint. *Clinical Biomechanics*, 14, 595-611.



- 183.RANAWAT, C. S. & SHINE, J. J. 1973. Duo-condylar total knee arthroplasty. *Clinical orthopaedics and related research*, 94, 185-195.
- 184.REINSCHMIDT, C., VAN DEN BOGERT, A., LUNDBERG, A., NIGG, B., MURPHY, N., STACOFF, A. & STANO, A. 1997. Tibiofemoral and tibioalcalneal motion during walking: external vs. skeletal markers. *Gait & Posture*, 6, 98-109.
- 185.REN, W., WU, B., MAYTON, L. & WOOLEY, P. H. 2002. Polyethylene and methyl methacrylate particle-stimulated inflammatory tissue and macrophages up-regulate bone resorption in a murine neonatal calvaria in vitro organ system. *J Orthop Res*, 20, 1031-7.
- 186.REVELL, P. A., WEIGHTMAN, B., FREEMAN, M. A. & ROBERTS, B. V. 1978. The production and biology of polyethylene wear debris. *Arch Orthop Trauma Surg*, 91, 167-81.
- 187.RIES, M. D. & PRUITT, L. 2005. Effect of cross-linking on the microstructure and mechanical properties of ultra-high molecular weight polyethylene. *Clin Orthop Relat Res*, 440, 149-56.
- 188.ROACH, M. 2007. Base metal alloys used for dental restorations and implants. *Dent Clin North Am*, 51, 603-27, vi.
- 189.ROBINSON, R. P. 2005. The early innovators of today's resurfacing condylar knees. *J Arthroplasty*, 20, 2-26.
- 190.SAIKKO, V. 1993. Wear and friction properties of prosthetic joint materials evaluated on a reciprocating pin-on-flat apparatus. *Wear*, 166, 169-178.

- 191.SCHMALZRIED, T. P., JASTY, M. & HARRIS, W. H. 1992. Periprosthetic bone loss in total hip arthroplasty. Polyethylene wear debris and the concept of the effective joint space. *J Bone Joint Surg Am*, 74, 849-63.
- 192.SCHOLES, S. & UNSWORTH, A. 2010. The wear performance of PEEK-OPTIMA based self-mating couples. *Wear*, 268, 380-387.
- 193.SCHOLES, S. C. & UNSWORTH, A. 2009. Wear studies on the likely performance of CFR-PEEK/CoCrMo for use as artificial joint bearing materials. *J Mater Sci Mater Med*, 20, 163-70.
- 194.SCHRODER, C., REINDERS, J., ZIETZ, C., UTZSCHNEIDER, S., BADER, R. & KRETZER, J. P. 2013. Characterization of polyethylene wear particle: The impact of methodology. *Acta Biomater*, 9, 9485-91.
- 195.SCHROER, W. C., BEREND, K. R., LOMBARDI, A. V., BARNES, C. L., BOLOGNESI, M. P., BEREND, M. E., RITTER, M. A. & NUNLEY, R. M. 2013. Why are total knees failing today? Etiology of total knee revision in 2010 and 2011. *The Journal of arthroplasty*, 28, 116-119.
- 196.SCOTCHFORD, C. A., GARLE, M. J., BATCHELOR, J., BRADLEY, J. & GRANT, D. M. 2003. Use of a novel carbon fibre composite material for the femoral stem component of a THR system: in vitro biological assessment. *Biomaterials*, 24, 4871-9.
- 197.SCOTT, M., MORRISON, M., MISHRA, S. & JANI, S. 2005. Particle analysis for the determination of UHMWPE wear. *Journal of Biomedical Materials Research Part B: Applied Biomaterials*, 73, 325-337.

198. SCOTT, M., WIDDING, K. & JANI, S. 2001. Do current wear particle isolation procedures underestimate the number of particles generated by prosthetic bearing components? *Wear*, 251, 1213-1217.
199. SEIREG, A. & ARVIKAR, R. 1975. The prediction of muscular load sharing and joint forces in the lower extremities during walking. *Journal of biomechanics*, 8, 89-102.
200. SHANBHAG, A. S., BAILEY, H. O., HWANG, D. S., CHA, C. W., EROR, N. G. & RUBASH, H. E. 2000. Quantitative analysis of ultrahigh molecular weight polyethylene (UHMWPE) wear debris associated with total knee replacements. *J Biomed Mater Res*, 53, 100-10.
201. SHANBHAG, A. S., JACOBS, J. J., BLACK, J., GALANTE, J. O. & GLANT, T. T. 1994a. Macrophage/particle interactions: effect of size, composition and surface area. *Journal of Biomedical Materials Research Part A*, 28, 81-90.
202. SHANBHAG, A. S., JACOBS, J. J., BLACK, J., GALANTE, J. O. & GLANT, T. T. 1995. Human monocyte response to particulate biomaterials generated in vivo and in vitro. *J Orthop Res*, 13, 792-801.
203. SHANBHAG, A. S., JACOBS, J. J., GLANT, T. T., GILBERT, J. L., BLACK, J. & GALANTE, J. O. 1994b. Composition and morphology of wear debris in failed uncemented total hip replacement. *J Bone Joint Surg Br*, 76, 60-7.

- 204.SHARKEY, P. F., LICHSTEIN, P. M., SHEN, C., TOKARSKI, A. T. & PARVIZI, J. 2014. Why are total knee arthroplasties failing today--has anything changed after 10 years? *J Arthroplasty*, 29, 1774-8.
- 205.SHEN, C. & DUMBLETON, J. H. 1976. The friction and wear behavior of polyoxymethylene in connection with joint replacement. *Wear*, 38, 291-303.
- 206.SHENOY, R., PASTIDES, P. & NATHWANI, D. 2013. (iii) Biomechanics of the knee and TKR. *Orthopaedics and Trauma*, 27, 364-371.
- 207.SIEVING, A., WU, B., MAYTON, L., NASSER, S. & WOOLEY, P. H. 2003. Morphological characteristics of total joint arthroplasty-derived ultra-high molecular weight polyethylene (UHMWPE) wear debris that provoke inflammation in a murine model of inflammation. *J Biomed Mater Res A*, 64, 457-64.
- 208.SMITH, R. A. & HALLAB, N. J. 2010. In vitro macrophage response to polyethylene and polycarbonate-urethane particles. *Journal of biomedical materials research Part A*, 93, 347-355.
- 209.SMITH, R. A., MAGHSOODPOUR, A. & HALLAB, N. J. 2010. In vivo response to cross-linked polyethylene and polycarbonate-urethane particles. *Journal of Biomedical Materials Research Part A*, 93, 227-234.
- 210.SOBIERAJ, M. C. & RIMNAC, C. M. 2009. Ultra high molecular weight polyethylene: mechanics, morphology, and clinical behavior. *J Mech Behav Biomed Mater*, 2, 433-43.

- 211.SONG, E.-K., SEON, J.-K., MOON, J.-Y. & JI-HYOUN, Y. 2013. The Evolution of Modern Total Knee Prostheses. *Arthroplasty-Update*. InTech.
- 212.TIPPER, J. L., GALVIN, A. L., WILLIAMS, S., MCEWEN, H. M., STONE, M. H., INGHAM, E. & FISHER, J. 2006. Isolation and characterization of UHMWPE wear particles down to ten nanometers in size from in vitro hip and knee joint simulators. *J Biomed Mater Res A*, 78, 473-80.
- 213.UTTING, M. R. & NEWMAN, J. H. 2004. Customised hinged knee replacements as a salvage procedure for failed total knee arthroplasty. *Knee*, 11, 475-9.
- 214.UTZSCHNEIDER, S., BECKER, F., GRUPP, T. M., SIEVERS, B., PAULUS, A., GOTTSCHALK, O. & JANSSON, V. 2010a. Inflammatory response against different carbon fiber-reinforced PEEK wear particles compared with UHMWPE in vivo. *Acta Biomater*, 6, 4296-304.
- 215.UTZSCHNEIDER, S., BECKER, F., GRUPP, T. M., SIEVERS, B., PAULUS, A., GOTTSCHALK, O. & JANSSON, V. 2010b. Inflammatory response against different carbon fiber-reinforced PEEK wear particles compared with UHMWPE in vivo. *Acta Biomaterialia*, 6, 4296-4304.
- 216.UTZSCHNEIDER, S., PAULUS, A., DATZ, J. C., SCHROEDER, C., SIEVERS, B., WEGENER, B. & JANSSON, V. 2009. Influence of design and bearing material on polyethylene wear particle generation in total knee replacement. *Acta Biomater*, 5, 2495-502.
- 217.VAN MEURS, J. B. 2017. Osteoarthritis year in review 2016: genetics, genomics and epigenetics. *Osteoarthritis Cartilage*, 25, 181-189.

- 218.VERMES, C., CHANDRASEKARAN, R., JACOBS, J. J., GALANTE, J. O., ROEBUCK, K. A. & GLANT, T. T. 2001. The effects of particulate wear debris, cytokines, and growth factors on the functions of MG-63 osteoblasts. *JBJS*, 83, 201.
- 219.VERTULLO, C. J., LEWIS, P. L., GRAVES, S., KELLY, L., LORIMER, M. & MYERS, P. 2017. Twelve-Year Outcomes of an Oxinium Total Knee Replacement Compared with the Same Cobalt-Chromium Design: An Analysis of 17,577 Prostheses from the Australian Orthopaedic Association National Joint Replacement Registry. *JBJS*, 99, 275-283.
- 220.WALKER, P., YILDIRIM, G., ARNO, S. & HELLER, Y. 2010. Future directions in knee replacement. *Proceedings of the Institution of Mechanical Engineers, Part H: Journal of Engineering in Medicine*, 224, 393-414.
- 221.WALKER, P. S., BLUNN, G. W., BROOME, D. R., PERRY, J., WATKINS, A., SATHASIVAM, S., DEWAR, M. E. & PAUL, J. P. 1997. A knee simulating machine for performance evaluation of total knee replacements. *J Biomech*, 30, 83-9.
- 222.WALKER, P. S., BLUNN, G. W. & LILLEY, P. A. 1996. Wear testing of materials and surfaces for total knee replacement. *J Biomed Mater Res*, 33, 159-75.
- 223.WALLDIUS, B. 1957. Arthroplasty of the knee using an endoprosthesis. *Acta Orthop Scand Suppl*, 24, 1-112.

224. WALLDIUS, B. 1960. Arthroplasty of the knee using an endoprosthesis. 8 years' experience. *Acta Orthop Scand*, 30, 137-48.
225. WANG, A., LIN, R., STARK, C. & DUMBLETON, J. 1999. Suitability and limitations of carbon fiber reinforced PEEK composites as bearing surfaces for total joint replacements. *Wear*, 225, 724-727.
226. WANG, A., STARK, C. & DUMBLETON, J. 1995. Role of cyclic plastic deformation in the wear of UHMWPE acetabular cups. *Journal of biomedical materials research*, 29, 619-626.
227. WANG, M. L., NESTI, L. J., TULI, R., LAZATIN, J., DANIELSON, K. G., SHARKEY, P. F. & TUAN, R. S. 2002. Titanium particles suppress expression of osteoblastic phenotype in human mesenchymal stem cells. *Journal of Orthopaedic Research*, 20, 1175-1184.
228. WILKINSON, J. M., HAMER, A. J., STOCKLEY, I. & EASTELL, R. 2005. Polyethylene wear rate and osteolysis: critical threshold versus continuous dose-response relationship. *J Orthop Res*, 23, 520-5.
229. WILLERT, H. G., BUCHHORN, G. H., FAYYAZI, A., FLURY, R., WINDLER, M., KOSTER, G. & LOHMANN, C. H. 2005. Metal-on-metal bearings and hypersensitivity in patients with artificial hip joints. A clinical and histomorphological study. *J Bone Joint Surg Am*, 87, 28-36.
230. WILLIAMS, D., MCNAMARA, A. & TURNER, R. 1987. Potential of polyetheretherketone (PEEK) and carbon-fibre-reinforced PEEK in medical applications. *Journal of materials science letters*, 6, 188-190.

- 231.WILLIAMS, P. A., BROWN, C. M., TSUKAMOTO, R. & CLARKE, I. C.  
2010. Polyethylene wear debris produced in a knee simulator model: effect of crosslinking and counterface material. *J Biomed Mater Res B Appl Biomater*, 92, 78-85.
- 232.XIA, B., DI, C., ZHANG, J., HU, S., JIN, H. & TONG, P. 2014.  
Osteoarthritis pathogenesis: a review of molecular mechanisms. *Calcif Tissue Int*, 95, 495-505.
- 233.XU, Y., MCKENNA, R. W., KARANDIKAR, N. J., PILDAIN, A. J. & KROFT, S. H. 2005. Flow cytometric analysis of monocytes as a tool for distinguishing chronic myelomonocytic leukemia from reactive monocytosis. *Am J Clin Pathol*, 124, 799-806.
- 234.ZHANG, L. & PIGGOTT, M. 2000. Water Absorption and Fiber-Matrix Interface Durability in Carbon-PEEK. *Journal of Thermoplastic Composite Materials*, 13, 162-172.